Design, synthesis, and evaluation of serum-stable peptide antagonists of the CGRP receptor as a novel treatment for migraine

Vera D'Aloisio

A thesis submitted in partial fulfilment of the requirements of
Liverpool John Moores University for the degree of Doctor of Philosophy.

In collaboration with The University of Edinburgh and PharmNovo AB.

April 2022

Declaration

The work presented in this thesis was carried out at the Byrom Street City Campus of Liverpool John Moores University and at the EaStChem School of Chemistry, Joseph Black Building, The King's Buildings at The University of Edinburgh. Unless otherwise stated, the work is the original work of the author.

While registered as a candidate for the degree of Doctor of Philosophy, for which submission is now made, the author has not been registered as a candidate for any other award. This thesis has not been submitted in whole, or in part, for any other degree.

James Parsons Building

Byrom Street City Campus

Liverpool John Moores University

3 Byrom Street

L3 3AF

Liverpool

UK

To the reader, who will be curious enough
to start reading this monograph.

And to my family, with all the gratitude I can think of.

Acknowledgements

There are many people I would like to thank for their contribution to this journey; without them, I would have never gone this far.

First, I would like to thank my supervisors. Professor Gillian A. Hutcheon, who believed in me since my first day at LJMU. Thank you for your guidance and support, not only research-wise, but also as the main point of reference during this journey, as an inspiring woman in STEM.

My sincere gratitude goes to Dr Chris R. Coxon; although the decision of moving to Edinburgh was a bit overwhelming for me at the time, sooner I understood that your promise of helping me from remote was a real commitment. I will never be grateful enough for your innovative ideas, your enthusiasm for research, your patient guidance, your encouragement, and advice, but also for the opportunity you gave me to join your research group at The University of Edinburgh.

A big thank you to Dr Amos Fatokun, for his help with the pharmacology section of this thesis, but also for his kindness and his humanity, which will never be forgotten.

I am grateful to Professor David Kendall, for starting the anti-migraine drug discovery programme, for believing in my competencies in carrying it on, and for his insightful advice.

A special mention goes to Dr Francesca Giuntini for her guidance and kindness: our conversations have been crucial part of my professional and personal growth.

I would like to thank my fellow lab mates (actually, I should say friends), both at Liverpool John Moores University and The University of Edinburgh, because we created a real squad which helped us overcoming the toughest times and allowed us to work in an amazing workplace. I feel blessed every time I think about you all.

I am grateful to Liverpool John Moores University and PharmNovo AB. (now InnoviPharm Ltd.) for the financial support to this research project. A special acknowledgement goes to The University of Edinburgh, for allowing me to join this research-intensive university during my placement at the EaSt Chem School of Chemistry.

Life is a cycle, and everything starts and goes back at the same spot. To me, the cycle starts and goes back to my family. Family is everything that matters. Therefore, I want to dedicate my thesis and all my achievements to my family.

The inspiration for pursuing a PhD came from both my nannas Vera and Anna, from their dedication, strength, and perseverance in any aspect of their lives, from my grandad Rolando, the backbone of the D'Aloisio's family and from my grandad Mimí and his dedication to study which brought him to achieve a degree in law in the 1960s with two daughters and a family to bring up.

My immense gratitude goes to my parents and my brother. To my mum Lia, always the right word at the right moment, a triumph of kindness and strength. You have been the backbone and the pillar of our family. To my dad Guido, the most ambitious, intelligent, and hilarious man I know, my light in the dark. To my brother Rolando, my flesh and blood, always there for me.

There are other people that made this journey the sweetest possible. First of all, Giulia, who has been my family in Liverpool during my PhD: you are the first person I think of when someone tells me "I am going to tell you a secret, but, please, tell no one". Without you, I would have not been here writing these acknowledgements. And thanks to your dad Ivano, who has watched and protected us during these years. I will never forget his smile.

Not less importantly, a huge thanks to David: you entered my life on tiptoe and you have always been there for me, no matter what. You are my sunshine even in the rainy UK, and I will be grateful forever for your smile and your kindness, for your love that gives and never asks back. Thank you.

A special thanks goes to the Italian and the international friends I met in Liverpool: Vale, Lally, Seba, Michele, Paolo, Ioannis, Ashley, Silvia, Kan, Paddy, Talhat, Thais, and Hique. We may now be far in distance, but never in my heart. I will always smile whenever I will think about you and about the good ol' times together.

I am grateful to my childhood friends. Thank you for your support from far away. The further we live from each other, the closer we are. I am lucky to have you in my life.

Finally, I should thank myself, for having faced every single situation with a big smile, even when the PhD research seemed to go nowhere. During this path, I learnt that to obtain something you must work hard, and if something goes wrong, you need to try again, and again, because if at first you do not succeed, you need to try two more times so that either you change your destiny, or your failure is statistically significant.

Abstract

Migraine, the third most prevalent disease in the world (global prevalence of 12-14.7%), is a complex and multifaceted neurovascular disorder, characterised by severe attacks of headache and often associated with nausea and sensory hypersensitivity. Numerous contraindications and adverse events are associated with traditional medicines and, more importantly, 40% of patients receive little-to-no benefit from them. Calcitonin gene-related peptide (CGRP) and its receptor are now recognised to play a key role in migraine pathophysiology and evidence suggests that the CGRP receptor could be antagonised with synthetic peptides obtained by truncation of the native CGRP.

Peptide-based therapeutics have been an active area of research for decades and have found clinical applications in a number of disease areas, e.g., metabolic disorders, cancers, cardiovascular diseases, and infection diseases, reaching the milestone of 100 approved peptide drugs in 2020. In this project, information on regulatory approved peptide therapeutics and diagnostics was collated in an open-source database, PepTherDia (http://peptherdia.herokuapp.com), and a detailed structural analysis was performed to uncover key structural trends to help with future peptide drug design.

The use of peptides as medicines is still limited due to poor bioavailability after oral administration and, more generally, poor stability due to their susceptibility to proteolytic degradation. Various strategies, including fluorine-editing, peptoid-editing, or lipidation, could be explored to prepare proteolytically stable peptide or peptidomimetic analogues. Towards this goal, a library of peptide and peptidomimetic analogues of the C-terminal portion of CGRP were designed and synthesised, starting from the structure of a potent CGRP receptor antagonist (P006) previously developed in collaboration with PharmNovo AB. These compounds were tested for antagonism at the CGRP receptor, lipophilicity and toxicity. Methods to assess peptide stability in blood and plasma protein binding were also optimised, validated, and applied to study the pharmacokinetic profile of the library of compounds. This led to the discovery of potent CGRP receptor antagonists with

extremely favourable pharmacokinetic profiles. Among them, the most promising compounds of the series were three N-terminal benzoylated analogues (i.e., LJMU027, LJMU017, and LJMU018) presenting significantly increased estimated half-lives (> 3 hours) compared to P006 (estimated half-life of ~13 min), while maintaining comparable activity against the CGRP receptor.

Due to first pass metabolism and poor oral absorption, peptides are often administered parenterally, thus usually resulting in low patient acceptability and compliance. Alternatively, peptides could be delivered *via* the intranasal route, offering the advantages of rapid direct delivery to the brain, greater acceptability and compliance, and lower adverse event profiles due to inferior systemic effects. Nano-sized structures derived from peptide self-assembly in water were obtained (diameter size between 14 and 30 nm) and peptide-loaded dry powder microparticles prepared from low molecular weight chitosan suitable for nasal delivery were manufactured (average diameter size of 9.55 ± 0.74 μm).

In conclusion, this investigation showed that benzoyl modifications performed at the N-terminus of P006 did not disrupt antagonistic activity but yielded stable analogues that were up to 90% intact after 60 min incubation in pooled human serum, with a tendency to bind to plasma proteins. The ability of these peptides to self-assemble was exploited to prepare nano-sized structures, which could be directly administered parenterally or loaded into mucoadhesive carriers for nasal delivery.

List of Abbreviations

5-FU = 5-fluorouracil

5-HT = Serotonin

AA = Amino acid

ACE = Angiotensin converting enzyme

ACN = Acetonitrile

ADD = Antidepressants drugs

ADME = Absorption, distribution, metabolism and excretion

AED = Antiepileptic drugs

AGP = α-1 acid glycoprotein

AM = Adrenomedullin

AMY = Amylin

ANOVA = Analysis of variance

AP = Aqueous phase

AT = Angiotensin II

ATP = Adenosine triphosphate

BBB = Blood brain barrier

Boc = t-butyloxycarbonyl

Bz = Benzoyl

CAC = Critical aggregate concentration

CAGR = Compound annual growth rate

cAMP = Cyclic adenosine monophosphate

CCB = Calcium channel blockers

CGRP = Calcitonin gene-related peptide

CGRP-R = Calcitonin gene-related peptide receptor

CHT = Chitosan

CLR = Calcitonin receptor-like receptor

CM = Chronic migraine

CMC = Critical micelle concentration

CNS = Central nervous system

CNS MPO = Central nervous system multiparameter optimization

COPD = Chronic obstructive pulmonary disease

CSD = Cortical spreading depression

CSF = Cerebrospinal fluid

CT = Calcitonin

DCC = N,N’-dicyclohexylcarbodiimide

DHE = dihydroergotamine mesylate

DIC = N,N’-diisopropylcarbodiimide

DIPEA = N,N-diisopropylethylamine

DLS = Dynamic light scattering

DMEM/F-12 = Dulbecco's Modified Eagle Medium: Nutrient Mixture F-12

DMF = Dimethylformamide

DoE = Design of experiments

DOTA = Tetraxetan

DPBS = Dulbecco’s Phosphate Buffered Saline

DPP IV = Dipeptidyl peptidase-4

EA = Enzyme acceptor

ED = Enzyme donor

ED = Equilibrium dialysis

EE% = Encapsulation efficiency percentage

EFC = Enzyme fragment complementation

EM = Electron microscopy

EM = Episodic migraine

EMA = European Medicines Agency

Exp. = Experiment

F-AAs = Fluorine-containing amino acids

FAs = Fatty acids

FDA = Food and drug administration

GBD = Global burden disease

GLP-1 = Glucagon-like peptide-1

GPCR = G-protein-coupled receptor

HF = Hydrofluoric acid

HSA = Human serum albumin

ICH = International Conference of Harmonization

ICHD = International Classification of Headache Disorders

IUPAC = International Union of Pure and Applied Chemistry

JCBN = Joint Commission on Biochemical Nomenclature

K = Equilibrium constant

KD = Dissociation constant

LCMS = Liquid chromatography mass spectrometry

LLOD = Lower limit of detection

LLOQ = Lower limit of quantification

LMW = Low molecular weight

LPPS = Liquid-Phase Peptide Synthesis

mAbs = Monoclonal antibodies

MEM = Minimum essential media

MPs = Microparticles

MWCO = Molecular weight cut off

No. = Number

NPs = Nanoparticles

NSAIDs = Nonsteroidal anti-inflammatory drugs

o/w = Oil-in-water

OP = Organic phase

PAC1 = Pituitary Adenylate Cyclase-Activating Polypeptide receptor

PACAP = Pituitary Adenylate Cyclase-Activating Polypeptide

PBD = Plackett-Burman design

Pbf = 2,2,4,6,7-pentamethyldihydrobenzofuran-5-sulfonyl

PBS = Phosphate buffer saline

PDI = Polydispersity index

PES = Polyethersulfone

PLGA = Poly(D,L-lactic-co-glycolic acid

PMDA = Pharmaceutical and Medical Devices Agency

PPB = Plasma protein binding

PTS = Peptide transporter systems

PVA = Polyvinyl alcohol

Pyr = Pyroglutamic acid

R2 = Regression coefficient

RAMP1 = Receptor activity-modifying protein 1

RED = Rapid equilibrium dialysis

RP-HPLC = Reversed-phase high-performance liquid chromatography

Rs = Resolution

RT = Retention time

SARs = Structure-activity relationship studies

SD = Spray-drying

SDI = Spreading depression inhibitors

SDS = Sodium dodecyl sulfate

SEM = Scanning electron microscopy

SN = Signal-to-noise

TCA = Trichloroacetic acid

TD = Taguchi design

TEM = Transmission electron microscopy

TFA = Trifluoroacetic acid

TGA = Thermogravimetric analysis

TIPS = Triisopropylsilane

Trt = Trityl

UC = Ultracentrifugation

UF = Ultrafiltration

w/o/w = water-in-oil-in-water

WHO = World Health Organization

ZP = Zeta potential

Amino acids

Alanine	Ala	A
Arginine	Arg	R
Asparagine	Asn	N
Aspartic acid	Asp	D
Cysteine	Cys	C
Glutamic acid	Glu	E
Glutamine	Gln	Q
Glycine	Gly	G
Histidine	His	H
Isoleucine	Ile	I
Leucine	Leu	L
Lysine	Lys	K
Methionine	Met	M
Phenylalanine	Phe	F
Proline	Pro	P
Serine	Ser	S
Threonine	Thr	T
Tryptophan	Trp	W
Tyrosine	Tyr	Y
Valine	Val	V
4-fluoro-phenylalanine	4-F-Phe	-
Pentafluoro-phenylalanine	F_5-Phe	-
Sarcosine	Sar	-
2,4-diaminobutyric acid	Dab	-
4-hydroxyproline	Hyp	-
Naphthyl-alanine	Nal	-
2,3,-diaminopropionic acid	Dap	-
Dehydroalanine	Dha	-
3-(3-pyridyl)-alanine	3Pal	-
N-methyl-leucine	N-Me-Leu	-
4-chloro-phenylalanine	Phe(4-Cl)	-
Ornithine	Orn	-
β-Lysine	βLys	-
3,4-dihydroxy-homotyrosine	(OH_2)-hTyr	-
2-aminoisobutyric acid	Aib	-
1,2,3,4-tetrahydroisoquinoline-3-carboxylic acid	Tic	-
Octahydro-1H-indole-2-carboxylic acid	Oic	-
Cyclic arginine	Cyclic Arg	-

List of Contents

List of Figures

List of Tables

1 General introduction

1.1 Migraine

1.1.1 Prevalence and burden of migraine

Migraine is the third most prevalent disease in the world, with an overall prevalence of between 12 and 14.7% over the world population [1,2], being disproportionally more common in women (~15-18%) than men (~6%) [3]. Its prevalence is probably underestimated as migraine tends to be underdiagnosed, and its importance for public health has only recently been recognised (in the 2000s) [2,4]. Migraine may first appear at any age, however, the greatest incidence occurs in early to mid-adolescence, being particularly burdensome among young and middle-age women [3,4]. Although not a fatal disease, migraine is listed by the World Health Organization (WHO) as the sixth most disabling disorder in the world and the most disabling of all the neurological conditions [5]. Indeed, in 2016 the Global Burden of Disease (GBD) ranked migraine as second globally in terms of years of life lived with disability [6].

It is well recognised that migraine is associated with a substantial socioeconomic burden, having a significant impact on both migraineurs' and their families' lives. The impact increases proportionally with the number of attacks per month, having the greatest burden on individuals with more than 15 headache days/month [7]. Thus, migraine, which mostly affects people during their period of family caring and professional achievements [8], heavily contributes to problems related to domestic and romantic relationships, parenting, finance, educational achievements, and career, as reported by a study conducted on ~13,000 patients [7]. Personal finances are endangered as migraine imposes a heavy economic burden through direct and indirect expenses. The main direct costs associated with migraine are pharmaceutical and non-pharmaceutical treatments, medical costs, and hospitalisation. The indirect costs, among which the most important are work loss and reduced productivity, greatly exceed the direct costs [2]. In Europe, it has been estimated that the migraine annual cost per-person is € 1,177, of which 93% is due to indirect costs [9]. In the UK

alone, more than 11 million people suffer from migraine, and 25 million days of school or work are lost every year due to migraine, with a huge impact on the economy, estimated to be £ 2.25 billion per year, due to short-term absence of non-manual employees in the UK [4,10,11].

1.1.2 Clinical manifestations of migraine

Migraine is a complex and multifaceted neurovascular disease, characterised by recurrent and severe attacks of headache, often unilateral, and frequently associated with nausea, vomiting and sensory hypersensitivity [1,3]. Migraine manifestations can be divided into four phases: premonitory, aura, headache, and postdrome phases, which can occur in a linear chronological order, or, in the majority of the cases overlap (Figure 1.1). On the other hand, some symptoms – e.g., drowsiness, tiredness, fatigue, sensory hypersensitivity, neck discomfort or concentration impairments – may appear in all phases [5,12]. The premonitory symptoms, which can last up to three days, include changes in mood and activity, irritability, tiredness, neck pain, sensitivity to light, food cravings and gastrointestinal problems [5,13]. Around 30% of people who suffer from migraine, experience the aura phase (~1 hour or more), characterised by transient neurological deficits, blind or scintillating spots in the visual field, and speech or motor disturbances [5,13,14]. The aura is followed by the headache phase, characterised by throbbing head pain, lasting up to 72 hours if untreated or unsuccessfully treated [3]. Headache is reported as the most impactful symptom by the sufferers and the most important reason for seeking medical advice and treatment [15]. The International Classification of Headache Disorders (ICHD) distinguishes episodic migraine (EM), appearing on less than 15 days a month, from chronic migraine (CM), occurring on 15 or more days per month [7,16,17]. Finally, the postdrome phase, arising after resolution of the headache, usually mirrors the symptoms observed during the premonitory phase and lasts on average for 25 hours [5,18].

1.1.3 Pathophysiology of migraine and risk factors

In recent years, the understanding of the pathophysiology of migraine has significantly advanced, although it is still not fully understood. Thus, improvements in its characterisation and diagnosis have led to the description of migraine as a complex neurovascular disorder, moving away from the now obsolete vascular theory, which described migraine as a primary vascular event [3]. Recent studies have provided new insights into various aspects of migraine, from its genetic causes to anatomical and physiological features, and pharmacological mechanisms [12]. The different phases described in section 1.1.2 can be used to study the physiological changes occurring at the beginning of the migraine attack, those responsible for the aura phase, those happening during the headache phase, and, finally, those involved in the process of recovery (Figure 1.1) [12].

Typical symptoms appearing during the premonitory phase suggest an involvement of the hypothalamus as the potential site of origin of the migraine attack, further proven by imaging studies (e.g., $H_2{}^{15}O$-Positron Emission Tomography) [5,13].

A well-established hypothesis is that the aura is a primary initiator of a migraine attack, leading to headache and other symptoms; however, migraine aura commonly occurs without head pain, and most migraine attacks occur without aura, indicating that aura is not necessary or sufficient to exacerbate headache [12]. Common manifestations of the aura phase – e.g., visual disturbances – and subsequent studies on patients suffering from migraine with aura suggested that visual aura in migraine may be a consequence of an event similar to a cortical spreading depression (CSD), where a slowly propagating wave of depolarisation in neuronal and glial cell membranes is followed by inhibition of the cortical activity for up to 30 minutes [5,13].

Nowadays, the characteristic throbbing headache in migraine is widely accepted as being a consequence of trigeminovascular pathway activation. Head pain begins when nociceptive neurons innervating the dura mater are stimulated, resulting in the

release of vasoactive peptides, such as calcitonin gene-related peptide (CGRP), substance P, neurokinin A, and pituitary adenylate cyclase-activating polypeptide-38 (PACAP-38), eventually causing signalling along the trigeminovascular pathway [5,13]. The role of these neuropeptides as mediators of migraine will be further explored in section 1.1.4.

Finally, the postdrome phase, occurring when the patient stops feeling head pain, while still experiencing other symptoms, has not been studied with imaging or other techniques, thus representing an opportunity for new findings [5].

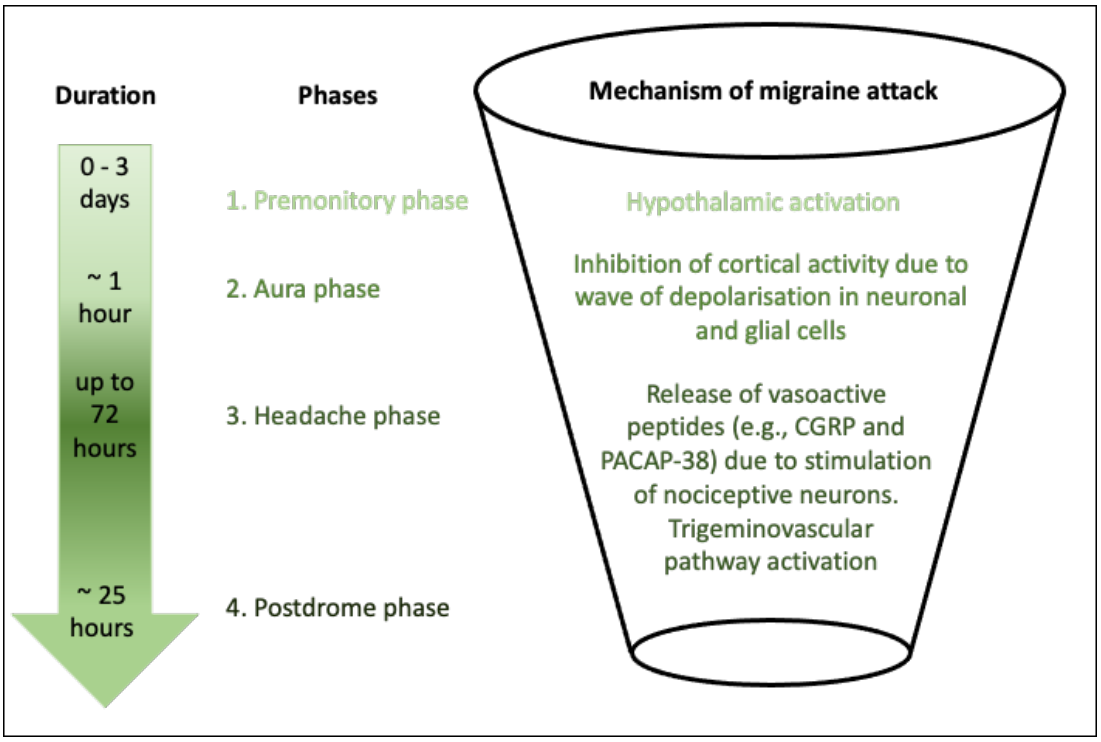

Figure 1.1. Duration, phases and mechanisms of a migraine attack.

Risk factors related to migraine can be divided into genetic factors, responsible for ~60% of the clinical cases, and non-genetic factors, being responsible for the residual 40% (Figure 1.2) [2]. More than 38 migraine-associated gene polymorphisms have been discovered so far, and this complex range of potential genetic mechanisms increases the chances of developing therapies tailored to individual patients [12]. Among the non-genetic factors responsible for triggering or worsening a migraine

attack, hormonal fluctuations, bad food habits, changes in sleeping or eating patterns, strong sensor stimuli, and comorbidity (e.g., allergies, respiratory diseases, psychiatric disorders, arthritis, obesity, head and neck injury, cardiovascular disorders, and ulcers) have the greatest impact [2,19].

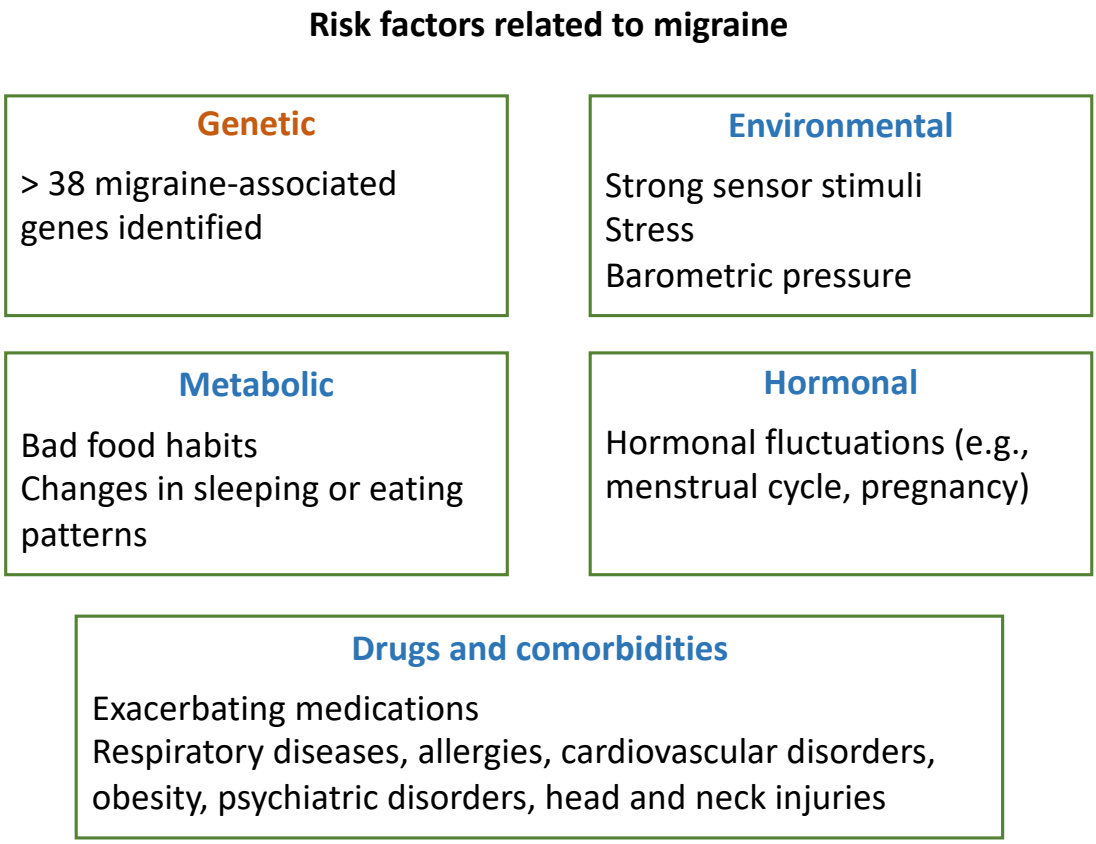

Figure 1.2. Genetic (orange) and non-genetic (blue) risk factors associated with migraine.

1.1.4 Neuropeptides as mediators of migraine

1.1.4.1 Calcitonin gene-related peptide (CGRP)

Accumulating evidence indicates a primary role for the calcitonin gene-related peptide (CGRP) as a key player in migraine pathophysiology, thus being an important target for migraine prevention and therapy [12,13].

CGRP is a 37-amino acid neuropeptide that belongs to the calcitonin family, comprising also calcitonin (CT), amylin (AMY), and adrenomedullin (AM) [20]. CGRP exists in humans in two isoforms (α and β) which derive from two different genes

and are distinguished by residues at positions 3, 22, and 25 [21]; both the isoforms show similarities with AMY and AM sequences (Figure 1.3) [22]. α and β CGRP isoforms are widely distributed in the central and peripheral nervous system where they have several physiological properties [22]. In the periphery, CGRP is released in the meninges, causing arterial vasodilation and, in some cases, plasma extravasation, sterile inflammation and activation of meningeal nociceptors [13,23]. Centrally, CGRP acts in the trigeminal ganglion, being involved in signalling between trigeminal ganglion neurons [13].

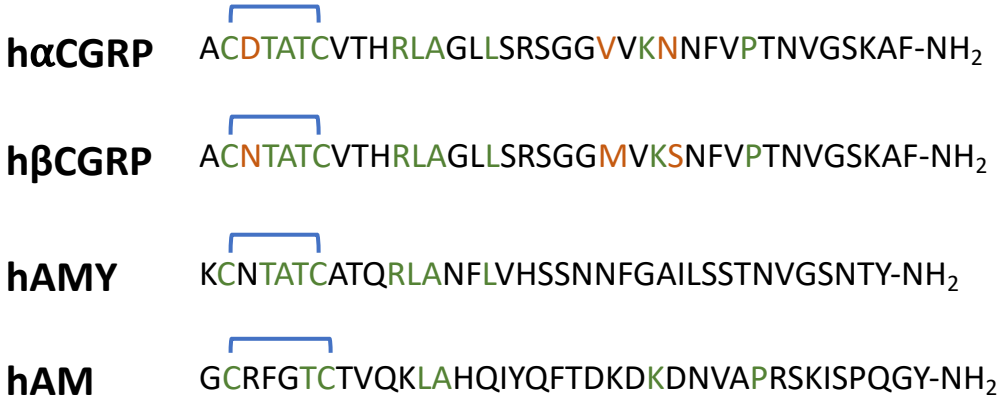

Figure 1.3. Amino acid sequence alignments of human α CGRP, β CGRP, AMY, and AM. They all present a C-terminal amide and a disulfide bond between two cysteine residues at the N-terminus. Similarities within the sequences of CGRP, AMY, and AM are coloured in green, while differences between the α and β isoforms of CGRP are highlighted in orange [20,22].

CGRP exerts its function by binding to the CGRP receptor complex, a heterodimer comprising the calcitonin receptor-like receptor (CLR), a class B G-protein-coupled receptor (GPCR), and receptor activity-modifying protein 1 (RAMP1), a type 1 transmembrane domain protein [20,24]. Activation of CGRP receptor (CGRP-R) by its endogenous ligand results in the induction of various downstream signalling pathways that, in turn, mediate physiological and pathophysiological effects [25]. It is now widely recognised that the CGRP-R couples to G-proteins to initiate signalling (Figure 1.4). Despite the fact that the CGRP-R is mainly considered a $G\alpha_s$-coupled

GPCR, it can also couple with $G\alpha_i$ and $G\alpha_{q/11}$ proteins. In particular, it has been demonstrated that CGRP-R couples to $G\alpha_s$-type G proteins to stimulate the activity of the cell-surface enzyme adenylate cyclase, which, in turn, converts adenosine triphosphate (ATP) to cyclic adenosine monophosphate (cAMP) [26]. On the other hand, $G\alpha_i$ proteins inhibit the activity of the catalytic domain adenylate cyclase, reducing the levels of cAMP. Finally, another GPCR-mediated effect is the mobilisation of intracellular calcium from the endoplasmic reticulum, due to activation of $G\alpha_{q/11}$-coupled proteins [24,27].

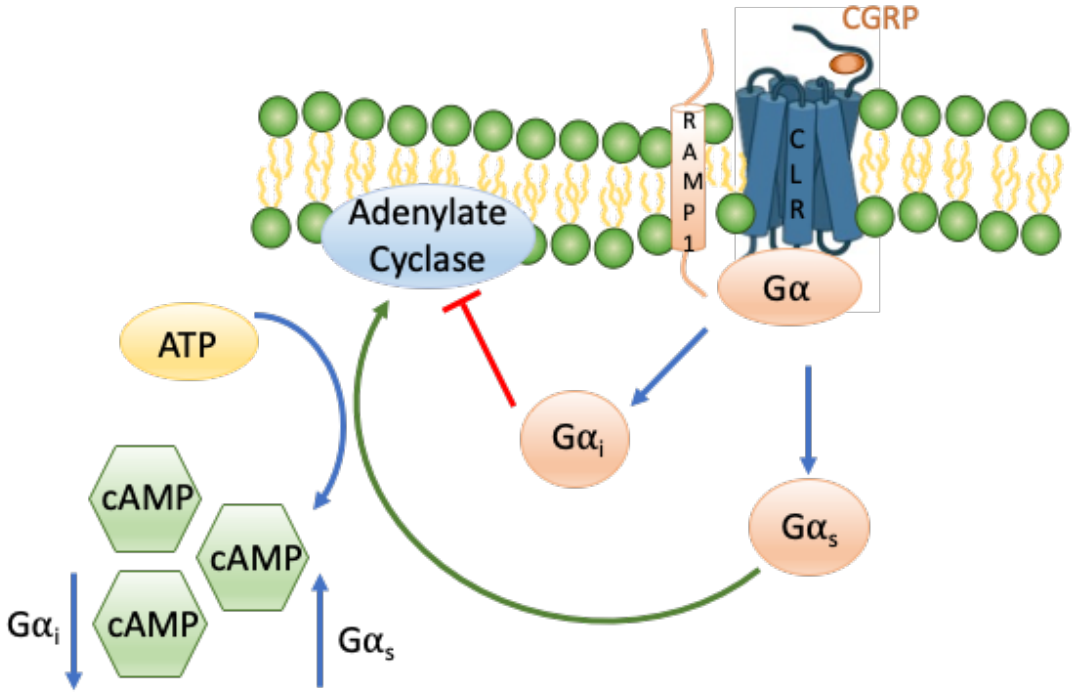

Figure 1.4. CGRP binding to CGRP receptor complex and cascade of Gα pathways activation.

In general, CGRP is considered a potent vasodilator and a mediator of pain transmission. Its involvement in migraine pathophysiology is supported by three different groups of studies: i) blood levels of CGRP in the external jugular vein, which drains extracranial tissue, are elevated during spontaneous migraine attacks [28,29]; ii) migraine patients present elevated CGRP levels in plasma, saliva [30–32], cerebrospinal fluid (CSF) [33], and tear fluids [34]; iii) intravenous administration of

αCGRP to migraineurs caused headache and moderate to severe migraine-like attacks [35].

1.1.4.2 Pituitary adenylate cyclase-activating polypeptide-38 (PACAP-38)

The neuropeptide PACAP-38 (Figure 1.5) is a C-terminally amidated 38-amino acid peptide found in sensory trigeminal neurons [36]. Similar to CGRP, PACAP-38 is now considered a mediator of migraine [37,38]. This evidence is supported by two groups of studies: i) intravenous diffusion of PACAP-38 has been shown to trigger migraine-like symptoms in susceptible individuals and anti-migraine drugs are effective in the treatment of PACAP-38-induced symptoms [39,40], ii) elevated concentrations of PACAP have been reported in patients during migraine attacks [41]. PACAP-27, the N-terminal 1-27 segment generated from cleavage amidation of PACAP-38, is responsible for the physiological activity of the peptide [42].

PACAP-27 fragment responsible
for physiological activity

PACAP-38 HSDGIFTDSYSRYRKQMAVKKYLAAVLGKRYKQRVKNK-NH_2

Figure 1.5. Amino acid sequence of the peptide PACAP-38 and resulting truncated peptide PACAP-27 (in green) [42].

These findings for CGRP and PACAP-38 opened the possibility of targeting CGRP and PACAP receptors (CGRP-R and PAC_1, respectively) as novel ways to treat migraine. While agents acting on PAC_1 are still in the development phase and have not yet reached regulatory approval, various medicines targeting both CGRP and its receptor have been approved for preventive and acute migraine therapy [43–49].

1.2 Management of migraine

1.2.1 Pharmacological treatments for migraine

After decades of little change, significant improvements in the understanding of migraine pathophysiology have occurred over the last 20 years, resulting in

innovative approaches to migraine treatment [50]. In 2018, various new preventive and acute migraine agents were launched, and the migraine market is expected to dramatically increase over the next 5 years, potentially tripling in size and reaching over $11 billion per year [51].

The burden of migraine is best treated through two parallel pharmacological approaches: i) prompt and effective abortive treatments to combat the disabling symptoms of the attack; ii) chronic use of effective preventive medications [52].

1.2.1.1 Acute therapy

Significant expansion of current medicines for treatment of migraine has translated to a need for regular updates to treatment guidelines. Categories of medicines currently approved for acute treatment of migraine include triptans, ergotamines, nonsteroidal anti-inflammatory drugs (NSAIDs), ditans, gepants, analgesics, and combination therapies [50]. First- and second-line approaches for acute treatment of migraine and their mechanism of action are summarised in Table 1.1, while key chemical structures of drugs approved for acute treatment of migraine are shown in Figure 1.6.

Table 1.1. Current pharmacological approaches for acute treatment of migraine. Drug classes used as first-line treatments are highlighted in bold.

Drug class	Examples	Mechanism of action
Antipyretics	Acetaminophen (paracetamol)	The mechanism of action of acetaminophen is still not fully understood, but its positive effects on migraine symptoms are probably attributable to the central inhibition of prostaglandin synthesis [53].
Triptans	Sumatriptan (**1**), Almotriptan (**2**), Eletriptan, Frovantriptan, Naratriptan, Zolmitriptan (**3**)	Triptans are potent agonist of 5-$HT_{1B/1D}$ receptor subtypes. They induce vasoconstriction through binding to 5-HT_{1B}. Sumatriptan was discovered to also inhibit neurogenic inflammation and the release of proinflammatory substances [50,52]. However, their use is hampered by contraindications in patients with cerebrovascular and cardiovascular disorders [50]. Moreover, sumatriptan does not provide full pain relief in more than 50% of patients [52].
Ergotamines	Dihydroergotamine mesylate (DHE, **4**)	DHE is an ergot alkaloid which putative activity is due to affinity for norepinephrine, epinephrine, dopamine, and serotonin receptors; however, the precise mechanism of action is not fully understood [54].
NSAIDs	Aspirin, Diclofenac K^+, Ibuprofen, Naproxen Na^+	NSAIDs inhibit the synthesis of prostanoids from arachidonic acid. They modify the activity of cyclooxygenase 1 and 2 (COX-1 and COX-2), responsible for catalysis of prostanoids and for inflammation, respectively [53].
Combined therapies	Acetaminophen/ Aspirin/Caffeine Sumatriptan/Naproxen	Combination therapies, obviously, combine the mechanisms of action of the drugs involved.

Drug class	Examples	Mechanism of action
Antiemetics	Chlorpromazine, Metoclopramide, Prochlorperazine, Promethazine	The effect of antiemetic agents may result from their dopamine antagonist properties, linked to the hypersensitivity to dopamine reported during a migraine attack. Antiemetics are also used as additional treatment for the nausea experienced during migraine attacks [53].
Gepants	Ubrogepant (**5**), Rimegepant (**6**), Atogepant (**7**)	Small molecule antagonists of the CGRP-R, known to be involved in migraine pathogenesis [49].
CGRP-targeted mAbs	Erenumab, Fremanezumab, Galcanezumab, Eptinezumab	Monoclonal antibodies targeting CGRP (Fremanezumab, Galcanezumab, Eptinezumab) or its receptor (Erenumab) [46,51].
Ditans	Lasmitidan	Selective 5-HT_{1F} receptor agonist, with no appreciable affinity for 5-HT_{1B}, thus avoiding vasoconstrictive effects of triptans [50,55].

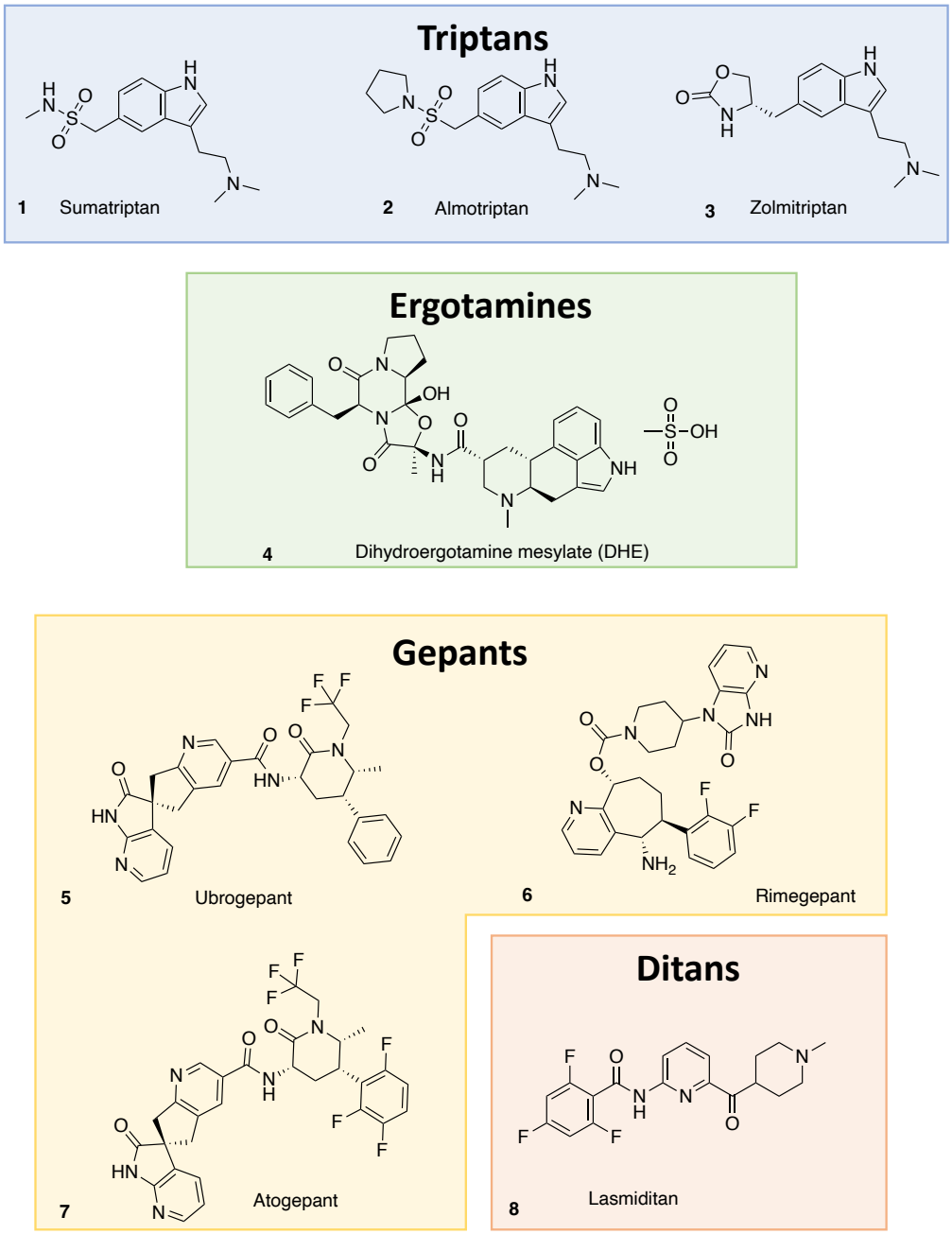

Figure 1.6. Chemical structures of drugs developed for acute treatment of migraine.

1.2.1.2 Preventive therapy

According to recommendations, preventive therapy should be offered to patients experiencing more than 6 headache days per month, should be considered in patients with 4 or 5 headache days a month, and for other special circumstances. The choice of medicine is based on patient preferences, side effects, efficacy, comorbidities, and drug-drug interactions [56].

Medicines for migraine prophylaxis comprise β-blockers, angiotensin modulators (i.e., angiotensin converting enzyme (ACE) inhibitors and angiotensin II (AT) blockers), antidepressants drugs (ADD), antiepileptic drugs (AED), calcium channel blockers (CCB), neurotoxins, serotonin (5-HT_2) modulators, spreading depression inhibitors (SDI), and CGRP-targeted drugs [52,57]. Among them, first-line treatments include AED (i.e., divalproex or topiramate) and β-blockers (i.e., propranolol, metoprolol, or timolol). If none of the first-line agents is effective and tolerable, the physician can consider alternative medicines, such as amitriptyline, venlafaxine, atenolol, or nadolol [57,58]. Finally, in the case in which at least 5 of the abovementioned substances are not effective, not tolerated, or if there are contraindications or warnings against their use, monoclonal antibodies (mAbs) against CGRP or its receptor can be considered for migraine prophylaxis [48]. Table 1.2 summarises the most commonly prescribed medicines used as preventive pharmacological treatments and their putative mechanism of action.

Table 1.2. Current migraine preventive pharmacological approaches. First-line treatments are highlighted in bold.

Drug class	Examples	Mechanism of action
β-blockers	**Propranolol**, **Metoprolol**, **Timolol**, Atenolol, Nadolol	β-blockers exert their effect mainly at the central nervous system level by tuning neuronal excitability. Blockade of β-1 receptors reduces the effects of adrenaline and noradrenaline, thus inhibiting the stimulating effect of the sympathetic nervous system [59].
Antiepileptic drugs (AED)	**Divalproex**, **Topiramate**	The mechanism of action of AED is still not fully understood. Their known action as Na^+ channel blockers may have an effect on the neural component of migraine pain [60]. The effect of topiramate on migraine is likely due to suppression of neuronal excitation [52].
Calcium channel blockers (CCB)	Verapamil, Flunarizine	CCB maintain a cerebral vasodilatory tone, thus preventing vasoconstriction, which may initiate the headache process [52].
CGRP-targeted mAbs	Erenumab, Fremanezumab, Galcanezumab, Eptinezumab	These mAbs specifically target CGRP (Fremanezumab, Galcanezumab, Eptinezumab) or its receptor (Erenumab) [46,51].

1.2.1.3 Contraindications and side effects of traditional treatments for migraine

There are numerous contraindications associated with traditional treatments for migraine. In particular, NSAIDs are contraindicated in patients with peptic ulcer disease, renal dysfunction, inflammatory bowel disease, gastric bypass surgery, aspirin allergy, and in patients on anticoagulant treatments [53,61]. Ergotamines are contraindicated in women who are pregnant or may become pregnant as this can harm the development of the foetus [53]. Moreover, ergotamines and triptan medicines are vasoconstrictors, thus they are contraindicated in patients with cardiovascular diseases (e.g., coronary artery disease, peripheral vascular disease, and stroke) [53,61]. β-blockers contraindications include asthma, hypoglycaemia associated with diabetes treatment, heart block, bradycardia, chronic obstructive

pulmonary disease (COPD), and hypotension [58,62]. Finally, anticonvulsant drugs are contraindicated in patients with liver disease or in pregnant women (topiramate in pregnancy only) [58].

Aside from contraindications, numerous potential adverse events are related to traditional medications for migraine. NSAIDs are associated with cardiovascular problems, nephrotoxicity and gastrointestinal side effects [50,53,55]. Combined therapies containing caffeine can cause sleep-related disturbances and caffeine withdrawal headaches, while some antiemetics may cause extrapyramidal side effects [53].

Triptans and ergotamines are associated with vasoconstrictive side effects which are more marked when administered subcutaneously [53,55]. The most common triptan adverse events are known as 'triptan sensations' and comprise paraesthesia, flushing, tingling, neck pain and mild transient chest pressure [55], while other side effects associated with triptans include nausea, dry mouth, dizziness, drowsiness, and somnolence [50]. Finally, DHE is associated with nausea and vomiting side effects when parenterally administered [53].

To conclude, despite the broad arsenal of traditional pharmacological therapies, several have unsatisfactory efficacy and may be poorly tolerated, resulting in a strong need for novel preventive and acute treatments [63].

1.2.1.4 Current and future CGRP-targeted drugs

To overcome the abovementioned limitations, recent years have seen the approval of novel acute and prophylactic treatments for migraine targeting different neuronal mechanisms. A new era was opened by the launch of two novel classes of migraine medicines (i.e., small molecules and mAbs) targeting CGRP or its receptor. Given the predicted growth of the migraine market in the next five years (over $11 billion/year), CGRP-targeted drugs should play a central role, reaching more than $6.5 billion of sales in 2027 [51]. Moreover, the CGRP pathway is of great interest not only for the treatment of migraine, but also for cluster headaches, post-traumatic headaches, fibromyalgia, and other pain conditions [64].

Small molecule CGRP-R antagonists, the so-called 'gepants', demonstrated an exceptionally high affinity for the CGRP-R, thus blocking the interaction between CGRP and its receptor. Except for atogepant, approved in September 2021 for migraine prevention, all the other gepants have been developed for acute migraine therapy [49]. Interestingly, gepants efficacy was not hampered by any cardiovascular and haemodynamic symptoms associated with their use. Hence, the efficacy of the gepants family, combined with their tolerability profile, make them a feasible therapeutic option for triptan non-responders, for patients with cardiovascular risks, and for those experiencing triptan-induced medication overuse headache [49].

CGRP-targeted therapy for migraine also includes fully humanised or human mAbs – i.e., erenumab, fremanezumab, galcanezumab, and eptinezumab. Their prolonged half-lives allow monthly administration. The most important difference between these agents is their mechanism of action: while erenumab binds to the CGRP-R, the other mAbs bind to different sites of the CGRP ligand [65].

Finally, increasing evidence suggests that the CGRP-R could be antagonised with truncated versions of natural CGRP [22,23,66–68]. Peptides derived from truncations of the N-terminal portion of CGRP are potential agents that could fill the gap between small molecules and large biologics, possibly combining the advantages of the two classes (Figure 1.7). These potential novel medicines may fulfil the current unmet medical need for migraine therapy and may be effective in patients suffering from refractory migraine who fail to tolerate and/or respond to the established treatments [63].

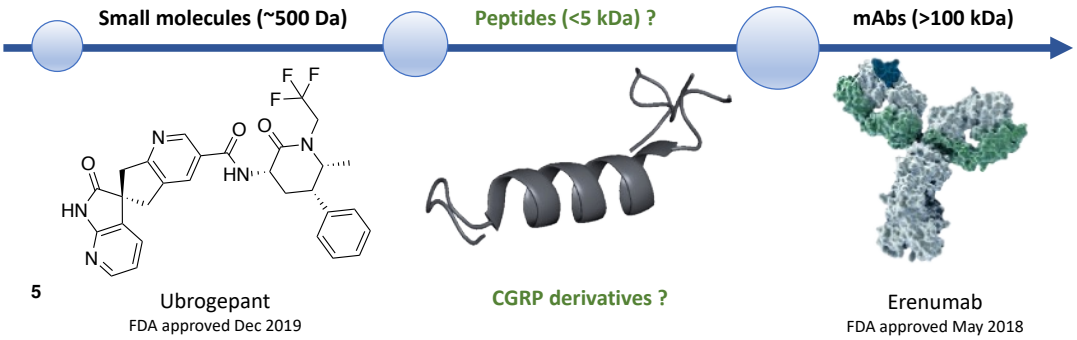

Figure 1.7. Ways of targeting the CGRP-R: small molecules, peptides, and monoclonal antibodies.

1.2.2 Routes of administration of antimigraine drugs

The majority of small molecule antimigraine medicines (e.g., acetaminophen, NSAIDs, triptans, and gepants) are administered orally [49,53]. However, some triptans are also available as nasal sprays (e.g., sumatriptan and zolmitriptan), suppositories or subcutaneous injections (e.g., sumatriptan), while DHE is available as a subcutaneous injection and nasal spray solution [53,61]. mAbs have to be administered either subcutaneously or intravenously, thus usually resulting in low patient acceptability and compliance, with dosing intervals depending on the half-life – i.e., 3 months for Fremanezumab and Eptinezumab, and 4 weeks for the others [48].

Due to first pass metabolism and poor oral absorption of peptides, similar problems may be encountered when administering peptides through the parenteral route. Hence, similarly to triptans and DHE, the intranasal route of administration could be explored to deliver future antimigraine peptide agents. This offers several advantages over the parenteral route, such as high absorption through the nasal mucosa with rapid direct delivery to the central nervous system, greater patient acceptability due to non-invasive mode of delivery, lower adverse event profile due to an inferior systemic effect [69].

1.3 Conclusions

Migraine is a largely widespread disabling neurological disorder with a significant personal, social, and economic burden for the sufferers and for their families. Despite the broad array of traditional medicines available, there is still a vast unmet medical need for novel treatments, including better tolerated and more effective abortive treatments alternative to triptans, as well as safer and patient-friendly preventive treatments [63]. In recent years, great advances have been achieved in terms of approvals of new classes of medicines for preventive and acute treatments. However, more could be done to increase patient compliance, tolerability, and efficacy.

Novel horizons could be opened by the development of novel peptidic modalities which provide advantages over small molecules – i.e., higher selectivity, specificity and potency, lower risk of systemic toxicity and accumulation in tissues – and proteins – i.e., deeper penetration into target tissue, lower immunogenicity, greater physicochemical stability, easier synthesis and lower production costs [70–73]. Although the use of peptides in medicine can be challenging, various synthetic and formulation strategies can be implemented to overcome these issues.

Finally, alternative administration routes, such as nasal delivery, already exploited for triptans and DHE administration, could support the delivery of peptides directly to the brain, in order to avoid first pass metabolism associated with oral administration as well as low patient compliance associated with subcutaneous and intravenous injections.

1.4 Thesis hypothesis

The aim of this thesis is to explore novel peptide antagonists of the CGRP-R and focus on innovative strategies i) to enhance efficacy *via* improvement of pharmacokinetic profiles and ii) to deliver them directly to the brain *via* a mucoadhesive dry powder platform.

The aim will be achieved by the following objectives to:

i) design and synthesise a library of P006 analogues comprising fluorinated peptides, peptide-peptoid hybrids, and N-terminally modified peptides and to test their activity against the CGRP-R;

ii) assess the pharmacokinetic profile of P006 and analogues *via* human blood stability testing and plasma protein binding testing;

iii) prepare a formulation comprising nano- and micro-structures suitable for nose-to-brain delivery.

2 Approved peptides database (PepTherDia) and structural analysis

2.1 Introduction

2.1.1 The current state of peptide therapeutics and diagnostics

Since the approval of insulin in 1923, peptides have established themselves as a major class of therapeutics and diagnostics [74,75]. As shown in Figure 2.1, the number of approved peptides has gradually increased over time, reaching the landmark of over 100 approved peptide drugs in 2020 across the main pharmaceutical markets (i.e., Europe, US, and Japan) [76–78].

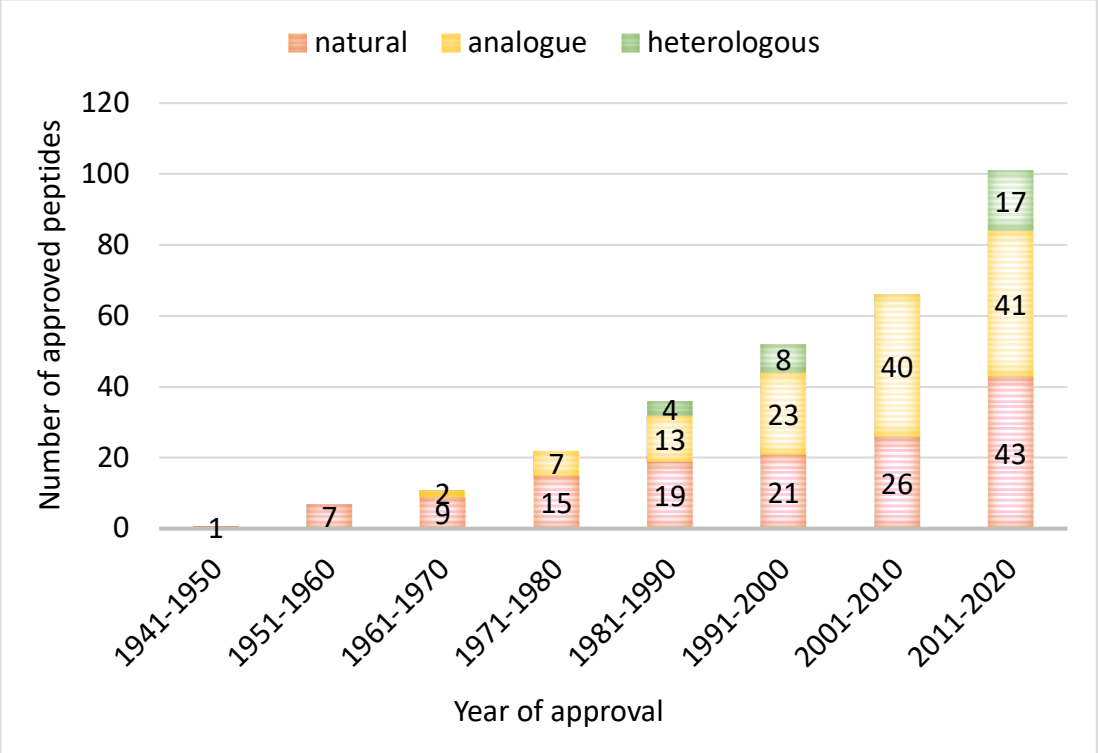

Figure 2.1. Cumulative peptide approvals by year, from 1941 to 2020. Peptides are divided into natural, analogue, and heterologous. Withdrawn peptides are not included. Graph derived from the analysis described in this chapter.

The main disease areas currently treated with peptide drugs are metabolic disorders, cancer, and cardiovascular diseases. However, other emerging therapeutic applications are in the areas of infectious disease, neurological disorders, pain, urinary tract, gastrointestinal and respiratory disorders [74,79,80]. With the growing incidence of metabolic disorders, cancer and cardiovascular diseases in the Western world, and the need for new effective therapies to treat emerging health problems, there may be an acceleration in the approval rate of peptide-based drugs in the coming years [81–83].

Of particular current interest is the impact of COVID-19 on the peptide therapeutics market as novel peptides are being developed and/or repurposed for the treatment of the disease caused by SARS-CoV-2. As of May 2020, there were 21 peptide drugs in development for the treatment of COVID-19 [84]. Not by chance, the first approved treatment for COVID-19 disease Pfizer's Paxlovid – nirmatrelvir (**9**) tablets and ritonavir (**10**) tablets, co-packaged for oral use – contains peptidomimetic molecules [85,86].

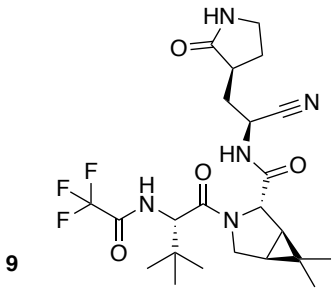

9

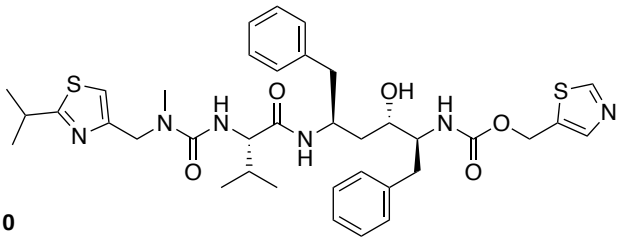

10

*Figure 2.2. Chemical structures of nirmatrelvir (**9**) and ritonavir (**10**), molecules contained in Paxlovid, the first medicine approved for the treatment of COVID-19.*

In general, the pharmaceutical industry is committed to exploring the role of peptide therapeutics in providing new opportunities for the modulation of difficult targets and addressing unmet medical needs. This is largely demonstrated by our analysis, showing that, as of January 2022, there are 111 peptide pharmaceutical products that have been granted regulatory approval in the major global markets – North

America, Europe and Japan – of which 95 are peptide drugs, 15 are diagnostic agents, and 1 is a theragnostic agent. Moreover, a great number of clinical studies involve peptide agents – 4,859 in total, 468 of which are in phase 3 [87].

In 2020, the peptide therapeutic market was valued at roughly $28.51 billion [84]. According to the "Global Peptide Therapeutics Market (by Type, Synthesis Technology, Manufacturing Type, Application & Region)", the global peptide-based therapeutics market is expected to increase over time with a Compound Annual Growth Rate (CAGR) of approximately 7%, from 2021 to 2025, reaching a value of $42.22 billion in 2025 [88], while according to the report compiled by Mordor Intelligence, the market is expected to yield a revenue of $51.36 billion in 2026, with a CAGR of 9.66% over the 5-years period 2021-2026 [84].

2.1.2 Advantages and drawbacks of peptide medicines

Table 2.1 illustrates the main advantages of peptides over small molecules and proteins and highlights how this class of compounds may complement or provide an alternative to small molecules and large biologics.

Table 2.1. Main advantages of peptides over small molecules and proteins [70–73]*. *Catabolism yields simple amino acids, recycled in the body through physiological metabolism.*

Advantages over small molecules	**Advantages over proteins**
- Higher selectivity and specificity - Higher potency - Lower risk of systemic toxicity* - Lower risk of accumulation in tissues	- Lower molecular weight - Easier synthetic procedures - Lower production costs - Deeper penetration into the target tissue - Lower immunogenicity - Greater physicochemical stability

Despite these important benefits, enthusiasm for the use of peptides as therapeutic agents has been tempered by significant limitations of natural peptides, exhibiting

many obstacles and consequent delays in the drug development process from laboratory to approval. Among these limitations is their typical susceptibility to proteolytic degradation, mainly due to the presence of numerous amide bonds, and rapid renal clearance, resulting in a generally short circulating half-life of natural peptides [71,74].

Peptide medicines are also challenged by chemical and physical instability. Chemical instability of peptides is caused by modification and/or alteration of amino acid residues; the most frequently encountered reactions are oxidation, reduction, deamidation, hydrolysis, arginine conversion, β-elimination and racemisation [89]. Physical instability involves changes in the secondary, tertiary and quaternary structures of these compounds due to various factors (e.g., temperature, pH, denaturing reagents) [89]. Additional limitations include poor membrane permeability, low aqueous solubility, and poor oral bioavailability due to intestinal pre-systemic degradation, which makes oral delivery of peptides a challenging task [90]. All these issues may hamper the development of peptide therapeutics and must be addressed to bring more peptides into clinical use. Nonetheless, in recent years, advances in drug delivery and emerging medicinal chemistry strategies have brought peptides to a significant renaissance, by overcoming their drawbacks and finally improving pharmacokinetic profiles and oral bioavailability [71,74].

2.1.3 Definition of 'peptide'

The International Union of Pure and Applied Chemistry (IUPAC) defines peptides as "amides derived from two or more amino carboxylic acid molecules (the same or different) by formation of a covalent bond from the carbonyl carbon of one to the nitrogen atom of another with formal loss of water" [91]. While the recommendations of the IUPAC-IUB Joint Commission on Biochemical Nomenclature (JCBN) defines a peptide as a chemical entity presenting between 2 and 50 amino acid residues [92], the currently used regulatory U.S. Food and Drug Administration (FDA) definition delineates a peptide as "any polymer composed of 40 or fewer amino acids" and regardless their production method [76,93]. Finally, the European

Medicines Agency (EMA), instead of describing peptides based on their size, considers them as small molecules if chemically synthesised, while treats them as biological entities (likewise proteins) if they are extracted from natural sources or produced with recombinant methodologies [94], which underlines that the definition of peptide is still ambiguous.

In conclusion, the above definitions demonstrate that the scientific community has different opinions on the definition of peptide, and, in particular, on where to stop using the term 'peptide' and start using the term 'protein'.

2.1.4 Peptide repositories and databases

In the last decade, with the growing interest in peptide-based therapeutic drugs, several research groups have tried to gain a better understanding of the properties of peptide medicines granted with marketing authorisation. In 2010, Vlieghe and collaborators compiled a list of synthetic therapeutic peptides that were approved in one (or more) of the main pharmaceutical markets (US, EU, and Japan) [70]. A few years later, Raghava *et al.* curated a repository named 'PEPlife' containing data on peptide half-lives [95], followed, one year later, by a database containing more than 800 FDA-approved biological molecules, among which 28 were peptides [96]. Recently, an extensive review on approved peptide therapeutics targeting GPCRs was published by Davenport and collaborators [97], demonstrating their leading presence in the market.

Yet, to the best of our knowledge, up to November 2020, a complete database containing information on pharmacokinetic properties (i.e., terminal half-life and protein binding), marketing authorisation, production methods, therapeutic indications, routes of administration, and structural features of regulatory-approved peptides was not freely available online. Moreover, there was an absence of guidelines for designing new peptides. Tyagi *et al*. highlighted that the use of "drug-likeness" criteria studied for small molecules – mainly, *Lipinski's Rule of Five,* Ro5 [98], and that models, such as the central nervous system multiparameter

optimization (CNS MPO) [99] – are not appropriate for peptides due to their entirely different intrinsic properties and applications [100].

Hence, the creation of a complete database containing information on peptides approved as therapeutic or diagnostic agents was undertaken, including the analysis of shared features that may lead to establish a set of guidelines on how to design a peptide candidate with favourable properties.

2.1.5 Software applications for prediction of drug properties

The use of *in silico* methods to predict key properties of drug candidates can reduce the attrition rate in drug design and development programmes by 'weeding out' compounds with unfavourable physicochemical and pharmacokinetic properties prior to synthesis and testing. Thus, reducing the number of compounds synthesised overall and ultimately reducing costs and time associated with it [99,101,102].

There are a great number of software applications and online resources available to predict the properties of small molecules with a surprisingly high degree of accuracy; nonetheless, their applicability to larger molecules (e.g., peptides) needs to be assessed. Under the supervision of Dr C. Coxon, MSc students from Heriot-Watt University compared different property prediction applications for their ability to estimate key physicochemical properties, such as lipophilicity and isoelectric point values of currently approved peptide medicines. This work showed discrepancies between predicted values and experimental values, in particular for medium-to-large size peptides (Liebnitz *et al.* unpublished). Hence, the reliability of predictions tools used for peptides should be carefully assessed.

2.1.5.1 Lipophilicity predictions

In the drug design and development process, lipophilicity is an important property that affects the absorption, distribution, metabolism and excretion (ADME) behaviour of a compound, and, at the same time, influences the solubility, toxicity and bio-activity [102,103]. Measuring and, if needed, tuning the physicochemical

properties is essential to enhance the drug-likeness of a compound. In peptide drug discovery and development, the importance of lipophilicity and its effect on pharmacokinetic behaviour is better exemplified by the FDA-approved integrin mimetic secretagogue peptide exenatide and its derivatives liraglutide and semaglutide. Careful tuning of exenatide's lipophilicity by addition of fatty acid appendages increased binding to human serum albumin (HSA) and protected against metabolism and/or excretion *via* renal clearance, ultimately increasing the plasma half-life from 2.4 h – in the case of exenatide – to 13 h and 168 h – in the case of liraglutide and semaglutide, respectively [104].

Most commonly, lipophilicity is quantified by LogP, the partition coefficient of a molecule between an aqueous medium (i.e., water) and a lipophilic phase (i.e., 1-octanol). However, the majority of drugs and potential drugs contain ionisable groups that are not taken into consideration in the LogP measurement. LogD is a better lipophilicity descriptor for most molecules because it is measured at a specific pH, accounting for the presence of different ionised microspecies that can form at different pH values. Of particular interest is the LogD at pH 7.4 (pH of blood serum). Thus, ideally, for the investigation of lipophilicity of peptides containing multiple ionisable groups, LogD would be the most appropriate value.

Various *in silico* approaches to calculate LogP have been extensively reviewed by Mannhold and collaborators [105]. In general, LogP prediction approaches can be divided into two major groups: substructure-based and property-based methods. In the first case, the molecules are cut down into fragments or single atoms and the final LogP is derived from the summation of known substructure contributions. cLogP and cLogD, ACD/LogP, and MiLogP used in this study fall into this category. In details, LogP and LogD calculation method of ChemAxon (Chemicalize) uses a (modified) algorithm developed by Viswanadhan *et al.*, in which the LogP value of a molecule is obtained by the summation of the increments of its atoms [106,107]. Moreover, Molinspiration Cheminformatics 2020 software takes into consideration intramolecular hydrogen-bonding contribution and charge interactions for its LogP

[108]. On the other hand, ChemDraw uses an algorithm licenced by BioByte for ClogP calculation [109]. This is based on a programmable method of dividing the structure of a solute into chemically meaningful fragments. Then, each fragment is searched in a table of measured fragment values. If the desired fragment is not found, the programme calculates the value by examining all atoms and their neighbours. Finally, the program sums fragment values and evaluates important interaction corrections when fragments are in proximity to one another [110]. Finally, ACD/LogP algorithm used by ACD/i-Labs is based on contribution of single atoms, structural fragments, and intramolecular interactions between different fragments; all this information is stored in internal databases [105].

2.1.6 Aim and Objectives

The aim of this chapter was to study approved peptide therapeutics and diagnostics and collect information on their physicochemical, conformational, pharmacodynamic, and pharmacokinetic properties, as well as on their routes of administration, production methods and marketing authorisation. Moreover, each peptide was analysed by type and properties of each component (amino acids or other structures), as well as global properties, such as molar mass and the nature of any macrocycle (if present), with the final goal of giving some insights into what a successful peptide agent looks likes.

2.2 Methods

2.2.1 Definitions

In this work, a peptide was considered to be a chemical entity composed of at least 2 amino acids, linked together by an amide bond, with a maximum of 50 amino acids and a molar mass lower than 5000 g/mol.

For the purpose of analysing peptide structures, three different types of building blocks were identified – natural amino acids, non-natural amino acids and modifications – referred altogether as constitutional members. An amino acid (AA) was considered to be a residue that presents both a carboxylic acid and an amine

functional group, capable of forming an amide bond. The 20 encoded proteinogenic AAs, presenting the amino group and the distinctive side chain appended to the α-carbon with an overall L-configuration, were defined as natural amino acids. In contrast, amino acidic residues with D-configuration, with non-native side chains, or bearing the amino group in a non-α-position (e.g., β-amino acids), as well as peptoid monomers (e.g., sarcosine) were defined as non-natural amino acids. Finally, non-amino acidic building blocks, named modifications, included lipids, sugars or other chemical entities that do not fall under any of the above definitions.

2.2.2 Data collection and peptide database construction

Compounds included in the database were selected according to the definitions provided in section 2.2.1 and to the key inclusion and exclusion criteria listed in Table 2.2.

The list of peptides was obtained by searching in DrugBank [111], FDA and EMA web pages [76,77], Pharmaceutical and Medical Devices Agency (PMDA) website [78], and Drug Central website [112].

*Table 2.2. Key inclusion and exclusion criteria used to compile PepTherDia database. *With the exception of tesamorelin which has a molar mass of 5005 g/mol.*

Structural criteria	Other criteria
- Lower length limit: two amino acids linked together by an amide bond. - Upper length limit: less than 50 amino acids and molar mass less than 5000 g/mol.* - Peptides conjugated to other molecules were included, as long as they met the other inclusion criteria (especially molar mass).	- Only non-insulin peptides were included. - Only peptides for human use were included. - Theragnostic and diagnostic peptides were included. - Peptides were included if approved in at least one of the main pharmaceutical market areas (North America, Western Europe, and Japan) or in one of the key countries in each region (United States, Germany, France, UK, Italy, Spain, Greece, the Netherlands, and Japan). - In the case of a mixture of components (e.g., Gramicidin D, > 80%), the main component was considered as the only one present for ease of calculation and classification.

Examples of approved peptides not included in the database and the reason for their exclusion are shown in Table 2.3.

*Table 2.3. Examples of excluded compounds and reason for exclusion. *Peptides withdrawn have not been included, with the exception of sinapultide, for which production has been deliberately ceased by the company in favour of the study of an improved formulation.*

Compound not included	Reason for exclusion
- Peginesatide	- 42 AAs + PEG: molar mass > 5000 g/mol
- Ritonavir and Lopinavir	- No amide bond between 2 amino acids
- Saralasin	- Peptide withdrawn *
- Bulevirtide	- Molar mass > 5000 g/mol
- Glatiramer acetate	- Mixture of random-sized peptides composed of four amino acids; no defined structure

With the aim of providing each peptide with a complete profile comprising relevant information regarding terminal half-life, protein binding, therapeutic indications, routes of administration, marketing authorisation, and production methodologies, specific searches were carried out in DrugBank [111], National Centre for Advancing Translational Sciences web page [113], Drugs.com [114], and pharmaceutical companies' websites, using the generic name of the individual peptide. References specific to each approved peptide and SMILES codes used for the calculations are reported on the website (http://peptherdia.herokuapp.com), on the specific peptide page.

2.2.3 Structural analysis methods

In agreement with the definitions given in section 2.2.1, peptides were divided into natural and non-natural amino acids by fragmenting the backbone in a manner consistent with amide bond retrosynthetic analysis. Non-amino acidic moieties, previously identified as modifications, were further detached from the amino acid they were linked to. Figure 2.3 shows an example of this theoretical process applied to the peptide daptomycin (**11**), along with the resulting building blocks.

Due to the structural complexity of glycopeptide antibiotics (i.e., dalbavancin, telavancin, oritavancin, and teicoplanin), there was no obvious way to rationally

divide and classify the building blocks as described above. Similarly, the complexity of multicyclic peptides, did not allow the identification of a defined single cycle and, therefore, the members of each cycle were not counted.

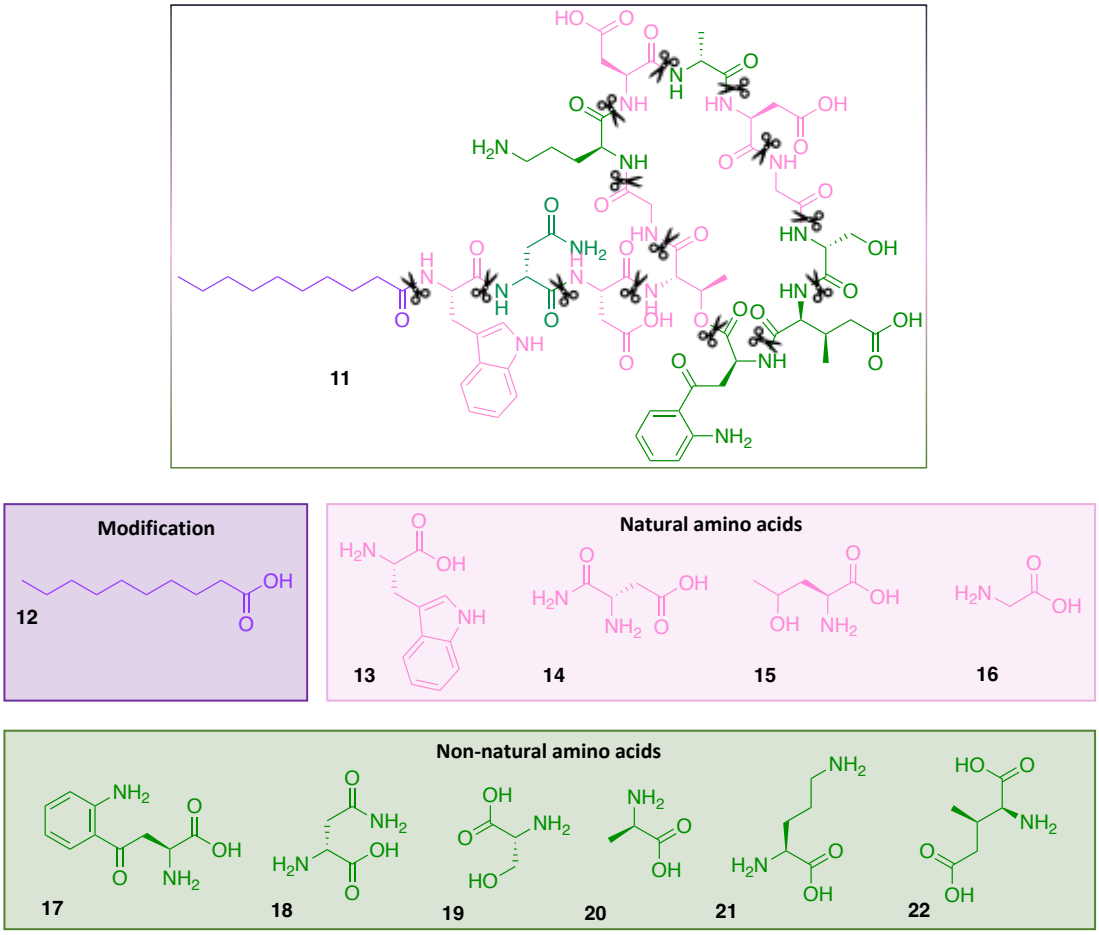

*Figure 2.3. Daptomycin (**11**) and its constitutional members obtained by fragmenting the backbone in a manner consistent with amide bond retrosynthetic analysis: decanoic acid (**12**), tryptophan (**13**), asparagine (**14**), threonine (**15**), glycine (**16**), kynurenine (**17**), D-asparagine (**18**), D-serine (**19**), D-alanine (**20**), ornithine (**21**), 3-methyl glutamic acid (**22**).*

Based on its structural and physicochemical characteristics, each constitutional member was further classified into five categories: polar, acidic, basic, nonpolar aliphatic, or aromatic.

For natural amino acidic residues, the designations polar, acidic, basic, nonpolar aliphatic, or aromatic were derived from literature precedent and ascribed by the

nature of the side chain [115]. Non-natural amino acids were classified following the same principles used for natural amino acids, as they form an amide backbone in the same way of natural amino acids. On the other hand, peptide modifications were classified by analysing both their structure and the way they were conjugated to the peptide. For example, in the case of daptomycin (**11**, Figure 2.3), decanoic acid (**12**) was classified as a nonpolar aliphatic modification because the carboxylic acid moiety is part of an amide and its contribution to the final polarity predominantly increases lipophilicity.

The complete list of non-natural amino acids and modifications, together with their polarity classification, can be found on the PepTherDia website, in the section named 'constitutional members' (http://peptherdia.herokuapp.com/members).

2.2.4 Calculations

ChemAxon's Chemicalize platform [116] and ACD/i-Labs [117] were used to calculate molar mass and lipophilicity (cLogP and CLogD at pH 7.4) of peptides, while ChemAxon's Chemicalize platform [116] was used to check the adherence to the Lipinski's rule of 5 for some peptides. The isomeric SMILES codes used for the calculations were derived from PubChem (computed by OEChem 2.1.5 – see PepTherDia website for the SMILES code used for each compound) [118].

2.2.5 Data Analysis

The data was collected in a manually curated repository in Microsoft Excel (version 16.58) and then was visualised with GraphPad Prism (version 9.3.1).

2.2.6 Website creation and development

The website PepTherDia was created and developed by Mr Daniele Tomasi. The admin functionality on the website allows the administrators to update it on a regular basis with new peptide approvals.

2.3 Results and Discussion

2.3.1 Development of PepTherDia and detailed structural analysis

A repository was built comprising 111 peptides, composed of 95 therapeutics, 15 diagnostics and 1 theragnostic. This repository was used to develop an online open-source database website 'PepTherDia' (Peptide Therapeutics and Diagnostics: accessible via http://peptherdia.herokuapp.com). The database included information on marketing authorisation (year and agency of first approval), therapeutic indications, routes of administration and production methodologies, as well as pharmacokinetic properties (i.e., terminal half-life and plasma protein binding) and structural features (i.e., molar mass, constitutional members, polarity, lipidation, glycosylation, cyclisation, N- and C-terminal features) of approved peptides. Its purpose was to assist medicinal chemists and scientists in the field of peptide drug discovery as the challenge of peptide rational design would be partially overcome by having a greater knowledge of the rules governing the sequence-to-function relationships, and a better understanding of the most successful patterns in the sequence of the drugs on the market [119]. To further assist the users on how to exploit the database, a tutorial was created, and is now available online (https://www.youtube.com/watch?v=c7xZeWqmCns).

2.3.2 Findings from structural analysis

In this structural study, important trends were identified to provide insights into the features and structural characteristics that are common in approved peptide agents. Previous attempts to describe the structure of peptide medicines on the market have been limited to specific indications (e.g., antimicrobial peptides), while, to the best of our knowledge, a comprehensive structural analysis has never been undertaken before [120].

2.3.2.1 Molar mass, constitutional members, and origin of peptide design

From this study, it emerged that nearly 70% of approved peptides are relatively 'small' peptides, composed of 2-16 constitutional members, with a second minor

cluster (27%) of larger size peptides with around 28-37 members (Figure 2.4A). Unsurprisingly, similar information was derived from the bimodal molar mass distribution, in which a bigger cluster was identified in the range 300-1750 g/mol (71%) and a minor cluster in the range 2770-4250 g/mol (22%), with an obvious lack of mid-length peptides (Figure 2.4B). This data suggests that even though in the last decades synthetic and manufacturing technologies have significantly improved, allowing the rapid synthesis of larger size peptides in high purities and quantities, this is not reflected in the approval of a great number of large peptides.

To understand if this bimodal distribution was due to the origin of these peptides, it was considered whether the design of peptides of certain sizes was intended to resemble the structure of specific biomolecules. As it is clear from Figure 2.4C, natural peptides (defined as drugs presenting an identical structure to the biomolecule of origin) account for 30% of the sample, while peptide analogues (described as drugs originating from the modifications of natural peptides) account for 54%. Peptides whose structure derives from a rational design or library screening and is not clearly related to any natural compound are defined as heterologous and account for 16% of the sample, clearly bringing to light the challenge in designing molecules *a priori*.

In light of the above findings, it can be speculated that for 84% of the peptides on the market there is a clear trend that design inspired by nature is a promoter of success and that the bimodal distribution is perhaps not accidental but may be attributed to the characteristics of the natural molecules that have inspired the design. Two examples of peptide design inspired by nature are the nonapeptide carbetocin, derived from oxytocin, and the 32-membered peptide pramlintide, derived from amylin. In both cases, even though being very different, their length is not fortuitous or designed *a priori*, but is due to the size of the natural molecule of origin.

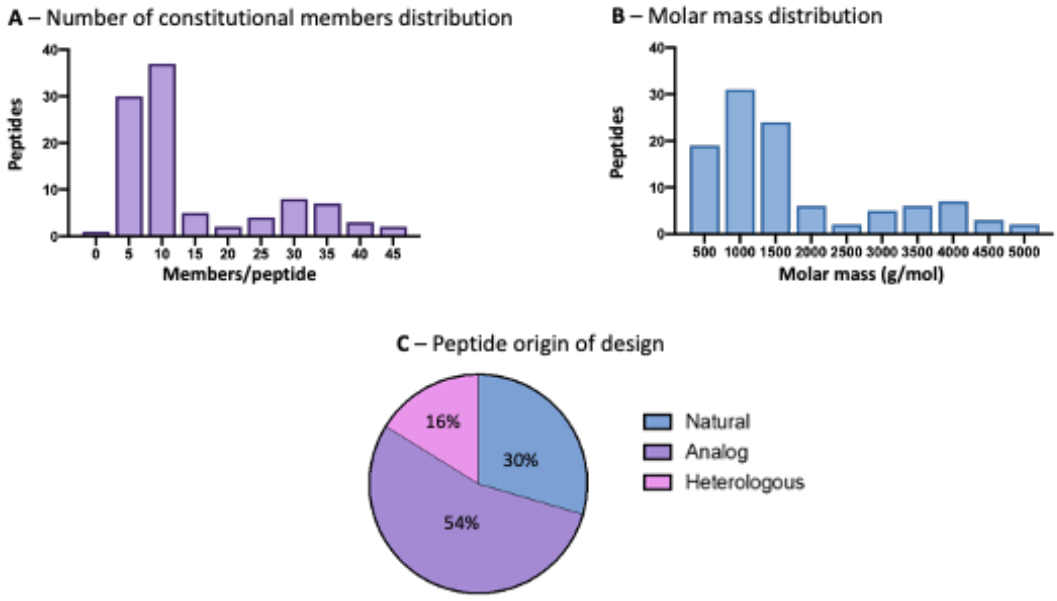

Figure 2.4. A. Number of constitutional members distribution; B. Molar mass (g/mol) distribution; C. Peptide origin of design, divided in natural, analogue, and heterologous.

2.3.2.2 Natural side-chain amino acids occurrence

By performing a retrosynthetic analysis, peptide structures were divided into their constitutional members, and classified as natural amino acids, non-natural amino acids, and modifications. This analysis showed that peptides on the market are mainly composed of natural L-amino acids (~81%). The remaining 19% is represented by non-natural amino acids and modifications. Moreover, by analysing the occurrence of each natural side-chain amino acid, the most common ones were identified as leucine (L), serine (S), and glycine (G), as shown in Figure 2.5. By contrast, the least commonly used amino acids are methionine (M), histidine (H) and isoleucine (I). These findings are largely mirrored in nature: the occurrence of natural amino acids in proteins are as follows: leucine (L) accounts for 9.1%, serine (S) for 6.8%, glycine (G) for 7.2%, and alanine (A) for 7.8%, being the most common amino acids. In contrast, methionine (M) and histidine (H) account each only for 2.3%, cysteine (C) for 1.9%, and tryptophan (W) for 1.4%, being the least common amino acid residues found in proteins [115]. The occurrence of cysteine (C) in approved peptides is higher than in proteins, which may be explained by the recurrent use of

disulfide bonds as a synthetic tool for macrocyclisation (see section 2.3.2.5). Amino acid occurrence is not usually mirrored in a single peptide (e.g., the high occurrence of leucine residues does not mean that majority of peptides contain leucine in their sequences). In fact, the amino acid composition of peptides and proteins is highly variable, meaning that some amino acid may not be present in one peptide and may be repeated several times in another peptide, increasing the overall occurrence of a specific amino acid. This is exemplified by sinapultide, designed to mimic the C-terminal domain of the surfactant protein B, which presents the repetition of the moiety KLLLL within its sequence, thus greatly increasing the overall occurrence of leucine [121].

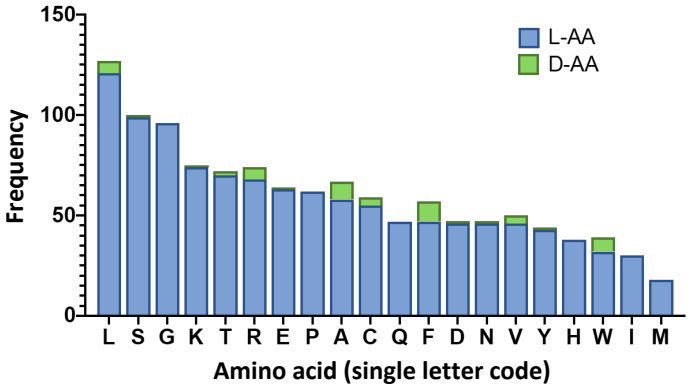

Figure 2.5. L-AAs (light blue) and D-AAs (green) occurrence in approved peptides.

D-amino acids with natural side chains, represented in green in Figure 2.5, account only for ~4% of the total number of amino acids with natural side chain. The most common ones are phenylalanine (F), alanine (A), and tryptophan (W). The selective replacement of L-amino acids by their enantiomers (D-AAs) is commonly studied in peptide design as it has been shown to protect the molecule from peptidase degradation [122]. However, proteolytic stabilisation of peptides through backbone modification causes conformational changes that may abort biological activity. An example in which proteolytic stabilisation has been achieved through replacement of L-amino acids with their mirror image forms is the somatostatin-like peptide

octreotide (**23**), in which L-Phe and L-Trp were replaced with their mirror-image forms, leading to a 100-fold increase in terminal half-life [123,124].

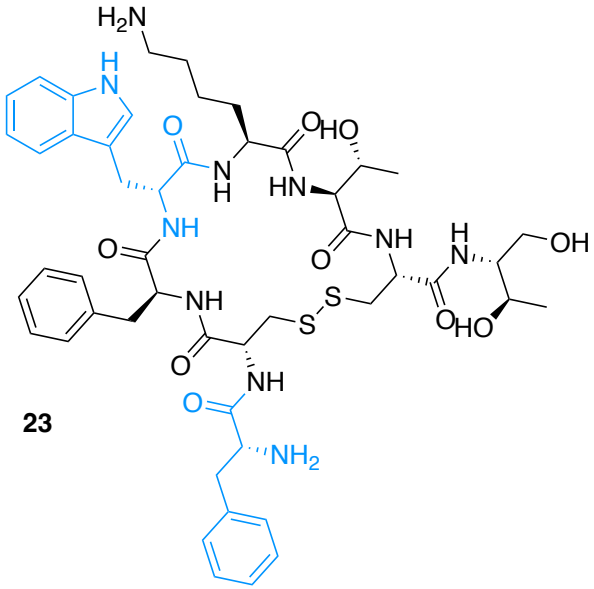

*Figure 2.6. Chemical structure of octreotide (**23**). D-amino acids are shown in light blue.*

2.3.2.3 Non-natural amino acid and non-amino acidic modifications occurrence

The exploitation of non-natural amino acids and conjugation with non-amino acidic modifications was shown to be a common strategy in drug discovery to overcome critical limitations typical of peptides [125,126]. Here, the occurrence of non-natural amino acids and modifications in approved peptides was examined, and the most frequently encountered are reported in Figure 2.7.

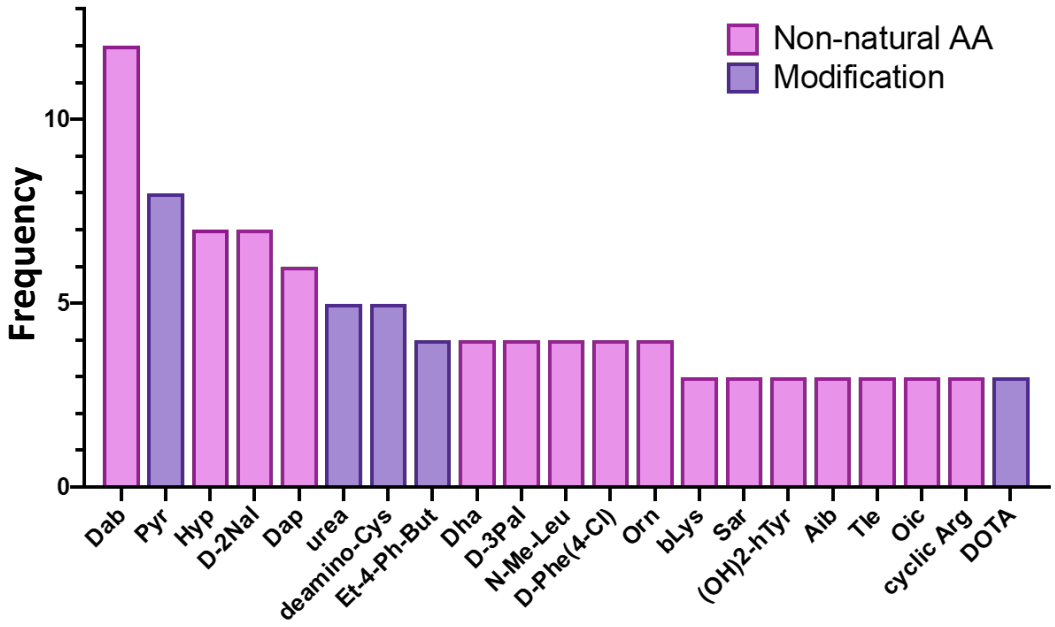

Figure 2.7. Most frequently encountered non-natural AAs, in pink, and modifications, in purple. Abbreviations: Dab = 2,4-diaminobutyric acid; Pyr = pyroglutamic acid; Hyp = 4-hydroxyproline; D-2Nal = 2-naphthyl-D-alanine; Dap = 2,3-diaminopropionic acid; deamino-Cys = deamino-cysteine; Et-4-Ph-But = ethyl-4-phenylbutanoate; Dha = dehydroalanine; D-3Pal = 3-(3-pyridyl)-D-alanine; N-Me-Leu = N-methyl-leucine; D-Phe(4-Cl) = 4-Cl-D-phenylalanine; Orn = ornithine; bLys = b-lysine; Sar = sarcosine (N-methylglycine); $(OH)_2$-hTyr = 3,4-dihydroxy-homotyrosine; Aib = 2-aminoisobutyric acid; Tic = 1,2,3,4-tetrahydroisoquinoline-3-carboxylic acid; Oic = octahydro-1H-indole-2-carboxylic acid; cyclic Arg = cyclic arginine; DOTA = tetraxetan.

Similar to the abovementioned incorporation of D-amino acids, position-specific incorporation of non-natural amino acids presenting various side chains can provide improvements in peptide physicochemical and biological properties [127]. In this study, the most common non-natural amino acids encountered were 2,4-diaminobutyric acid (Dab), 4-hydroxyproline (Hyp), D-2-naphthyl-alanine (D-2Nal), and 2,3-diaminopropionic acid (Dap); less common but still important were dehydroalanine (Dha), 3-(3-pyridyl)-D-alanine (D-3Pal), N-methyl-leucine (N-Me-Leu), 4-Cl-D-phenylalanine (D-Phe(4-Cl)), and ornithine (Orn). Not only heterologous peptides (e.g., ACE inhibitors, macimorelin, argatroban) and peptide analogues (e.g., GnRH agonists, buserelin, carbetocin, icatibant, pasireotide, carfilzomib), but also

one third of the natural peptides contain non-natural amino acids. Paradoxically, natural peptides antibiotics (e.g., capreomycin, vancomycin, bleomycin, oritavancin), despite being derived from natural sources, contain a very low percentage of proteinogenic amino acids (between 0 and 10% of all the constitutional members), significantly lower than the mean percentage of proteinogenic amino acids in approved peptides (~81%).

Dab, Dap, and Orn are three lysine homologues, containing an amino group on the side chain which contributes to the overall basicity of the molecule and, at the same time, allows opportunities for cyclisation or conjugation. It has been demonstrated that the use of lysine homologues protects the peptide from instability; examples are the use of Dab, Dap, and homoarginine in antimicrobial peptides (AMPs) to prevent Arg or Lys haemolytic activity or tryptic digestion [128,129], but also, the replacement of Lys with Orn to reduce the susceptibility to tryptic hydrolysis [130]. Generally, amino acid side chains bearing a primary amine, such as lysine and its homologues, are among the most frequently used amino acids (around 7% of the total amino acids). Specifically, the Dab residue was encountered 12 times in total, but this amino acid appears only in two peptide structures (i.e., colistin and polymyxin B), while Orn appears only four times, each in a different peptide (i.e., daptomycin, ornipressin, atosiban, bacitracin).

Hyp, a proline structure bearing a hydroxyl group in position 4 of the pyrrolidine ring, is encountered in 7 approved peptides (i.e., icatibant, pasireotide, anidulafungin, caspofungin, micafungin, paritaprevir, and grazoprevir). Hyp may be introduced for the possibility of further conjugation and/or for its ability to enhance polarity and improve hydrogen-bonding capacity. In addition to this, Hyp may stabilise peptide secondary structure, similarly to the way this residue stabilises the triple-helical structure of collagen [131].

Naphthyl-alanine (Nal) is an amino acid often used to replace tryptophan (Trp) and to explore potential improvements in peptide pharmacological profiles [132–134].

However, the consequences of this replacement should be judiciously evaluated as this may result in a decrease in potency, as reported by Rodriguez *et al.*, who studied the effect of the substitution of Trp with 1-Nal and 2-Nal in cholecystokinin analogues [135]. On the other hand, this strategy has been successfully used in the development of GnRH receptor (GnRH-R) antagonists (i.e., abarelix, ganirelix, degarelix, and cetrorelix) and other peptides (e.g., lanreotide, nafarelin, pralmorelin).

Improvement of peptide drug-likeness can be also achieved through the introduction of non-amino acidic modifications, usually linked to the main chain at different sites (i.e., amino acid side chains functional groups or N- or C-termini) by one functional group (e.g., carbonyl in the case of fatty acids or hydroxyl in the case of sugars). Among the various modifications encountered, the most common ones are lipid acylation and glycosylation. Enhancement of stability, protein binding, and membrane permeability can be obtained through peptide lipid acylation, while improved solubility and bioavailability can be achieved through glycosylation [136,137].

13% of the peptides on the market present a lipophilic carbon chain attached to their structure. Lipid acylation of peptides can enhance stability, protein binding, and membrane permeability by modulating hydrophobicity and secondary structure [137]. Examples of lipidated peptides presenting an extended terminal half-life and high plasma protein binding are the GLP-1 receptor agonists liraglutide (conjugated with palmitic acid) and semaglutide (conjugated with an octadecanedioic acid), used for the treatment of diabetes. They both bind with high affinity to plasma proteins (~98-99% bound), promoting greater peptide stability that results in significantly extended half-lives of 13 and 168 hours, respectively, compared with the parent peptide GLP-1 (half-life of 1.5-5 min) [138,139].

Although less frequent than lipidation, glycosylation is a meaningful modification, found in ~7% of the marketed peptides. Examples of glycosylated peptides are mifamurtide, bleomycin, vancomycin, dalbavancin, telavancin, teicoplanin, and oritavancin, all natural or naturally derived peptides, probably due to the synthetic

challenges that glycochemistry presents. Analogously to recombinant glycoprotein therapeutics, where carbohydrates are commonly N-linked to Asn or O-linked to Ser and Thr, in these peptides glycosyl units are attached to the main structure *via* an N-terminal NH_2 group or a side-chain OH group [140]. In contrast with lipidation, glycosylation enhances solubility and increases bioavailability and oral absorption [94,137]. It is probably not by chance that, out of 7 glycosylated peptides, 6 of them present an aliphatic chain or a large aromatic core, where the hydrophobic nature is balanced by the presence of one or more carbohydrate groups.

An important role is played by pyroglutamic acid (Pyr) – cyclic lactam of glutamic acid – found in 8 approved peptides (i.e., leuprolide, buserelin, triptorelin, goserelin, gonadorelin, nafarelin, histrelin, and protirelin, all GnRH agonists). In nature, N-pyroglutamyl is found in many neuronal peptides and hormones but its function in living cells is still unclear [141]. In drug design, capping the N-terminus with Pyr is a common strategy to modulate peptide activity and increase resistance to degradation [142]. Indeed, in some cases, Pyr has shown to be essential in order to achieve full biological activity [143].

Notably, although fluorine is largely used in small molecule design, the only example of an approved fluorinated peptide is Voxilaprevir (**24**), used in combination with Sofosbuvir/Velpatasvir in Vosevi to treat chronic Hepatitis C [139]. The exploitation of fluorine in peptides is predicted to become a key medicinal chemistry tool in which the judicious addition of a small and highly electron-withdrawing atom, has been shown to have a key role in improving PK and physicochemical properties [144].

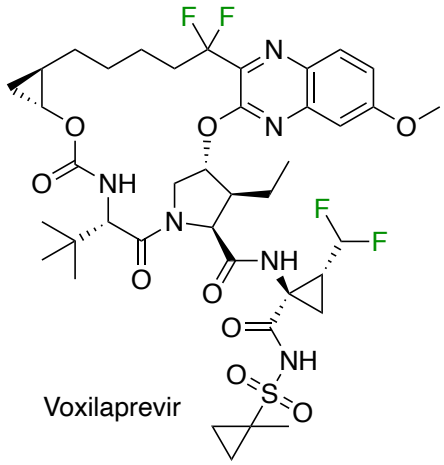

24 Voxilaprevir

*Figure 2.8. Chemical structure of voxilaprevir (**24**), the first fluorinated peptide approved.*

Finally, other non-aminoacidic appendages include metal cation-chelating agents (e.g., DOTA in dotatate and DTPA in pentetreotide), typically found in diagnostic agents, or linkers (e.g., 2-amino-4,6-dimethyl-3-oxo-3H-phenoxazine-1,9-dicarbonyl in dactinomycin).

2.3.2.4 Polarity trends of approved peptides

Examination of the structural features of the constitutional members of approved peptides revealed that, on average, peptides present a balance between polar and hydrophobic residues, where the polar contribution is derived by the summation of the polar, basic and acidic constitutional members and the hydrophobic contribution is the summation of the aromatic and aliphatic constitutional members. The distribution chart in Figure 2.9A shows that, not surprisingly, most approved peptides include between 35 to 75% polar residues, indicating that these molecules do not contain an excess of either hydrophilic or lipophilic components. In fact, both polar and hydrophobic components are generally required to obtain drugs with acceptable pharmacokinetic profiles. However, a small number of outliers that comprise 100% polar or 100% hydrophobic constitutional members are present. By closely examining these, it is clear that these exceptions are represented by very small-size peptides (2-5 constitutional members), more similar to small molecules than to

peptides. Indeed, the hydrophilic dipeptide spaglumic acid as well as the hydrophobic tripeptides ACE inhibitors (enalapril, perindopril, ramipril, quinapril, and trandolapril) all respect the Lipinski's rule of five tailored for small molecules (computed by ChemAxon [116]). Other exceptions are represented by macimorelin, a growth hormone secretagogue receptor agonist composed of only 3 building blocks, and the hydrophobic antiviral peptides telaprevir, boceprevir, and ombitasvir, composed of 4 or 5 members. Finally, cyclosporine is the only case in which a marketed peptide composed of more than 5 members (11 in this case) completely lacks the polar component. This is reflected in its prolonged half-life of 19 hours and its attitude to bind to serum plasma proteins (~90% bound to serum proteins) [145,146]. Notably, the classification of natural and non-natural amino acids is solely based on the nature of the side chain, ignoring the polar contribution of the backbone, as this seems the clearest way to distinguish between hydrophilic and hydrophobic amino acids, without overshadowing the contribution of the side chain with that of the backbone. However, when encountering an all-hydrophobic peptide such as cyclosporine, it is important to remember that the backbone will contribute to the overall polarity of the molecule. Figure 2.9B, in which the constitutional members are colour-coded according to their properties (polar, acidic, basic, non-polar aliphatic, and aromatic), allows the reader to clearly visualise the composition of each approved peptide.

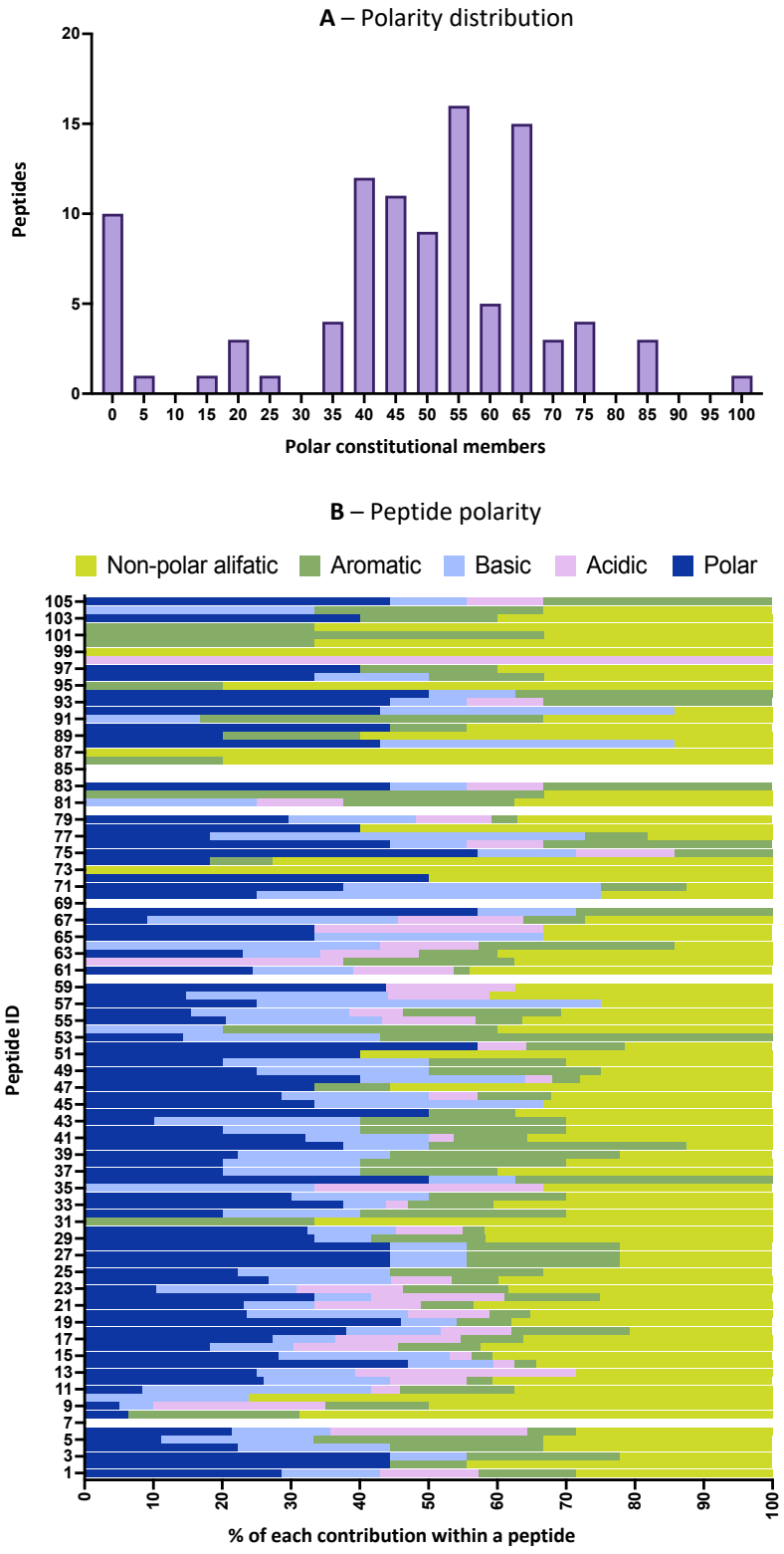

Figure 2.9. Peptide polarity evaluation. ***A.*** *Polarity distribution within the pool of approved peptides;* ***B.*** *Colour-coded plot to show the aliphatic (light green), aromatic (green), polar (blue), basic (light blue), and acidic (pink) contributions in each peptide under evaluation.*

2.3.2.5 Conformational properties of approved peptides

An important aspect of this study was the discrimination between linear peptides and peptides containing one or more macrocycles, followed by further evaluation of the structure of the cyclic ones. As shown in Figure 2.10A, 53% of the marketed peptides are linear, while 47% present one or more macrocycles in their structure. Among the cyclic peptides, 39% are of natural origin, 55% are analogues and only 6% are heterologous, once again proving the strong influence of nature in the development of stable, biocompatible peptides, being a rich source of inspiration for candidates with optimal drug-like properties [147].

Interestingly, as illustrated in the distribution graph in Figure 2.10B, the majority of peptide macrocycles consists of 5-to-7 members. Examples of this include the therapeutic agents eptifibatide, human calcitonin, desmopressin, lanreotide, and pramlintide, as well as the diagnostic agents edotreotide Gallium Ga-68 and pentetreotide Indium In-111. Exceptions to this general trend are represented by the cardiovascular drugs nesiritide and carperitide, both containing a 17-membered ring.

Generally, smaller macrocycles present greater conformational stability due to physical restraints and fewer rotatable bonds. Indeed, macrocyclisation is a very common technique to enhance peptide conformational stability and restrict the usual peptide chain flexibility [148,149]. In turn, this conformational stabilisation may result in optimal complexation with the target receptor or confer a protein-like secondary and tertiary structure [149–151].

Cyclisation can occur at various sites of the peptide structure – i.e., the C-terminal moiety (‘head’), N-terminal moiety (‘tail’), or amino acid side chains. Depending on the desired site of cyclisation, the strategy to choose to generate cyclic peptides varies [152]. The findings of this study, summarised in the pie chart in Figure 2.10C, indicate that the most common technique used is the side chain-to-side chain cyclisation (58% of all the marketed cyclic peptides), with 25 out of 26 side chain-to-side chain macrocycles formed by a disulfide bond between cysteine thiol pairs. The only exception is bremelanotide, in which a lactam is formed between the amine side

chain of a lysine residue and the carboxylic acid side chain of an aspartic acid residue. However, disulfide bridges are not always metabolically stable *in vivo*, leaving space for the exploration of alternative strategies [153]. Another approach to yield macrocycles within a peptide structure is the head-to-side chain cyclisation (24%), mainly *via* lactamisation between the C-terminal carboxylic acid and a side chain amine (e.g., lysine). The head-to-tail cyclisation between the N- and C-termini (7%), generates an all-amide end-to-end cyclic lactam, thus abrogating exopeptidase hydrolysis. Finally, two cyclic peptides (i.e., grazoprevir and elcatonin) present a macrocycle formed by side chain-to-tail macrocyclization. In general, participation of the head and/or the tail of a peptide in a macrocycle prevents the action of carboxy- and/or amino-peptidases, respectively, thus increasing resistance to proteolysis [154]. This figure is well represented by the pool of approved peptides, with the mean experimental terminal half-life of cyclic peptides being more than 2-fold greater than that of linear peptides (27 h and 12 h, respectively).

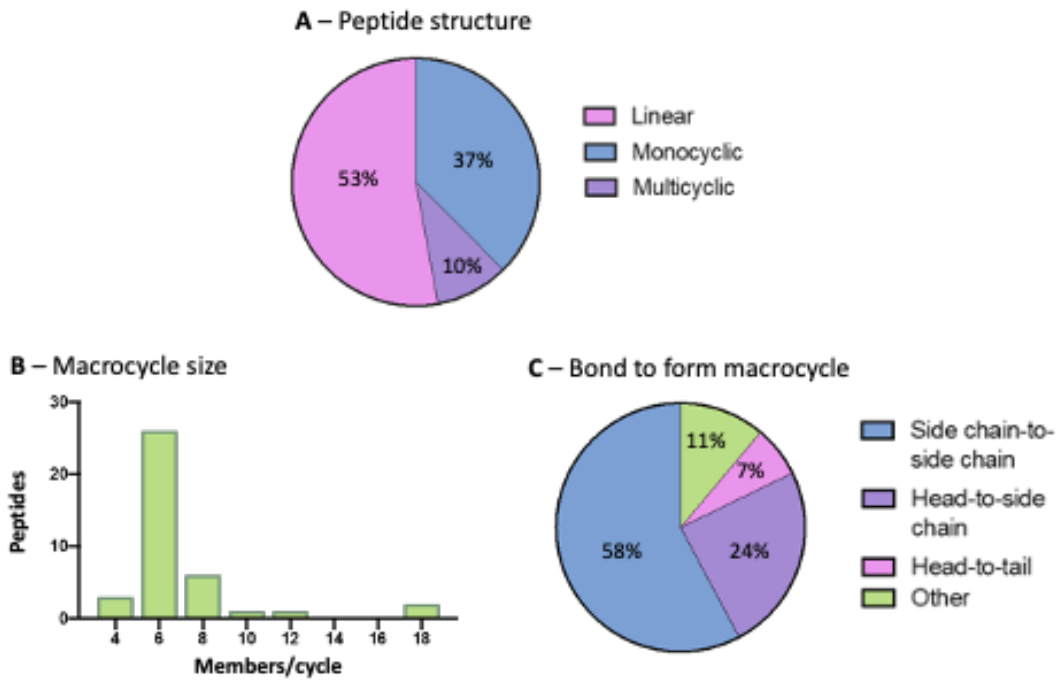

Figure 2.10. A. Peptide structure, divided in linear, monocyclic and multicyclic. B. Macrocycle size, shown as number of constitutional members per cycle; C. Type of bond to form the cycle within the peptide structure.

In the pool of approved peptides, 38% present an amidated C-terminus (Figure 2.11A), while 10% present an acetyl group at the N-terminus (Figure 2.11B). Modifications of peptide N-terminus also include the addition of the previously mentioned pyroglutamic acid (7%) or deamination of the last amino acid (4%). Similar to the head-to-tail cyclisation, masking amino- and carboxyl- termini abrogates exopeptidase hydrolysis [155]. Additionally, N-terminal acetylation or C-terminal amidation preclude ionisation and hydrogen-bonding of NH_2 and COOH groups, respectively, thus better mimicking natural proteins [156,157].

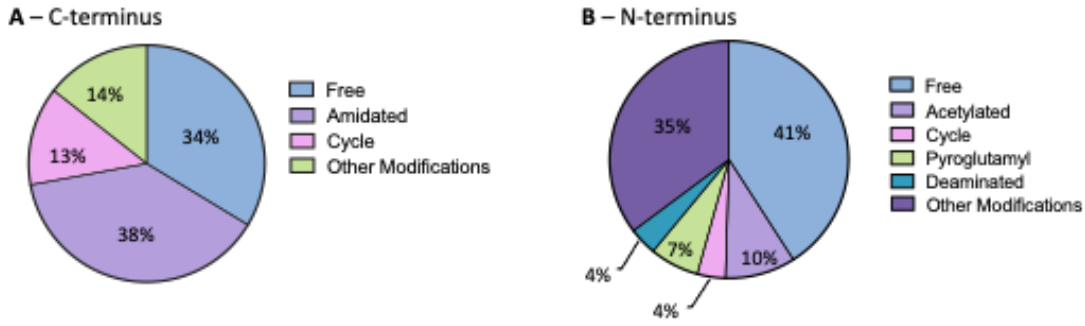

Figure 2.11. A. C-terminal modifications in the pool of approved peptides; B. N-terminal modifications in the pool of approved peptides.

2.3.3 Lipophilicity predictions (cLogP and cLogD)

To investigate whether there were any trends in the physicochemical properties of approved peptides, an initial test was conducted on predicted lipophilicity values. Unfortunately, LogD predictions is permitted only with ChemAxon (Chemicalize) and ACD/i-Labs and LogD experimental data for comparison with the *in silico* data are rarely available. However, LogP can be used as a reasonable proxy for LogD in trend analysis of compounds below 2,000 g/mol (correlation R^2 ~0.93 using ChemAxon and R^2 ~ 0.80 for ACD/i-Labs), as previously proven by our research group (Liebnitz *et al*., unpublished).

In the case of approved peptides for which experimental values were available in the literature, calculations with two software applications (Chemicalize and ACD/i-Labs)

were performed. Predicted values, reported in Table 2.4, were then compared with experimental values (previously gathered and listed in an internal database by our research group).

Table 2.4. LogP experimental values of approved peptides collected from literature (exp. LogP), and LogP and LogD values calculated with Chemicalize ChemAxon (cLogP and cLogD, respectively), LogP and LogD calculated with ACD/i-Labs (ACD/LogP and ACD/LogD, respectively).

Generic Peptide Name	Molar Mass (g/mol)	Exp. LogP	cLogP	cLogD	ACD/ LogP	ACD/ LogD
Perindopril	368	2.6	0.631	-0.85	3.36	-5.45
Enalapril	376	0.07	0.588	-1.06	2.43	-3.11
Lisinopril	405	-1.01	-3.103	-3.18	1.19	-1.06
Ramipril	417	2.9	1.474	-0.18	3.41	-4.22
Trandolapril	431	3.5	1.947	0.29	3.97	-4.48
Quinapril	439	0.86	1.964	0.31	4.32	-1.99
Argatroban	509	1	-0.97	-0.97	2.56	-2.4
Carbetocin	988	-2	-3.584	-3.58	-3.59	0.84
Octreotide	1019	-0.49	-1.411	-4.28	0.77	-2.5
Desmopressin	1069	-4.2	-6.128	-7.78	-5.82	-1.93
Caspofungin	1093	0	-4.824	-7.54	-5.05	-7.16
Anidulafungin	1140	2.9	-1.5	-1.46	-	-
Colistin	1155	-2.4	-8.096	-18.57	-3.68	-11.97
Gonadorelin	1182	-3.6	-6.319	-7.98	-2.02	-2.32
Cyclosporine	1203	1.4	3.638	3.64	3.35	2.34
Polymyxin B	1203	-4.9	-7.249	-17.72	-	-
Dactinomycin	1255	1.6	-0.097	-0.1	-4.03	-0.43
Goserelin	1269	-2	-5.084	-6.51	-0.95	-3.98
Micafungin	1270	-1.5	-6.338	-6.74	-	-
Capreomycin	1321	-9.609	-11.314	-17.18	-9.89	-3.561
Bacitracin	1423	-0.8	-6.838	-6.79	-	
Vancomycin	1449	-3.1	-4.39	-4.85	-1.44	-3.84
Dotatate Gallium Ga-68	1502	-3.69	-8.352	-14.46	-	-
Telavancin	1756	0.6	-6.163	-5.93	-	-
Oritavancin	1793	4.1	0.205	-1.56	-	-
Exenatide	4187	-2	-29.357	-41.8	-	-

As shown in Figure 2.12, for small-size peptides (i.e., below ~1100 g/mol), the reliability of the predictions, expressed as the difference between the experimental values and the calculated values, was overall within an acceptable range. However, for peptides with molar mass greater than ~1100 g/mol, the difference between predicted and experimental values was too significant to be used for further considerations. In light of these findings, predictions of lipophilicity were not employed in further studies and trends, considered not sufficiently reliable, are not described.

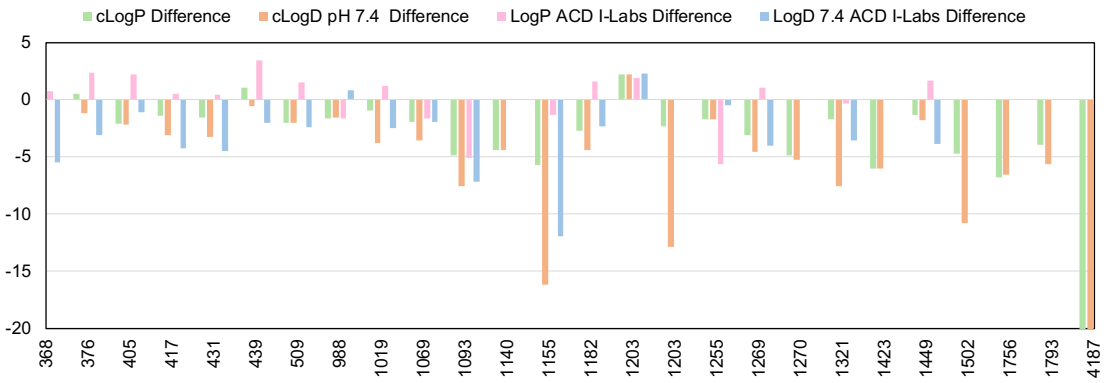

Figure 2.12. Comparison of predicted cLogP and cLogD values with literature LogP values, ranked by increasing molar mass.

2.4 Conclusions

This chapter, together with the production of a freely available database PepTherDia, offers the opportunity to explore common trends in approved peptide therapeutics and diagnostics. Here, some of the strategies most commonly used in peptide drug design to successfully bring these peptides to the market have been highlighted. Most approved peptides (~84%) are natural or analogues of natural compounds, following the rules of nature established over several millennia of evolution.

Key observations include the emergence of a bimodal distribution of peptide molar mass, with the large majority being smaller than ~1750 g/mol and others being larger than ~2700 g/mol. This is mirrored in a bimodal distribution of the number of constitutional members. Among all the peptide constitutional members, most

(around 81%) are represented by natural L-amino acids, while the residual 19% comprises non-natural amino acids and modifications. In addition to frequently encountered natural AAs, commonly used non-natural AAs introduced to enhance properties or opportunities for further diversification were analysed, as well as strategies to modify peptides with non-amino acidic appendages. Indeed, conjugation with fatty acids or sugars are well represented in various approvals, suggesting that they are promising tools to modify peptidic structures while retaining favourable pharmacological properties. Moreover, careful characterisation of constitutional members derived from our retrosynthetic analysis showed a balance between polar and hydrophobic residues within the peptide structures. Finally, 47% of the approved peptides are cyclic and, interestingly, 5- to 7-members macrocycles are the most common encountered.

On account of this analysis, it was concluded that a peptide most likely to become a drug will have a molar mass lower than 2000 g/mol and will present a balance between hydrophobic and polar contributions. Furthermore, careful evaluation of the C- and N-terminal modifications will be key for the PK properties as well as for the desired activity. A starring role for peptide therapeutics is predicted in the next few years and it is envisaged that this information will aid the scientific community to more carefully design and pre-screen peptide candidates at an early stage to increase longitudinal approval rates.

Among the successful strategies analysed in this work, modifications, such as fluorination and lipid acylation, but also peptidomimetic molecules are of great interest to improve the drug-likeness of novel peptides. Hence, these strategies will be applied to the design of anti-migraine peptide drug candidates of interest.

3 Design, synthesis and testing of potent peptide and peptidomimetic antagonists of the CGRP receptor

3.1 Introduction

3.1.1 Peptide synthesis

3.1.1.1 Peptide early developments

140 years ago, Theodor Curtius synthesised and characterised the first N-protected dipeptide (benzoyl glycylglycine, **25**), obtained from the reaction of a silver salt of glycine with benzoyl chloride [158]. Twenty years later, Emil Fischer and Ernest Fourneau synthesised, for the first time, a native peptide (glycylglycine, **26**) and coined the term 'peptide', initiating the so-called 'peptide chemistry' research field [159].

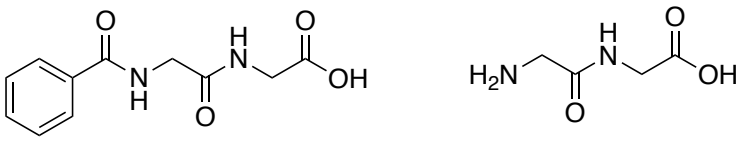

25 benzoylglycylglycine

26 glycylglycine

*Figure 3.1. Benzoylglycylglycine (**25**) and glycylglycine (**26**) structures.*

For the first half of the 20th century, peptide synthesis was performed in homogenous solution. Liquid-phase peptide synthesis (LPPS), also called 'classical synthesis', is based on the reversible blocking of the carboxylic acid group of the C-terminal amino acid (e.g., H_2N-Phe-OBz, **28**) and the amino group of the N-terminal amino acid (e.g., Boc-Ala-OH, **27**), and finally on the activation *via* dicyclohexylcarbodiimide (DCC) of the free carboxylic acid of the N-terminal amino acid, to yield the peptide bond (Figure 3.2).

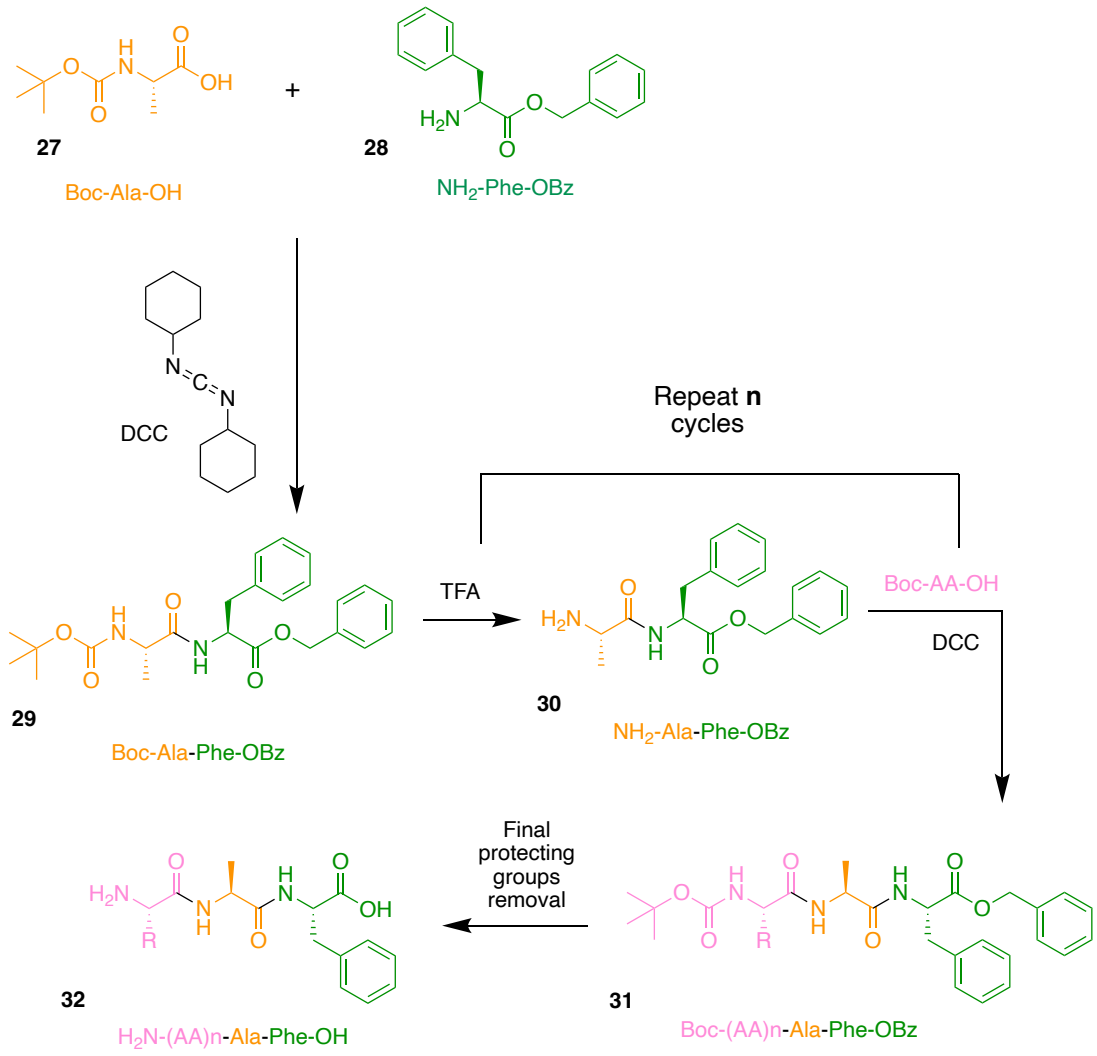

Figure 3.2. Liquid-Phase Peptide Synthesis (LPPS) steps.

This process may be limited to short (~5 amino acids) sequences due to low solubility issues. Moreover, it is time-consuming and laborious as it requires isolation and purification of each intermediate before this can be utilised for further elongation steps [160].

However, in 1963, Robert Bruce Merrifield revolutionised the field of peptides by developing a methodology for chemical synthesis on a solid matrix, in which iterative couplings are performed in a single reaction vessel (Figure 3.3) [161,162], receiving the Nobel Prize in Chemistry for 1984 for "Development of methodology for chemical synthesis on a solid matrix" [163].

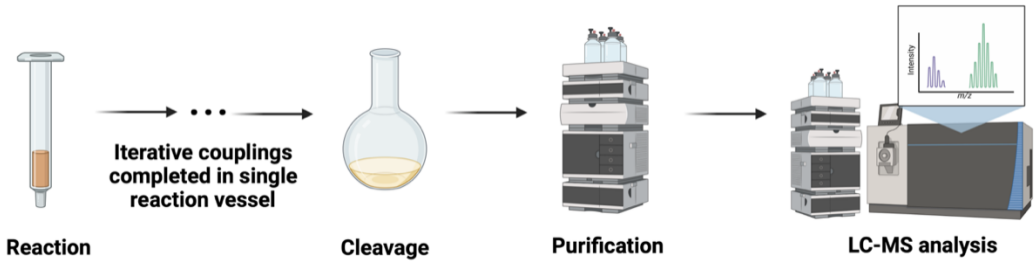

Figure 3.3. General scheme for Solid-Phase Peptide Synthesis (SPPS) steps. Image created with BioRender.com.

The idea underpinning the development of Solid-Phase Peptide Synthesis (SPPS) is to maintain the same chemistry used in liquid-phase but on an insoluble solid polymeric support (resin), where the nascent peptide chain is linked by a covalent bond [164]. The chain elongation reactions are performed in an excess of soluble reagents that can be easily removed by filtration and washing steps without peptide loss, avoiding tedious crystallisation steps, and eventually yielding greatly improved peptide purity [162]. Merrifield's original approach to SPPS (Figure 3.4) used amino acids protected at the amine with a Boc group (**32**) and covalently attached to the solid support as a benzyl ester linker (**34**) *via* reaction at a chloromethylphenyl group (**33**); here, the peptide chain could be extended with sequential deprotection, neutralisation and coupling steps for each succeeding amino acid. The elongation process was facilitated by DCC which activated the acid of the Boc-amino acid. The Boc group could be completely removed with 50% TFA in dichloromethane, while the side chain protecting groups as well as the covalent bond between the first amino acid and the solid support required treatment with a strong anhydrous acid such as hydrofluoric acid (HF) [161,164].

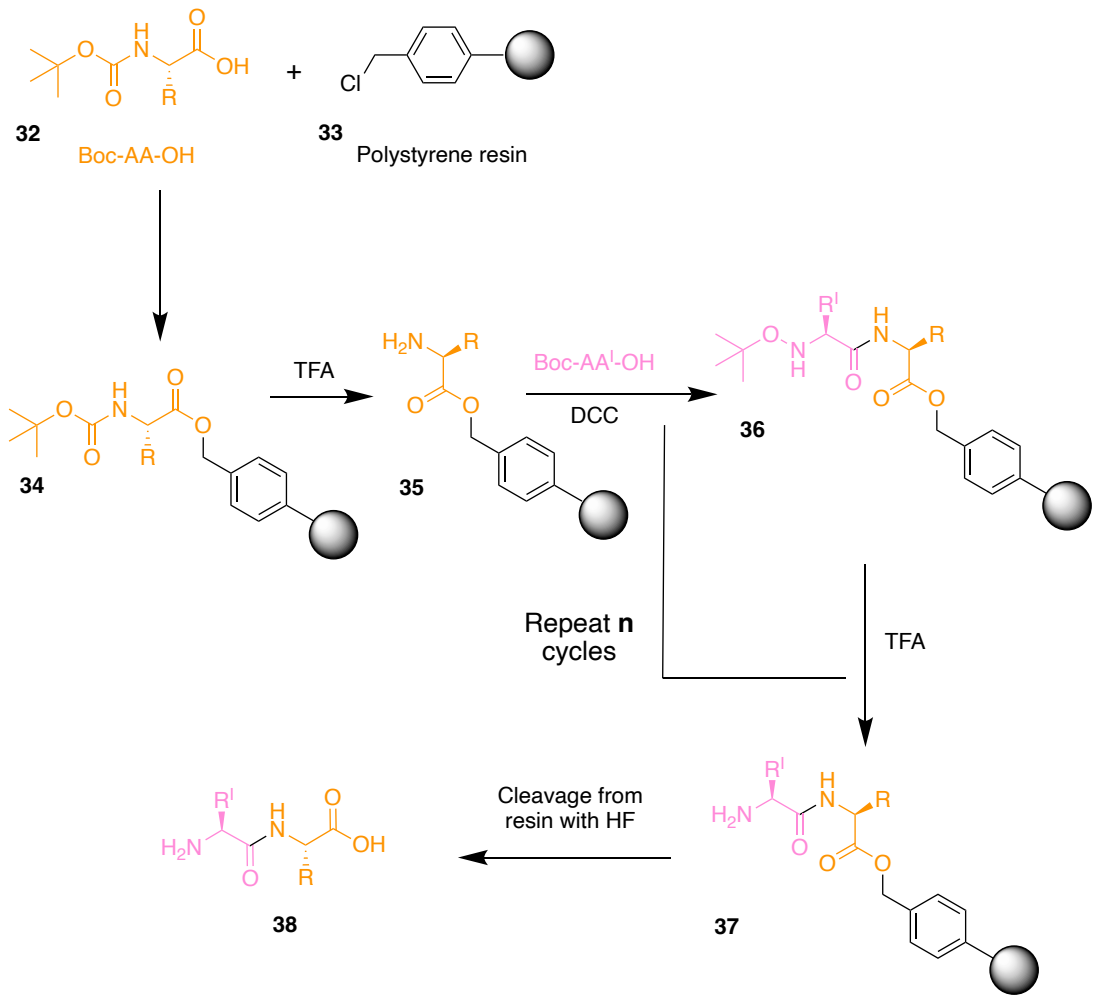

Figure 3.4. Solid-Phase Peptide Synthesis (SPPS): Merrifield's original approach [164].

3.1.1.2 Fmoc solid-phase peptide synthesis (Fmoc-SPPS)

Among the strategies for peptide synthesis on solid support, Fmoc (9-fluorenylmethyloxycarbonyl, **39**) and Boc (*tert*-butyloxycarbonyl, **40**) are the most commonly used [165].

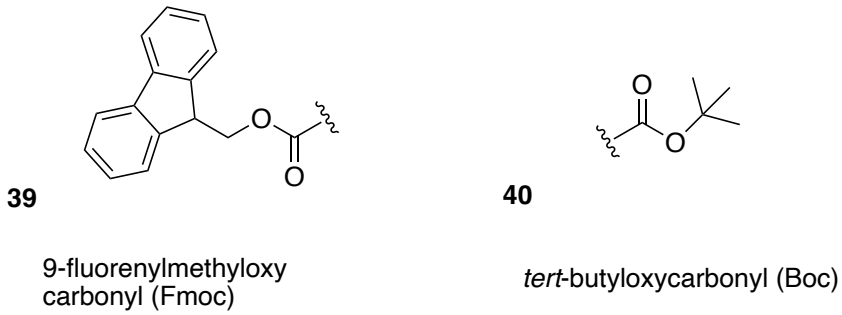

Figure 3.5. Backbone NH_2 protecting group structures used for SPPS.

In recent years, Fmoc SPPS has superseded the Boc methodology, by overcoming the issues related to the use of Boc [166]. Thus, the combination of Fmoc and acid-labile protecting groups provides an orthogonal combination of temporary and permanent side-chain protecting groups [167].

In Fmoc-SPPS, all amino acid derivatives present the Fmoc (**39**) as a temporary protecting group of the amino group that is removed at each elongation step of the synthesis. The removal of the Fmoc group requires a base, normally piperidine or, alternatively, 4-methylpiperidine [165]. Permanent protecting groups of the amino acid side chains – e.g., *t*-butyl (^{t}But, **41**), O-*t*-butyl (O-^{t}But, **42**), trityl (Trt, **43**), 2,2,4,6,7-pentamethyldihydrobenzofuran-5-sulfonyl (Pbf, **44**), and t-butyloxycarbonyl (Boc, **40**) groups – remain intact during the synthesis and are removed only during cleavage to prevent side reactions [165].

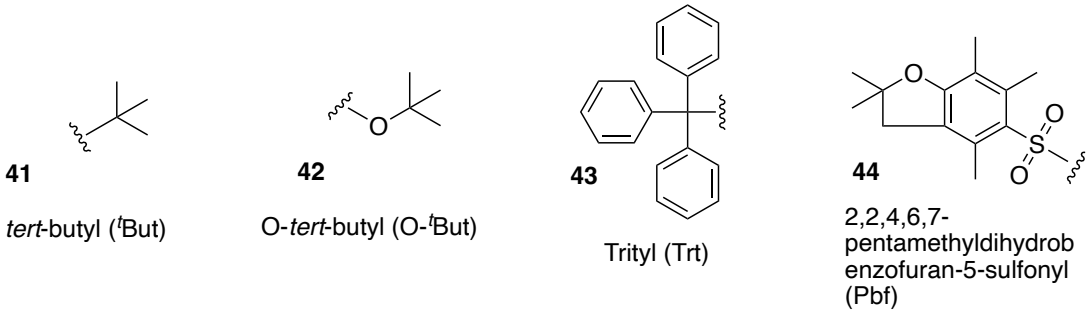

Figure 3.6. Side chain protecting group structures in Fmoc-SPPS.

A general reaction scheme for Fmoc SPPS using Rink Amide ProTide resin as the solid support is shown in Figure 3.7.

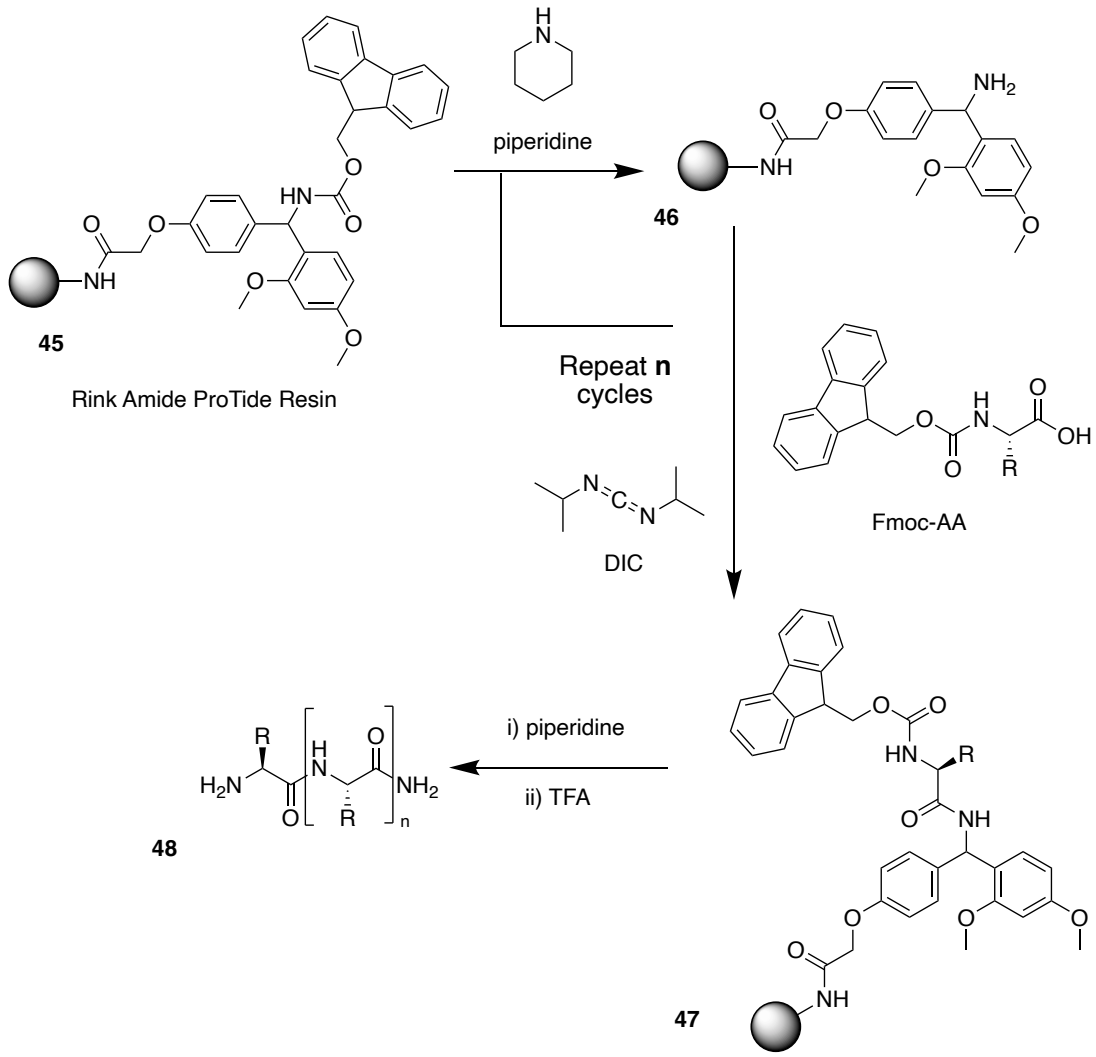

Figure 3.7. Fmoc SPPS general reaction scheme with Rink Amide ProTide Resin as solid support. DIC = N,N'-Diisopropylcarbodiimide; TFA = trifluoroacetic acid.

3.1.1.3 Microwave-assisted automated peptide synthesis

The cyclic procedure of peptide assembly on a solid support offers the ideal settings for automation [160]. In 1965, Merrifield described the process of the automation of SPPS, offering great advantages over manual synthesis [168]. This was followed by improvements in coupling reagents, solid supports, linkers and the development of the Fmoc-SPPS technology.

Instruments for solid-phase peptide synthesis (e.g., CEM Liberty Blue Peptide Synthesizer, Figure 3.8) can now be purchased from numerous companies; some of the most commonly used have been reviewed [160,169].

Over the last two decades, precise microwave irradiation applied to peptide synthesis has become increasingly popular, due to the reduction in synthesis time (1-2 min per coupling), and increase in crude peptide purity [170–173].

Figure 3.8. CEM Liberty Blue Peptide Synthesizer.

Microwave-assisted Fmoc SPPS can be efficiently employed to prepare libraries of biologically relevant peptides and peptidomimetics in high yields in relatively short times.

3.1.2 Calcitonin gene-related peptide (CGRP) and structure-activity relationship studies

As previously described in Chapter 1, in the last two decades, CGRP and its receptor (CGRP-R) have been recognised as important mediators of neurogenic inflammation and are heavily involved in migraine pathophysiology [29,35,174].

Structure-activity relationship studies (SARs) conducted on the natural hormone CGRP demonstrated that different parts of the sequence are responsible for activity or affinity (Figure 3.9). The C-terminal segment of CGRP (amino acids 8-37) determines affinity for the receptor, whereas the N-terminal disulfide bridged ring structure (amino acids 1-7) is responsible for receptor activation [175–179]. Dennis *et al.* demonstrated that, while CGRP analogues lacking the portion 9-37 had reduced

affinity, the CGRP segment 2-7 was not essential for binding [175]. Furthermore, a study conducted by Chiba and collaborators demonstrated an inhibitory effect of the segment 8-37 on the CGRP-R. They showed that this fragment did not activate adenylate cyclase in rat liver plasma membrane, but it significantly inhibited the activation of adenylate cyclase induced by CGRP and human calcitonin [176]. Additionally, Rovero and collaborators studied the activity of the segments 19-37 and 23-37 of CGRP, confirming their ability to act as antagonists of the CGRP-R [177]. The natural hormone CGRP and the relevance of its regions in relation to the CGRP-R as well as the CGRP amino acid sequence are represented in Figure 3.9.

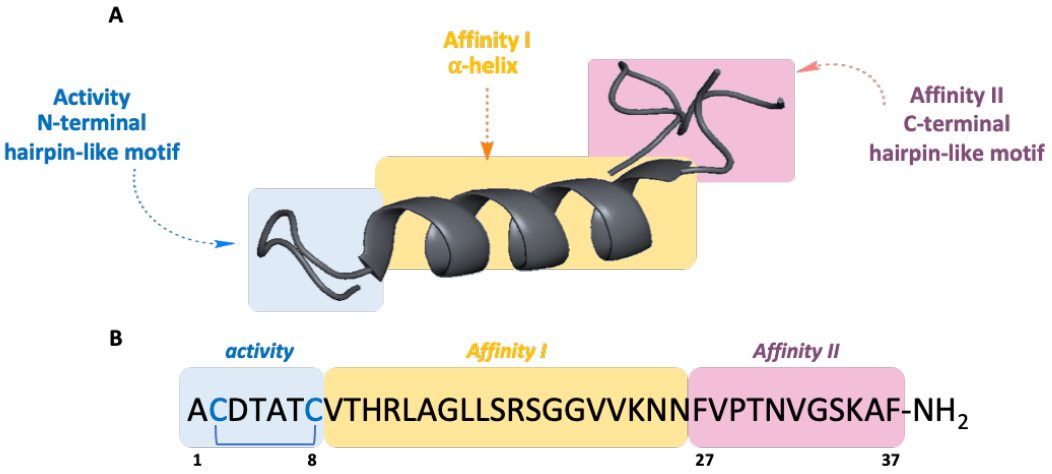

Figure 3.9. A. CGRP structure constructed on PyMol (version 2.3.4); B. CGRP amino acid sequence. In both cases, portion 1-8 is highlighted in light blue, helical portion 9-26 is coloured in yellow, while portion 27-37 is highlighted in pink.

These findings were followed by studies performing a variety of systematic modifications on the C-terminal segment to optimise the C-terminal part of CGRP and identify the primary structure necessary for high CGRP-R affinity, eventually found to be the portion CGRP 27-37 (**49**) or 28-37, as Phe27 could be removed without loss of activity [66,179].

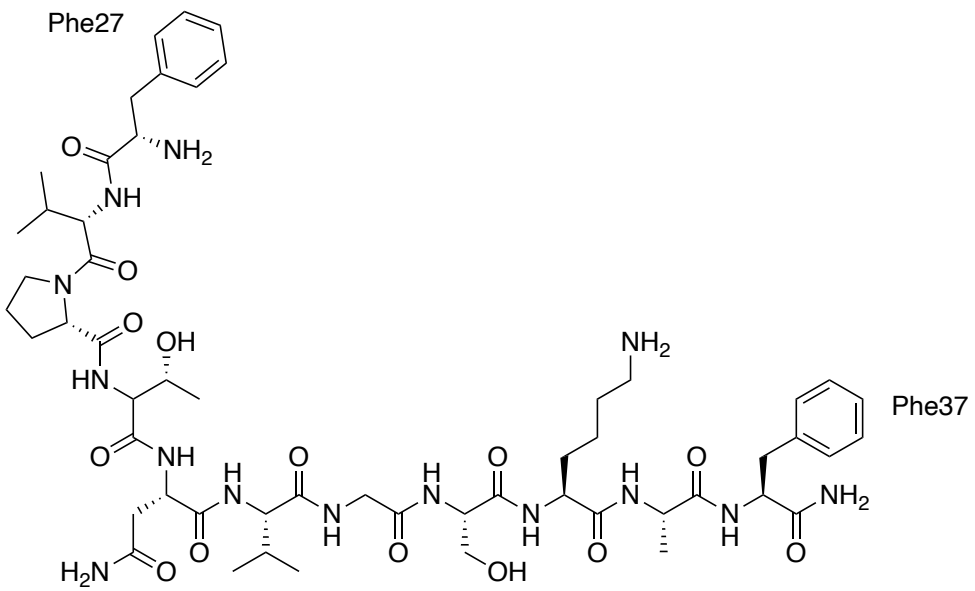

Figure 3.10. Chemical structure of the portion 27-37 of the natural hormone CGRP.

Rist and co-workers made possibly the greatest contribution towards the understanding of the CGRP 27-37 structure-activity relationships, eventually identifying various CGRP-R antagonists with moderate-to-high receptor affinity, including [Pro34, Phe35] CGRP 27-37 and [Asp31, Pro34, Phe35] CGRP 27-37 (Table 3.1) [66,67].

Table 3.1. Early development of peptide CGRP-R antagonists. Modifications from the CGRP 27-37 amino acid sequence are highlighted in bold.

Peptide Name	Sequence	hCGRP K_i [nM]	Ref.
CGRP 27-37	FVPTNVGSKAF-NH_2	728	[67]
[Pro34, Phe35] CGRP 27-37	FVPTNVG**PF**AF-NH_2	19	[67]
[Asp31, Pro34, Phe35] CGRP 27-37	FVPT**D**VG**PF**AF-NH_2	14	[67]
[Asp31, Pro34, Phe35]-CGRP 30-37	T**D**VG**PF**AF-NH_2	29.7	[180]
[Ala34, Phe35]-CGRP 28-37	VPTNVG**AF**AF-NH_2	495	[180]

The predicted turn structures centered at Pro29 and Pro34 of [Asp31, Pro34, Phe35] CGRP 27-37 were investigated by replacing Pro with proline mimetics, such as (1S,2S,3S)-β-aminocyclopropane carboxylic acid (**50**), (1R,2R,3R)-β-

aminocyclopropane carboxylic acid (**51**), aminoisobutyric acid (**52**), tetrahydroisoquinoline-3-carboxylic acid (**53**), L-homoproline (**54**), and L-4-hydroxyproline (**55**). Modifications in position 29 resulted in compounds with greater affinity than the same modifications in position 34, so the former was identified as a key position [22].

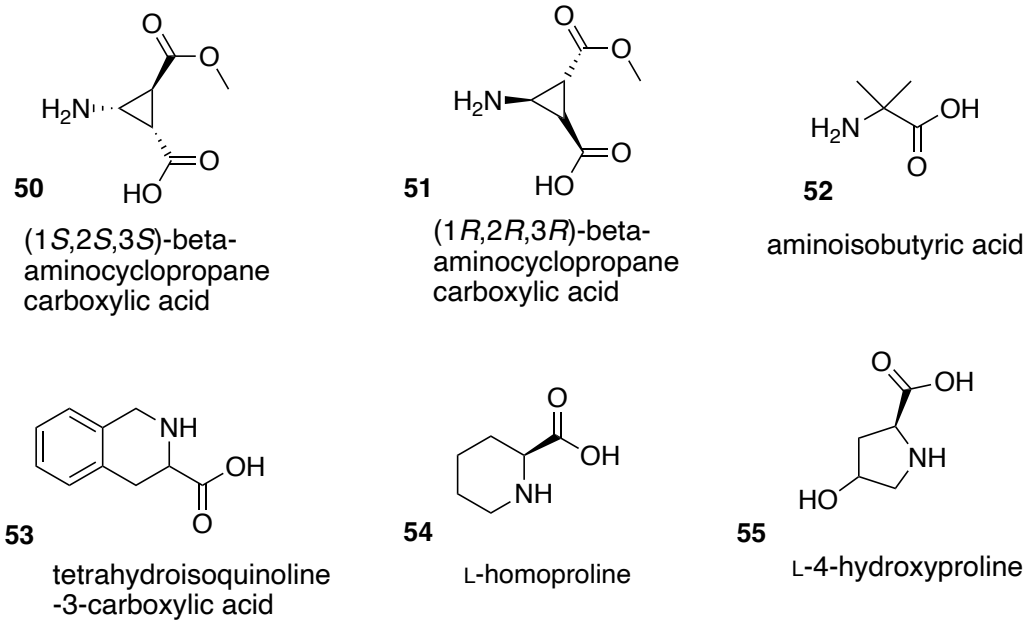

Figure 3.11. Chemical structures of the turn-inducing amino acid derivatives introduced in the sequence of the CGRP 27-37 by Lang et al. [22].

In 2001, Astra Zeneca (Montreal, Canada) carried out SAR studies on [Asp31, Pro34, Phe35]-CGRP 27-37 which resulted in [Asp31, Pro34, Phe35]-CGRP 30-37, the shortest CGRP C-terminal peptide analogue showing CGRP receptor affinity (K_i = 29.6 ± 6.1 nM) (Table 3.1) [180]. In addition, through alanine-scanning mutagenesis on [Ala34, Phe35]-CGRP 28-37 the critical residues for the CGRP-R binding were identified as Thr30, Val32, and Phe37 (Table 3.1) [180].

Ten years later, Lilly Research Laboratories (Indianopolis, USA) carried out a ligand optimisation strategy that combined positional scanning, N-terminal modifications, and the use of disulfide-induced constraint, eventually leading to a series of potent cyclic peptides with subnanomolar K_b values at the CGRP-R. However, further *in vivo*

studies were hampered by the unacceptably low aqueous solubility of these compounds [68].

A summary of the modifications explored on the C-terminal segment of CGRP and the resulting outcomes is shown in Figure 3.12.

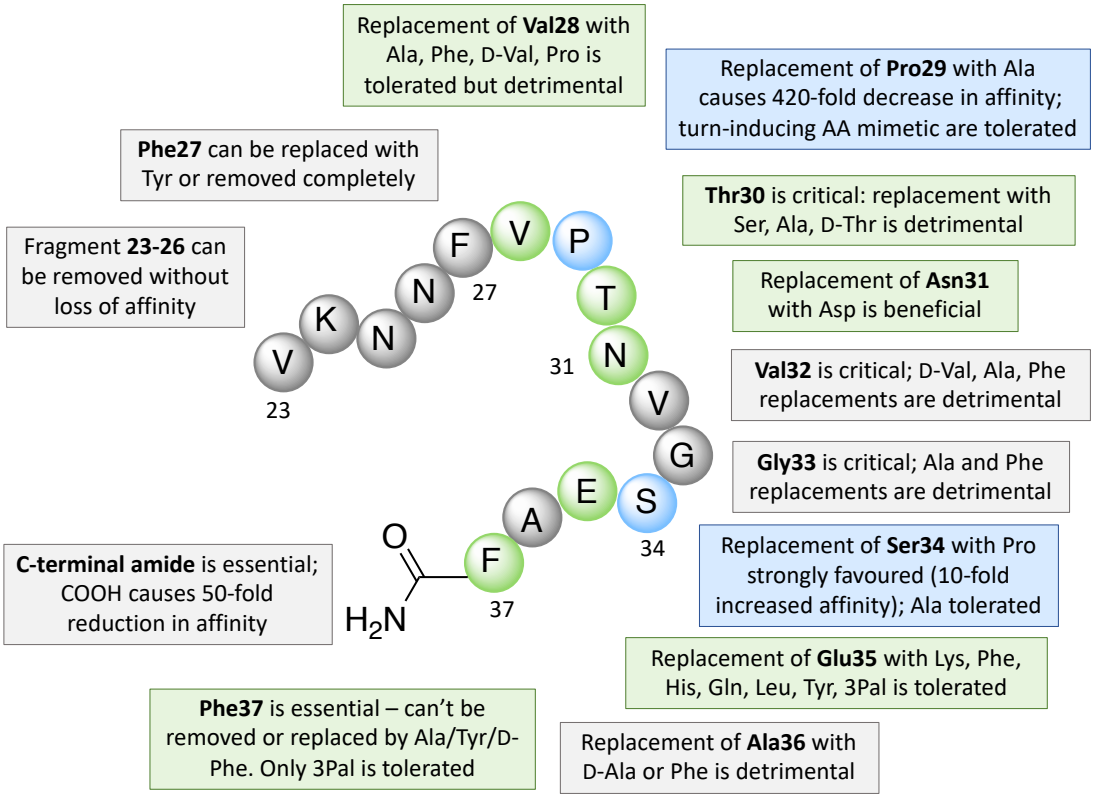

Figure 3.12. Summary of SAR studies on C-terminal segment of CGRP in literature precedent [66,68,180,181]. *3pal is 3-pyridyl-L-alanine.*

Our research group previously reported that the peptide [Pro34, Phe35]-CGRP 27-37 is a potent CGRP-R antagonist both *in vitro* and *in vivo*. *In vitro* activity was studied in SK-N-MC cells with a functional assay detecting inhibition of CGRP-stimulated cAMP accumulation at different concentrations of [Pro34, Phe35]-CGRP 27-37 (K_b = 79 ± 0.8 nM). For *in vivo* activity, the effect of [Pro34, Phe35]-CGRP 27-37 in the presence of CGRP was studied in mice, by subcutaneous injection of agonist and antagonist compounds into one hind paw and testing the resulting extravasation into the surrounding tissue, eventually demonstrating that CGRP-induced plasma protein

extravasation could be significantly reversed by co-administration of the peptide antagonist [23].

From a collaboration between our research group and PharmNovo AB. (now InnoviPharm Ltd.), six novel 8-11 amino acid peptide antagonists of the CGRP-R were designed, synthesised, and tested (Table 3.2, Killoran *et al*., unpublished data). The parent compound from which these analogues were derived is the peptide [Pro34, Phe35]-CGRP 27-37. In all cases (**P001**-**P006**), Phe27 was removed because it is not essential for binding activity, as previously demonstrated by alanine scanning studies [68,180]. Modifications included the substitution of Pro34 with Ala, the replacement of Asn31 with Asp, bearing a carboxylic acid side chain to increase water-solubility, and truncations of the N-terminal Val-Pro motif (**P001**-**P003**). For **P004**-**P006**, Pro34 was retained in the sequence, while Asn31 was replaced with Asp and the effect of truncations of Val-Pro motif was studied. Compared to [Pro34, Phe35]-CGRP 27-37, all the peptide antagonists showed a decrease in antagonist potency and binding affinity. This suggested that the conformational arrangement favoured by the presence of Pro34 results in low energy receptor binding, while the alanine analogue adopts a different conformation that results in challenging binding. On the other hand, sequential truncations of **P006** by removal of Val28, in **P005**, and Val28-Pro29, in **P004**, afforded a lower binding affinity.

Table 3.2. Development of small peptide antagonists of the CGRP receptor (Killoran et al., unpublished data). Modifications from [Pro34, Phe35] CGRP 27-37 are highlighted in bold.

Peptide Name	Sequence	CGRP Antagonist potency (pK_B)	CLR Binding Affinity (pK_i)
***hα*CGRP** [182]	ACDTATCVTHRLAGLLSRSGGVVKNNFVPTNVGSKAF-NH_2	-	9.7
[Pro34, Phe35] CGRP 27-37	FVPTNVG**PF**AF-NH_2	8.1	8.0
P001	T**D**VG**A**FAF-NH_2	6.7	6.8
P002	PT**D**VG**A**FAF-NH_2	6.7	6.8
P003	VPT**D**VG**A**FAF-NH_2	6.9	7.3
P004	T**D**VGPFAF-NH_2	7.5	7.4
P005	PT**D**VGPFAF-NH_2	7.7	7.7
P006 (56)	VPT**D**VGPFAF-NH_2	7.9	7.8

The peptide **P006** (**56**) was selected at this stage for further development in hit-to-lead studies. Modifications comprising fluorination, peptide-peptoid hybridisation, and lipophilic modifications were considered in order to improve the predicted poor pharmacokinetic profile of **P006** and optimise its drug-likeness, in the development of a lead candidate to use for further studies.

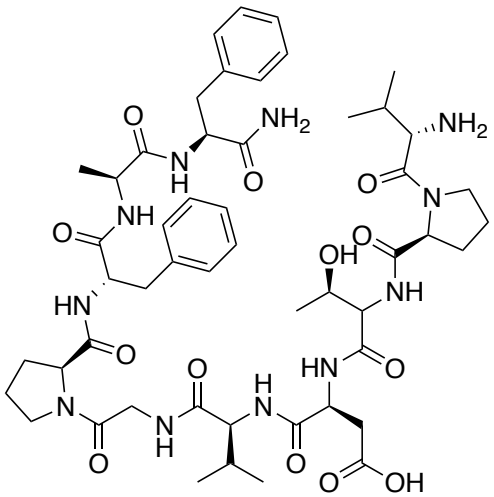

56

Figure 3.13. Peptide P006 structure. pK_b = 7.9.

3.1.3 Modification of peptides via 'fluorine-editing'

3.1.3.1 The role of fluorine in medicinal chemistry

The first example of the application of organic fluorine in the pharmaceutical industry was the development of fludrocortisone (**57**). This was achieved through the introduction of a fluorine atom into the 9α position of cortisol, by reaction of the corresponding alcohol with anhydrous hydrogen fluoride. In 1954, Fried and Sabo demonstrated that this modification increased glucocorticoid activity by a factor of 10 [183–185]. Another early example of synthetic fluorinated drug dates back to 1957, when the antineoplastic agent 5-fluorouracil (5-FU, **58**) was first synthesised [186]. 5-FU acts as an antimetabolite of uracil and, through inhibition of thymidylate synthase (TS), has a remarkable anti-tumour activity [185]. These two drugs (Figure 3.14) constituted a breakthrough in the role of fluorine in the design and development of biologically active compounds.

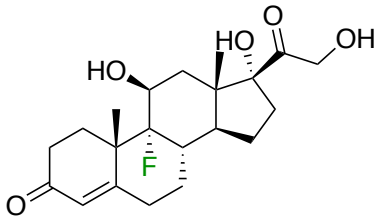

Fludrocortisone

57

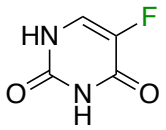

5-Fluorouracil

58

Figure 3.14. Chemical structures of the first two fluorinated drugs approved.

In contemporary medicinal chemistry, fluorination is considered a powerful tool not only to increase the therapeutic index – i.e., the range of doses at which a drug is effective without unacceptable adverse events – but also to tune pharmacokinetic, physicochemical (e.g., pKa values of neighbouring functional groups and hydrophobicity), and conformational properties, and to improve target affinity of pharmaceutical products [144,184,186,187]. Nowadays, 'fluorine-scanning' and/or 'fluorine-editing' is a routine procedure in drug discovery [188]. Fluorinated compounds now play a central role in healthcare, being present in more than 200 clinically approved small molecule drugs (around 20-30% of all the drugs and more than 50% of the so-called blockbuster drugs) [188–191]. Approved drugs containing

fluorine include anti-cancer agents, antibiotics, antidepressants, anti-migraine medicines, anti-inflammatory drugs, anaesthetics, antiacids, and neuroleptics [144,184,186,188].

Of pivotal importance to the focus of this research were the FDA approvals of two fluorinated antagonists of the CGRP-R, ubrogepant (**59**, Ubrelvy™, December 2019), developed by Allergan and licensed by Merck, and atogepant (**60**, Qulipta ™ September 2021, Abbvie), the first and only oral CGRP-R antagonists specifically developed for the preventive treatment of episodic migraine. Of interest is also the fluorinated small molecule CGRP-R antagonists telcagepant (**61**), a drug candidate from Merck which reached Phase III clinical trial for treatment of migraine but was then excluded due to liver toxicity, but also olcegepant (**62**), a CGRP-R antagonist containing two bromine atoms on a 4-OH-benzyl ring. This evidence suggests that the judicious use of halogens in CGRP-R antagonists does not interfere with receptor binding, while it may result in improvements of molecules' drug-likeness [24,192–196].

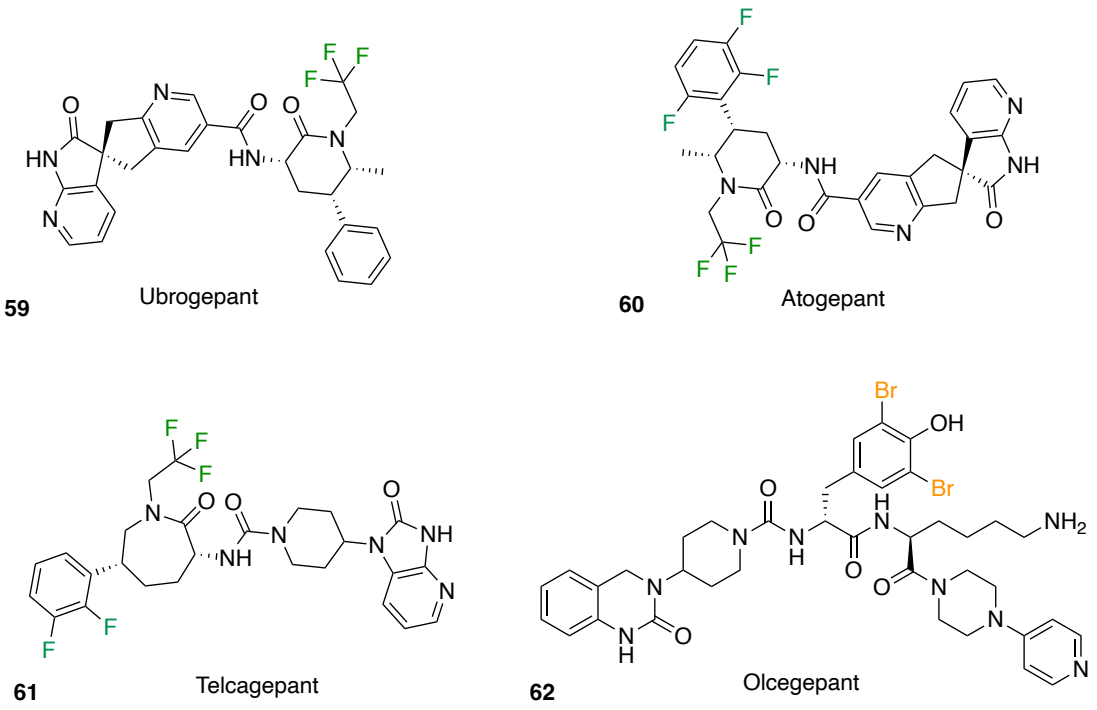

*Figure 3.15. Chemical structures of small molecule antagonists of CGRP-R containing halogens: ubrogepant (**59**), atogepant (**60**), telcagepant (**61**), and olcegepant (**62**).*

However, the presence of organic fluorine in peptide and protein therapeutics is relatively low compared to that of small molecules. As underlined in the work undertaken with PepTherDia, as of 2020, the only peptide therapeutic agent containing fluorine atoms on the market is Voxilaprevir (**24**), used in combination with Sofosbuvir/Velpatasvir in Vosevi to treat chronic Hepatitis C [139].

It is possible that, in the future, fluorinated peptides will become key players in the pharmaceutical market due to their improved drug-likeness properties compared to nonfluorinated counterparts [144].

3.1.3.2 Fluorinated amino acids

Despite the lack of fluorinated approved peptides, a large selection of fluorine-containing amino acids (F-AAs) is commercially available [197]. The introduction of F-AAs into peptides/proteins has a variety of applications, ranging from conformational investigation *via* ^{19}F NMR to tuning molecules properties [198–202]. Replacement of problematic natural amino acids with fluorinated bioisosteres (e.g., substitution of cysteine (**63**) with (S)-2-amino-4,4-difluorobutanoic acid (**64**)) may solve problems related to the presence of natural amino acids without altering the overall structure [197]. Moreover, fluorine atoms or fluorine-containing groups may be installed on the natural amino acid proline to study structural aspects of polyproline as well as to induce conformational changes by influencing the *cis-trans* preferences of the amide bond between Pro and any other amino acid, as extensively explained by Verhoork *et al.* [203]. Additionally, the introduction of even a single fluorine atom into the amino acid sequence of a peptide or protein can significantly modify the pharmacokinetic and biological properties. An example is the design of fluorinated analogues of the gut hormone peptide (GLP-1); this study, conducted by Meng and collaborators, showed that the introduction of 5,5,5,5',5',5'-2S-hexafluoroleucine (**65**) into GLP-1 at strategic sites retains efficacy while conferring resistance against its regulatory protease, dipeptidyl peptidase-4 (DPP IV) [201]. Other studies have investigated the effect of the substitution of fluorinated amino acids on the stability

towards enzymatic digestions [198–200]. Finally, a recent study from the Koksch group have investigated the replacement of a critical Ile residue within an approved peptide-based fusion inhibitor (enfuvirtide) with fluorinated amino acid analogues (difluoroethylglycine (**66**), 5,5,5-trifluoroisoleucine (**67**), and 5,5,5,5',5',5'-hexafluoroleucine (**65**)), confirming the concrete great interest of numerous research groups in fluorine-editing of drugs [187].

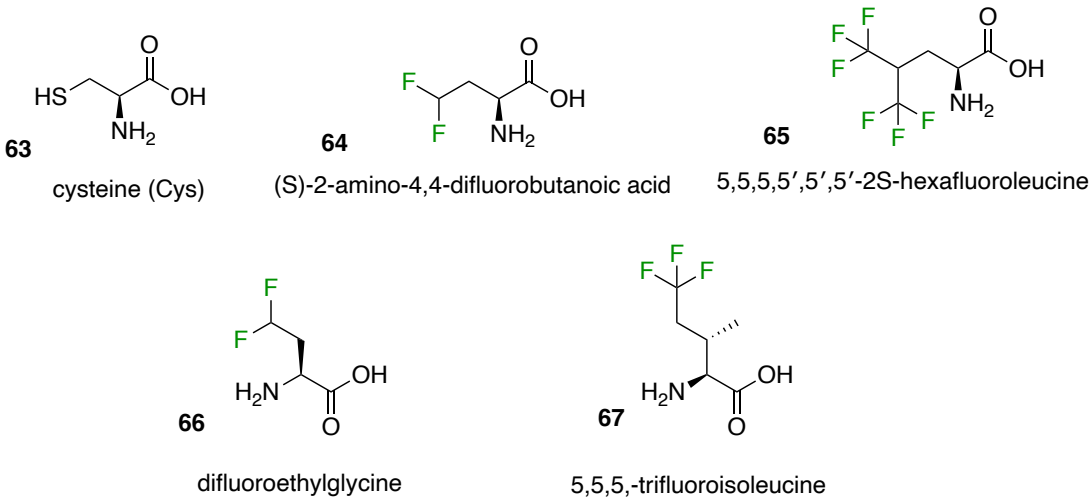

*Figure 3.16. Structures of cysteine (**63**), (S)-2-amino-4,4-difluorobutanoic acid (**64**), and 5,5,5,5',5',5'-2S-hexafluoroleucine (**65**), difluoroethylglycine (**66**), 5,5,5-trifluoroisoleucine (**67**).*

Among the aromatic amino acids, the behaviour of fluorinated phenylalanine has been extensively studied; nowadays, a large number of fluorinated Phe analogues are commercially available (Figure 3.17), the majority at an affordable price, which makes them more attractive than other fluorinated amino acids.

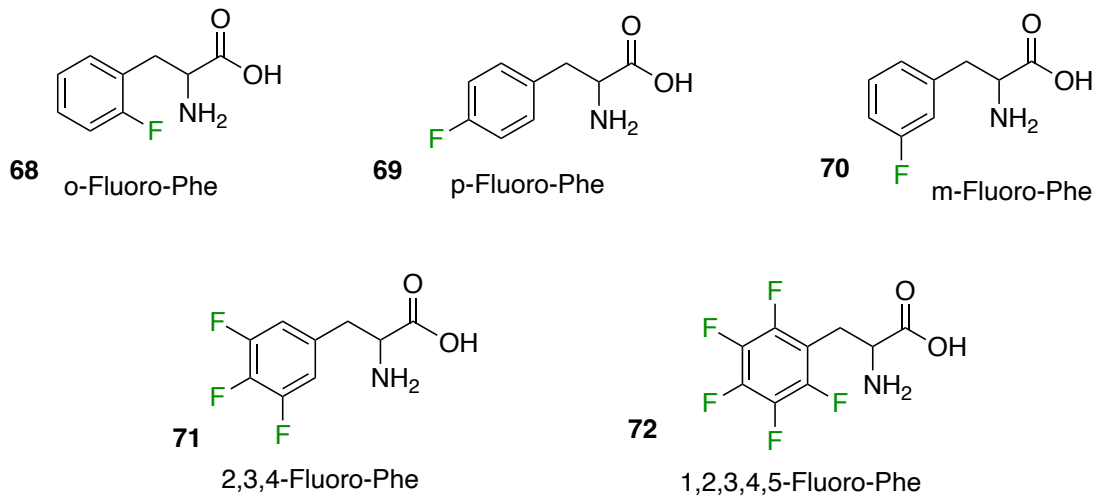

Figure 3.17. Commercially available fluorinated phenylalanine structures.

The substitution of fluorine for hydrogen on the aromatic ring of the natural amino acid phenylalanine results in a rearrangement of the electrostatic potential, a decrease in polarizability, and an increase in strength of the covalent bond to carbon [204,205]. This results in the modulation of a number of properties of the analogue. Specifically, fluorination of Phe may eventually tune acidity/basicity, conformation and geometry, lipophilicity of the aryl side chain, and finally, the activity and bioavailability of the counterpart peptide [205].

It is generally accepted that the replacement of hydrogen atoms with fluorine results in an increase in hydrophobicity. However, some exceptions to this generalisation have been highlighted [206]. In fact, while the substitution of a single H on the aromatic ring causes, in general, minor perturbation of lipophilicity, the significant increase in size of polyfluorinated Phe should be careful assessed as it may result in destabilisation of the molecule due to steric repulsion. On the other hand, the presence of multiple fluorine atoms on the aromatic ring may enhance attractive interactions with non-fluorinated phenyl rings [204].

In peptide design and development, monofluorinated phenylalanines have been used to study the role of fluorine in membrane binding properties and activity of antimicrobial peptides, revealing that 4-F-Phe residues (**69**) are deeply embedded in

the hydrophobic region of the SDS micelles used to resemble the bacterial cytoplasmic membrane [207].

In general, greater alteration is afforded when Phe is replaced with phenylalanine residues bearing multiple fluorine atoms. In particular, pentafluorophenyalanine (F_5-Phe, **72**) was used in a study on the influence of *i, i* + 4 aromatic side chain to side chain interactions on α-helix stability, showing that Phe – F_5-Phe greatly enhanced helicity of peptides [208]. Moreover, Geurink *et al*. demonstrated that incorporation of F_5-Phe (**72**) in proteasome inhibitors yielded one of the most β5 selective inhibitors [209], while Senguen and collaborators focused its effect on the self-assembly of the amyloid β-fragment Aβ(16-22), concluding that fibrils formation is influenced together by the aromatic, hydrophobic, and steric nature of the amino acids [210]. Finally, Tantry *et al*., used both mono- and poly-fluorinated Phe residues to study the interactions between the 13-membered α-factor peptide and the G-protein coupled receptor Ste2p [211].

3.1.3.3 'Fluorine-editing' in peptide CGRP-R antagonists

Given the favourable effects of the introduction of fluorine atoms in peptides and that this has not been explored for peptidic CGRP-R antagonists, our research group explored the effect of 'fluorine-editing' on P006. Previous work from our group included the use of fluoroprolines substitutions in positions 29 and 34 of P006. Pro29 and Pro34 are proposed to play a pivotal role in stabilising bioactive conformation of the truncated analogues: adoption of a type I β-turn centred at Pro29 and a γ-turn centred at Pro34 have been confirmed through a combination of molecular dynamics, NOE NMR, and infra-red experiments [180]. Pro29 is generally tolerant to substitution with turn-inducing amino acids, yet replacement with Ala led to a 420-fold decrease in affinity for the CGRP-R [181]. On the other hand, the replacement of Ser34 with Pro in CGRP 27-37 brought about a 10-fold increase in receptor affinity and any further modification resulted to be detrimental [66,181]. Therefore, former members of our research group replaced independently, and in combination, each proline of P006 with 4*R*-fluoro, 4*S*-fluoro, or 4,4-difluoro proline to probe

conformational sensitivity at each position and to understand conformational requirements to improve binding affinity. Despite the relatively minor modification, fluorination at proline residues proved to have a profound effect upon biological activity, confirming that, while Pro29 is more tolerant to modifications, the introduction of fluorine at Pro34 was deleterious in each case (Killoran *et al*., unpublished data). However, this work was useful in estimating the population of *cis* vs *trans* peptidylprolyl bond conformers at each fluoroproline residue through ^{19}F NMR analysis.

Considering the tuning of physicochemical properties and, in turn, pharmacokinetic properties via fluorine addition, a feasible option would be the fluorination of Phe35 and/or Phe37 of P006 to provide additional hydrophobicity without causing disruption of conformation. In fact, the small molecule antagonists atogepant (**60**), telcagepant (**61**), and olcegepant (**62**) contain hydrophobic aromatic motifs (i.e., 2,3-difluorophenyl-, 2,3,6-trifluorophenyl-, and 3,5-dibromo-4-hydroxyphenyl-, respectively), that likely mimic the Phe35 residue of peptide CGRP-R antagonists [192,193,212]. A local increase of hydrophobicity at these positions may result in enhanced affinity for the receptor, as well as more favourable pharmacokinetic properties.

3.1.4 Peptoids and peptide-peptoid hybrids

As discussed in previous chapters, natural amino acid containing peptides present several limitations due to their intrinsic physicochemical properties and pharmacokinetic profiles. However, these limitations may be overcome through transformation into stable mimics with similar biological effects to their parent peptide but with higher target specificity, greater stability and enhanced cell membrane penetration [70,213].

Peptoids (N-substituted polyglycines) are oligomeric synthetic polymers in which the amino acid side chain is relocated from the α-carbon to the adjacent backbone nitrogen atom of the peptide bond (Figure 3.18) [214]. This subtle structural modification confers to the peptoids various advantages; most importantly

significantly enhanced resistance to proteolysis that provides them with wide opportunities for biomedical applications [215]. Other advantages include, ease and economy of synthesis, high flexibility, achirality, non-immunogenicity, backbone variability and greater side-chain chemistry possibilities [214,216]. Various potential therapeutic applications of peptoids are described in the literature, such as antimicrobial agents against *Pseudomonas Aeruginosa* [217], *Mycobacterium Tuberculosis* [218], and *Escherichia Coli* [219], Alzheimer's disease treatment [220], cholecystokinin (CCK) receptors antagonistic activity [221], neuroprotective action in brain inflammation [222], and diagnosis and treatment of cancer [223]. Moreover, their low immunogenicity and capacity for intranasal administration make peptoids a novel and valuable neurotherapeutic path [214,221]. Finally, polypeptoids have been studied as a promising class of bioinspired polymers, having unique properties that fill the material gap between proteins and bulk polymers [224].

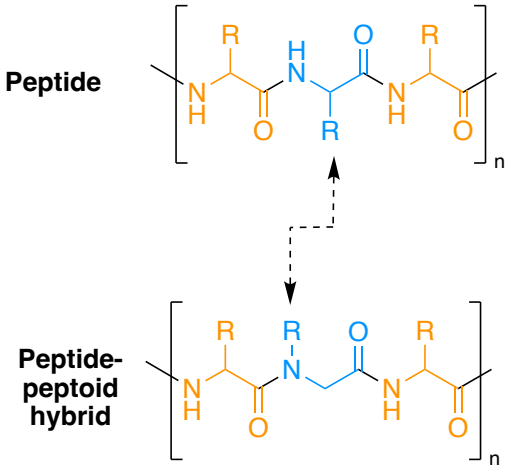

Figure 3.18. The structural difference between peptides and peptide-peptoid hybrids.

3.1.4.1 Peptoid synthesis

Peptoid synthesis has been approached with two different strategies, as shown in Figure 3.19. The monomer approach is analogous to Merrifield's Fmoc solid-phase peptide synthesis method [161,225]. The submonomer method**,** pioneered by Zuckermann *et al.*, considers the peptoid chain as a copolymer composed by a succession of acetate and amine units [226]. This process consists of two chemical

steps: acylation with readily available haloacetic acid (commonly, bromoacetic acid) and N,N'-diisopropylcarbodiimide (DIC) as activating agent, followed by a nucleophilic displacement with a monosubstituted amine. In this case, there is no need for protecting groups on the main chain as the two chain-elongation steps are self-limiting [226]. This approach presents the advantage of avoiding tedious synthesis and deprotection steps of the N-terminal Fmoc-protected glycine building block as well as its complete control over chain length, side-chain chemistry and monomer sequence [216,227]. Finally, the submonomer approach is automatable making it suitable for microwave automated synthesis, as proven in 1992 by Zuckermann *et al.* [226].

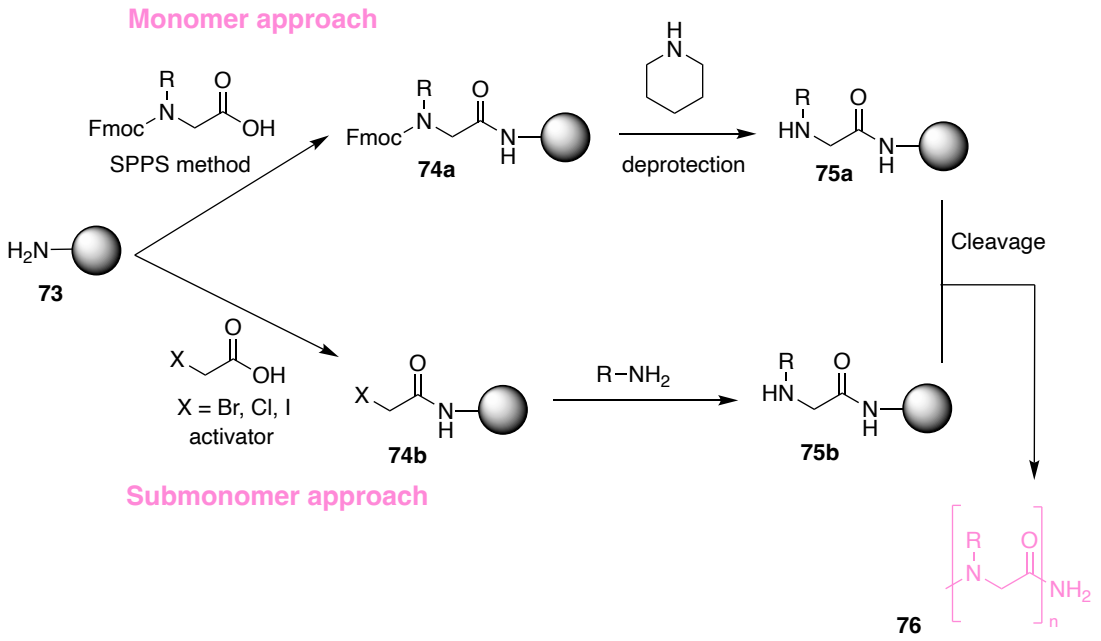

Figure 3.19. Reaction schemes for monomer and submonomer approaches used for peptoid synthesis.

3.1.4.2 'Peptoid-editing' on CGRP-R antagonists

The use of peptoids in CGRP-R antagonist discovery is still an unexplored yet interesting field, as this structural modification may promote enhanced biological stability. However, while significantly improving pharmacokinetic properties of peptides, the replacement of amino acids with structural isomers – i.e., peptoid monomers – may affect the activity at the receptor site due to a lack of hydrogen

bond donors and presence of tertiary amide bonds [214,228]. Hence, a study of the effects of peptoid replacement in each independent position of P006, through peptoid-scanning, is a means to identify residues tolerant to relocation of the side chain and, at the same time, beneficial for stability. Once replaceable residues have been identified, these modifications can be combined and this, in turn, may result in the design of a potent antagonist with enhanced resistance to peptidase activity.

3.1.5 Modification of peptides via lipidation

3.1.5.1 Lipidation of peptides

In the last decades, many modifications have been studied in an attempt to boost the properties of peptides. Lipidation, developed in the mid-1990s while researching strategies to prolong insulin half-life, is probably the most important modification used to convert peptides into drug leads [73]. As of 2020, 13% of the peptides on the market contained a lipophilic carbon chain, confirming the success of this modification [139]. There are three different ways to obtain a lipidated peptide, based on the type of lipid bond formation method used with either the peptide backbone or with side chains; these include amidation, esterification, and S-bond (thioether or disulfide) formation, involving lysines, cysteines, or N-termini [136,229].

Lipid-acylation of peptides provides a simple way to modulate peptide physicochemical properties, in particular peptide lipophilicity that, in turn, affects the absorption, distribution, metabolism, and excretion (ADME), as well as bioavailability [136,230]. One of the main drawbacks of peptides is their poor oral bioavailability (usually below 1%), mainly due to their liability to peptidase metabolism, but also due to their relatively high molecular weight, which limits peptides to paracellular absorption, and their excessive hydrophilicity, which prevents them from penetrating cell membranes [231]. These issues may be overcome through the introduction of lipophilic groups that results in a reduction of hydrogen bond potential. Moreover, conjugation of lipids to peptides is expected to increase their half-life by stabilising the structure and increasing binding to human serum albumin, which sequesters them from circulation, preventing degradation and eventually

improving their circulating time [73,230,232,233]. Finally, an important feature of lipidated peptides is their tendency to form self-assembling structures (e.g., micelles, vesicles, tubules, nanofibers) and aggregates which may, in turn, protect them from metabolism and prolong their half-life [73,136].

3.1.5.2 N-terminal modifications

Among lipidation methods at various sites of the peptide sequence, the N-terminal position is an attractive target, because, generally, there is only one such group within a peptide molecule [229]. This is a common strategy in protein design too, as the N-terminus is typically exposed to solvent and offers unique sites for many protein targets [234]. The terminal amine functionality can be modified with an acetyl group, small alkyl groups (e.g., ethyl, propionyl, butyryl, isobutyryl, pentanoyl, and hexanoyl), bigger alkyl groups (decanoyl, undecanoyl, and octanoyl), or aromatic groups (e.g., Fmoc and benzoyl) [68,235,236].

In some cases, these potentially beneficial changes may result in a partial (or total) loss of biological activity [231]. However, this should not prevent researchers from exploiting N-terminal modifications in peptides and proteins; in fact, even in the case of a decrease in binding affinity and/or potency compared to the parent peptide, the N-terminally modified analogues may benefit from greater stability and have the best *in vivo* efficacy, eventually demonstrating that a reduction in binding affinity can be largely counterbalanced by increased *in vivo* stability [236].

The idea of capping the N-terminus of a peptide with a lipophilic carbon chain to tune its properties can be expanded further to include modifications that go beyond the conjugation of fatty acids. A field that has seldom been explored is the conjugation of benzoyl derivatives at the N-terminal end of a peptide to increase lipophilicity without dealing with a long carbon chain.

Few examples of the use of benzoyl moieties have been reported. Sonzini *et al*. incorporated a fluorinated benzoyl moiety (3,5-bis(trifluoromethyl)-benzoic acid) in a short amyloid β sequence to explore the possibility of recording Transmission Electron Microscopy (TEM) images without any staining procedure [237]. Moreover,

introduction of benzoyl moieties by benzoyl derivatization of primary amines of short peptides has been studied by Julka *et al*. as a tool to enhance sequence coverage in tryptic peptide mapping, by obtaining an increase in chromatographic retention time [238]. Another study included the coupling of N-(ferrocenyl) benzoic acids to tri- and tetra-peptide ethyl esters of glycine [239].

3.1.5.3 Effect of N-terminal benzoylation on peptide CGRP-R antagonists

As opposed to fluorination and peptoid replacement, the effect of N-benzoylation on binding affinity of CGRP derivatives has been explored by two research groups. Smith and colleagues described N-benzoylation of CGRP 8-37, showing a 53-fold increase in affinity compared to CGRP 8-37 [240]. Yan *et al*. from Lilly Research Laboratories (Indianopolis, USA) evaluated the possibility of N-benzoylating cyclic peptide CGRP-R antagonists, and demonstrated that no losses in activity were obtained with this modification; however, the solubility of the benzoyl cyclic analogues (~0.02 mg/mL) was too low to proceed with *in vivo* studies [68]. The most relevant compounds from this work are summarised in Table 3.3.

Table 3.3. Relevant compounds from Yan et al. work [68]*. Modifications from CGRP 27-37 are highlighted in bold. Antagonistic data are reported as K_b obtained from SK-N-MC cells, using a cAMP accumulation fluorescence assay kit. 3-Hyp = 3-OH-proline, Bz = benzoyl, 3Pal = 3-pyridyl alanine, Dap = diaminopropionic acid.*

No.	Sequence	K_b (nM)
3	FVPT**D**VG**PF**AF-NH_2	1.72 ± 1.19
4	FV-**3-Hyp**-T**D**VG**PF**AF-NH_2	1.12 ± 1.51
14	**Bz**-TDV-**cyclo**[**C**G**PFC**]-F-NH_2	> 100
23	**Bz**-V**Y**-**cyclo**[**C**TDVG**PFC**]-F-NH_2	0.126 ± 0.042
35	(**4-F-Bz**)-**v**Y-**cyclo**[**C**-**Dap**-**D**VGPF**C**]-**3Pal**-NH_2	0.0491 ± 0.0032

3.1.6 Assays for quantifying CGRP-R activation and antagonism

As previously described in Chapter 1, the effects of CGRP are mediated by the binding to the CGRP-R complex, a heterodimer of the calcitonin receptor-like receptor (CLR), a class B GPCR, and the receptor activity-modifying protein 1 (RAMP1), a type 1 transmembrane domain protein [241–243].

As with other GPCRs, the CGRP-R activates a range of different protein kinase cascades, notably cAMP-dependent protein kinase, and CGRP-R activation can be studied by monitoring cAMP accumulation. This can be measured using a range of commercially available kits – e.g., Eurofins DiscoverX kit, Creative Biomart kit, R&D System kit, and cisbio cAMP Gs dynamic kit (cisbio PerkinElmer) [244–246].

In particular, the cAMP Detection Assay (Eurofins; DiscoverX) is described as an easy-to-use high-throughput assay that detects cAMP production in cells using Enzyme Fragment Complementation (EFC). In this assay, two recombinant β-galactosidase fragments – a large protein fragment, the enzyme acceptor (EA), and a small peptide fragment, the enzyme donor (ED) – only when combined form an enzyme that hydrolyses a substrate to produce a chemiluminescent signal [244]. To obtain a luminescent signal proportional to the levels of intracellular cAMP, the ED fragment is labelled with cAMP. A separate cAMP antibody competes with the EA fragment to inhibit formation of the active enzyme complex. Changes in the amount of intracellular cAMP levels affect the levels of free cAMP antibody available to bind to the ED: the higher the concentration of cAMP, the greater the amount of antibody bound to it, leaving the ED free to form the active enzyme complex that hydrolyses the substrate to produce a luminescent signal [247]. A representation of the assay principle is shown in Figure 3.20, while Figure 3.21 shows a schematic protocol of the assay.

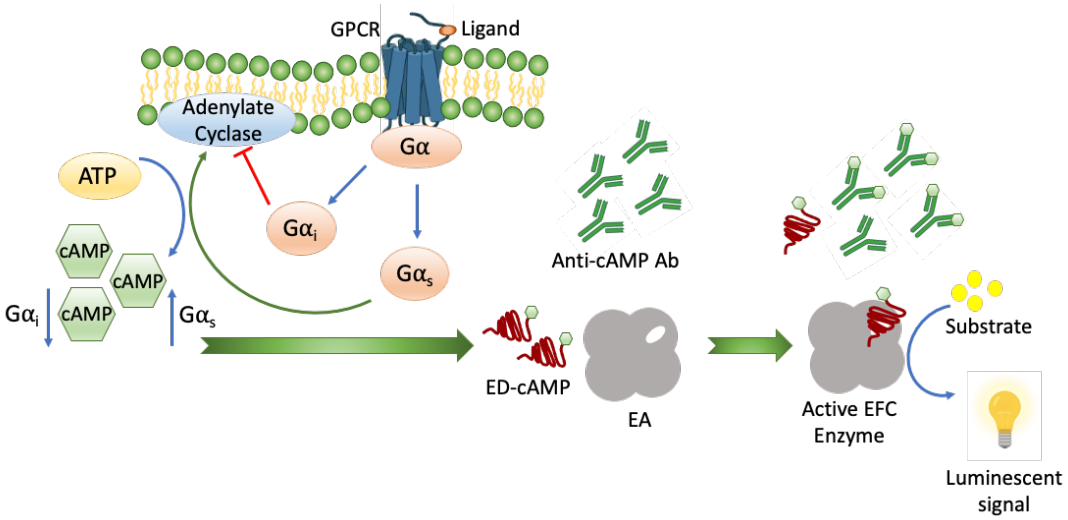

Figure 3.20. cAMP Hit Hunter eXpress (DiscoverX-Eurofins) GPCR Assay principle.

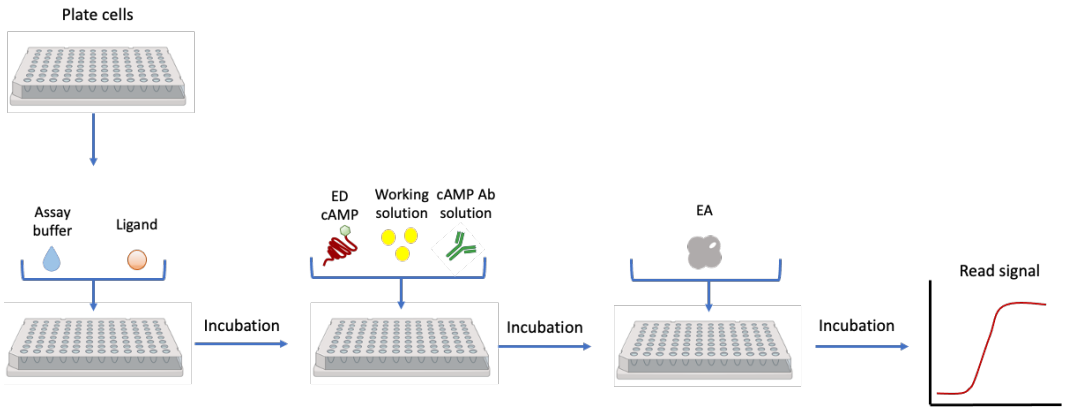

Figure 3.21. cAMP Hunter eXpress GPCR Assay Schematic Protocol.

3.1.7 Cytotoxicity assay – Alamar Blue

An ideal test for *in vitro* proliferation and cytotoxicity should be easy-to-use, rapid, efficient, reliable, sensitive, safe, and cheap. These requirements are met by the Alamar Blue cytotoxicity test, used for the past 50 years to assess cell viability and cytotoxicity of compounds [248–250].

As shown in Figure 3.22, Alamar blue monitors the reducing environment of living cells by detecting the presence of molecules produced by the mitochondrial respiratory chain (i.e., $NADH/H^+$ and $NADPH/H^+$) which reduce resazurin (blue and nonfluorescent, **77**) to resorufin (pink and highly fluorescent, **78**) [248,250,251].

Thus, given that only living (and metabolically active) cells produce molecules that can reduce resazurin to resorufin, high fluorescence in a sample indicates the presence of viable cells. Moreover, the fluorescent signal, measured at an excitation wavelength of ~530-560 nm, and an emission wavelength of ~590-600 nm, is proportional to the number of living cells in the sample [250].

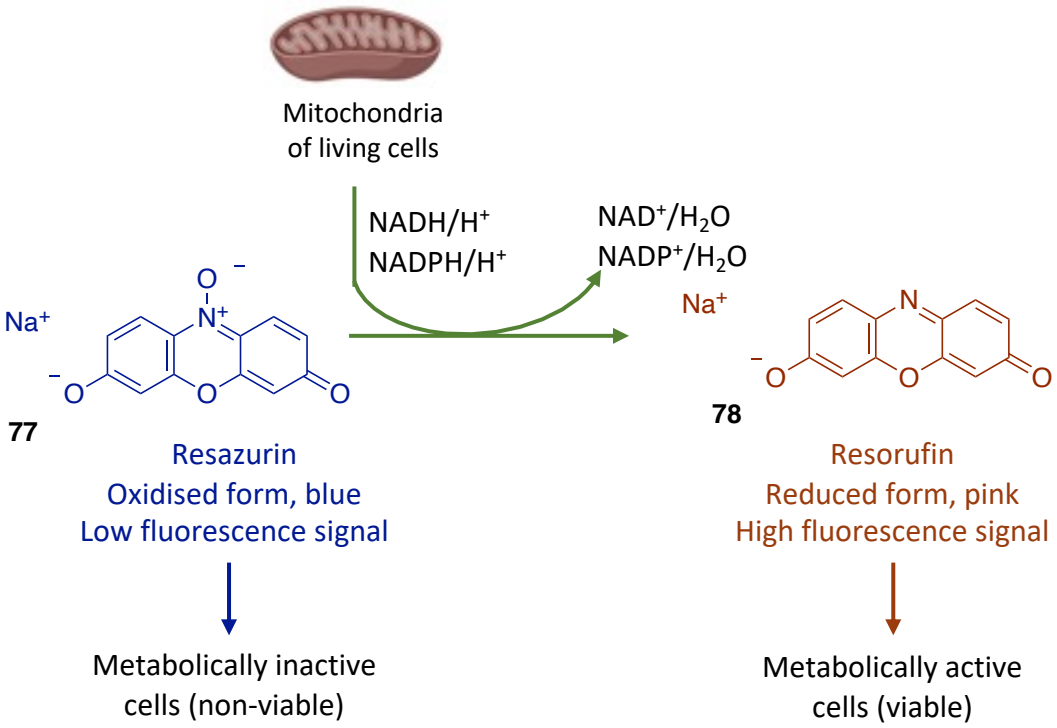

*Figure 3.22. Mechanism of resazurin (**77**) reduction to resorufin (**78**) by NADH and NADPH molecules produced by mitochondria of metabolically active cells* [251].

3.2 Aims and Objectives

The aim of the work reported in this chapter was to design, build and test a library of peptide antagonists of the CGRP-R *via* modification of **P006**, a potent CGRP-R antagonist. Modification strategies included fluorination, peptoid replacement, and N-terminal lipidation. Characterisation of peptides involved RP-HPLC for purity assessment, LC-MS and LC-MS/MS for mass identification, and ^{19}F NMR, where possible, to study peptide conformation. The effect of the above-mentioned modifications on lipophilicity was assessed through experimental shake-flask method, *in silico* predictions, and hydrophobicity index derived from RP-HPLC retention time. Finally, antagonist potency was studied by cAMP accumulation assay, while *in vitro* toxicity was evaluated through the Alamar Blue cytotoxicity test (experiment performed by Giulia Scagnetti, PhD student at LJMU).

3.3 Materials and Methods

3.3.1 Materials

All Fmoc proteinogenic L-amino acids (CEM), Fmoc-sarcosine (Fmoc-Sar; Novabiochem), Fmoc-fluorinated amino acids (Fluorochem UK), Rink Amide ProTide resin (100-200 mesh, 0.56 mmol/g; CEM), N,N'-diisopropylcarbodiimide (DIC; Sigma), Oxyma Pure™ (CEM), N,N-dimethylformamide (DMF; Acros Organics), bromoacetic acid (Acros Organics), benzylamine (Acros Organics), isopropylamine (Sigma), t-Butyl glycine ester (Alfa Aesar), N,N-diisopropylethylamine (DIPEA; Sigma), piperidine (Sigma), benzoyl chloride (Alfa Aesar), trifluoroacetic acid (TFA; Sigma), triisopropylsilane (TIPS; Sigma), Phosphate Buffered Saline (PBS) tablets (unless otherwise stated, tablet formulation: sodium chloride 137 mM, phosphate buffer 10 mM, potassium chloride 2.7 mM, Fisher Chemicals), 1-octanol (Alfa Aesar), 2,3,4,5,6-pentafluorobenzoyl chloride, and 4-fluorobenzoyl chloride (Fluorochem UK) were purchased from commercial suppliers and used without further purification steps. Solvents for liquid chromatography (i.e., acetonitrile HPLC-grade, methanol HPLC-grade) were purchased from Fisher Scientific UK.

CHO-K1 CALCRL RAMP1 cells and reagents for cAMP detection were purchased from Eurofins (DiscoverX, Part#95-0164E2; Lot#16A0503 and #19F2604) and used as described in the appropriate experimental procedures. Human lung adenocarcinoma cell line (Calu-3) was purchased from American Type Culture Collection (ATCC). Dulbecco's Phosphate Buffered Saline (DPBS) solution (Gibco), Dulbecco's Modified Eagle Medium: Nutrient Mixture F-12 (DMEM/F-12, Gibco), Minimum Essential Media (MEM, Sigma), TrypLe (Gibco), Foetal Bovine Serum (Sigma), Pen/Strep (10,000 units penicillin and 10 mg streptomycin/mL) (Sigma), resazurin (Sigma) were purchased from commercial suppliers and used without further treatment.

3.3.2 Standard methods for solid-phase peptide synthesis

3.3.2.1 Prediction of difficult coupling reactions

The Peptide Companion Excel spreadsheet was used to predict difficult couplings within the peptide sequences (http://www.spyderinstitute.com/software.html). Peptides were examined with this tool to predict challenging coupling steps requiring double coupling to increase the likelihood of high synthesis yields.

3.3.2.2 Microwave-assisted automated solid peptide synthesis

Peptides were prepared using automated Fmoc-SPPS methods on a Liberty Blue microwave-assisted peptide synthesiser (CEM). Solid phase synthesis was conducted at 0.1 mmol scale using Rink amide ProTide resin (179 mg, 0.56 mmol/g loading)*. Amino acid coupling reactions were performed employing the required Fmoc-amino acids (0.2 M in DMF, 5 eq.) with DIC (1 M in DMF; 10 eq.) and Oxyma Pure™ (1 M in DMF, 5 eq.) and Fmoc deprotection was performed with piperidine (20% *v/v* in DMF, 4 mL). Standard coupling procedures employed single coupling of each amino acid (2.5 min, 90˚C).

* With the exception of CGRP 8-37 which was prepared using Rink amide ProTide resin (556 mg, 0.19 mmol/g loading).

3.3.2.3 Peptide-peptoid hybrid synthesis

Peptide-peptoid hybrids were prepared at 0.1 mmol scale using a Liberty Blue microwave-assisted automated peptide synthesiser (CEM) on a Rink Amide ProTide resin (179 mg, 0.56 mmol/g loading), following the procedure described in the CEM application note ap0116 [252]. Amino acid coupling reactions were performed as described in section 3.3.2.2. Following Fmoc deprotection of the peptide (20% piperidine in DMF, 4mL), peptoid motifs were introduced using the submonomer approach, following a two-step procedure. Acylation was achieved with bromoacetic acid (0.6 M, 4.5 eq., or 2 M, 15 eq., in DMF) and DIC (1 M in DMF, 25 eq.), while nucleophilic displacement was performed with the appropriate primary amine (1.5 M in DMF, 75 eq.). Both acylation and displacement steps were performed twice.

3.3.2.4 N-terminal capping

Upon completion of SPPS synthesis of the appropriate sequence and final deprotection, N-terminal benzoylation was performed manually on resin (100 mg) with benzoyl chloride or benzoyl chloride derivatives (4 eq.) and DIPEA (8 eq.) in DMF (1 mL) in a 10 mL syringe equipped with filter, with shaking at room temperature for 30 min [68]. This procedure was repeated once more, and completion of reaction was checked by the Kaiser test procedure, described in section 3.3.2.5.

3.3.2.5 Kaiser test for coupling completion

For the Kaiser test, two stock solutions were prepared; A) ninhydrin in ethanol (50 mg/mL) and B) phenol in ethanol (4 mg/1 mL) . Approximately 2 mg of resin was added to a 1.5 mL Eppendorf tube, then 5 drops of solution A and 5 drops of solution B were added to the Eppendorf tube and mixed. The tube was heated at 100°C for 5 min. The colour of the resin beads was evaluated. An intense blue colour (Ruhemann's blue) of the resin beads was generated by reaction of ninhydrin with a free primary amine, thus representing an incomplete N-capping (or amino acid coupling), while a yellow/transparent colour was the evidence of a successful capping (or amino acid coupling) [253].

3.3.2.6 Cleavage of peptides and peptide-peptoid hybrids from resin

After completion of the on-resin synthesis, the resin was shrunk in diethyl ether (Et_2O) and the compounds were cleaved from the resin as the C-terminal amide using a cleavage cocktail (3 mL; comprising TFA, TIPS and water (8:1:1 *v*/*v*)) with regular shaking (Eppendorf Thermomixer comfort) at room temperature for 3 h. Following the cleavage step, crude samples were precipitated dropwise in cold Et_2O, kept in the freezer for 30 min to facilitate precipitation, then the suspension was centrifuged (3,500 rpm, 5 min). The isolated pellet was resuspended in diethyl ether and centrifuged again to remove residual TFA. Finally, the isolated solid was dissolved in water (where possible) or in water/MeOH (for LJMU017, LJMU018, LJM027), flash-frozen using liquid N_2, and lyophilised.

3.3.3 General procedures for peptide and peptidomimetic purification

3.3.3.1 Preparative-HPLC

For preparative-HPLC purification, crude samples (10 mg/mL) were purified using Agilent Infinity 1260 equipped with a Waters XBridge Peptide BEH C18 Prep 130 Å column (5 µm particle size, 10 x 150 mm). A gradient elution method used MeOH / H_2O (30 min: from 30 to 99% MeOH, with 0.1% TFA) at a flow rate of 8 mL/min and 50-800 µL injection volumes. The column was kept at room temperature and signals were recorded at 215 nm. Isolated pure compound solutions were concentrated *in vacuo* to remove residual organic solvents. The resulting aqueous solutions were flash frozen with liquid N_2, lyophilised, and stored at -20˚C.

3.3.3.2 Flash chromatography

Flash purification of peptides and peptomers was performed using a Teledyne ISCO Combi*Flash*® NextGen 300+ instrument. Crude samples (8-16 mg/mL; 1mL) were separated using RediSep Rf C18 Gold® 5.5 g cartridges (Teledyne ISCO) with a binary eluent system comprising water (A) and MeOH (B) as mobile phase, from 10% to 90% B in 8.8 min. Flow rate was set at 13 mL/min and wavelengths detected were 214 nm and 254 nm. Solutions containing isolated pure compounds were concentrated *in*

vacuo to remove residual MeOH and the resulting aqueous solutions were flash frozen with liquid N_2, lyophilised, and stored at -20 °C.

3.3.4 Characterisation by HPLC, LC-MS, LC-MS/MS, and ^{19}F NMR

3.3.4.1 Analytical high performance liquid chromatography (HPLC)

Analytical purity of peptides was determined by high performance liquid chromatography (HPLC) with an Agilent 1100 equipped with a Phenomenex Aeris PEPTIDE XB-C18 LC Column (150 x 4.6 mm, particle size 3.6 µm), by measuring the UV absorbance at 215 nm. Samples were prepared by dissolving the compounds in water. The HPLC was used with a two-component system of H_2O/0.05% TFA, and MeCN/0.05% TFA for a run time of 20 min at a flow rate of 1 mL/min and a temperature of 65˚C. After analytical method optimisation (see section 4.4.2.3), the elution method was set up as follows: from 0 to 10 min, a gradient was applied from 80% H_2O/0.05% TFA to 40% H_2O/0.05% TFA, after which the system was flushed with 95% MeCN/0.05% TFA for 2 min and, finally, equilibrated back to initial conditions for 8 min. Operating pressures were in the range of 150-200 bar.

3.3.4.2 Low-resolution LC-MS analysis

Characterisation of crude and purified compounds was performed with an oa-TOF mass spectrometer (Waters LCT), using an XBridge (Waters) C18 analytical column (5 µm particle size, 4.6 x 150 mm) with a binary eluent system comprising MeCN / H_2O (20 min gradient: from 90% H_2O/10% MeCN to 100% MeCN with 0.1% formic acid) as mobile phase. Operating pressures were in the range of 2000-3000 PSI. Electrospray ionisation mass spectrometry was conducted in positive ion mode (*m*/*z* range: 600–1700) using a cone voltage of 50 V, desolvation temperature of 300 °C and source temperature of 100 °C. Exact mass measurements of the products were based on the protonated molecules $[M+H]^+$.

3.3.4.3 High-resolution (accurate) LC-MS analysis

Purified peptides and peptomers were analysed using an Agilent 1260 Infinity II LC system with Agilent 6530 Accurate-Mass QToF spectrometer, using an Agilent

ZORBAX Eclipse Plus C18 Rapid Resolution HD analytical column (1.8 µm particle size, 2.1 x 50 mm) with a binary eluent system comprising MeCN / H_2O with 0.1% formic acid (from 1% to 99% MeCN over 12 min gradient) as mobile phase. Operating pressures were in the range of 2000-3000 PSI. Electrospray ionisation mass spectrometry was conducted in positive ion mode (*m/z* range: 50 – 3200) using a fragmentor voltage of 150 V, gas temperature of 325 °C (flow 10 L/min) and sheath gas temperature of 400 °C (flow 11 L/min). Reference ions were Purine (*m/z* 121.0509) and Hexakis(1H,1H,3H-tetrafluoropropoxy)phosphazine (*m/z* 922.0098) (API-TOF Reference Mass Solution Kit, Agilent). Exact mass measurements of the products were based on the protonated molecules $[M+H]^+$.

3.3.4.4 ^{19}F NMR analysis

NMR spectra for fluorinated peptides were recorded using a Bruker 600 MHz Ascend NMR (operating transmitter frequency offset at field of 600 MHz was ~564.63 MHz) at 298 K. Peptides were prepared at a concentration of 1 mg/mL in purified H_2O and analysed by ^{19}F NMR (64-256 scans, proton decoupled). Where assignment was possible, signal multiplicities were reported as s (singlet), d (doublet), and t (triplet) or combinations thereof; where the signal was too complicated to resolve, this was reported as m (multiplet). Where relevant, signals were referenced to TFA (-76.55 ppm) as an internal standard. Raw data were processed and analysed using Bruker Top Spin (version 4.0.6) and signals were automatically integrated, where possible (4-F-Phe, 4-F-benzoyl, and F_5-benzoyl analogues) or manually integrated (F_5-Phe analogues).

3.3.5 Lipophilicity assessment

3.3.5.1 Software applications to predict cLogP and cLogD at pH 7.4

Calculated LogP values were obtained using ChemDraw (cLogP, version 19.0.1.32), Molinspiration Cheminformatics 2020 web application (miLogP, https://www.molinspiration.com/cgi-bin/properties), and Chemicalize ChemAxon (cLogP, https://chemicalize.com/welcome), while $logD_{7.4}$ was calculated using Chemicalize ChemAxon (cLogD, https://chemicalize.com/welcome).

3.3.5.2 Shake-flask method for LogD evaluation

For LogD assessment at pH 7.4, peptides were dissolved at 300 µM in PBS aq. solution saturated with 1-octanol. Partition experiments were carried out by putting 500 µL of saturated octanol in contact with 500 µL of saturated PBS aq. containing peptide (300 µM) in a 1.5 mL sealed glass vial. The samples were allowed to equilibrate at room temperature under gentle agitation (50 rpm) for 150 h. After this point, samples (100 µL) were taken from the PBS aq. phase, added to a 96-well UV-vis transparent plate, and analysed by spectroscopy (λ=220 nm) using a Tecan Spark 10M plate reader. The absorbance of a blank sample (100 µL of PBS saturated with 1-octanol) was subtracted from the resulting sample absorbance. The concentration in the PBS aq. phase was obtained by comparison with a calibration curve in saturated PBS aq. solution (250, 200, 100, 75, 50, 25, 10 µM) and the concentration in the organic phase was obtained as the difference between the total starting peptide (300 µM) and the peptide in the aqueous phase. Each peptide was tested in triplicate.

3.3.5.3 Determination of peptide hydrophobicity through RP-HPLC

The peptides and peptidomimetics hydrophobicity index derived from RP-HPLC retention time (RT) was obtained using the chromatography method described in section 3.3.4.1. Peptide solutions of 0.125 mg/mL were prepared in H_2O. All RP-HPLC analyses were conducted in triplicate. The difference in RT between P006 and the analogues (Δ RT) was calculated with the following equation:

$$\Delta \mathrm{RT} = RT\ (P006) - RT\ (analogue)$$

Equation 3.1

A software package (https://ispso.unige.ch/labs/fanal/hplc_calculator:en) developed by Guillarme and collaborators was used to calculate the elution composition (% MeCN) of P006 and analogues, taking into consideration the dwell

volume of the system and the specific HPLC method conditions. The difference between P006 elution composition and the analogues elution composition (Δ %MeCN) was calculated with the following equation:

$$\Delta\ \%\mathrm{MeCN} = \%MeCN\ (P006) - \%MeCN\ (analogue)$$

Equation 3.2

3.3.6 Computational alanine-scanning study

A computational alanine-scanning mutagenesis experiment was performed using the BAlaS web application, through a molecular docking engine named BUDE AlaScan (https://pragmaticproteindesign.bio.ed.ac.uk/balas/) [254,255]. Receptor (CGRP-R) and ligand (P006) were loaded in PDB format (6E3Y), the receptor chains and the ligand chain were specified, and the energetic contribution of each residue to the interaction energy ($\Delta\Delta G_{res}$) was calculated with the following equation:

$$\Delta\Delta G_{res} = \Delta Gint_{mut} - \Delta Gint_{wt}$$

Equation 3.3

where $\Delta Gint_{mut}$ is the interaction energy between the ligand and the receptor when the amino acid is alanine, while $\Delta Gint_{wt}$ is the interaction energy between the wild-type ligand and the receptor before mutation.

3.3.7 cAMP accumulation assay

CGRP-stimulated cAMP accumulation was assessed in CHO-K1 CALCRL RAMP1, which were Chinese Hamster Ovary (CHO) cells overexpressing the human CGRP-receptor complex (receptor activity-modifying protein-1 (RAMP1) and calcitonin receptor-like receptor (CLR)), using a commercial kit from Eurofins (DiscoveRx HitHunter Assay Kit). CHO-K1 cells were cultured in DMEM/F-12 supplemented with FBS (10%) and 1% penicillin/streptomycin (10000 U/mL). When 60-80% confluent, cells were washed

with DPBS and detached from T-75 flasks using 5 mL trypsin, followed by addition of complete media to inactivate the trypsin, after which the cells were pelleted by centrifugation at 100 g for 5 min at room temperature. The supernatant was removed, cell pellets were re-suspended in cell plating reagent provided in the kit and the cells were counted using a haemocytometer. $4x10^4$ cells/well were seeded in cell plating reagent into a white-walled, transparent-bottom, 96-well plate and incubated overnight. On the day of the assay, cell plating reagent was aspirated from the plate and replaced with 30 µL of cell assay buffer (DiscoveRx HitHunter Assay Kit). Cells were treated in their respective wells with peptide/peptidomimetic antagonists (7.5 µL, $6x10^{-5}$ M in cell assay buffer, diluted to 10^{-5} M in the plate) and incubated for 15 min at 37°C. Then, increasing concentrations of α-CGRP (from $6x10^{-11}$ M to $6x10^{-6}$ M, 7.5 µL in cell assay buffer) were added and the plate was incubated for 30 min at 37 °C. cAMP accumulation was detected through luminescence reading after cell lysis (achieved with Lysis Buffer provided in the kit) and addition of cAMP DiscoveRx HitHunter assay reagents, as written in the protocol (in this order: cAMP antibody solution, working detection solution containing lysis buffer, and solution A). The chemiluminescent signal was detected using a Tecan Spark 10M plate reader.

Antagonist potency (competitive antagonism) was determined from binding affinity, as indicated by the equilibrium dissociation constant (K_b), which was estimated from the functional assay (cAMP accumulation assay). Each estimated affinity value (K_b, or expressed as pK_b) was calculated from the parallel shift of the agonist (α-CGRP) concentration-response curve in the presence of a fixed concentration of the tested peptide antagonist, using the Schild analysis equations below:

$$K_b = \frac{[B]}{(dr - 1)}$$

Equation 3.4

$$dose\ ratio\ (dr) = \frac{EC_{50}[A_2]}{EC_{50}[A_1]}$$

Equation 3.5

where EC_{50} [A_2] is the EC_{50} in the presence of the antagonist, EC_{50} [A_1] is the EC_{50} in the absence of the antagonist, and [B] is the concentration of the antagonist [256,257].

3.3.8 Cytotoxicity assay (Alamar Blue)

For cytotoxicity determination, Calu-3 cells were grown in Minimum Essential Media (MEM) (Sigma) supplemented with 10% FBS and 1% penicillin/streptomycin (10000 U/mL). Cells grown in T-75 flasks were kept in an incubator at 37°C in a humidified atmosphere of 5% CO_2. Confluent cells (60-80%) were washed with PBS and detached from T-75 flasks using 5 mL of TrypLE solution, followed by addition of complete media to inactivate TrypLE. Afterwards, cells were pelleted by centrifugation at 1,200 rpm for 5 min at room temperature. Supernatant was removed, cell pellets were re-suspended in complete media and the density of the suspension was determined by cell counting using a haemocytometer. Cell density was adjusted to $5x10^4$ cells/mL, and a 96-well plate was prepared by adding 200 μL of cell suspension to each well (10^4 cells/well). The plate was incubated at 37 °C, 5% CO_2 overnight to allow for attachment and recovery. 24 h later, media was removed from wells and replaced with 200 μL of peptide solutions at various concentrations (ranging from 100 μM to 1 mM, three wells for each concentration to control for inter-well variability). The negative control (100% viability) was cells treated with complete media, while the positive control (0% viability) was cells treated with 10% DMSO (dilution in complete media), a highly toxic concentration of DMSO that should kill all the cells. A further control was included to assess the potential cytotoxicity of the solvent used to dissolve the peptide (mock treatment): solutions of DMSO and media were prepared at the same ratio of solvent/media mixtures used to prepare peptide dilutions. 200 μL of each solution was added to the plate as previously described. The plate was incubated at 37°C, 5% CO_2 for 24 h, after which the treatment solution was removed, and the cell layer washed with 200 μL of PBS (Oxoid, BR0014G, pH 7.3; sodium chloride 8.0 g/L, potassium chloride 0.2 g/L, di-sodium hydrogen phosphate 1.15 g/L, potassium dihydrogen phosphate 0.2 g/L). 100 μL of resazurin solution (1 mg/mL in PBS) was added to each well (peptide solutions, controls, mock

treatments). The plate was incubated at 37°C for 3 h. To assess cell viability after treatment, fluorescence was measured at an excitation wavelength of 545 nm and an emission wavelength of 600 nm: as living cells oxidise resazurin (blue, non-fluorescent) to resorufin (red, fluorescent), the amount of resorufin produced by the cells and detected was considered proportional to the number of living cells in each well. The experiment was run two independent times.

3.3.9 Data analysis and statistical analysis

Results were recorded and evaluated with Microsoft Excel (version 16.58) or GraphPad Prism (version 9.3.1). One-way ANOVA was performed using GraphPad Prism to investigate statistical significance of differences between group means. A p value less than 0.05 was considered statistically significant.

3.4 Peptides and peptidomimetics characterisation

The library of peptides and peptidomimetics synthesised is reported in Table 3.4.

*Table 3.4. Library of peptides and peptidomimetics synthesised. Modifications are color-coded in green (fluorination), orange (benzoylation), and pink (peptoids). * data shown in bold have been obtained with LC-MS/MS system (Agilent 1260 Infinity II LC system and Agilent 6530 Accurate-Mass QToF spectrometer). ** by measuring the area under the peak from the HPLC chromatogram. RT = retention time.*

Entry	Sequence	Formula	Exact Mass	Calculated *m/z* $[M+H]^+$	Observed *m/z* $[M+H]^+$ *	Purity (%)**	RP-HPLC RT (min)
P006	**VPTDVGPFAF-NH_2**	$C_{51}H_{73}N_{11}O_{13}$	1047.540	1048.5400	**1048.55055**	96.6	5.424
LJMU011	**VPTDVGPFA-4-F-Phe-NH_2**	$C_{52}H_{73}FN_{10}O_{13}$	1064.530	1065.5300	**1066.54100**	95.0	5.668
LJMU012	**VPTDVGP-4-F-Phe-AF-NH_2**	$C_{52}H_{73}FN_{10}O_{13}$	1064.530	1065.5300	**1066.53710**	94.3	5.633
LJMU013	**VPTDVGP-4-F-Phe-A-4-F-Phe-NH_2**	$C_{52}H_{72}F_2N_{10}O_{13}$	1082.520	1083.5200	**1084.52984**	98.0	5.850
LJMU014	**VPTDVGPFA-F_5-Phe-NH_2**	$C_{51}H_{68}F_5N_{11}O_{13}$	1137.490	1138.5000	**1138.49881**	90.3	6.589
LJMU015	**VPTDVGP-F_5-Phe-AF-NH_2**	$C_{51}H_{68}F_5N_{11}O_{13}$	1137.490	1138.5000	**1138.49917**	92.3	6.601
LJMU016	**VPTDVGP-F_5-Phe-A-F_5-Phe-NH_2**	$C_{51}H_{63}F_{10}N_{11}O_{13}$	1227.440	1228.4500	**1228.45216**	90.0	7.735
LJMU017	**4-F-Bz-VPTDVGPFAF-NH_2**	$C_{58}H_{76}FN_{11}O_{14}$	1169.560	1170.5600	1170.8380	92.6	8.961
LJMU018	**F_5-Bz-VPTDVGPFAF-NH_2**	$C_{58}H_{72}F_5N_{11}O_{14}$	1241.270	1242.5200	1242.8564	99.5	10.015
LJMU019	**VPTDVGPFA-NPhe-NH_2**	$C_{51}H_{73}N_{11}O_{13}$	1047.540	1048.5400	**1048.54688**	91.5	5.295

Entry	Sequence	Formula	Exact Mass	Calculated *m/z* $[M+H]^+$	Observed *m/z* $[M+H]^+$ *	Purity (%)**	RP-HPLC RT (min)
LJMU020	**VPTDVGPF-Sar-F-NH_2**	C_{51} H_{73} N_{11} O_{13}	1047.540	1048.5400	**1048.54854**	87.5	5.288
LJMU021	**VPTDVGP-NPhe-AF-NH_2**	C_{51} H_{73} N_{11} O_{13}	1047.540	1048.5400	**1048.54796**	97.5	5.435
LJMU022	**VPTD-NVal-GPFAF-NH_2**	C_{51} H_{73} N_{11} O_{13}	1047.540	1048.5400	**1048.54869**	79.7	5.160
LJMU023	**VPT-NAsp-VGPFAF-NH_2**	C_{51} H_{73} N_{11} O_{13}	1047.540	1048.5400	1048.3901	77.0	5.453
LJMU024	**NVal-PTDVGPFAF-NH_2**	C_{51} H_{73} N_{11} O_{13}	1047.540	1048.5400	**1048.54870**	95.4	5.451
LJMU025	**TDVGPFAF-NH_2**	C_{41} H_{56} N_8 O_{12}	852.400	853.4000	852.5260	96.0	5.073
LJMU026	**VPSDVGPFAF-NH_2**	C_{50} H_{71} N_{11} O_{13}	1033.520	1033.5200	**1034.53094**	91.7	5.468
LJMU027	**Bz-VPTDVGPFAF-NH_2**	C_{58} H_{77} N_{11} O_{14}	1151.565	1151.5651	1153.0021	88.9	8.718
CGRP 8-37	**VTHRLAGLLSRSGGVVKNNF VPTNVGSKAF-NH_2**	C_{139} H_{230} N_{44} O_{38}	3123.742	3124.7451	$[M+2H]^+$ 1563.3038	83.5	4.231

3.4.1 ^{19}F NMR chemical shifts

3.4.1.1 LJMU011

^{19}F NMR (564.63 MHz H_2O, {^1H}): δ, ppm: -116.38 (1F, s, 4-F-Phe37; *cis* prolyl bond rotamer), -116.45 (1F, s, 4-F-Phe37; *trans* prolyl bond rotamer) - 1 : 3.15 ratio.

3.4.1.2 LJMU012

^{19}F NMR (564.63 MHz H_2O, {^1H}): δ, ppm: -115.74 (1F, s, 4-F-Phe35; *cis* prolyl bond rotamer), -116.40 (1F, s, 4-F-Phe35; *trans* prolyl bond rotamer) - 1 : 3.20 ratio.

3.4.1.3 LJMU013

^{19}F NMR (564.63 MHz H_2O, {^1H}): δ, ppm: -115.74 (1F, s, 4-F-Phe35; *cis* prolyl bond rotamer), -116.41 (1F, s, 4-F-Phe35 *trans* & 1F, s, 4-F-Phe37 *cis* prolyl bond rotamer), -116.46 (1F, s, 4-F-Phe37; *trans* prolyl bond rotamer) - 1 : 4.21 : 3.25 ratio.

3.4.1.4 LJMU014

^{19}F NMR (564.63 MHz H_2O, {^1H}): δ, ppm: *Trans prolyl bond* rotamer: -143.07 (2F, dd, J_o = 22.14 Hz, J_m = 7.44 Hz, *ortho*-ArF), -156.49 (1F, t, J_o = 20.83 Hz, *para*-ArF), -163.08 (2F, m, *meta*-ArF).

Cis prolyl bond rotamer: -143.14 (2F, dd, J_o = 22.56 Hz, J_m = 7.79 Hz, *ortho*-ArF), -156.47 (1F, t, J_o = 21.09 Hz, *para*-ArF), -163.08 (2F, m, *meta*-ArF). Prolyl bond rotamers observable but not quantifiable. *para*-ArF multiplets poorly resolved due to overlapping rotamers.

3.4.1.5 LJMU015

^{19}F NMR (564.63 MHz H_2O, {^1H}): δ, ppm: *Trans prolyl bond* rotamer: -143.20 (2F, dd, J_o = 23.20 Hz, J_m =7.3 Hz, *ortho*-ArF), -156.3 (1F, t, J_o = 21.10 Hz, *para*-ArF), -162.9 (2F, dt, J_o = 22.17 Hz J_m = 6.57, *meta*-ArF); *Cis prolyl bond* rotamer: -142.90 (2F, dd, J = 25.00 Hz, J = 8.5 Hz, *ortho*-ArF), -155.48 (1F, m, *para*-ArF), -162.58 (2F, m, *meta*-ArF) - 1 : 5 ratio.

3.4.1.6 LJMU016

^{19}F NMR (564.63 MHz H_2O, {^{1}H}): δ, ppm: δ, ppm: *Trans prolyl bond* rotamer: -143.23 (2F, dd, J_o = 22.65 Hz, J_m = 6.67 Hz, *ortho*-ArF, Phe37), -143.5 (2F, dd, J_o = 23.43 Hz, J_m = 6.85 Hz, *ortho*-ArF, Phe35), -156.49 (1F, t, J_o = 20.96 Hz, *para*-ArF, Phe37), -156.75 (1F, t, J_o = 20.85 Hz, *para*-ArF, Phe35), -163.24 (4F, m, *meta*-ArF); *Cis prolyl bond* rotamer: -143.18 (4F, m, *ortho*-ArF, Phe37 and Phe35), -155.68 (1F, m, *para*-ArF, Phe35), -156.68 (1F, m, *para*-ArF, Phe37), 162.82 (4F, m, *meta*-ArF) - 1 : 10 ratio.

3.4.1.7 LJMU017

^{19}F NMR (564.63 MHz H_2O, {^{1}H}): δ, ppm: -109.67 (1F, s, ArF), -109.72 (1F, s, ArF), -109.78 (1F, s, ArF) - 1 : 0.2 : 0.05 ratio.

3.4.1.8 LJMU018

^{19}F NMR (564.63 MHz H_2O, {^{1}H}): δ, ppm: -142.99 (2F, m, *ortho*-ArF), -154.79 (1F, m, *meta*-ArF), -163.40 (1F, m, *para*-ArF).

3.5 Results and Discussion

3.5.1 Peptides and peptidomimetics synthesis

3.5.1.1 Automated microwave-assisted peptide synthesis

The library of peptides and peptidomimetics was synthesised by automated microwave solid-phase peptide synthesis, recognised to significantly reduce coupling times and enhance product purity [258,259].

CGRP 8-37 is a well-known CGRP-R antagonist [176,240,260,261]; hence, it was synthesised for use as a reference for biological activity. Its synthesis may be jeopardised by its length so a low loading resin was chosen to allow lower steric obstruction from the nearby peptide chains [262]. Examination of CGRP 8-37 with the Peptide Companion Excel spreadsheet showed that the most challenging amino acid couplings were Arg11, Arg18, Gly20, Gly21, Val22, Val23, Lys24

(http://www.spyderinstitute.com/software.html). Hence, these seven amino acids were coupled twice during the synthesis.

P006 was taken as the starting point of the anti-migraine drug discovery project. P006 was also examined with Peptide Companion Excel spreadsheet to predict difficult couplings, and in this case single coupling of each amino acid was sufficient.

As represented in Figure 3.23, peptides listed in Table 3.4 can be further categorised into fluorinated analogues (LJMU011-LJMU016, light green), peptide-peptoid hybrids (LJMU019-LJMU024, pink), N-terminally modified analogues (LJMU017, LJMU018, LJMU027, yellow, among which LJMU017 and LJMU018 are also fluorinated, light green), and the remaining peptides are CGRP 8-37, the known CGRP-R antagonist taken as the reference, P006, the peptide CGRP-R antagonist from which this project has started, LJMU025, the main metabolite of P006, and LJMU026, a P006 analogue in which Thr30 has been replaced with serine to study the importance of the side chain length of this crucial residue.

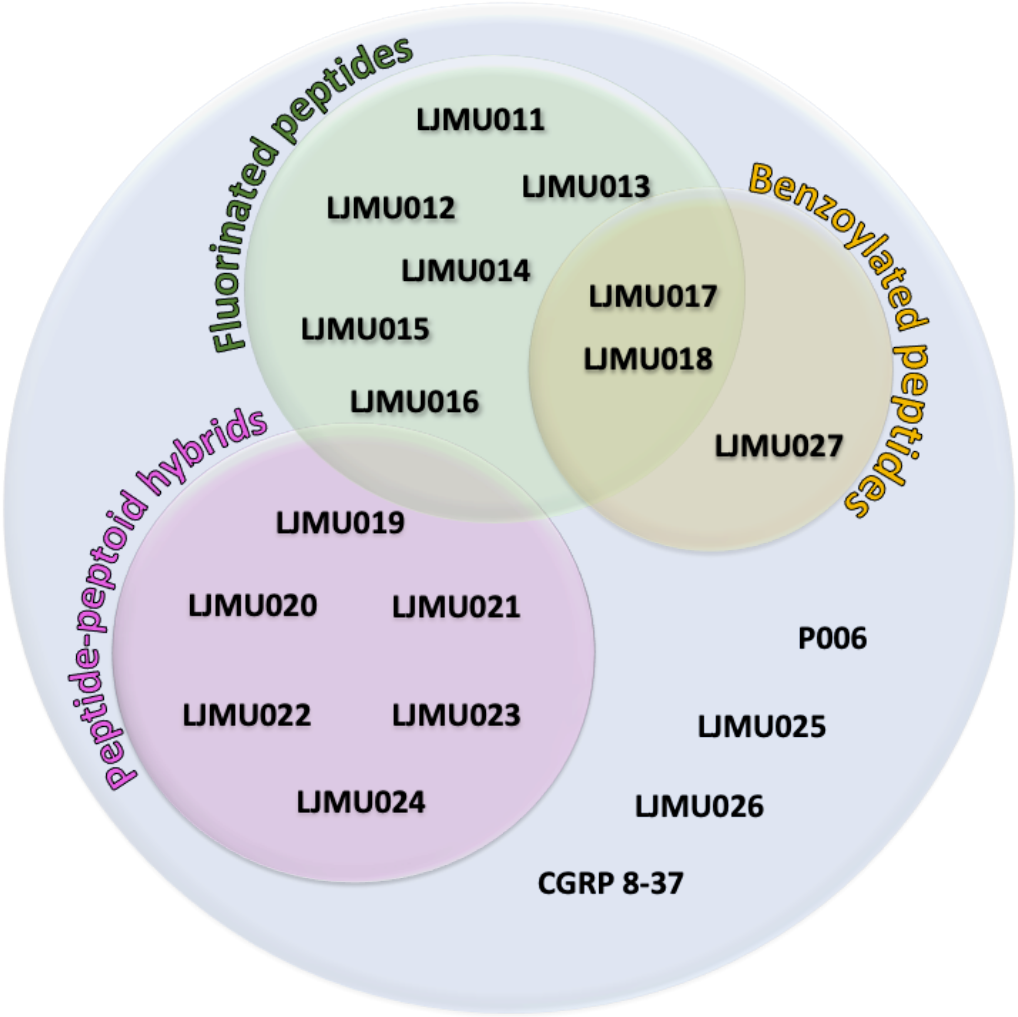

Figure 3.23. Classification of the library of peptides into fluorinated peptides (light green), benzoylated peptides (orange), and peptide-peptoid hybrids (pink).

3.5.2 Fluorinated P006 analogues preparation

To study the effect of fluorination on peptide conformation, physicochemical properties, activity, and stability, Phe37 and Phe35 were replaced with two fluorinated counterparts (i.e., 4-F-Phe and F_5-Phe; Figure 3.24). A local increase in hydrophobicity at these positions (in particular, Phe35) may follow the path of the successful halogenation of the aromatic motif of small molecule CGRP-R antagonists atogepant (**60**), telcagepant (**61**), and olcegepant (**62**) [192,193,212].

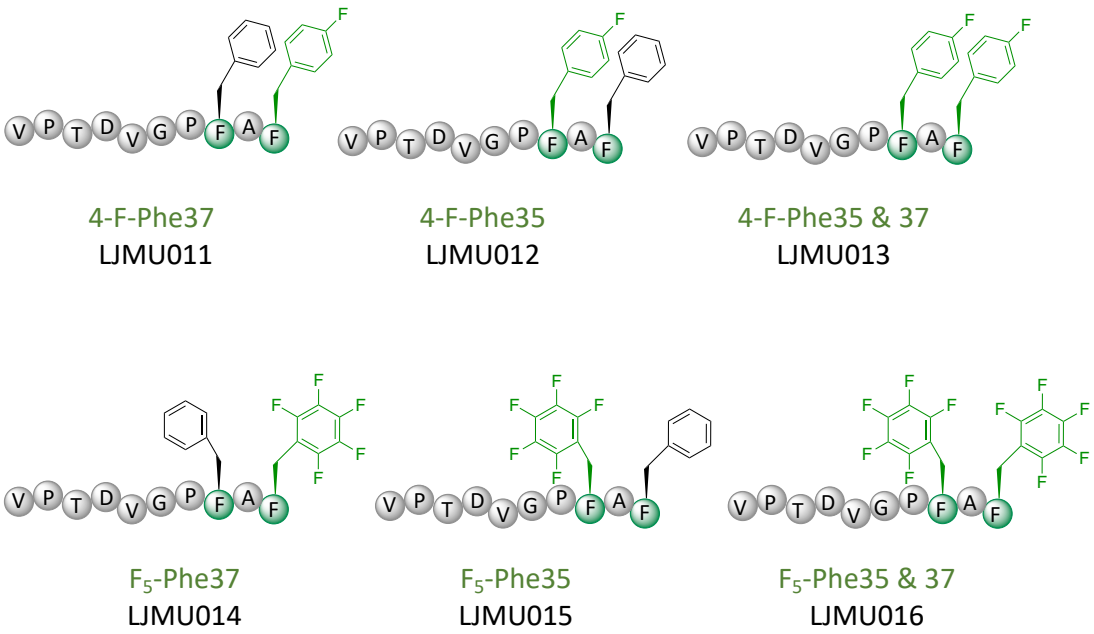

Figure 3.24. Schematic representation of P006 amino acid sequence and modifications performed to include fluorinated Phe residues.

3.5.2.1 ^{19}F NMR analysis

Peptides containing fluorine atoms were analysed by ^{19}F NMR. Interestingly, two distinct sets of well-resolved resonances were observed in most cases, which our group has previously ascribed to both cis and trans conformers of the peptidylprolyl bond (Killoran et al., unpublished data). This was despite the fluorine nucleus being distal to the site of conformational change (attributed at Pro34). Prolyl bond trans-cis isomerism occurs relatively slowly on the NMR timescale and therefore affords distinct signals that indicate the conformational equilibrium [203]. The quantitative nature of ^{19}F NMR allowed the integrated signals to be converted where possible into trans:cis ratios (Table 3.5).

*Table 3.5. Fluorinated peptide sequences and corresponding trans/cis ratios obtained by integration of ^{19}F NMR signals. In spectra where the trans/cis signals were not clearly resolved, the ratio was defined as N.A. * for the pair of signals with same chemical shift as 4-F-Phe35 alone (LJMU012).*

Entry	Sequence	trans/cis ratio
P006	VPTDVGPFAF-NH_2	-
LJMU011	VPTDVGPFA-4-F-Phe-NH_2	3.15
LJMU012	VPTDVGP-4-F-Phe-AF-NH_2	3.20
LJMU013	VPTDVGP-4-F-Phe-A-4-F-Phe-NH_2	3.25 *
LJMU014	VPTDVGPFA-F_5-Phe -NH_2	N.A.
LJMU015	VPTDVGP-F_5-Phe-AF-NH_2	5
LJMU016	VPTDVGP- F_5-Phe -A-F_5-Phe-NH_2	10
LJMU017	4-F-Bz-VPTDVGPFAF-NH_2	N.A.
LJMU018	F_5-Bz-VPTDVGPFAF-NH_2	N.A.

Peptides containing 4-F-Phe at position 35 or 37 (i.e., LJMU011 and LJMU012) showed well resolved *trans* and *cis* signals and reported ~3:1 *trans:cis* conformer ratio, probably due to Pro34, as shown in Figure 3.25 and Figure 3.26. Similarly, for LJMU013, containing two fluorine atoms (i.e., two 4-F-Phe), it was possible to detect *trans:cis* ratio at Pro34 using the two different reporters; however, signals with chemical shift of -116.41 ppm due to the presence of 4-F-Phe in position 37 tend to be overlapped and not well-resolved. ^{19}F NMR spectra of LJMU013 is shown in Figure 3.27.

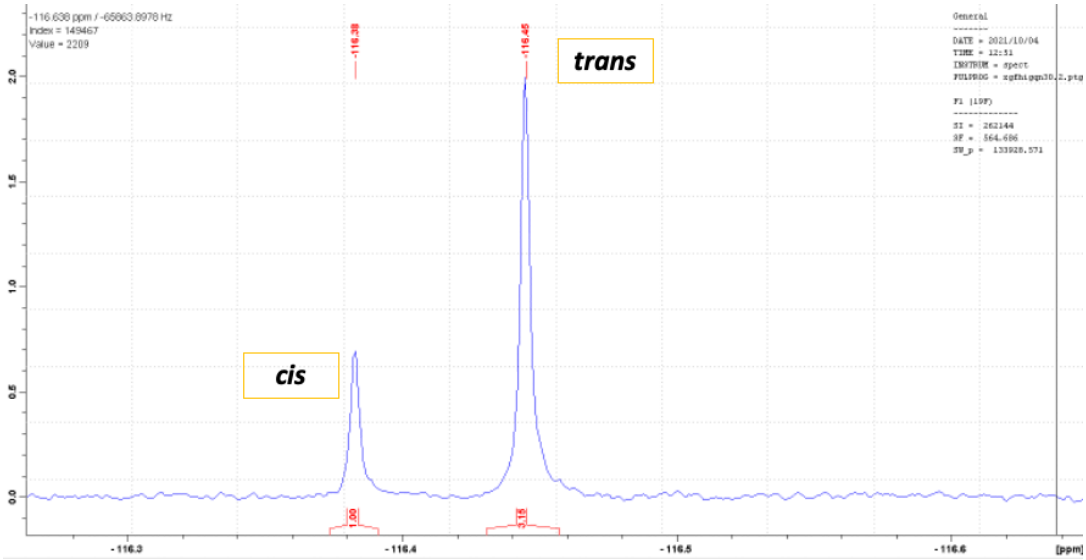

Figure 3.25. ^{19}F NMR spectrum of LJMU011, containing 4-F-Phe in position 37. cis and trans population are reported in the figure.

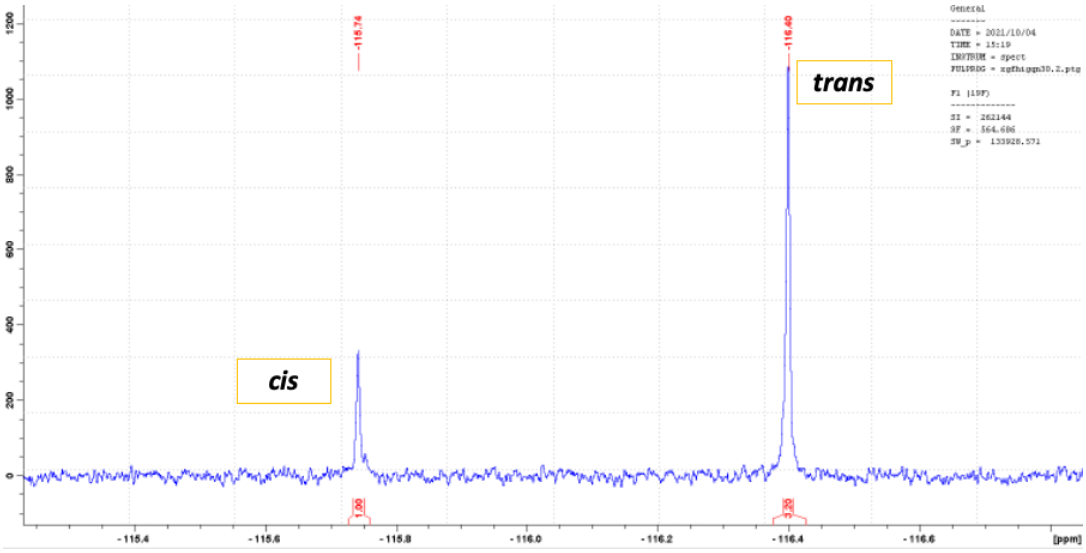

Figure 3.26. ^{19}F NMR spectrum of LJMU012, containing 4-F-Phe in position 35. cis and trans population are reported in the figure.

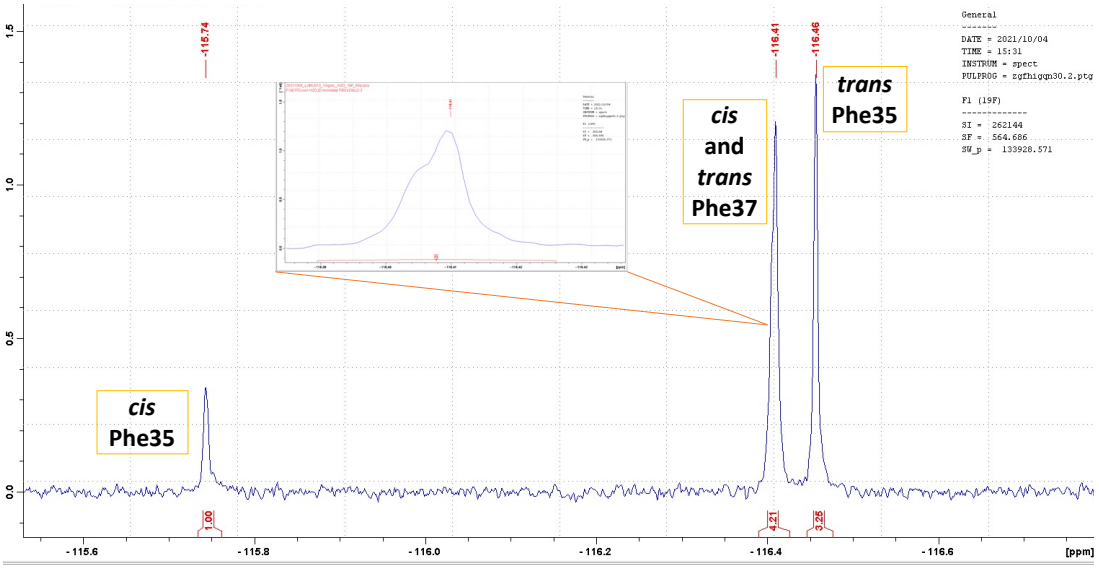

Figure 3.27. ^{19}F NMR spectrum of LJMU013, containing two 4-F-Phe residues in positions 35 and 37. cis and trans population are reported in the figure.

Peptides containing one or two F_5-Phe – i.e., LJMU014, LJMU015, and LJMU016, represented in Figure 3.28, Figure 3.29, and Figure 3.30, respectively – presented more complicated spectra, but still showed a trend in the *trans:cis* ratio, similar to that of 4-F-Phe replacements but with higher ratios (e.g., 1:5 or 1:10).

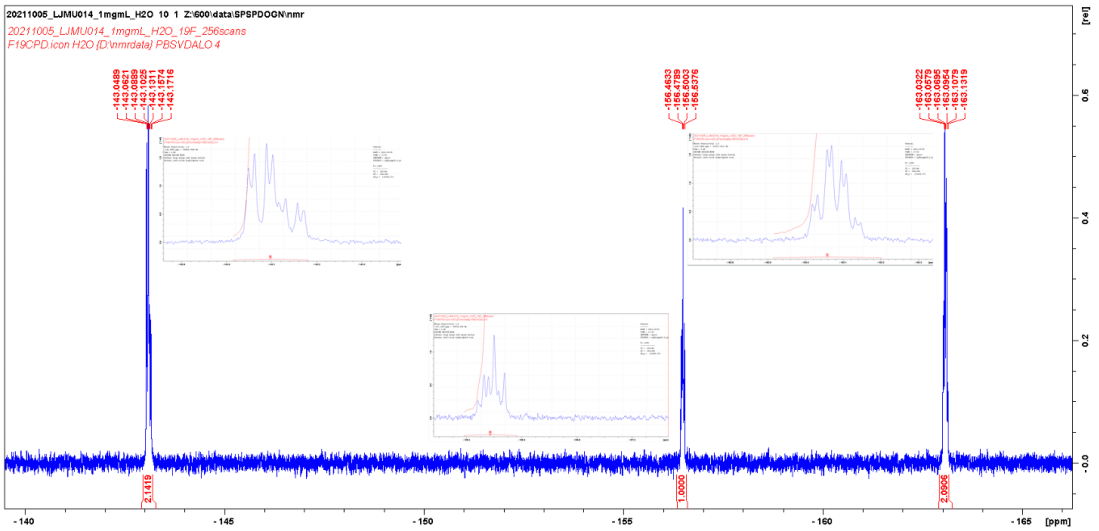

Figure 3.28. ^{19}F NMR spectrum of LJMU014, containing F_5-Phe in position 37.

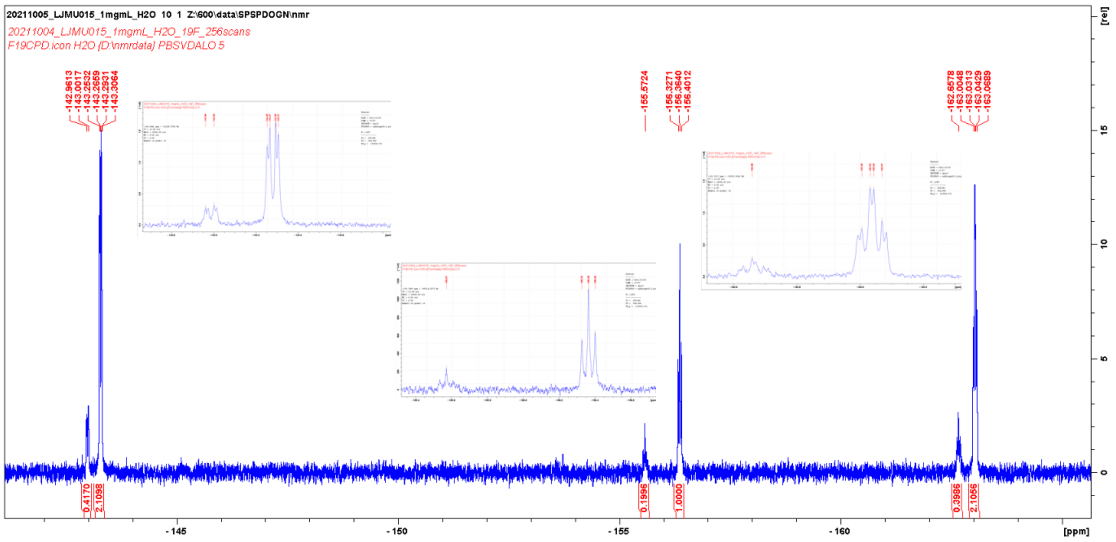

Figure 3.29. ^{19}F NMR spectrum of LJMU015, containing F_5-Phe in position 35.

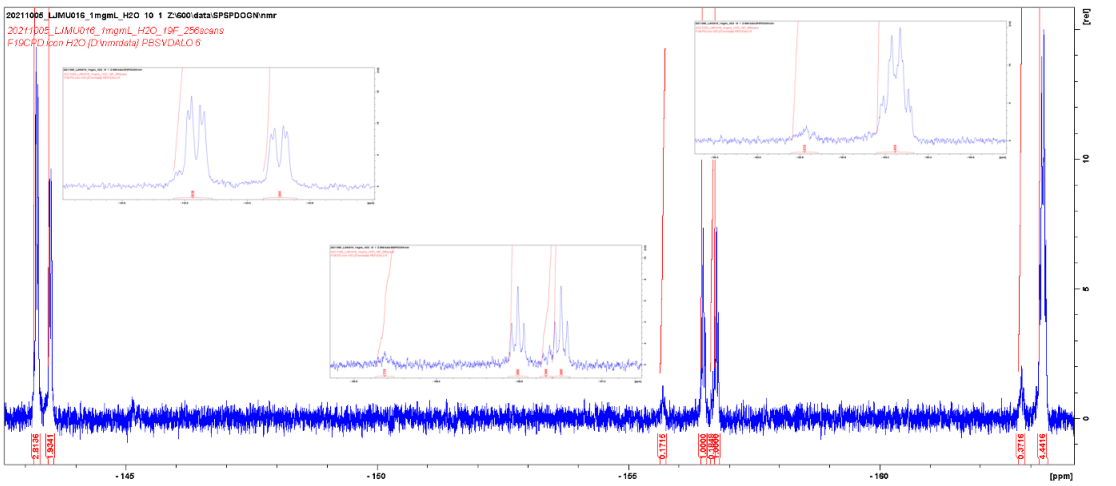

Figure 3.30. ^{19}F NMR spectrum of LJMU016, containing two F_5-Phe residues in positions 35 and 37.

Similarly, ^{19}F NMR analysis of fluorinated N-benzoyl derivatives showed the presence of *cis-trans* isomerism. In particular, LJMU017 spectra (Figure 3.31) showed the presence of at least three distinct conformers probably related to isomerism around the prolyl bond at position 29. The *trans-trans* conformer, likely being the most abundant should correspond to the signal at chemical shift -109.67 ppm, while the other two signals (δ, ppm -109.72 and -109.78) should correspond to *trans-cis* and *cis-trans* conformers but there was no unambiguous way to distinguish between the

two. Finally, in LJMU018 spectra (Figure 3.32) prolyl bond rotamers were observable but not well resolved.

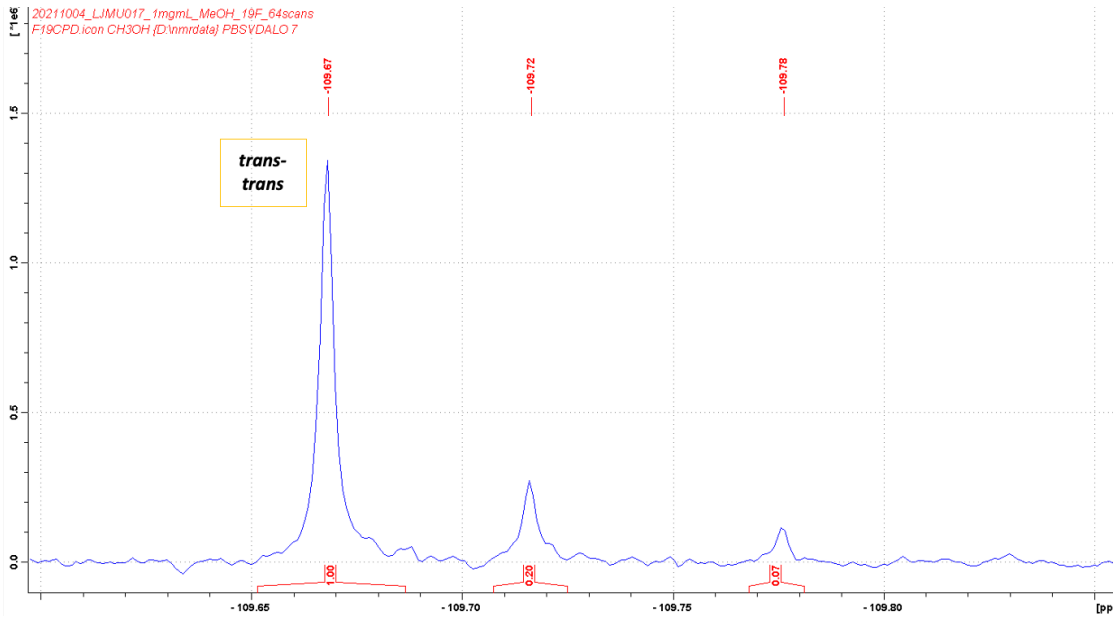

Figure 3.31. ^{19}F NMR spectrum of LJMU017, containing 4-F-benzoyl at the N-terminus.

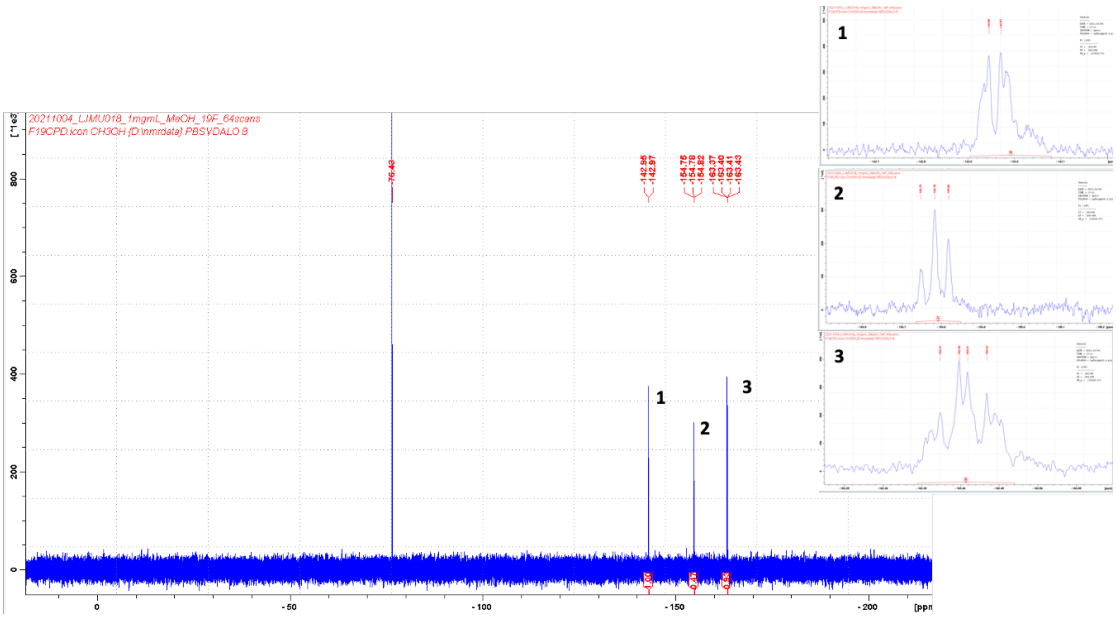

Figure 3.32. ^{19}F NMR spectrum of LJMU018, containing F_5-benzoyl at the N-terminus.

Interestingly, ^{19}F NMR analysis of P006 analogues where Phe residues were replaced with fluorinated counterparts proved that the conformation of a peptide containing proline residues can be studied by fluorination of an amino acid distal from the

proline to avoid having a direct influence on it while still obtaining information on the peptidylprolyl bond conformation. This work is currently being further explored in the Coxon Lab at The University of Edinburgh.

3.5.3 P006 peptomer analogues preparation

Six peptide-peptoid hybrid analogues of P006 (LJMU019-LJMU024) were prepared by replacing amino acids at six positions of P006 with the peptoid counterpart (Figure 3.33).

Figure 3.33. Schematic representation of P006 amino acid sequence and modifications performed to amino acid residues at various positions with peptoid counterparts.

The presence of peptoid monomers within a peptide sequence may enhance metabolic stability, as the relocation of the side chain to the N in α position of the carbonyl group should prevent access of the peptidases responsible for hydrolysing the peptide bond. However, as biological activity can be easily influenced by even minor structural changes, peptide residues tolerant to peptoid replacement should be carefully pinpointed to successfully develop a therapeutically attractive peptidomimetic [263]. Thus, initial approaches to the use of peptoids were through positional scanning. Positional 'peptoid-scanning' is an already known approach in which one amino acid at the time along the peptide sequence is replaced with a peptoid monomer [263–266]. This scanning approach resembles the idea behind

alanine-scanning, usually employed to reveal the presence of residues critical for biological activity, conformational and physicochemical properties, and protein-protein interactions by replacing one amino acid at the time with the simplest natural chiral amino acid.

The portion 27-37 of the natural hormone CGRP has already been subject to positional scanning studies. Indeed, the significance of each amino acid and the role of their side chain has been evaluated through replacement of each residue of the sequence with L-Ala and L-Phe [66]. However, the tolerance of peptoid monomer in place of each amino acid has not been evaluated for CGRP 27-37. Moreover, the study of each amino acid replacement distinctly facilitates the final design of a successful peptide-peptoid hybrid in which only specific residues – the ones in which the replacement is beneficial for activity and stability – are substituted.

For peptide-peptoid hybrids preparation, the submonomer approach was chosen, as this allowed rapid synthesis from cheap commercially available starting materials and did not require main-chain protecting groups [226,267,268]. Peptoid monomers were built by sequential haloacetylation of an amine functionality linked to a solid support, followed by displacement of the halogen (bromide) using a primary amine, chosen according to the amino acid side chain to replace [267]. The advantage of this method was that the side chain of interest only required a reactive primary amine to be successfully coupled into the sequence. Primary amines chosen for this study were isopropylamine (**79**) – when the amino acids to be replaced were Val28 (LJMU024) or Val32 (LJMU022) – and benzylamine (**80**), in place of Phe37 (LJMU019) or Phe35 (LJMU021). Moreover, for replacement of Ala36 (LJMU020), a commercially available amino acid, named sarcosine or N-methylglycine (**81**) was used, presenting a methyl group on the nitrogen in α position. Finally, LJMU023 was produced by replacing Asp31 with its peptoid analogue. This synthesis was achieved by using bromoacetic acid in the haloacetylation step to deprotected Val32, followed by manual double coupling of *t*-butyl glycine ester (**82**).

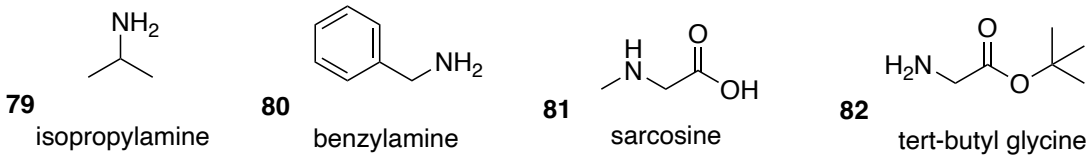

Figure 3.34. Chemical structures of primary amines used for peptide-peptoid hybrids preparation.

The remaining four amino acidic residues (i.e., Pro34, Gly33, Thr30, Pro29) were not replaced with peptoid monomers. Glycine does not present any side chain that can be moved to the N in α position; proline, responsible for the 3D-structure of the backbone, is the only naturally occurring N-substituted amino acid, and indeed can be considered a natural candidate for peptoid substitutions [263]. Finally, Thr30 was not replaced with its peptoid corresponding analogue because this amino acid is known to be of crucial importance for activity [66,180]. At the same time, a commercially available amine presenting the Thr side chain (1-amino-1-ethanol) is not available and the synthesis of the entire peptoid monomer (to follow a monomer approach) is tedious and time-consuming [269,270].

In general, the yield of the crude peptide-peptoid hybrids analogues was lowered by incomplete coupling of $BrCH_2COOH$ to the free amine of the neighbour amino acid and any deletion product detected in the crude mixture was due to the presence of a peptide lacking the peptoid monomer. An attempt to increase crude purity was performed on LJMU019 by repeating the $BrCH_2COOH$ coupling three times instead of two, by increasing the number of equivalents of $BrCH_2COOH$ (from 0.6 M to 2 M), and by prolonging the coupling times, without obtaining any increase in the final yield.

3.5.4 Purification by preparative-HPLC and flash-chromatography

Solid-phase synthesis is a straightforward procedure for small-size peptides, and it generally yields relatively pure products (~50 to 80%) [168]. However, purification is needed in most cases to remove large quantities of salts and to yield purity

percentages higher than the 90% required for further biological testing [271]. This can be achieved through both preparative-HPLC and flash chromatography. The choice of the technique to use depends on the chromatography of the crude product. If the unwanted side product(s) is (are) eluting closely to the compound of interest, generally preparative HPLC is the technique of choice. However, if the two products are well separated, flash chromatography is the best option, as it can afford faster, easier, and cheaper purification on a larger scale.

To compare the results obtained with both approaches, the example of LJMU019 purification is reported here and published in an application note (AN115) in collaboration with Teledyne Isco Ltd. [272]. Figure 3.35A shows the HPLC chromatogram of the crude peptide-peptoid hybrid; at 8.06 min an unwanted side product, derived from unsuccessful coupling of the bromoacetic acid and subsequent deletion of the peptoid monomer in position 37, is present in the crude sample; this required purification of the mixture to isolate the peptide-peptoid hybrid LJMU019 from its close-running impurity.

Purification was attempted with both the approaches; chromatographic separation achieved through preparative HPLC (Figure 3.35B) and through flash chromatography (Figure 3.35C) are shown. With the two approaches, comparable high purity products (> 90%) were obtained (Figure 3.36A and B), demonstrating that, for compounds appearing well-separated in HPLC chromatograms, flash chromatography may be used in place of prep-HPLC to save time and sources.

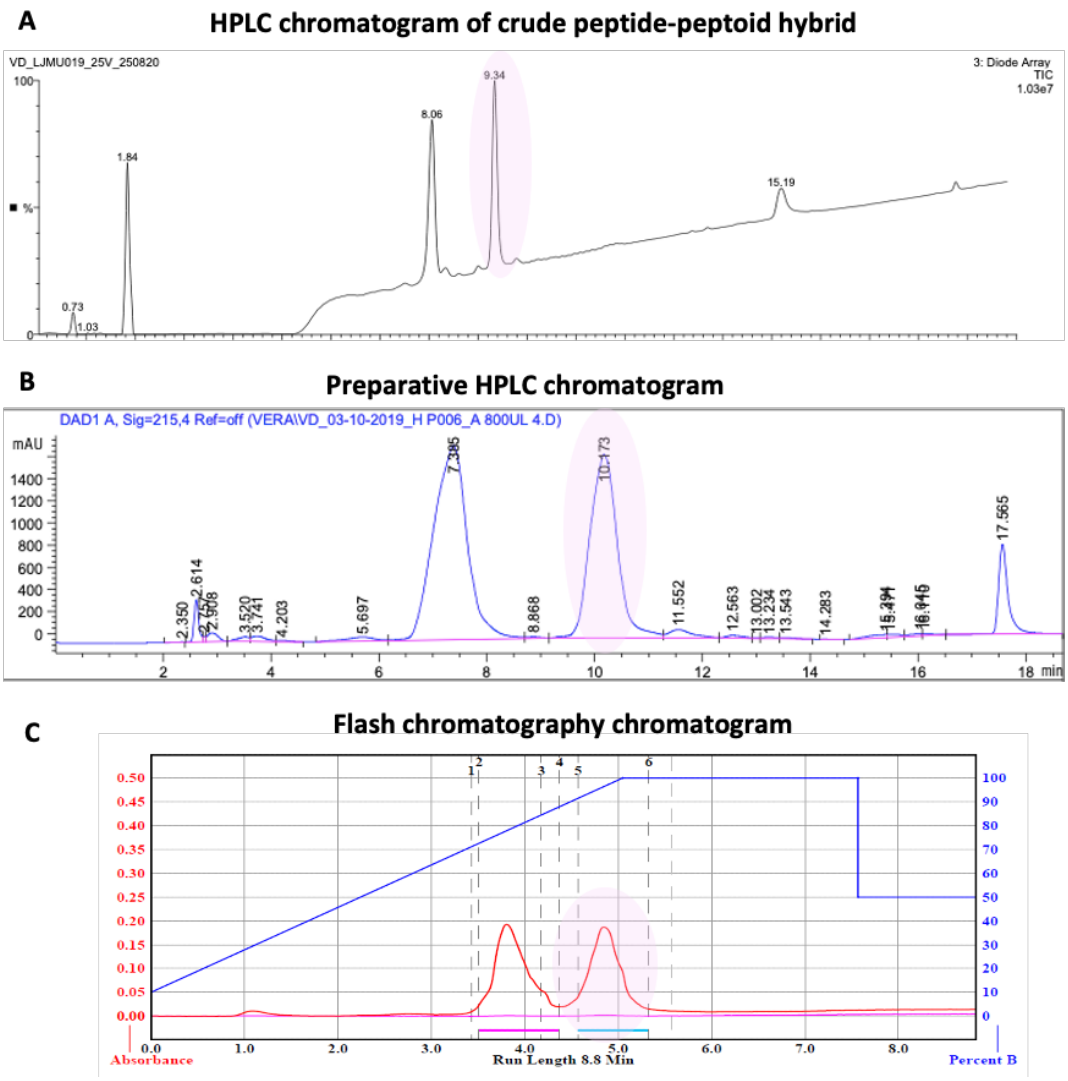

Figure 3.35. A. HPLC chromatogram (DAD1) of crude LJMU019 after automated synthesis. B. HPLC chromatogram of crude LJMU019 from preparative-HPLC. C. HPLC chromatogram of crude LJMU019 from flash-chromatography. The peak of interest is highlighted in pink.

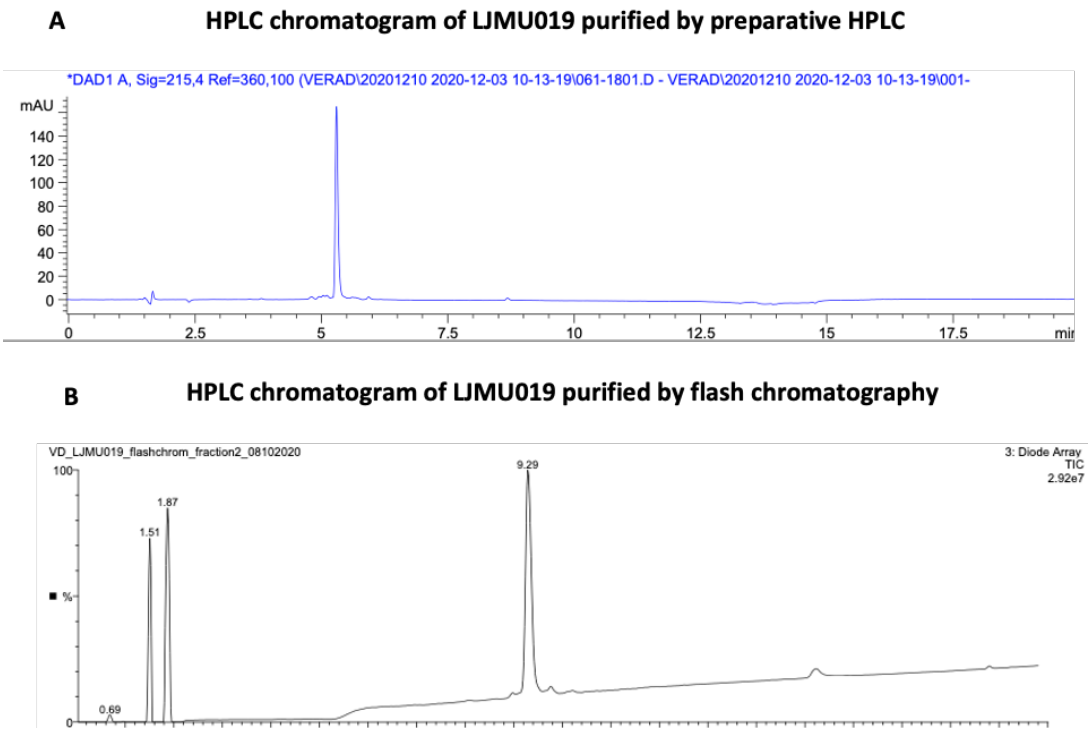

Figure 3.36. A. HPLC chromatogram of purified LJMU019 after preparative-HPLC; B. HPLC chromatogram of purified LJMU019 after flash chromatography. The difference in retention times is due to two different analytical methods employed for the characterisation, a gradient from 30% to 60% MeCN in the first case, and a full gradient from 5% to 95% in the second case.

In light of these findings, when possible, peptides and peptide-peptoid hybrids were purified by flash chromatography due to easiness and quickness of the technique, especially when high amounts of purified compounds were required for further studies (e.g., formulation and self-assembly, see Chapter 5).

3.5.5 N-terminally modified P006 analogues preparation

The idea of developing P006 analogues bearing a benzoyl group at the N-terminus was considered as a judicious option to cap the N-terminus and protect it from cleavage, to increase peptide lipophilicity, and, in turn, prolong its circulating half-life, without impacting on the pharmacophore responsible for binding and activity.

Benzoyl capping provides a fast, cheap, flexible, and straightforward synthetic route to add lipophilic moieties to the terminal amine of a peptide sequence. Here, the peptides were prepared by treating P006 linked on resin with an excess of benzoyl chloride (or fluorinated analogues, i.e. 4-F-benzoyl chloride and F_5-benzoyl chloride) in the presence of an excess of base (DIPEA) to mop up any HCl produced and avoid subsequent protonation of -NH_2 [68]. The reaction successfully yielded the products of interest (i.e., LJMU027, LJMU017 and LJMU018, Figure 3.37) in relatively high conversions (~70 to 90%). The attempts to increase conversion by repeating the capping reaction more than twice or treating the resin for longer times (e.g., 1 h or 2 h) were not successful. Moreover, among the side-products, the starting material was not detected, meaning that the reaction went to completion within the indicated time frame (i.e., 30 min).

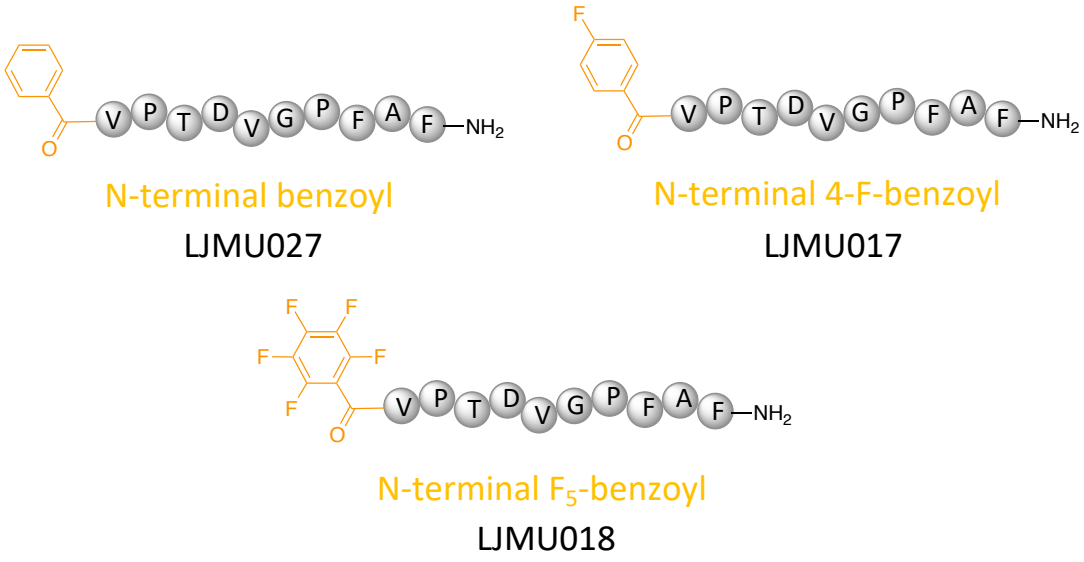

Figure 3.37. Schematic representation of P006 amino acid sequence and modifications performed at the N-terminus.

3.5.6 Lipophilicity assessment

The lipophilicity (or hydrophobicity) of a molecule is defined as its tendency to partition into a non-polar phase versus an aqueous phase [103]. Most commonly, the discovery phase starts with selection of active molecules from a large pool of

candidates, by testing them against the biochemical target of interest. The subsequent step is to screen compounds according to their hydrophobicity, as this is one of the key factors determining ADME properties and efficacy [273,274]. To elicit an effect, a drug molecule should first be absorbed into the blood stream, which depends on the ability of a compound to cross a series of barriers by passive diffusion or mediated by carriers [274–276].

In particular, for peptides or peptidomimetics of potential therapeutic interest, the ADME properties and, indirectly, the pharmacokinetic behaviour, the metabolic properties, and the bioactivity, are strictly linked to their lipophilic propensity [273,277]. For this reason, it is pivotal to assess the change in lipophilicity due to modifications performed on the parent peptide.

The most common indexes for lipophilicity are LogP and LogD, for neutral and ionisable compounds, respectively. LogP is described as follows:

$$LogP = \mathrm{Log10}\left(\frac{[\mathrm{compound}]\mathrm{octanol}}{[\mathrm{compound}]\mathrm{water}}\right)$$

Equation 3.6

where $[\mathrm{compound}]_{\mathrm{octanol}}$ and $[\mathrm{compound}]_{\mathrm{water}}$ represent the concentrations of the analyte in the phase indicated.

LogD, employed in place of LogP when the lipophilicity of an ionisable compound is under investigation, is described by the following equation:

$$LogD\ at\ pH(x) = \mathrm{Log10}\left(\frac{[\mathrm{compound}]\mathrm{octanol}}{[\mathrm{compound}]\mathrm{aq.\ buffer\ at\ pH(x)}}\right)$$

Equation 3.7

where $[\mathrm{compound}]_{\mathrm{octanol}}$ and $[\mathrm{compound}]_{\mathrm{aq.\ buffer\ at\ pH(x)}}$ represent the concentrations of the analyte in 1-octanol and aqueous buffer at specific pH, respectively.

In this study, the lipophilicity of peptides and peptidomimetics was carefully evaluated using different approaches, including RP-HPLC, prediction tools and an experimental shake-flask method. The results were then compared to understand (i) the advantages and disadvantages of each method; and (ii) how the lipophilicity was affected by changes in the structure of P006. This is important to explain the behaviour of the parent peptide and analogues in further studies (e.g., activity, metabolic stability, protein binding).

A modified shake-flask method, previously employed by Bolt and colleagues on a library of antimicrobial peptoids was used to determine LogD at pH 7.4 of P006 and 8 analogues [278,279].

RP-HPLC was employed to compare retention times of each analogue, to examine the overall hydrophobicity. In liquid chromatography, the separation is influenced by the composition of the binary hydro-organic mobile phase and by the properties of the column packing material [280]. If these conditions are kept constant, the way in which the analyte interacts with the stationary/mobile phases, and, ultimately, the retention time can be considered as an index of the overall lipophilicity of the molecule.

Finally, LogD at physiological pH (where possible) or LogP values were calculated using *in silico* predictor tools. These novel computational methodologies are fuelling a shift away from the traditional *in vitro* experiments as they present a lower variability between experiments, they are faster and cheaper [274]. Four *in silico* prediction programs were used (i.e., ChemAxon, ACD/i-Labs, ChemDraw, and Molinspiration), each of them employing a similar substructure-based method to compute LogP (and LogD) values.

However, the lack of large, robust, and standardised peptide training sets may affect the reliability of LogP and LogD *in silico* predictions. Moreover, the tendency to fold and to assume secondary and tertiary structures may not be taken into account if the tools are not tailored on a training set that includes peptides. Therefore, the

calculated values obtained were considered as a means of ranking compounds within a library and not as absolute values of LogP (or LogD).

The addition of fluorine atom(s) on the benzyl ring of Phe residues (LJMU011-LJMU016) resulted in an increase of the overall lipophilicity of the molecule, proportional to the number of fluorine atoms added. This was shown by experimental LogD data (increase in LogD compared to P006 between ~1.8 and ~3.6, with the highest values of LogD yielded by LJMU016, presenting two F_5-Phe residues), but also by RP-HPLC index, where the addition of fluorine atom(s) (LJMU011-LJMU016) caused an increase in RT proportional with the number of fluorine atoms added, and, finally, by *in silico* prediction tools, as shown in Figure 3.38 (green).

Similarly, an increase in lipophilicity was produced by capping the N-terminus of P006 with benzoyl moieties (LJM017, LJMU018, and LJMU027, Figure 3.38). Here, the experimental LogD values were measured for LJMU027 and LJMU017, while LJMU018, bearing five fluorine atoms on the benzoyl ring, was found to be unsuitable for this experiment as it was not soluble in the aqueous buffer at the desired concentrations. Yet, the LJMU017 LogD value (-1.2) was unexpectedly lower than that of LJMU027 (-0.3) and this could be attributed to solubility issues (PBS aq. buffer was cloudy after an attempt to solubilise LJMU017, even after long sonication times). Notably, *via* RP-HPLC, the increase in hydrophobicity after addition of N-benzoyl moiety was clear as it yielded the highest increase in RT of the entire library, with a Δ RT of 3.3 - 4.6 min (Figure 3.38, yellow).

Finally, peptoid replacements (LJMU019-LJMU024, Figure 3.38, pink) did not considerably affect the overall lipophilicity, as shown by RP-HPLC analysis (Δ RT < 0.2 min) and *in silico* predictions (cLogP and cLogD comparable to that of P006). For this reason, experimental LogD measurements were not performed.

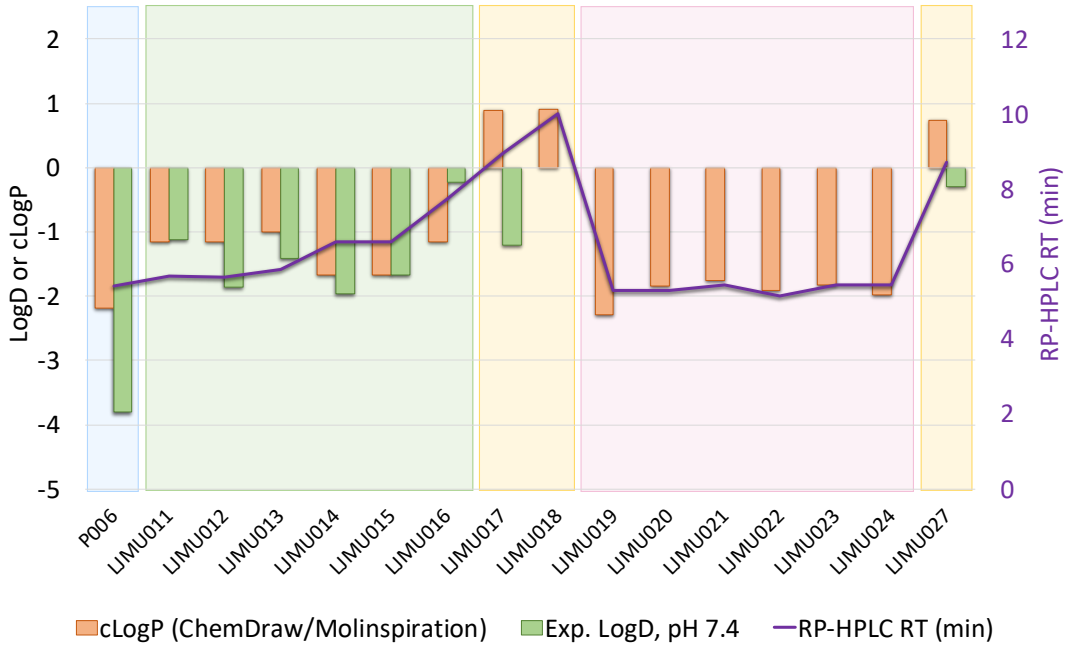

Figure 3.38. Computationally derived LogP values versus experimental LogD (pH 7.4) versus RP-HPLC retention time (min). Peptides are color-coded as follows: P006 in light blue, internally fluorinated analogues in light green, benzoylated analogues in pale yellow, and peptide-peptoid hybrid analogues in pink.

A full data set comprising experimental LogD values, RP-HPLC hydrophobicity index, and *in silico* predictions, is reported in the Appendix.

3.5.7 BUDE AlaScan

To predict the energetic contribution of each amino acid side chain in forming an interaction with the CGRP-R, a computational alanine-scanning mutagenesis experiment was performed on P006 using the interactive web application BAlaS, developed by Wood *et al*. This also allows the identification of the residues that contribute the most to the free energy of binding, expressed as $\Delta\Delta G_{res}$, which is higher when a residue makes a significant contribution to the overall interface energy [254]. Table 3.6 shows the $\Delta\Delta G_{res}$ for P006, confirming the importance of Phe37, followed by Val32, Thr30, Phe35, Pro34. On the other hand, residues Asp31, Pro29, and Val28 were predicted to contribute little to the receptor interaction.

Table 3.6. BUDE AlaScan results for P006 and CGRP-R. Amino acid residues making the greatest contribution to the overall interface energy are highlighted in bold.

Residue	Amino Acid	$\Delta\Delta G_{res}$ (kJ/mol)
28	Val	0
29	Pro	0.6
30	**Thr**	4.9
31	Asp	0.1
32	**Val**	6.6
34	**Pro**	2.1
35	**Phe**	3.8
37	**Phe**	12.7

Information derived from the computational alanine-scanning mutagenesis experiment would be helpful when analysing binding affinity data obtained with cAMP accumulation experiment (section 3.5.8.2).

3.5.8 Biological Activity

This lead optimisation strategy focused on the C-terminal segment of CGRP, starting from P006 (**56**), the lead compound in this series. P006 derives from Phe27 truncation of the well-known potent antagonist [Asp31, Pro34, Phe35]-CGRP 27-37 [66–68]. P006 was previously tested by our research group, using the DiscoverX HitHunter Assay kit, and its antagonist potency $pK_b = 7.9$ ($K_b = 1.26 \times 10^{-8}$ M) (Killoran *et al*., unpublished).

For this study, P006 and the library of P006 analogues were tested using CHO-K1 cells engineered to overexpress the CGRP-R complex (in particular, CALCARL-RAMP1) on the cell surface. Binding of α-CGRP to the receptor was estimated through intracellular accumulation of cAMP derived from activation of $G\alpha_s$ protein-coupled receptor pathway, with conversion of ATP to cAMP due to activation of the cell-surface enzyme adenylate cyclase. Accumulation of cAMP, in turn, was measured through the chemiluminescent signal derived from gain-of-signal competitive immunoassay based on Enzyme Fragment Complementation (EFC) technology. The amount of signal produced was considered directly proportional to the amount of

cAMP produced in the cells. The response curve for the effects of the agonist (α-CGRP) is shown in light blue in each of the representative concentration-response curve graphs in Figure 3.39.

When the cells were pre-treated with the antagonist (e.g., P006, 10^{-5} M) for 15 min and then with increasing concentrations of the agonist in the continued presence of the antagonist, the agonist (α-CGRP) concentration-response curve was shifted to the right, with the slope and the maximum effect (top of the curve) unchanged, indicative of competitive antagonism, as shown in Figure 3.39A. With a pK_b of 6.26 in this functional assay, P006 was more than 43-fold less potent than previously determined (pK_b of ~7.62, a representative concentration-response curve previously obtained for P006 is shown in Figure S48 of the Appendix). Despite a protracted period of troubleshooting to investigate factors such as the roles of peptide purity, media used to prepare peptide stock solution, cell density, agonist and antagonist incubation times, and plasticware used, the reason for the observed decrease in antagonist potency was not clear. To identify any potential confounding effect of the decreased potency of P006 on our analysis, potencies of the library of CGRP-R antagonists were compared both with P006 and with a known CGRP-R antagonist synthesised in-house (i.e., CGRP 8-37).

3.5.8.1 CGRP 8-37 as reference antagonist in the estimation of antagonist potencies

The portion 8-37 of CGRP is known to bind to the receptor without causing activation, hence behaving as a CGRP-R antagonist [176,240,261]. Its potential to bind to the receptor without causing an effect was proven in the 1990s in rat liver plasma membrane and in guinea-pig isolated left atria, where the peptide showed no activation of the adenylyl cyclase pathway and a positive inotropic effect following binding, respectively [260,281,282]. Ten years later, various N-terminal modifications (acetylation, benzoylation, and benzylation) of CGRP 8-37 were explored by Smith *et al*., who assessed the IC_{50} of these peptides using a radioligand assay (IC_{50} of CGRP 8-37 = 14.4 ± 0.38 nM) and their antagonist potencies through a coronary artery relaxation assay (K_b of CGRP 8-37 = 970 ± 300 nM), underlying that the K_b values

determined in the relaxation assay were probably an underestimation of the affinities due to proteolytic degradation which could not be prevented with bacitracin (used in binding experiment) because of incompatibility with the procedure [240]. Finally, studies previously carried out on CGRP 8-37 (von Mentzer *et al*., unpublished) reported a K_b of 38 nM for CGRP 8-37 when the peptide was analysed by DiscoverX cAMP accumulation assay.

Hence, CGRP 8-37 was chosen as a reference antagonist with which to compare the potencies of antagonists in our library of P006 analogues. When re-tested using the DiscoverX cAMP accumulation assay, CGRP 8-37 produced a parallel rightward shift in the CGRP concentration response curve (Figure 3.39B), with a K_b of 230.18 nM $\pm$ 3.60 nM (pK_b = 6.64 $\pm$ 0.00), suggesting that the results hereby obtained for P006 (K_b of 560.57 $\pm$ 47.58 nM instead of 12.6 nM) were probably an underestimation of its antagonist potency. The antagonist potency values obtained for the library of P006 analogues were, therefore, compared with both P006 and CGRP 8-37.

3.5.8.2 cAMP accumulation assay and antagonist potencies of P006 and its derivatives

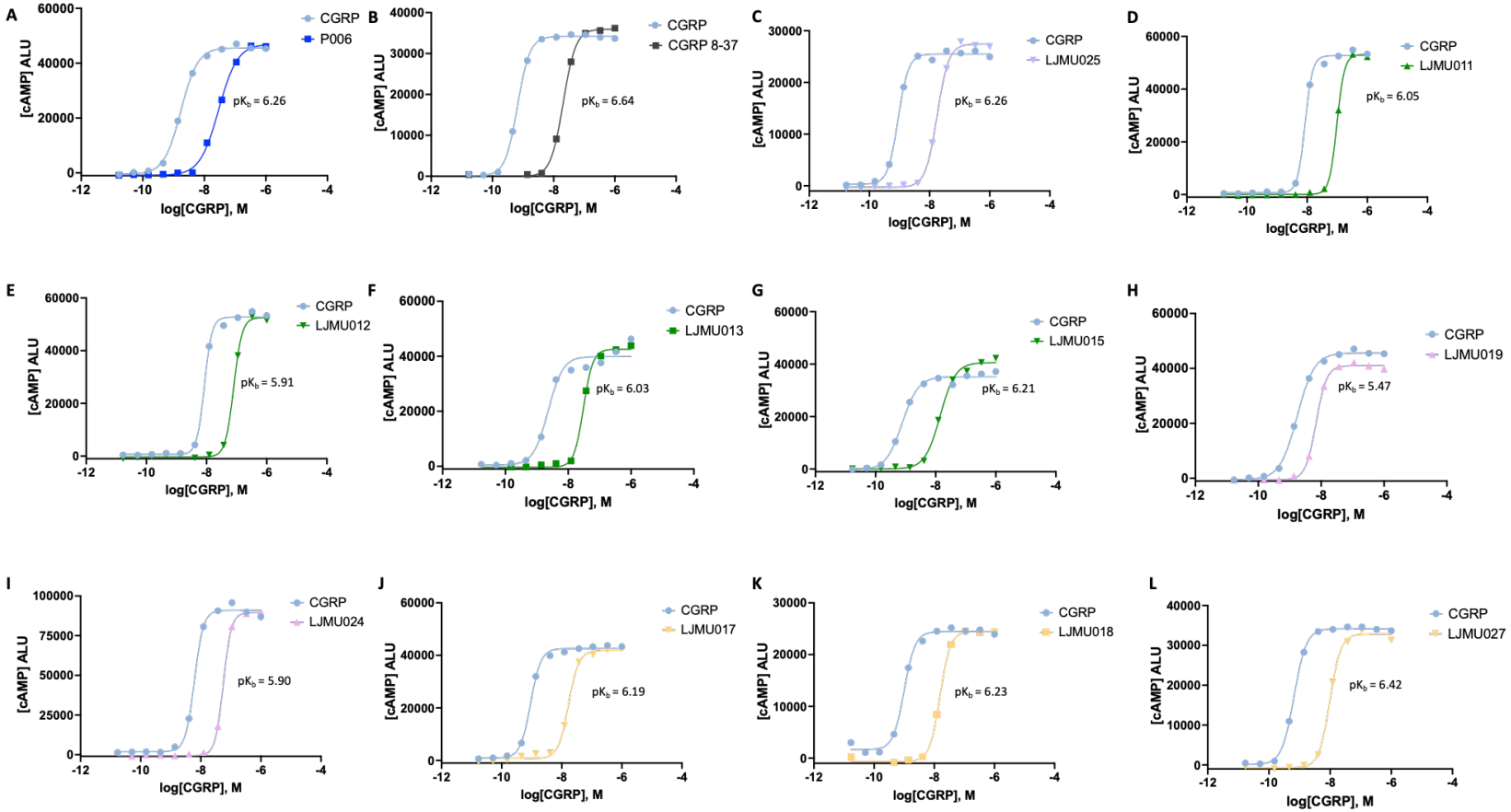

*Figure 3.39. Representative cAMP concentration-response curves for active peptides. From top left to bottom right: P006 (**A**), CGRP 8-37 (**B**), LJMU025 (**C**), LJMU011 (**D**), LJMU012 (**E**), LJMU013 (**F**), LJMU015 (**G**), LJMU019 (**H**), LJMU024 (**I**), LJMU017 (**J**), LJMU018 (**K**), and LJMU027 (**L**).*

As shown in Figure 3.39, active peptides produced rightward, parallel shifts in the concentration-response curve of the agonist CGRP. Notably, of the peptides shown, those that produced a parallel rightward shift comparable to that of P006 (dose ratio > 17) were LJMU015, LJMU017, LJMU018, LJMU025, and LJMU027. On the other hand, peptides LJMU014, LJMU016, LJMU020, LJMU021, LJMU022, LJMU023, and LJMU026 did not produce any significant shift in the CGRP concentration-response curve (data shown in Figure S49 of the Appendix).

Potency data for active compounds are reported in Table 3.7; K_b values were also transformed into pK_b values to reduce the heteroscedasticity of the data. Reductions (as fold change) in the potencies of the compounds in comparison with CGRP 8-37 or P006 are shown in Table 3.8.

*Table 3.7. Affinities of active antagonist compounds of the peptide library, expressed in K_b and pK_b. The data shown are means ± SEM. Statistical significance (Stat. Sign.) was calculated using one-way ANOVA. *p≤0.05, **p≤0.01, ***p≤0.001 and ****p≤0.0001 compared to P006; #p≤0.05, ##p≤0.01, ###p≤0.001 and ####p≤0.0001 compared to CGRP 8-37; ns=non-significant (p> 0.05).*

Peptide	dose ratio (dr)	K_b (nM)	pK_b	Stat. Sign. pK_b
CGRP 8-37	44.45 ± 2.12	230.18 ± 58.26	6.64 ± 0.05	**** -
P006	19.28 ± 0.63	560.57 ± 47.58	6.26 ± 0.02	- ####
LJMU011	12.21 ± 0.33	897.58 ± 49.84	6.05 ± 0.02	* ####
LJMU012	9.13 ± 1.44	1231.40 ± 125.86	5.91 ± 0.06	*** ####
LJMU013	11.78 ± 0.83	944.67 ± 32.62	6.03 ± 0.02	* ####
LJMU015	17.40 ± 0.97	612.98 ± 39.50	6.21 ± 0.03	ns ####
LJMU017	16.57 ± 1.93	647.11 ± 61.70	6.19 ± 0.05	ns ####
LJMU018	18.28 ± 0.09	592.60 ± 100.48	6.23 ± 0.01	ns ####
LJMU019	3.92 ± 2.01	3427.37 ± 320.16	5.47 ± 0.11	**** ####
LJMU024	9.48 ± 0.66	1327.32 ± 20.56	5.90 ± 0.02	*** ####
LJMU025	19.34 ± 2.38	546.79 ± 34.86	6.26 ± 0.04	ns ####
LJMU027	27.22 ± 0.39	384.56 ± 2.08	6.42 ± 0.00	ns #

Table 3.8. Reduction (fold change) in potency (expressed as K_b) of P006 derivatives compared to CGRP 8-37 and P006.

Peptide	Fold K_b (vs. CGRP 8-37)	Fold K_b (vs. P006)
CGRP 8-37	1.0	0.4
P006	2.4	1.0
LJMU011	3.9	1.6
LJMU012	5.3	2.2
LJMU013	4.1	1.7
LJMU015	2.7	1.1
LJMU017	2.8	1.2
LJMU018	2.6	1.1
LJMU019	14.9	6.1
LJMU024	5.8	2.4
LJMU025	2.4	1.0
LJMU027	1.7	0.7

Fluorination is a powerful tool to tune physicochemical and conformational properties of peptides; however, its effect upon receptor binding may be deleterious, especially when occurring at amino acids highly involved in binding. Not surprisingly, this was the case for LJMU014 and LJMU016, presenting F_5-Phe in position 37 and F_5-Phe both in positions 35 and 37, respectively. While the addition of a single fluorine atom through replacement of Phe with 4-F-Phe in positions 35 and/or 37 only caused a minor decrease in potency (from 1.6 to 2.2-fold reduction compared to P006, Table 3.8), the replacement of the hydrogen atoms with five highly electronegative atoms around the Phe37 benzene ring abolished the activity. As expected, the only tolerated F_5-Phe replacement was in position 35 (LJMU015), known to have less involvement in the binding to the receptor, as proven by BUDE AlaScan and as shown in Figure 3.40 A and B. Moreover, as mentioned in section 3.1.3.3, Phe35 resembles the aromatic structures of the small molecules atogepant (**60**) and telcagepant (**61**) – containing 2,3,6-trifluorophenyl-, and 2,3-difluorophenyl-, respectively – where fluorination is known to be tolerated [192,193,212].

As with fluorination, peptoid replacement may disrupt interactions with the hydrophobic pocket of the receptor; hence, peptoid-scanning was performed to

understand which residues tolerated the relocation of the side chain on the nitrogen of the peptide backbone. Surprisingly, moving Phe37 side chain from the α–carbon to the nitrogen did not completely disrupt the potency of the analogue (LJMU019), even though this was severely affected (6-fold reduction compared to P006's K_b value). Probably neither the polar interactions – occurring between the C-terminal amide and the carbonyl of Thr122 of the CLR, and between the carbonyl of the Phe37 and the N of the Thr122 of the CLR – nor the π stacking that may occur with Trp72 of the CLR were majorly disrupted by this modification (Figure 3.40A). In contrast, the replacement of Ala36 with its corresponding peptoid monomer (i.e., sarcosine or N-methylglycine) (LJMU020) appeared to be detrimental to the binding affinity; this is in accordance with Rist *et al.* study, which showed that alanine replacement with Gly as well as its stereochemical inversion resulted in a great loss of affinity for the CGRP-R [66]. Similarly, the replacement of Phe35 with its peptoid analogue (LJMU021) resulted in total loss of affinity, even though previous studies reported that in the natural segment CGRP 27-37, position 35 (Glu) had little influence on binding and its substitution with Lys, Phe, His, Gln, Leu, and 3-Pal were all tolerated [66,68]. However, it has also been described that the substitution of Glu35 with Pro was not tolerated, probably due to a decrease in H bonding capacity of the Nα, while polar interactions occurring between the carbonyl group of Phe35 residue and Arg119 are reported in the cryo-EM structure (Figure 3.40B). Similarly, a reduction of H bonding capacity of the nitrogen due to relocation of the side chain was not tolerated [66,214,228]. The shift of the isopropyl group of Val32 on the Nα (LJMU022) resulted in a loss of CGRP-R affinity; this scenario was expected from BUDE AlaScan predictions – where a ΔΔG of 6.6 kJ/mol was associated with this residue – as well as from previous studies. Rist *et al.* previously demonstrated that Val32 was critical, as its replacement with Ala, Phe, Pro or D-amino acid led to a total loss of receptor interaction [66]. Again, replacement of Asp31 with its peptoid monomer (LJMU023) was not well tolerated, causing a loss of activity against the CGRP-R. In general, as previously demonstrated by SAR studies conducted on the 27-37 region of CGRP, the most sensitive segment is between Thr30 and Gly33 (Figure 3.40D and E); and, basically, any modification there was detrimental to the binding affinity. This is

explained by the cryo-EM structure studied by Liang *et al*. in which there was clear evidence that Thr30, Val32 as well as Phe37 form persistent contacts with two amino acids ($Trp72^{ECD}$ and $Gln93^{ECD}$) of the CLR's extracellular domain [242]. Finally, the replacement of Val28 with the corresponding peptoid monomer analogue (LJMU024) resulted in the smallest disruption of receptor interaction (only 2-fold decrease compared to P006). This is in accordance with the SARs studies on CGRP 27-37, as well as with the BUDE predictions, as Val28 is known to be the least sensitive amino acid in the segment [66].

N-terminal benzoylation of P006 (LJMU027) resulted in a compound slightly more active than P006 (1.3-fold compared to P006). Benzoylation at the N-terminus of P006 did not seem to disrupt interactions with the receptor, as it is probably involved in interactions with the hydrophobic pocket, similar to that of Phe27 of the natural hormone CGRP. In fact, both the benzoyl modification and the Phe27 form an amide bond with Val28 and present a benzyl ring which may be involved in stacking interactions. Fluorine additions on the aromatic ring in *para*-position (LJMU017) or in *para*-, *meta*-, and *ortho*- positions (LJMU018) of the benzoyl ring were slightly detrimental compared to LJMU027, even though the activity of the analogues against the receptor was still comparable to that of P006.

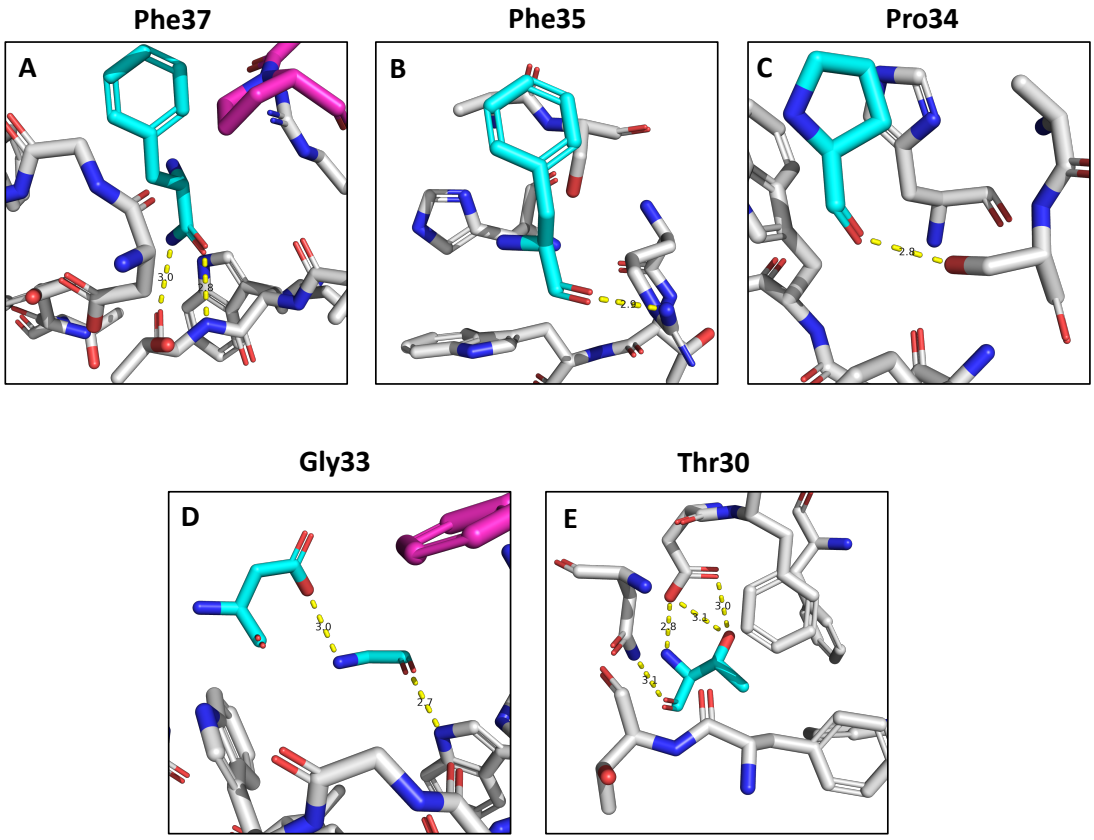

Figure 3.40. Polar interactions between P006 (light blue) and CLR (grey)/RAMP1 (pink) of the CGRP receptor. Oxygen atoms are coloured in red and nitrogen atoms in blue. (A) Phe37 residue interacting with Thr122 through carbonyl and amide groups. (B) Carbonyl group of Phe35 residue interacting with Arg119. (C) Pro34 carbonyl group interacting with Ser117. (D) Gly33 carbonyl group interacting with Trp121; side-chain carbonyl group of Asp31 interacting with nitrogen of Gly33 of P006. (E) Thr30 interacting with Asn128 through carbonyl group and with Asp94 through amine and OH. Lengths of the H bonds are reported in Å (between 2.8 and 3.3 Å) and shown with a dashed yellow line.

3.5.9 Cytotoxicity assay (Alamar Blue)

LJMU017 (4-F-benzoyl P006), the first N-benzoylated compound synthesised, was selected as an example and tested for cytotoxicity through the resazurin assay (Alamar blue). A mock treatment was performed to prove that the media containing DMSO used to dilute the peptide stock solution did not influence cell survival. The resazurin assay showed that, at the concentrations tested, LJMU017 did not

significantly influence Calu-3 cell survival, even though a decrease in cell survival proportional to the concentration used was detected (Figure 3.41). Notably, the concentration used in the cAMP accumulation assay (10^{-5} M) resulted in a cell survival higher than 90% compared to untreated cells.

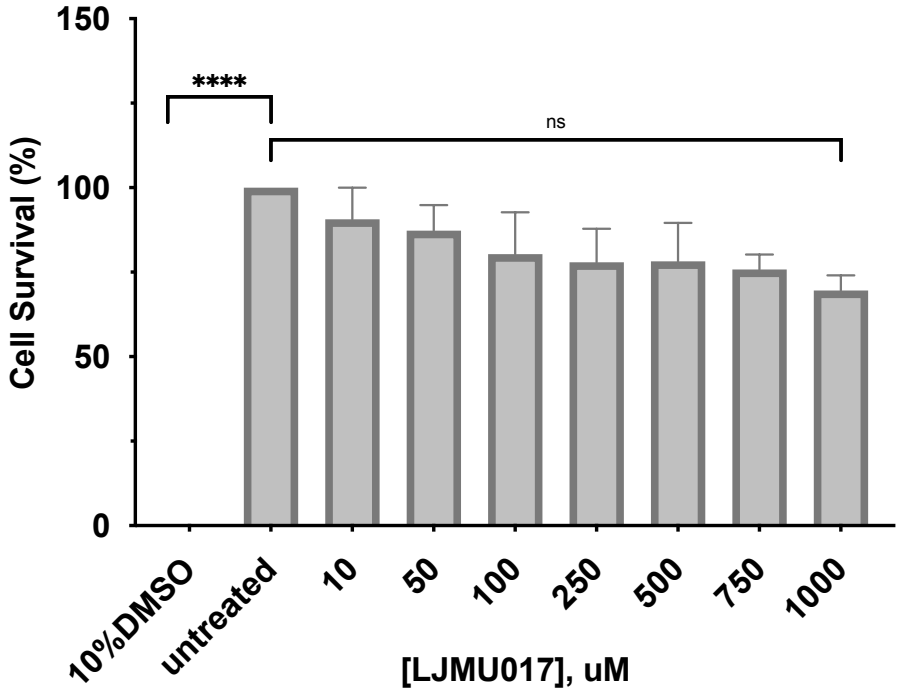

*Figure 3.41. Alamar Blue assay for LJMU017 (n=2). Cell survival after treatment of Calu-3 cells with increasing concentrations of peptide. Statistical analysis performed with ordinary one-way ANOVA in GraphPad Prism is reported in the graph; ns=non-significant (p> 0.05, applies to comparison of each tested concentration with the 'untreated' control); ****p≤0.0001.*

3.6 Conclusions

In this chapter, we described the design and synthesis of a library of peptide and peptidomimetic antagonists of the CGRP-R. Various strategies were considered to modify the lead compound (P006), including fluorination, peptoid replacement and N-terminal modifications.

P006 and derivatives were all synthesised by automated microwave peptide synthesis in high yields (~50-90%). Purification through preparative-HPLC or flash chromatography was needed in each case to obtain purity suitable for further biological testing (>90%). LJMU019 was used to test the efficiency of the two purification methods, finally demonstrating that for well separated chromatographic peaks, flash chromatography is a cheap and quick technique to purify peptides.
^{19}F NMR was used to study P006 conformation, proving that information on *cis* and *trans* populations can be obtained by adding fluorine atoms distal from the peptidylprolyl bond.

The effects of these modifications on lipophilicity were assessed both experimentally and *in silico.* While peptoid-editing at various positions did not cause any major effect on lipophilicity, the addition of fluorine atoms to Phe residues caused an increase in lipophilicity proportional to the number of fluorine atoms added. Similarly, aromatic appendages at the N-terminus yielded compounds with increased lipophilicity.

The affinity of the peptides for the CGRP-R was studied indirectly through a cAMP accumulation assay. Fluorination was generally found to be detrimental for activity either abolishing the antagonist activity (in LJMU014 and LJMU016) or significantly reducing it (in LJMU011, LJMU012, LJMU013), with the exception of LJMU015, where the activity was comparable to that of P006. Peptoid replacement was only tolerated in two positions, being Phe37 (LJMU019) and Val28 (LJMU024). Finally, N-benzoylated analogues (i.e., LJMU017, LJMU018 and LJMU027) exhibited activity comparable with or better than P006. Hence, as proof of principle, the toxicity

potential of LJMU017 was assessed in lung cancer cells (Calu-3), in which it had no significant effect on cell survival.

This hit-to-lead development study suggested that N-benzoylated analogues are promising compounds and the evaluation of putative improved pharmacokinetic profile is key to identifying the future lead compound of the series. Finally, aromatic appendages at the N-terminus may conceptually result in peptide self-assembly due to the final amphiphilic behaviour of the deriving peptides. All these aspects will be further explored in the subsequent chapters.

4 Pharmacokinetic evaluation of P006 and analogues – method development and testing

4.1 Introduction

When evaluating the potential of a bioactive compound to become a clinically used drug, many factors should be taken into consideration. Biological activity is undoubtedly the most studied property. However, other important considerations for drug development include the evaluation of pharmacokinetic properties e.g. biological stability and plasma protein binding. These aspects will be covered in this chapter.

4.1.1 Proteolytic stability of peptides

Determination of peptide serum stability constitutes a pivotal screening assay for eliminating unstable peptides at an early stage of drug development. For peptide candidates, the path to becoming a successful drug is often challenging due to various ADME issues, such as poor oral bioavailability, low permeability, low metabolic stability, short half-life, and inadequate residence time in tissues [283]. Notably, many peptides showing promising *in vitro* pharmacological activities fail to show good *in vivo* effects. Classically, one of the main reasons is their low metabolic stability becoming the chokepoint to overcome for a peptide candidate to become a drug [283,284].

4.1.1.1 Peptidases

Peptides are subject to proteolysis by peptidases due to the presence of amide bonds in their structures. According to the positional specificity of their activity, peptidases can be classified as exopeptidases, when they act near either end of the peptide chain, or endopeptidases, when they act on the internal bonds of the peptide chain [285]. Further classification of peptidases according to positional specificity is shown in Figure 4.1 [285].

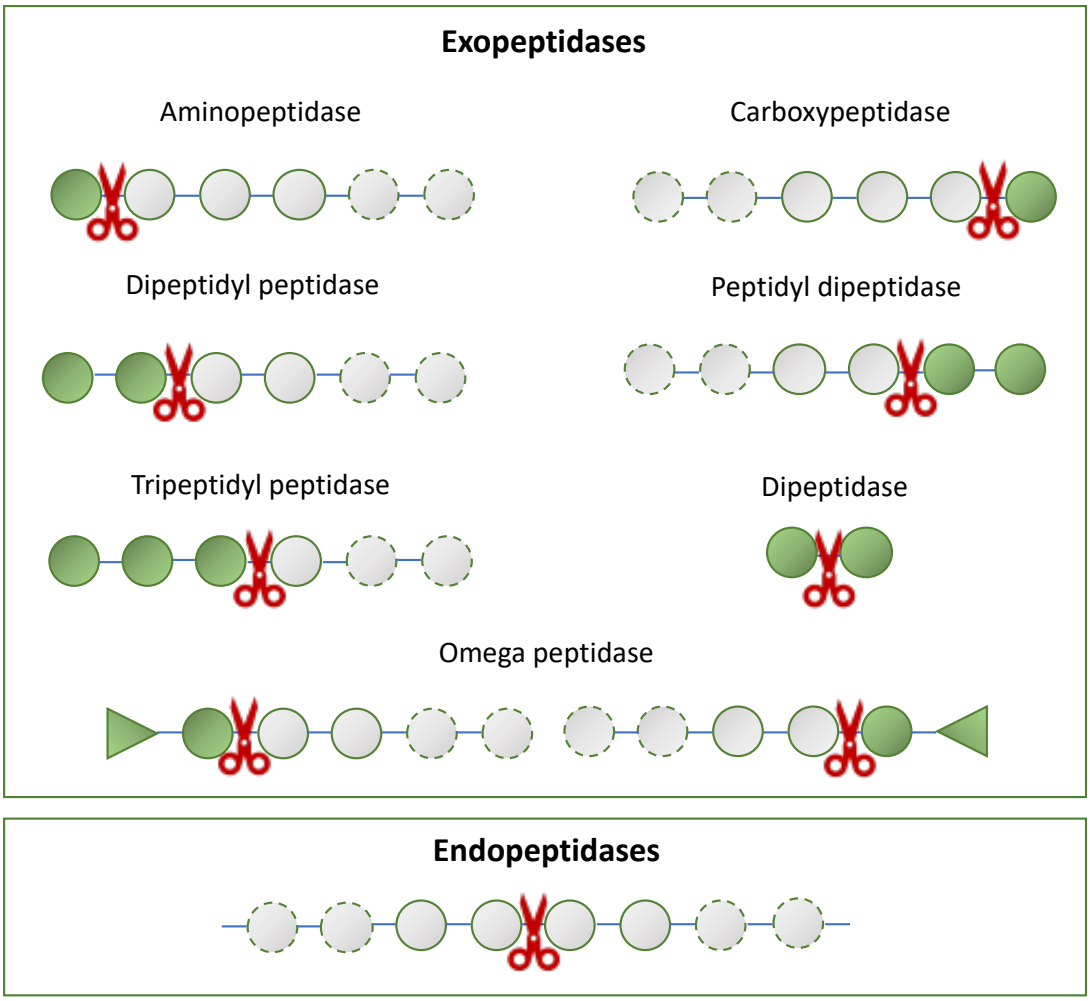

Figure 4.1. Classification of peptidases based on positional specificity [285]. *The spheres represent amino acid residues, and the red scissors are placed on the hydrolysed bond.*

In addition to this classification, according to the chemistry of the catalytic site, peptidases can be categorised into six catalytic types, namely serine, threonine, cysteine, aspartic, glutamic, or metallo-peptidases [285].

4.1.1.2 Methods for proteolytic stability evaluation of peptides

Common methods to evaluate peptide stability include the incubation of the drug candidate at 37 °C in blood serum or plasma or in a medium containing one or more isolated enzymes [284]. Various research groups have attempted to estimate the proteolytic stability of compounds in serum or plasma [286]. After incubation of the

compound in serum/plasma at realistic temperature conditions (i.e., 37 °C) and for various time intervals (from minutes up to 24 h), the reaction is stopped with a quenching reagent, which is typically an aqueous acidic solution composed of hydrochloric acid or trichloroacetic acid, or alternatively an organic solvent (e.g., methanol, acetonitrile, ethanol or a mixture of those). This should ensure the precipitation of larger serum proteins, while leaving peptides and peptide metabolites in solution for further analysis. The precipitation step is followed by the isolation of proteins *via* centrifugation. Subsequent analysis of the intact peptide after incubation is performed using liquid chromatography (RP-HPLC) and/or mass spectrometry (LC-MS, LC-MS/MS or MALDI-TOF) [287–294].

4.1.1.3 Optimisation of the chromatography method to measure intact peptide

Reverse-phase high-performance liquid chromatography (RP-HPLC) is the most widely used technique for separation of peptides and proteins [295]. Usually, the elution/retention of analytes is controlled by increasing the concentration of organic solvent (i.e., methanol or acetonitrile), hereby changing the polarity of the aqueous mobile phase [296]. The ability of a chromatographic method to successfully separate a compound from one or more close-running impurities depends on numerous factors, that can be easily studied and controlled. When designing an optimisation strategy, it is necessary to define a mathematical function to reflect the quality of the separation as a single number [297]. Resolution (R_S) can be defined as the measure of a column to separate chromatographic peaks, and can be calculated through Equation 4.1:

$$\mathrm{Rs} = \frac{2 * (RT_2 - RT_1)}{W_1 + W_2}$$

*Equation **4.1***

where RT_2 is the retention time in minutes of the compound eluted second, RT_1 is the elution time of the compound eluted first, and W_1 and W_2 are their peak widths at half height [295,298].

The easiest way to determine conditions that afford optimal analyte resolution is using multifactorial approaches, such as Design of Experiments (DoE). This allows the identification of the most significant factors affecting the resolution and subsequent optimisation, within a relatively small number of experiments and without requiring a deep knowledge of the physicochemical properties of the system [299]. Orthogonal array designs are employed in analytical method optimisation to create a series of experimental combinations the result of which, expressed as a mathematical function, can be used to extract independently the main effects of each factor [297].

The Plackett-Burman Design (PBD) is a screening tool widely used as a prelude to HPLC method optimisation, to identify which factors under investigation significantly contribute to the response [299–301]. It helps in deciding which factors to concentrate on, thereby reducing the number of experiments to run. Once the most important factors have been identified, a fractional design (e.g., Taguchi design) can be employed to study those factors only. The use of a fractional design allows the user to reduce costs and time associated with the experiments, while still obtaining sufficient information.

Existing literature includes numerous methods for quantification of peptides in biological matrixes using HPLC or LC-MS/MS; however, very little has been done to validate these methods according to International Conference of Harmonization (ICH) guidelines [296,302,303]. Validation of an analytical technique is of pivotal importance as it proves that the technique is adequate for its planned purpose [304].

4.1.1.4 Half-life: definition, kinetic considerations, and strategies to enhance half-life

Half-life ($t_{1/2}$) is defined as the time needed for the concentration of a substrate (typically in blood or plasma) to decrease to half of its initial value [305,306]. This is the most frequently reported pharmacokinetic parameter as it carries important implications for dosing regimens [306]. For this reason, developing an effective approach with which to estimate half-life is of significant importance in peptide research and development.

Chemical reactions can be categorised into zero, first, and second order reactions based on their reaction kinetics. The classical one compartment pharmacokinetic model assumes that both absorption and elimination happen *via* a first-order rate, represented by the constants K_a and K_{el}, respectively. Under these conditions, K_{el} can be calculated from the slope obtained from a graph where the natural logarithm of the concentration of intact drug is plotted against time, as shown in Figure 4.2 [305].

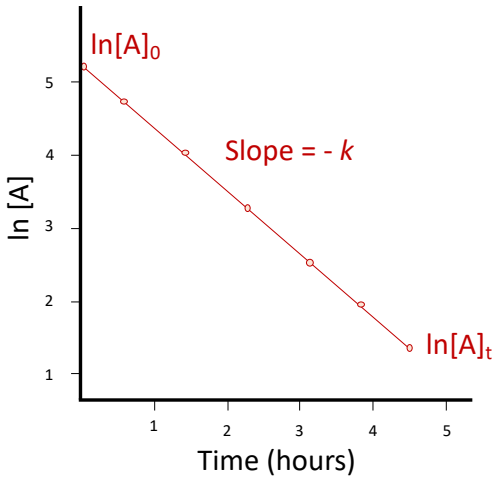

Figure 4.2. Kinetic profile of a first order reaction, characteristic of the once compartment pharmacokinetic model.

A first-order kinetic reaction is represented by Equation 4.2:

$$\ln[A]_t - \ln[A]_0 = -kt$$

Equation 4.2

where $\ln[A]_t$ is the natural logarithm of the concentration of the analyte at time t, $\ln[A]_0$ is the natural logarithm of the concentration of the analyte at time zero, while *k* is the rate constant, and t is the time. This equation can be simplified with Equation 4.3:

$$[A]_t = [A]_0 * e^{-kt}$$

Equation 4.3

From the definition of half-life ($t_{1/2}$), we can state that $[A]_t = [A]_0/2$. Hence, Equation 4.3 can be re-arranged as follows (Equation 4.4) where 0.693 is the natural logarithm of 2 and k (or k_{el}) is the constant of elimination:

$$t_{\frac{1}{2}} = \frac{0.693}{k}$$

Equation 4.4

Half-life reflects on the *in vivo* efficacy of a drug: in most cases, when the half-life is of only a few minutes, the peptide candidate does not exhibit a significant *in vivo* effect as the amount of intact drug that reaches the target tissue is too low and, for this reason, an increase in stability is a prerequisite for clinical use [284]. In general, proteolysis is the main elimination pathway for most peptides and, therefore, a clear understanding of their kinetics and products of degradation is necessary. By detecting the cleavage sites, it is possible to design *ad-hoc* modifications to minimise enzymatic degradation, eventually extending the half-life [283]. As already mentioned, there are several proteolytic enzymes acting at the peptide N- or C-termini, therefore, modifications at this level may be beneficial for the enzymatic stability [284]. Another strategy includes the replacement of specific amino acids known to be susceptible to proteolysis with D-amino acids or with peptoid monomers to delay degradation [215,287].

Octreotide is an example of an approved peptide derived from the modification of an endogenous peptide with a short half-life. Octreotide is an 8-mer synthetic analogue of somatostatin that has a similar pharmacological effect but much longer duration of action due to shortening of the somatostatin sequence (from 14 to 8 amino acids) and replacement of L-amino acids with D-amino acids, leading to an elimination half-life of 1.5 hours, compared to a few minutes for the natural peptide (Figure 4.3) [139,284,307,308].

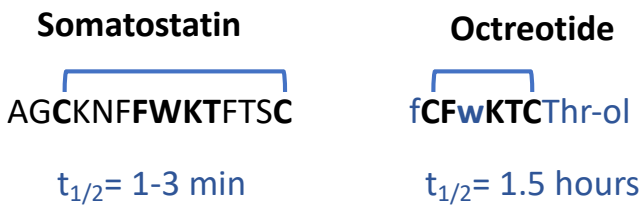

*Figure 4.3. Amino acid sequences, and elimination half-lives of somatostatin and its synthetic analogue octreotide (**23**). Residues not replaced nor eliminated in somatostatin are highlighted in bold in the amino acid sequence.*

4.1.2 Plasma protein binding

Reversible plasma protein binding plays a pivotal role in the pharmacokinetics, pharmacodynamics and availability of a drug in the blood stream; therefore, a careful evaluation of this aspect is necessary in the development of therapeutic agents [309]. The reversible binding of a ligand to serum proteins can significantly alter the free fraction of a drug, leading to pharmacokinetic changes that, in turn, can affect both the therapeutic effect and toxic effect of the drug [310]. This concept relies on the idea that only the unbound fraction can partition into the site of action to interact with its molecular target [311], as represented in Figure 4.4.

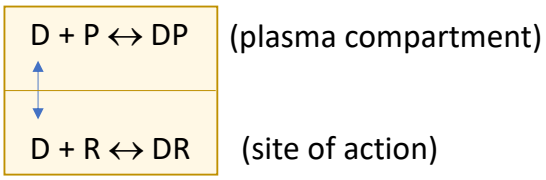

Figure 4.4. Equilibrium equations representing plasma protein binding and drug receptor binding, where D is the free drug, P represents plasma proteins, DP is the complex drug-plasma proteins, R is the receptor at the site of action, and finally DR is the complex drug-target receptor.

Reversible protein binding can be exploited to increase the efficacy of a drug candidate that undergoes fast elimination due to enzymatic degradation and/or fast renal clearance, since the protein-bound fraction is essentially shielded from these

various elimination pathways [312]. When elimination happens at the renal level through glomerular filtration it can be significantly slowed down by excluding bound drugs from filtration [311].

4.1.2.1 Abundant proteins in human plasma

In human blood, endogenous and exogenous compounds are generally transported by plasma proteins, such as lipocalins (e.g., α-1-acid glycoprotein, AGP) and human serum albumin (HSA) [313]. It is generally accepted that acidic drugs favourably bind to HSA, while basic and neutral drugs are mainly bound to AGP. However, in many cases, both HSA and AGP contribute almost equally to binding and transportation of some drugs [313]. HSA is the most abundant protein in human plasma, with an average concentration of ~7.5×10^{-4} M, 100-fold more abundant than AGP (~2×10^{-6} M) [313,314]. Although AGP plasma concentration is lower than that of HSA, levels of this protein may increase in certain pathological conditions (e.g., cancer, infections, cardiovascular, inflammatory, kidney, and liver diseases). Hence, this 42 kDa glycoprotein is of great relevance in the transport of drugs, particularly basic and neutral compounds.

HSA is a globular protein with a molecular weight of ~66 kDa, characterised by a monomeric multi-domain macromolecule and composed by almost all α-helices [313–316]. HSA plays a key role in plasma oncotic pressure and fluid distribution between body compartments, but more importantly, shows a unique capacity to bind ligands [313,314]. The natural ligands of HSA are long-chain fatty acids (FAs), which bind to seven primary binding sites (from FA1 to FA7) and two secondary pockets (FA8 and FA9). On the other hand, HSA contains three flexible primary sites for drugs binding (FA1, FA3-FA4, and FA7) and several secondary binding sites (FA2, FA5, FA6, FA8, and FA9), scattered across the protein (Figure 4.5) [313].

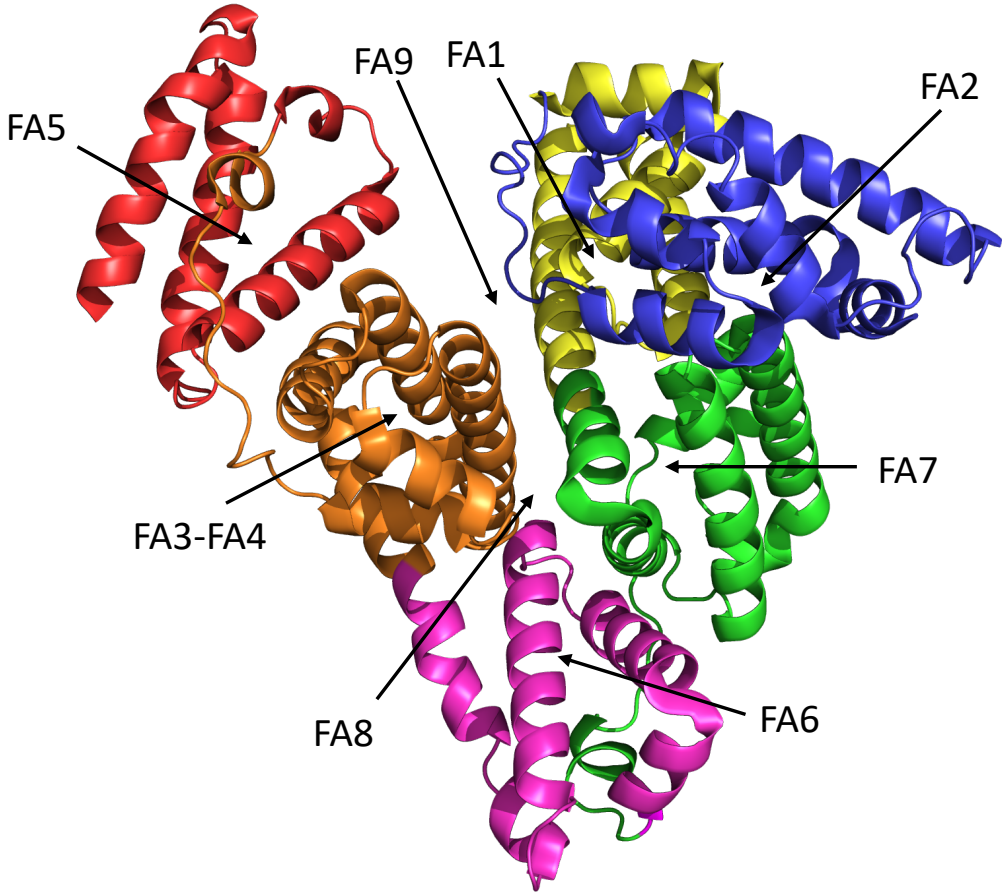

Figure 4.5. Three-dimensional structure of HSA and FA binding sites (PDB: 2BXG). The subdomains of HSA are represented with different colours: Domain Ia (res 5-118, tv_blue, N-terminal), Domain Ib (res 119-195, tv_yellow), Domain IIa (res 196-313, tv_green), Domain IIb (res 314-383, magenta), Domain IIIa (384-509, tv_orange) Domain IIIb (res 510-582, tv_red, C-terminal) [313,316,317].

4.1.2.2 Dissociation constant (K_D)

Generally, an equilibrium constant (*K*) is defined as the ratio of the equilibrium concentrations of the reaction products to reactants or vice versa. In a simple bimolecular model reaction such as:

$$P + L \underset{k_{off}}{\overset{k_{on}}{\rightleftharpoons}} PL$$

Equation 4.5

where P and L are protein and ligand, respectively, K_{on} is the association rate constant for the forward reaction, while K_{off} is the dissociation rate constant for the backward reaction [318,319].

At the steady state, the rate of forward reaction is equal to the rate of backward reaction and both the equilibrium association and the dissociation constants, reciprocally related, can be defined [320,321]. In particular, the equilibrium association constant (K_a) can be described with the following equation:

$$K_a = \frac{[PL]}{[P] * [L]}$$

Equation 4.6

In contrast, the dissociation constant (K_D), defined as the concentration of ligand at which half the ligand binding sites of the protein are occupied, can be described with the equation:

$$K_D = \frac{[P] * [L]}{[PL]}$$

Equation 4.7

In this situation, increasing amounts of P may be titrated against a fixed amount of ligand and the equilibrium concentration of the product PL may be determined.

4.1.2.3 Methods to measure plasma protein binding in vitro

In vitro quantification of small molecule drug candidates binding to plasma proteins has been attempted using numerous strategies. These approaches include equilibrium dialysis (ED), ultrafiltration (UF), ultracentrifugation (UC), as well as more innovative techniques, such as immobilised HSA chromatography, micropartitioning and biosensor-based analysis [309,311,322]. However, only ED, UF and UC are extensively accepted and used [322,323], and they all rely on the physical separation of the bound drug from the unbound and on the quantification of the two, to finally

calculate their relative fractions. In particular, ED and UF use semipermeable membranes, where the unbound drug can be separated from the protein-drug complex and then quantified with a suitable analytical technique (e.g., HPLC, LC-MS) [311]. On the other hand, UC relies on the use of centrifugal forces to separate the protein fraction from the free drug fraction according to their different densities [323–325].

4.1.2.3.1 Equilibrium dialysis (ED)

Equilibrium dialysis (ED) is the method of choice for studying plasma protein binding as it is a straightforward but effective technique and is less susceptible to experimental artifacts (e.g., volume shifts or apparent binding due to drug trapping by the UF membrane) [326–328]. Generally, the final aim is to indirectly measure the amount of a ligand bound to a protein by dialysing the unbound fraction through a membrane, until its concentration is at equilibrium. A standard equilibrium dialysis set-up includes two chambers separated by a membrane, which only the ligand is able to cross, as the molecular weight cut off (MWCO) is chosen such that it will retain the protein component [310,311]. A ligand solution of known concentration and volume is placed into the sample chamber and the time for it to equilibrate through the system is studied. When the protein is added to the sample chamber, only the free ligand will diffuse across the membrane and equilibrate, while the bound ligand will be retained. A schematic diagram of a standard equilibrium dialysis assay is represented in Figure 4.6.

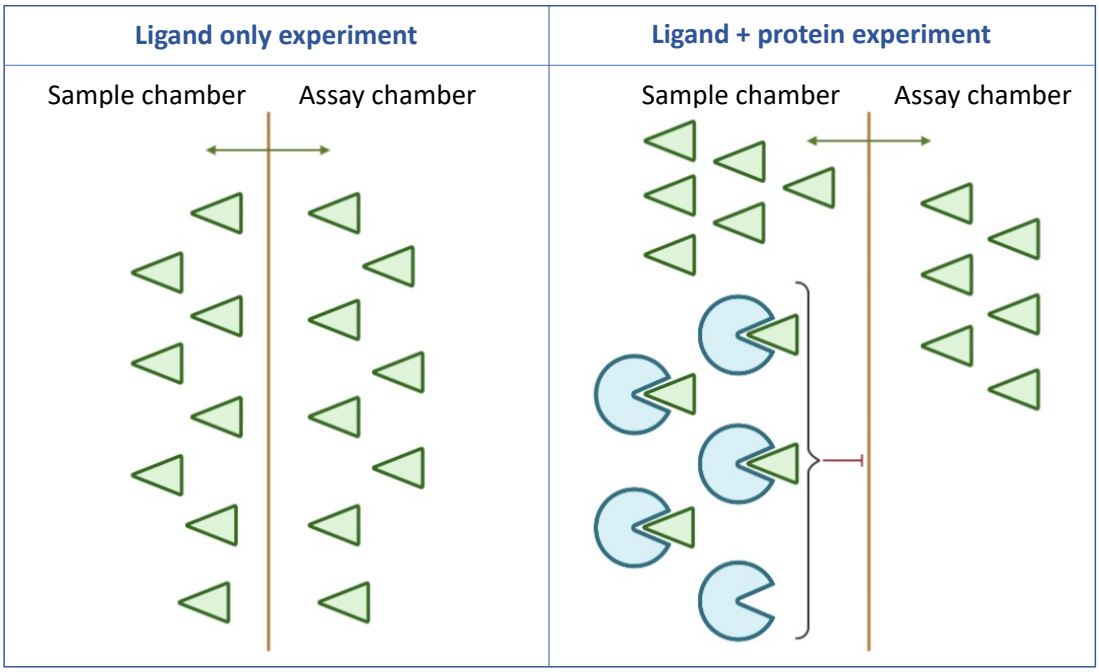

Figure 4.6. Schematic diagram of protein binding experiment through ED.

Various kits are commercially available for ED experiments. In recent years, to facilitate the determination of protein binding for large compound libraries, high throughput parallel sample processing devices were designed; a few examples are the 96-well Rapid Equilibrium Dialysis (RED) device from Thermo Scientific, the 96-well Equilibrium Dialyzer from Harvard Bioscience, and the 96-well Micro Equilibrium Dialysis Device from HT-dialysis LLC [311,326,329].

Figure 4.7 shows a schematic representation of the Thermo Fisher RED device experimental procedure. In detail, a RED device is composed of a Teflon base plate that can hold up to 48 disposable dialysis inserts. Each insert is made of two side-by-side chambers (coloured in red and white), separated by a vertical cylinder of cellulose dialysis membrane that allows the passage of the compound but retains the proteins [330,331].

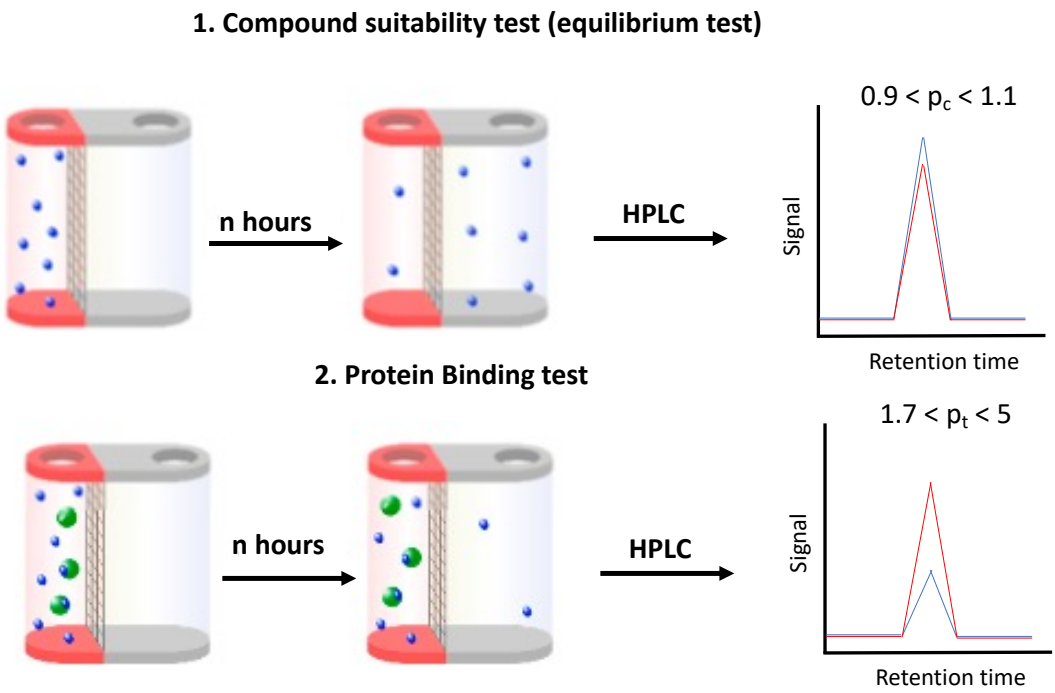

Figure 4.7. Schematic representation of the two-step RED experimental procedure. Step 1 is the compound-only experiment to check if the compound is suitable for dialysis and to find the time necessary to reach equilibrium. p_c is the partition coefficient of the compound in the absence of protein. In step 2, the step 1 is repeated under identical conditions but adding protein in the sample chamber. p_t is the partition coefficient in the presence of the target protein [329].

4.1.2.3.2 Ultrafiltration (UF)

Ultrafiltration (UF) is a reliable routine technique for estimating drug protein binding. With this methodology, the free drug is separated from the bound fraction in an easy and rapid way [311,332–334]. The idea behind UF is to separate small volumes of protein-free phase by applying centrifugal forces to a solution containing both the protein-drug complex and the free drug. UF devices available are composed of two compartments separated by a semipermeable membrane with a molecular weight cut off (MWCO) that limits the protein filtration while allowing the free drug filtration [322]. Advantages related to the use of UF methodology include speed, simplicity, and achievement of accurate and quantitative data. However, some of the major limitations to consider are the nonspecific binding of drugs to the semipermeable

membrane and to the material of the UF device, as well as the sieving effect typical of high MW molecules, protein leakage, and influence of experimental conditions (i.e., pH, temperature and relative centrifugal force) [322]. A schematic diagram of an UF apparatus is shown in Figure 4.8.

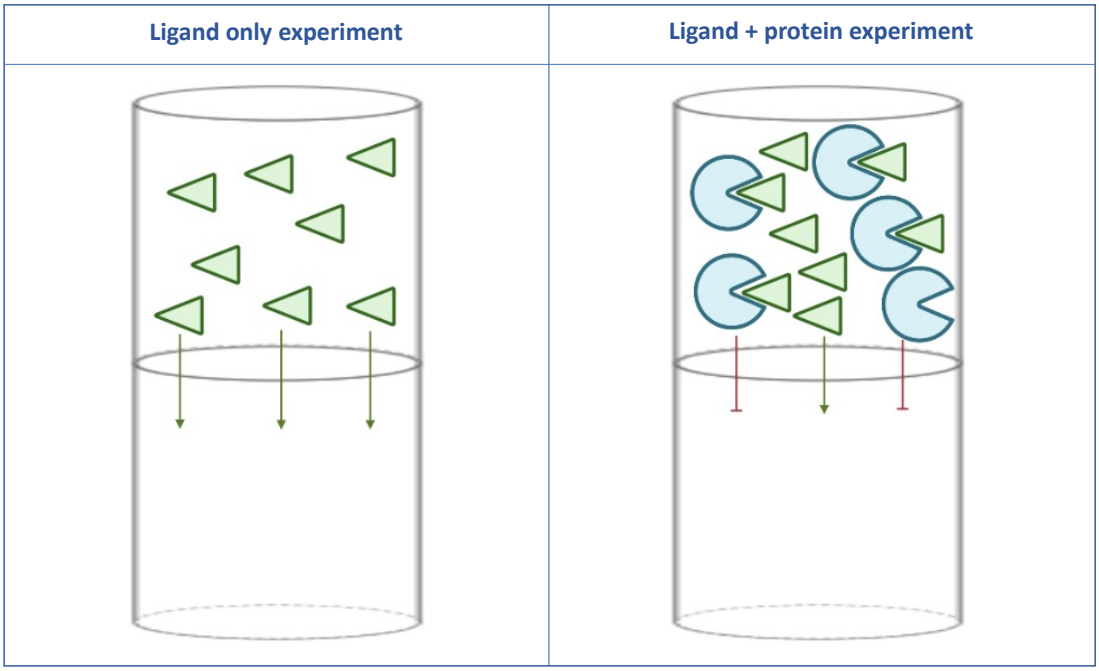

Figure 4.8. Schematic diagram of an ultrafiltration device used for plasma protein binding estimation. The ultrafiltration unit allows the filtration of free drug (in green), while protein and protein-drug complexes (in blue and green) are retained in the upper compartment.

Commercially available kits for ultrafiltration include disposable centrifugal concentrators containing a vertical membrane and thin channel filtration chamber (e.g., Sartorius Vivaspin 500 equipped with polyethersulfone membrane), as well as kits for high throughput studies, used for automating early drug discovery assays and pharmacokinetic studies (e.g., Millipore Corp. kit). A picture of the Sartorius Vivaspin 500 apparatus and the structure of polyethersulfone (PES, **83**) are shown in Figure 4.9.

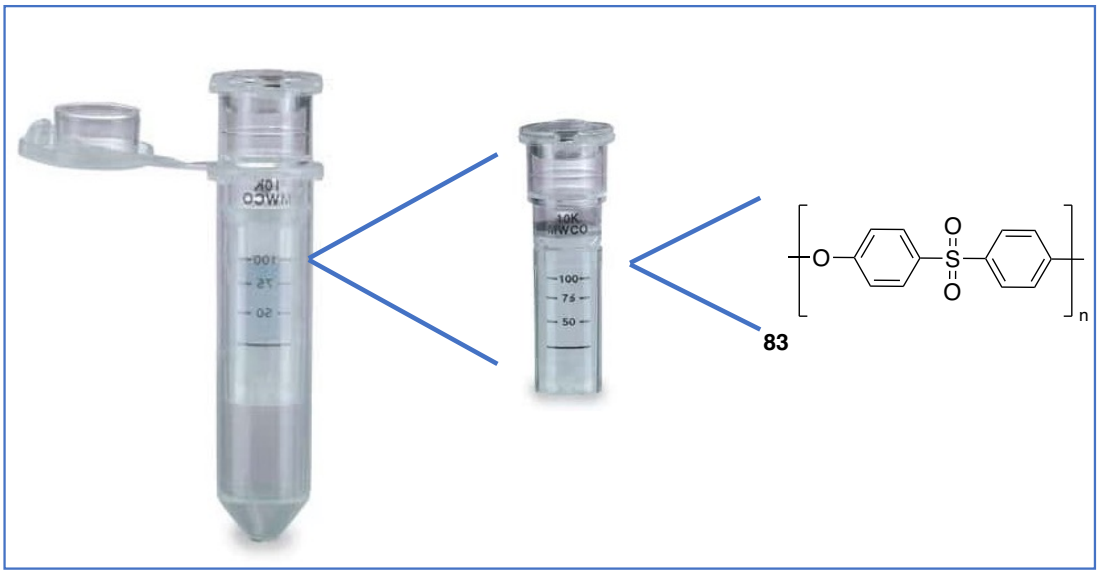

*Figure 4.9. Sartorius Vivaspin 500, 10 kDa MWCO apparatus and polyethersulfone (PES, **83**) structure* [335,336].

4.1.2.3.3 Ultracentrifugation (UC)

Ultracentrifugation (UC) is a widely used method for determination of the free fraction of drugs in blood plasma, especially for highly lipophilic compounds [323]. UC methods simply encompass sample spinning to separate the free drug phase from the protein-containing phase [323,324]. Hence, compared to ED and UF, UC overcomes the issue of non-specific binding due to drug absorption to the membrane, emblematic of lipophilic drugs, as it does not employ a membrane [323–325]. However, in the calculation of the free drug using UC, two critical assumptions are necessary. The first one is that the free drug fraction contains no protein, while the second one is that ultracentrifugation causes no alteration of binding equilibrium, both of which are difficult to prove [323].

4.1.2.4 Peptide plasma protein binding

To the best of our knowledge, the abovementioned techniques to quantify the extent of plasma protein binding have all been explored, studied, optimised, and validated for small molecule candidates. However, *in vitro* protein binding studies have rarely been exploited specifically for peptides. One example is the joint work between different departments of Novo Nordisk A/S (Måløv DK-2760, Denmark) where a novel

methodology, named reiterated stepwise equilibrium dialysis method, was used to measure the *in vitro* plasma protein binding of liraglutide (molar mass of 3751.262 g/mol) [337]. Moreover, Greco and collaborators explored the extent of protein binding of two small peptidomimetics (molar mass of 1050-1200 g/mol) by using Thermo Fisher RED kit [338].

The optimisation and validation of methodologies to study plasma protein binding of peptides is necessary as this is a key property with which to make an informed decision when selecting the best candidates to bring forward during the drug discovery and development stage.

As previously discussed, the approval of a large number of peptide leads has been impeded by their short *in vivo* half-life and fast elimination. The majority of peptides are subject to enzymatic degradation and fast renal clearance. One way to reduce the rate of clearance is to chemically conjugate them to small moieties that, by increasing binding to circulating proteins, can prevent their fast filtration through the kidneys [312]. Examples of albumin binders are shown in Figure 4.10, of particular interest are palmitic acid (**85**) and stearic acid (**86**) which have been conjugated to the glucagon-like peptide-1 (GLP-1) receptor agonists, liraglutide and semaglutide, respectively. By doing so, their half-lives (liraglutide: $t_{1/2}$ = 13 h; semaglutide: $t_{1/2}$ = 168 h) were significantly improved compared to exenatide ($t_{1/2}$ = 2.4 h), the parent peptide containing only natural amino acid residues [139].

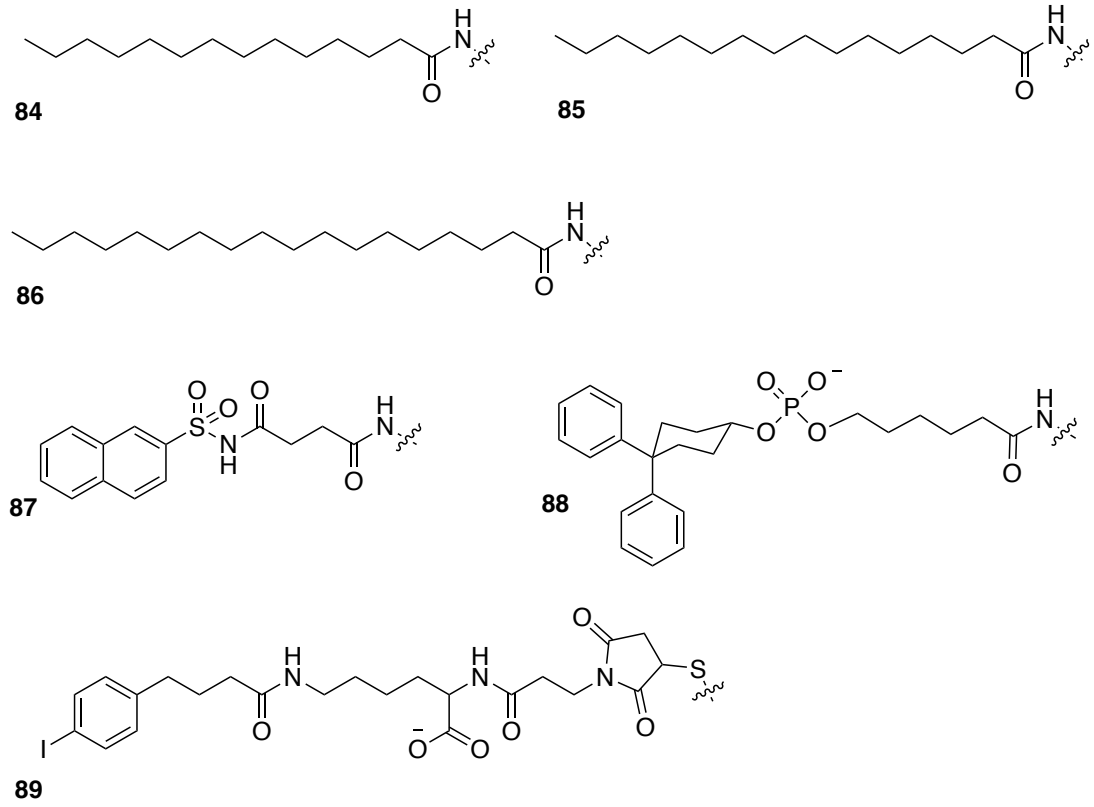

*Figure 4.10. Chemical structures of albumin-binders: myristic acid (**84**), palmitic acid (**85**), stearic acid (**86**), naphthalene acylsulfonamide (**87**), diphenylcyclo-hexanol phosphate ester (**88**), 6-(4-(4-iodophenyl) butanamido) hexanoate ('Albu'-tag, **89**)* [139,312,339–341].

4.1.3 Effect of modifications on pharmacokinetic properties

4.1.3.1 Fluorine modifications

The benefits of introducing fluorine atoms into organic molecules are mostly related to the modification of physicochemical properties (e.g., control of conformational properties, modulation of acidity and lipophilicity), as well as interference with metabolic pathways, ultimately resulting in alteration of the biological and/or pharmacological properties [189,197]. In drug candidate optimisation, 'fluorine-editing' has become a widely accepted strategy to tune properties not only of small molecules, but also of peptides and proteins.

In the past two decades, fluorine-containing amino acids have gained increasing attention, and the effect of these modifications on peptide conformation, activity,

folding, and physicochemical and biological stability has been widely studied [200,204]. The impact of fluorination on rate, route, and extent of peptide metabolism was explored by numerous research groups with conflicting results, depending on the amino acid replaced and on the position of the modification in relation to the cleavage site [144,198,199]. Various fluorinated amino acids (e.g., 4-F-Phe, 3-F-Phe, HfVal, HfLeu) have been investigated for their ability to tune the proteolytic stability of biologically active peptides and proteins [200]. In particular, HfLeu substitution has been explored in GLP-1 analogues to improve binding affinity and protease (DPP IV) stability [201]. A study carried out by Middendorp *et al*. explored the effect of various modifications on the affinity and stability of Factor XIIa inhibitors, proving that the replacement of Arg1 with 4-F-Phe resulted in increased affinity but a 1.4-fold reduction in half-life [342]. A similar outcome was derived from a study of fluorine substitution on the trypsin inhibitor SFTI-1, where the replacement of Lys5 with 4-F-Phe increased the inhibitory activity with no significant influence on the resistance to proteolysis [200].

4.1.3.2 Peptoids

Peptoids are emerging therapeutics that evade proteolytic degradation yet maintaining the same properties that confer peptides a great potential [343].

When the amino acid side chains and carbonyl groups are misaligned, the peptide bond is out of range of the usual nucleophilic catalyst active sites, resulting in impeded cleavage, and consequent improved stability [215]. However, only few research groups have reported evidence of this increased proteolytic stability. The positive effect of peptoid introduction on the extent of cleavage by various peptidases was confirmed by Miller *et al*. [215]. Moreover, complete stability of antimicrobial peptoids against tryptic digestion compared to the natural occurring peptide was confirmed by Luo and collaborators [344]. Finally, Greco *et al*. studied, for the first time, the ADME profile of a peptide-peptoid hybrid and a peptoid with antimicrobial activity. The stability study using proteases, plasma or liver microsomes showed great resistance to degradation, while a plasma protein binding study using RED devices showed high protein binding (>98%) [338].

4.1.3.3 N-terminal modifications

As common in numerous drug discovery programs, while the effect of N-benzoylation on receptor affinity has been studied for CGRP 8-37 and CGRP 27-37 cyclic derivatives [68,240], the effect on the pharmacokinetic properties has never been explored. In particular, the proteolytic stability of N-benzoyl derivatives may be affected, when the peptide is attacked by aminopeptidases because protecting the N-terminus by addition of lipophilic groups may preclude hydrolytic cleavage, leading to a greater *in vivo* efficacy due to longer residence of the peptide at the site of action [236]. Moreover, plasma protein binding may be promoted by the increased lipophilicity conferred to the peptide by the aromatic appendages as well as by the fact that the N-benzoyl moiety may act as an HSA binder, similarly to those described in Section 4.1.2.4.

4.2 Aims and Objectives

The aim of the work reported in this chapter was to develop appropriate methods to assess the biological stability and plasma protein binding of modified peptides.

4.3 Materials and Methods

4.3.1 Materials

Serum from human male AB plasma (USA origin, sterile-filtered, H4522, Lot#SLCF0252), trichloroacetic acid, trifluoroacetic acid, and DMSO were purchased from Sigma and used without further treatment. RED device for Rapid Equilibrium Dialysis (single-use plate with 8 kDa MWCO inserts (cat. number 90006) and single use plate with 12 kDa MWCO inserts (cat. number 91012), Thermo Fisher Scientific) and Sartorius Vivaspin 500 10 kDa MWCO PES devices (Fisher Scientific) were purchased from commercial suppliers and used as indicated in the appropriate experimental procedures. Non-denatured Human Serum Albumin was purchased from EMD Millipore Corp.

Solvents for liquid chromatography (i.e., acetonitrile HPLC-grade, methanol HPLC-grade) and Phosphate Buffered Saline (PBS) tablets (tablet formulation: sodium

chloride 137 mM, phosphate buffer 10 mM, potassium chloride 2.7 mM) were purchased from Fisher Chemicals.

4.3.2 Peptide chemical stability

4.3.2.1 Stability over 24 h at 37 °C

Peptide solutions (200 µL, in H_2O, 5% DMSO) at different concentrations (500, 250, 100, 50 µM) were incubated at 37 °C for 24 h while shaking at 200 rpm. Then, the solutions were centrifuged for 5 min at 13,200 rpm. The supernatant was analysed by RP-HPLC using method described in section 4.3.5.5. The resulting area under the peak of interest was analysed against a calibration curve (serial dilutions of peptide in PBS, 5% DMSO). Retention time of the peak of interest was used to check possible peptide degradation. The experiment was performed in duplicate.

4.3.2.2 Stability in acidic conditions

A peptide solution (200 µL, 125 µM, in PBS, 5% DMSO) was incubated at 37 °C for 15 min with shaking at 200 rpm. After addition of TCA aq. (40 µL, 15% *w/v*), the peptide solution was cooled in ice for 15 min and then spun at 13,200 for 5 min. The resulting supernatant was analysed by RP-HPLC using the method described in section 4.3.5.5. Control samples were prepared under the same conditions but adding H_2O instead of TCA aq. solution and taken as 100% against the TCA samples. Retention time of the peak of interest was checked to exclude the possibility of peptide degradation. The experiment was performed in duplicate.

4.3.3 Biological stability of peptides in human serum

4.3.3.1 Biological stability procedure A – TCA quenching

For blood stability evaluation, aqueous pooled human serum (25% *v/v*) temperature-equilibrated at 37°C for 15 min was spiked with the compound under evaluation to a final concentration of 0.1 mg/mL and final volume of 200 µL (five samples in total). Samples were mixed in a sample mixer (HulaMixer, orbital mixing at 20 rpm) at 37 °C. At known time intervals (i.e., 0, 15, 30, 45, 60 min), the reaction was stopped by

adding TCA aq. (40 μL, 15% *w/v*). The cloudy reaction samples were cooled in ice (>15 min) to precipitate serum proteins, before centrifugation at 13,200 rpm (Eppendorf centrifuge 5415 D) for 2 min to pellet the precipitated proteins. The resulting supernatant was analysed by RP-HPLC using a method specifically optimised and validated for the stability study (see section 4.3.5.4). The concentration of intact peptide at time zero was taken as 100% and concentrations were measured against a calibration curve (see Appendix). A blank control experiment was carried out under the same conditions but adding deionised H_2O in place of peptide stock solution. The experiment was performed in triplicate.

4.3.3.2 Biological stability procedure B (for P006, 017, 018, 027) – MeOH quenching

An alternative procedure for assessment of peptide stability in serum included the use of MeOH for protein precipitation, as follows. Pure human serum (47.5 μL) was added to five 2-mL Eppendorf tubes. Both the serum containing Eppendorf tubes and the peptide stock solution (0.13 mg/mL in H_2O, 1.2% DMSO) were temperature-equilibrated at 37 °C for 15 min. Peptide stock solution (153.5 μL) was added to each Eppendorf tube to reach a final concentration of peptide of 0.1 mg/mL and to dilute serum to 25% *v/v*. A control experiment was carried out under the same conditions but adding 153.5 μL of deionised H_2O (1.2% DMSO) in place of peptide stock solution. Samples were mixed at 37 °C in a sample mixer (HulaMixer, orbital mixing at 20 rpm). After 0, 15, 30, 45, and 60 min, the reaction was stopped by adding MeOH (200 μL). The cloudy reaction samples were chilled in ice (>15 min) to precipitate serum proteins, before centrifuging at 13,200 rpm (Eppendorf centrifuge 5415 D) for 10 min to pellet the precipitated proteins. The resulting supernatant was analysed by RP-HPLC using a method specifically optimised and validated for this study (see section 4.3.5.4). The concentration of intact peptide at each time point was measured against a calibration curve; the peptide concentration at time zero was taken as 100%. The experiment was repeated three times for each peptide.

4.3.4 Plasma protein binding method development

4.3.4.1 Human Serum Albumin (HSA) precipitation method

A solution of peptide (200 µL; in PBS, 5% DMSO, 500 or 125 µM) and HSA (80 µM) was incubated with shaking at 200 rpm for 15 min, 30 min, 60 min, and 24 h at 37 °C. HSA was then precipitated by addition of TCA aq. (40 µL; 15% *w/v*) or pure MeOH (600 µL). The samples were kept in ice for 15 min, then centrifuged at 13,200 rpm for 5 min. As a control, a solution of peptide (500 or 125 µM, in PBS, 5% DMSO) was treated under the same conditions. Protein binding was then estimated using Equation 4.8:

$$\%\ unbound\ peptide = \frac{[peptide] in\ PBS\ solution\ containing\ HSA}{[peptide] in\ PBS\ only\ solution} * 100$$

Equation 4.8

4.3.4.2 K_D determination by HSA precipitation method

A peptide solution (50 µM, 200 µL, in PBS, 5% DMSO) was incubated with HSA at various concentrations (10, 25, 50, 80, 100, 150, 200, 250, 400 µM) for 15 min at 37°C with shaking at 200 rpm. HSA was precipitated by addition of TCA aq. (40 µL; 15% *w/v*) and samples were refrigerated in ice for 15 min to facilitate HSA precipitation. The protein was then pelleted by centrifugation (13,200 rpm for 5 min) and the supernatant was analysed by RP-HPLC with method described in section 4.3.5.5. A solution of peptide without protein (50 µM, in PBS, 5% DMSO) was treated under the same conditions and used as a control. Each experiment was performed in triplicate. K_D was determined by estimating the concentration of HSA at which 50% of the peptide was bound.

4.3.4.3 Rapid Equilibrium Dialysis (RED) method

The Teflon base plate was washed thoroughly with 20% ethanol and allowed to dry before use. The RED inserts (both MWCO 8 kDa and 12 kDa) were then inserted in the Teflon base, taking care of not damaging the membranes. Each peptide was

tested to assess the diffusion rate and the time interval necessary for the two compartments to reach equilibrium. To do so, a peptide solution (100 µL, 500 µM, in PBS at pH 7.4, 5% DMSO) was added to the sample chamber (red), while aq. PBS buffer (300 µL, pH 7.4, 5% DMSO) was added to the adjacent chamber (white). The plate was sealed with parafilm and tape, and the system shaken at 200 rpm at room temperature or 37 °C for the required time (4, 6, 8, and 24 h), depending on the experiment), after which, the seal was removed from the plate and 80-100 µL aliquots were taken from each side of the insert and analysed by RP-HPLC (method described in section 4.3.5.5). The peptide concentration was obtained by measuring the area under the peak at the retention time corresponding to the peptide, and comparison against a calibration curve (peptide serial dilutions prepared in PBS, 5% DMSO – see Appendix). The retention time was used to check if the peptide was degraded. The compound was considered suitable for dialysis under certain conditions if the partition coefficient (p_c) was between 0.9 and 1.1, calculated with Equation 4.9:

$$p_c = \frac{[compound]_{red\ chamber}}{[compound]_{white\ chamber}}$$

Equation 4.9

For the protein binding experiment, a solution of peptide and HSA (500 µM and 80 µM, respectively, in PBS, 5% DMSO) was added to the sample chamber (red), while buffer (300 µL, PBS, 5% DMSO) was added to the adjacent chamber. The plate was sealed, and the system was equilibrated at 37 °C for 12 h (12 kDa devices) or 24 h (8 kDa devices) while shaking at 200 rpm. At the established time points, the parafilm was removed and 100 µL of solution was taken from the buffer chamber and analysed by RP-HPLC as it was, while 80 µL of HSA-containing solution was added to MeOH (240 µL) to precipitate HSA. The sample was cooled in ice for 15 min and then centrifuged at 13,200 rpm for 5 min prior RP-HPLC analysis of the supernatant (method described in section 4.3.5.5).

The % of free peptide was calculated with the following equation:

$$\%\ free\ compound = \frac{C_1}{C_2} * 100$$

Equation 4.10

where C_1 is the concentration of peptide in the white chamber and C_2 is the concentration of peptide in the red chamber in the protein binding experiment. Both the equilibrium experiment and the HSA binding experiment were conducted in duplicate.

4.3.4.4 Ultrafiltration membrane method

Peptides (200 µL, 125 µM, in PBS, 5% DMSO) were incubated for 24 h at 37 °C with HSA (80 µM) while shaking at 200 rpm. After 24 h, free peptide was isolated from the protein by ultrafiltration. An aliquot of solution (150 µL) was added to a Vivaspin 500 ultrafiltration device equipped with a 10 kDa MWCO PES membrane. First, the samples were centrifuged at 13,200 for 7 min, then additional PBS buffer solution (100 µL, 5% DMSO) was used to wash the membrane and the solution was centrifuged again at 13,000 for 7 min at room temperature. The washing step was repeated twice. Finally, the peptide concentration in the filtrate was measured by RP-HPLC, using the analytical method described in section 4.3.5.5. A parallel control experiment for each replicate was carried out under the same conditions without the HSA in solution to assess the percentage of recovered peptide in the retentate in the absence of protein (taken as 100%). The experiment was conducted in duplicate.

4.3.4.5 K_D determination by ultrafiltration membrane method

Determination of K_D through ultrafiltration was carried out by incubating the peptide with HSA at different concentrations. PBS aq. solution (5% DMSO) containing peptide (125 µM) and HSA at different concentrations (100, 200, 300, 400 µM) was incubated for 15 min at 37 °C while shaking at 200 rpm. An aliquot of the solution (150 µL) was

added to a Vivaspin 500 ultrafiltration device equipped with a 10 kDa MWCO PES membrane and centrifuged for 7 min at 13,200 rpm. Then, the PES membrane was washed twice by adding PBS buffer solution (100 µL, 5% DMSO) and centrifuging at 13,200 rpm for 7 min. The filtrate solution was analysed by RP-HPLC (see section 4.3.5.5 for analytical method's details).

Two control samples of peptide solution (PBS, 5% DMSO, 125 µM) were prepared for each replicate and treated under the same conditions (incubated for 15 min at 37 °C while shaking at 200 rpm), then 150 µL of one was added to the ultrafiltration device and spun for 7 min at 13,200 rpm, and finally washed twice with PBS solution (100 µL), while 150 µL of the second one was added to an Eppendorf tube (in the absence of PES membrane), centrifuged for 7 min at 13,200 rpm, then centrifuged two more times after dilution aq. PBS (100 µL, 5% DMSO). Each experiment was performed in duplicate.

4.3.5 Analytical methods

4.3.5.1 Standard HPLC method for peptides prior optimisation

Initially, quantification of intact peptides and peptoid-peptide hybrids in the supernatant solution derived from stability study was carried out by RP-HPLC using a standard HPLC method for peptide quantification. Samples were analysed using an Agilent 1100 HPLC system equipped with a Phenomenex Aeris PEPTIDE XB-C18 LC Column (150 x 4.6 mm, pore size: 3.6 µm) and UV detector (absorbance measured at 215 nm), employing a binary eluent system of H_2O/0.1% TFA, and MeCN/0.1% TFA. A gradient method from 99% H_2O/0.1% TFA to 99% MeCN/0.1% TFA was employed, with a run time of 22 min at a flow rate of 1 mL/min, injection volume of 10 mL, and a temperature in the column compartment of 25 °C. Finally, the column was equilibrated back to initial conditions for 2 min. Operating pressures were in the range of 140-180 bar.

4.3.5.2 HPLC Method optimisation (DoE)

To optimise the HPLC conditions, two design of experiments (DoE) were carried out in triplicate: a Plackett-Burman Design and a Taguchi Design. The endpoint of the two designs was evaluated as the resolution (R_s, Equation 4.1) between the two peaks [298].

In the Plackett-Burman design (PBD), seven factors were studied, as listed in Table 4.1: column pore size (Phenomenex Aeris PEPTIDE XC-C18 LC Column 150 x 4.6 mm C18 particle size 3.6 μm and YMC 150 x 4.6 mm C18 particle size 5 μm); % of organic modifier at start of the gradient (5% MeCN and 20% MeCN); % of organic modifier at end of the gradient (50% MeCN and 60% MeCN); gradient time (10 min and 30 min); flow rate (0.5 mL/min and 1 mL/min); column temperature (25°C and 65°C); and TFA concentration in mobile phases (0.05% and 0.1%). The HPLC system (Agilent 1100), sample concentration (0.2 mg/mL), wavelength (215 nm, band width 4 nm), injection volume (10 μL), and preparation of sample mixture (P006 0.2 mg/mL + LJMU025 0.2 mg/mL) were kept constant. 36 randomised runs (12 runs, 3 replicates) were suggested from Minitab Software (version 12.2020.2.0).

Table 4.1. Factors under evaluation in the Plackett-Burman Design.

Factor under evaluation	Level 1	Level 2
Column particle size (μm)	3.6	5
Initial gradient (% of MeCN)	5	20
Final gradient (% of MeCN)	50	60
Gradient time (min)	10	30
Flow Rate (mL/min)	0.5	1
Column Temperature (°C)	25	65
TFA in mobile phases (%)	0.05	1

Taguchi Design of Experiment (TD) was constructed with Minitab Software (version 12.2020.2.0) by choosing the L9 3^3 array (3 factors evaluated at 3 levels). As shown in Table 4.2, factors under evaluation were column temperature (35, 50, and 65 °C), flow rate (0.5, 0.8 and 1 mL/min), and acidic modifier in the mobile phases (0.05%; 0.08%, 0.1%). On the other hand, parameters kept constant during the investigation included HPLC system, injection volume, sample concentration, column, wavelength,

gradient time, % of organic modifier at start of the gradient, % of organic modifier at end of the gradient, as illustrated in Table 4.3.

Table 4.2. Factors under evaluation in the TD experiment and levels at which the factors were evaluated.

Factor under evaluation	Level 1	Level 2	Level 3
Column Temperature (°C)	35	50	65
Flow Rate (mL/min)	0.5	0.8	1
TFA in mobile phases (%)	0.05	0.08	0.1

Table 4.3. Parameters kept constant in the TD experiment.

Fixed parameters in the TD
1. HPLC system: Agilent 1100
2. Wavelength: 215 nm, band width 4 nm
3. Sample: P006 0.2 mg/mL + LJMU025 0.2 mg/mL
4. Injection Volume: 10µL
5. Column: Phenomenex Aeris, 3.6 µm XB-C18 LC-Column 100 Å 150 x 4.6 mm
6. Gradient time: 10 min
7. Initial gradient: 80% H_2O, 20% MeCN
8. Final gradient: 40% H_2O, 60% MeCN

4.3.5.3 HPLC method validation (ICH guidelines)

The developed HPLC method was validated according to the ICH guidelines [302]. Linearity, range, intraday and interday precision, sensitivity, specificity, robustness, and stability were evaluated [302,345]. P006 was taken as reference peptide for the validation.

Linearity was evaluated in triplicate by calculating the regression line from the graphical plot of the area derived from the chromatographic peak (y) versus the peptide concentration (x) of eleven standard solutions (5, 7.5, 10, 25, 50, 75, 100, 250, 500 750, 1000 mg/mL), obtaining a calibration curve. This analysis was followed by the corresponding statistical study using a linear least-squares regression method

and by analysis of the respective response factors. The specified range was derived from linearity studies.

For investigation of precision, repeatability was calculated on 3 levels (50, 100, 250 mg/mL), as the standard deviation of three replicates on the calibration curve on the same day (intraday precision). Interday variation was calculated by determination of the same samples at three concentration levels (50, 100, 250 mg/mL) in the analysis series on three different days. Repeatability of injection was assessed by the analysis of three standard solutions (50, 100, 250 mg/mL) injected five times in the same day. Sensitivity was evaluated through the values of the lower limit of detection (LLOD) and lower limit of quantification (LLOQ). LLOD and LLOQ were calculated with the following equations:

$$LLOD = 3.3 * \frac{S_Y}{S}$$

Equation 4.11

$$LLOQ = 10 * \frac{S_Y}{S}$$

Equation 4.12

where Sy is the standard deviation of the response of the curve and S is the slope of the calibration curve.

Specificity was evaluated by analysing P006 in deionised H_2O, in H_2O + TCA (2.5% *w/v*), and in relevant supernatant solutions. To assess the robustness of the method, flow rate (± 0.1 mL/min), wavelength (± 2 nm) and column compartment temperature (± 2°C) were changed during analysis. Sample solution of 250 μg/mL was prepared and injected for every condition and retention time was derived.

Storage stability at 25°C ± 2°C was evaluated at different time intervals up to 72 h.

4.3.5.4 Optimised HPLC method for stability study

For the stability study, the supernatant solutions derived from pelleting the serum proteins were analysed by RP-HPLC (Agilent 1100, fitted with a C-18 Column Phenomenex Aeris particle size 3.6 µm peptide XB-C18 100 Å LC Column 150 x 4.6 mm) using a linear gradient from 80% solution A (H_2O, 0.05% TFA) to 60% solution B (MeCN, 0.05% TFA) over 10 min. A flow rate of 1 mL/min was used, the absorbance was detected at 215 nm and the analysis was performed at 65 °C. The amount of the intact peptide/peptomer was quantified measuring the peak areas against the appropriate blank and the standard curves in blank serum supernatant ($r^2 > 0.997$, see Appendix)*. The amount of compound at time 0 min was used as 100% and the remaining intact peptide/peptomer at various time points was calculated as a percentage of the initial concentration, as shown in the following equation (Equation 4.13):

$$\%\ Remaining\ intact\ compound = \frac{Concentration\ at\ time\ T * 100}{Concentration\ at\ time\ zero}$$

Equation 4.13

* with the exception of LJMU017, LJMU018, and LJMU027 where samples for the calibration were prepared in H_2O due to solubility issues.

4.3.5.5 HPLC method for protein binding studies and chemical stability studies

Solutions were analysed by RP-HPLC (Agilent 1100, equipped with a YMC 150 x 4.6 mm C18 particle size 5 µm) using a linear gradient from 80% solution A (H_2O, 0.05% TFA) to 60% solution B (HPLC grade, 0.05% TFA) over 10 min. A flow rate of 1 mL/min was used, the absorbance was detected at 215 nm and the analysis was performed at 40 °C. The concentration of peptide was obtained by measuring the area under the peak of interest against the appropriate blank and the standard curves (obtained by analysing peptide serial dilutions prepared in PBS, 5% DMSO – $r^2 > 0.999$, see Appendix).

4.3.5.6 Low resolution LC-MS analysis

LC-MS (Waters LCT system fitted with a Waters XBridge BEH C18 130 Å, 5µm, 4.6 x 150 mm, 1p/kg) column was used to monitor parent peptide/peptomer depletion and examine the structures of the degradation products. Briefly, for the LC, a linear gradient of 10 min from 80% A (H_2O, 0.1% formic acid) to 60% B (MeCN, 0.1% formic acid) was employed; absorbance was detected at 215 nm, a flow rate of 1 mL/min and an injection volume of 10 µL were used, and the column compartment was kept at 60 °C. Electrospray ionisation mass spectrometry was conducted in positive ion mode (*m*/*z* range: 600–1700) using a cone voltage of 50 V, desolvation temperature of 300 °C and source temperature of 100 °C. Exact mass measurements of the products were based on the protonated molecules $[M+H]^+$.

4.3.6 Data analysis and statistical analysis

Results were reported and evaluated with Microsoft Excel (version 16.58) or GraphPad Prism. One-way ANOVA or unpaired two tailed t-test were performed using GraphPad Prism (version 9.3.1) to investigate statistical significance of data. A p value smaller than 0.05 was considered significant.

4.4 Results and Discussion

4.4.1 Peptide physicochemical stability

Serum stability and protein binding experiments required conditions that may cause peptide instability (e.g., incubation at 37 °C over 24 h, or acidic conditions). Hence, P006 and benzoylated analogues were chosen as examples to study the physicochemical stability under these conditions prior to adding any plasma protein or peptidases.

4.4.1.1 Thermal stability and solubility of peptides over 24 hours at 37 °C

Solutions of P006 and LJMU027 at various concentrations (500, 250, 100, 50 µM) were tested for thermal stability at 37 °C. As shown in Figure 4.11, P006 was completely stable and remained in solution at every concentration over 24 h.

However, LJMU027 was subject to precipitation or instability and resulted in recovery >90% only for lower concentrations (250, 100, and 50 μM), while showed high variability for the highest concentration (500 μM).

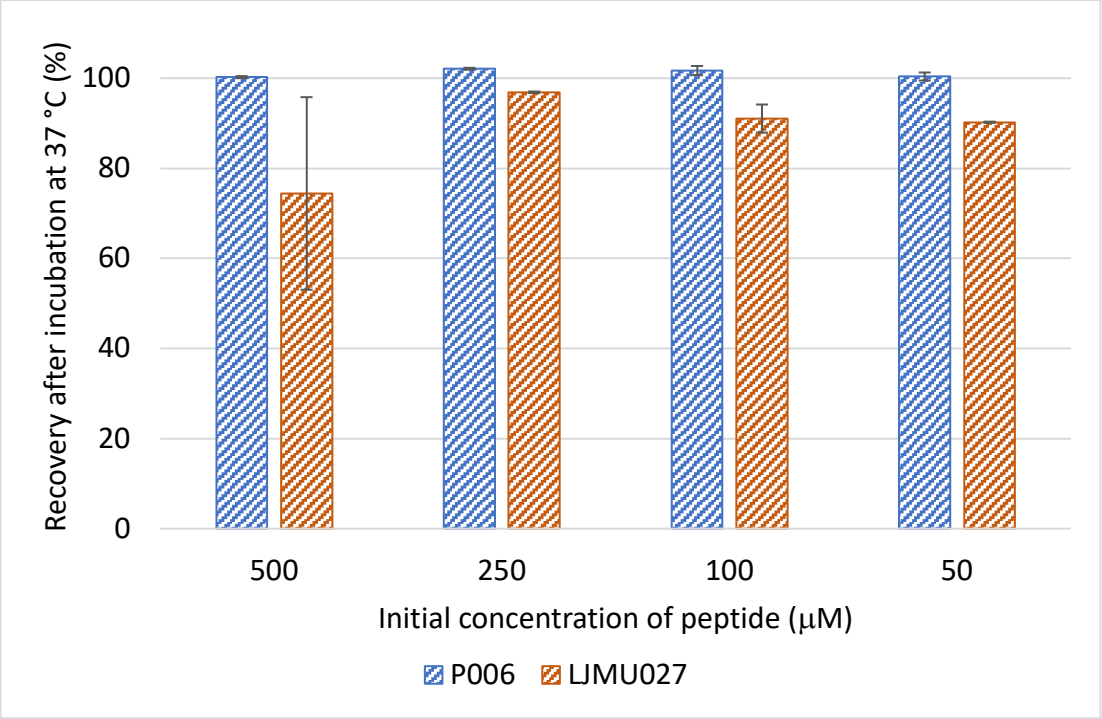

Figure 4.11. Thermal stability of P006 (in blue) and LJMU027 (in yellow) over 24h at 37 °C with shaking, expressed as percentage of recovery compared to a standard solution.

4.4.1.2 Chemical stability of peptides in acidic conditions

To test if the addition of TCA (15% *w/v*) to peptides in solution caused instability and/or precipitation, four peptides (i.e., P006, LJMU027, LJMU017, LJMU018) were analysed before and after addition of the acidic solution. As represented in Figure 4.12, in each case, peptide recovery after addition of TCA aq. solution was higher than 94%, demonstrating that TCA does not cause peptide precipitation and is a valuable option to precipitate serum proteins without significantly affecting peptide concentration in solution.

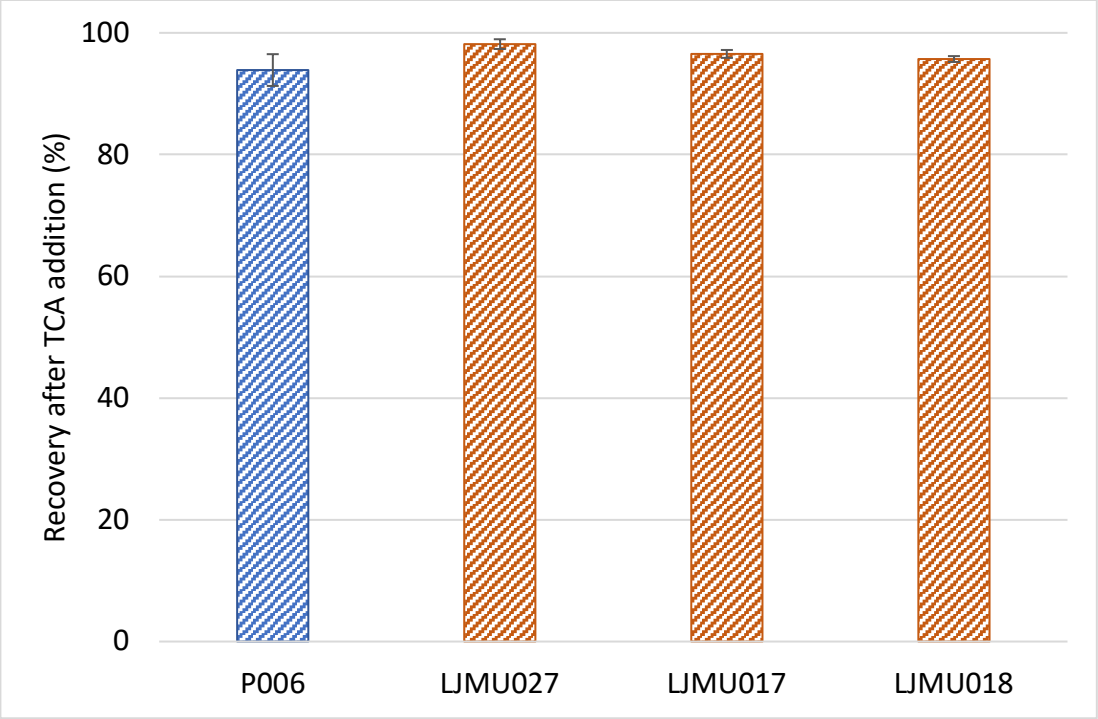

Figure 4.12. Recovery of peptides after addition of TCA aq. solution (40 µL, 15% w/v). P006 is represented in blue, while benzoylated derivatives are shown in yellow.

4.4.2 Blood stability method development

4.4.2.1 Stability method development

In order to investigate the blood stability of P006 and analogues, the presence of intact peptide after incubation with diluted serum was detected and quantified. Notably, it has been reported that *in vivo* peptide stability can be modelled by *in vitro* stability in human serum or plasma with a high grade of accuracy, even though the stability in serum or plasma may be underestimated compared to whole blood [287,346]. Incubation times were selected between 15 and 60 min, using 0 min as the reference sample (100% of intact peptide). Incubation times shorter than 15 min resulted in highly variable results, while incubation times longer than 60 min resulted in no intact peptide detected for P006 (the lead compound used for the optimisation strategy).

The use of diluted serum has previously been explored by various research groups [287,289,291,294,347]. In this study, by using diluted human serum (25% *v/v*, in H_2O) it was possible to detect changes in peptide concentration with a higher grade of

precision due to the longer time needed for the peptide to degrade, eventually yielding more accurate stability profiles over 60 minutes. The initial concentration of peptide in diluted serum was fixed at 100 µg/mL as per literature precedent [289].

As a standard method of choice, denaturation of serum proteins was obtained by adding trichloroacetic acid (TCA) aq. solution. Initially, 6% *w/v* TCA aq. solution was added in a ratio 1:1 (200 µL) to the samples, as reported in literature [287]. However, this resulted in a superfluous dilution of the starting concentration of intact peptide and, for this reason, protein denaturation data was finally obtained by adding a lower volume of a more concentrated solution of TCA (15% *w/v*, 40 µL), as previously explored by Cudic *et al.* and Nguyen *et al.* [291,294]. Otherwise, precipitation of serum proteins can also be achieved by mixing diluted serum with MeOH in a 1:1 ratio. This was used as an alternative to TCA when the use of the acidic solution resulted in ambiguous results (see section 4.4.3.4). Finally, quantification of intact peptide after incubation in serum was performed by RP-HPLC, but an optimisation of the liquid chromatography method was necessary to achieve high accuracy of detection.

4.4.2.2 First attempts and issues with chromatographic separation

RP-HPLC is one of the most commonly used techniques for the separation and purification of peptides and proteins [295]. Standard methods for HPLC peptide separation involve the use of a gradient of H_2O and MeCN from 1% to 99% MeCN over 10-20 min [348]. Hence, a standard HPLC gradient method over 22 min at room temperature was initially employed to quantify the intact peptide remaining in serum at various time points. However, this method was unable to separate P006 (or analogue peptides) from its metabolite(s) (Figure 4.13). The main identified metabolite (RT 9.19 min, *m/z* 852, Figure 4.14) eluted very close to the intact peptide (RT 9.31 min, *m/z* 1048, Figure 4.15) and, for this reason, further optimisation was required to obtain full resolution of the two peaks, enabling accurate quantification of intact compound.

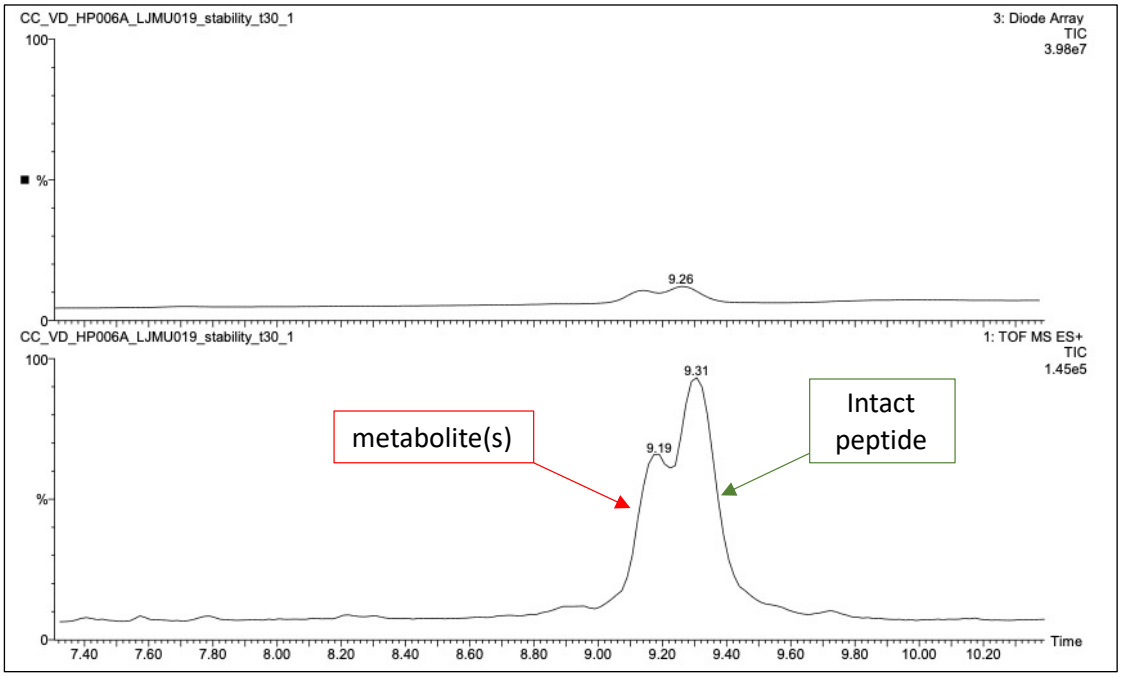

Figure 4.13. HPLC chromatogram and TIC spectra of LJMU019 after 30 min incubation in diluted human serum.

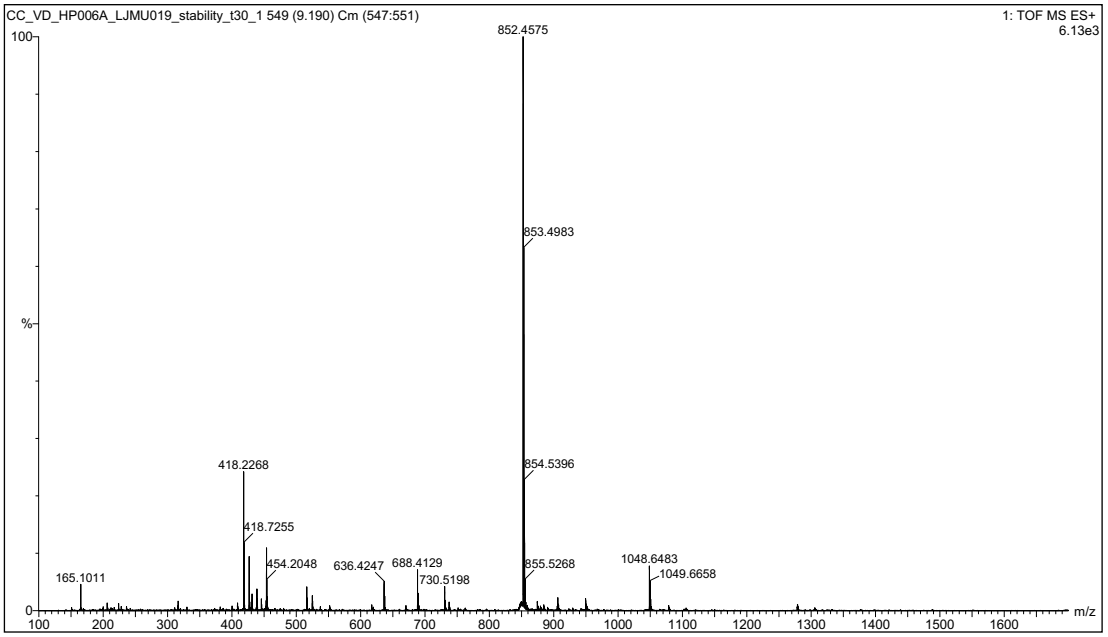

Figure 4.14. ESI mass spectrum of main metabolite of LJMU019 [main metabolite ([M+H]$^+$ 852.4575) of P006 and derivatives].

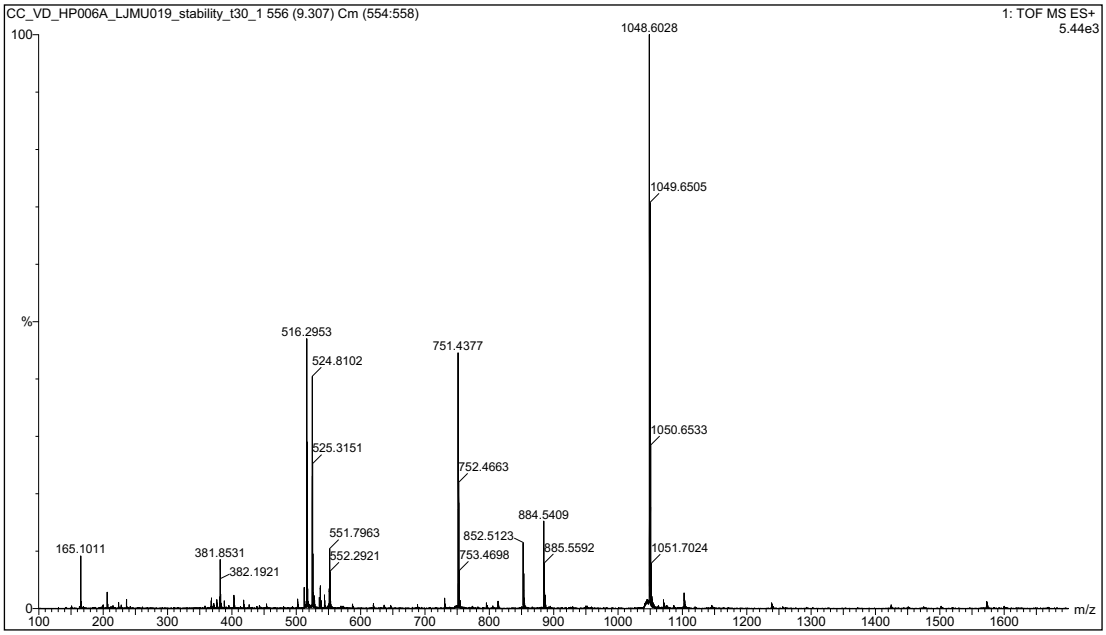

Figure 4.15. ESI mass spectrum of intact peptide LJMU019 after 30 min incubation in serum.

4.4.2.3 HPLC method optimisation

The first step towards the HPLC method optimisation was to synthesise the main metabolite identified by LC-MS (*m/z* 852), corresponding to the peptide sequence TDVGPFAF-NH_2 (LJMU025). Following synthesis, purification and characterisation (Chapter 3, section 3.4), this compound was mixed in solution with P006 (1:1) to optimise the chromatographic separation.

The development of an optimised method potentially requires a large number of experiments that increases exponentially with the number of independent influencing factors under evaluation. To decrease the number of experiments required a preliminary screening study was performed to exclude independent variables that had no significant effect on the outcome. Hence, RP-HPLC method optimisation was carried out through two design of experiments approaches, an initial PBD to identify the factors that mainly influenced the resolution of the two peaks, followed by a TD to investigate the most important factors at different levels and to define the final parameters to use.

The quantifiable endpoint was the resolution (R_s) between the two peaks deriving from elution of LJMU025 and P006 [295,297]. R_s may also be represented in the Resolution Equation (Equation 4.14) as a combination of three factors (efficiency, separation, and retention) that affect this value:

$$R_S = \frac{k}{k+1} * \frac{a-1}{a} * \frac{\sqrt{N}}{4}$$

Equation 4.14

where k, a, and *N* represent the retention, the selectivity, and the efficiency, respectively [349]. In light of this, it was decided to increase R_s through improvement in efficiency (by studying column particle size and temperature) and selectivity (by changing mobile phases and mobile phases pH).

In the standardised main effect Pareto chart (Figure 4.16), obtained from the PBD study, the length of the bar is proportional to the significance of the variables for R_s. Hence, the factors that most influence the resolution of the peaks were found to be column compartment temperature (**F**), flow rate (**E**) and TFA % in the mobile phases (**G**). Other significant variables were column particle size (**A**), the % of organic modifier at the beginning of the gradient (initial gradient, **B**), and gradient time (**D**), while the % of organic modifier at the end of the gradient (final gradient, **C**) had no significant influence on the outcome.

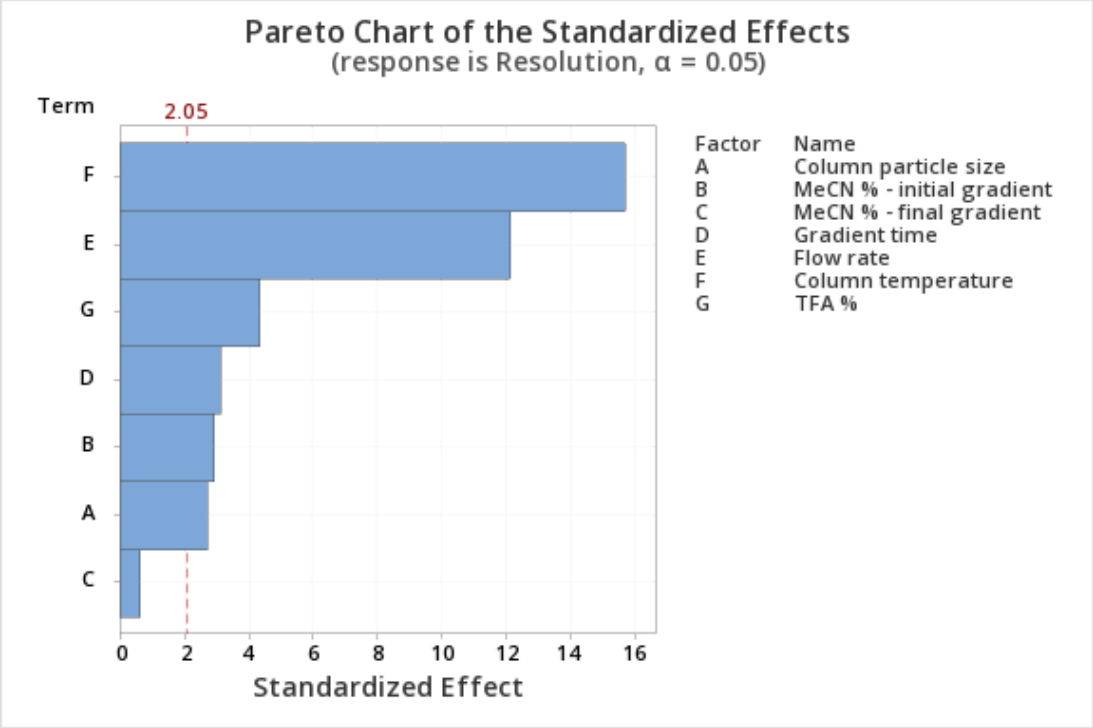

Figure 4.16. Standardised main effect Pareto chart for the Plackett-Burman Design experiment. The vertical red line in the chart defines the 95% confidence level; the bars that cross the reference line are statistically significant.

Consequently, the three factors that had the greatest significance were further investigated with a fractional design. TD with three factors evaluated (column temperature, flow rate, and TFA % in the mobile phases) at three levels (L9, 3^3) was chosen [350,351].

The analysis of the TD outcome was obtained using the criterion “the larger the better”: the higher the resolution of the two peaks, the better for our purpose of separating P006 from its metabolite. By visually inspecting the main effect plot of means (Figure 4.17), it was clear that resolution linearly increased with an increase in temperature (Figure 4.17A) and flow rate (Figure 4.17B). No such clear linear relationship was observed for the TFA percentage in the mobile phases which had a very subtle effect on the outcome (Figure 4.17C). Hence, the parameters that yielded the greater resolution of the two peaks were column compartment temperature at 65 °C and flow rate at 1 mL/min, while TFA % in mobile phases had almost no

influence on the outcome and, for this reason, was chosen as 0.05%, to reduce the waste of reagents.

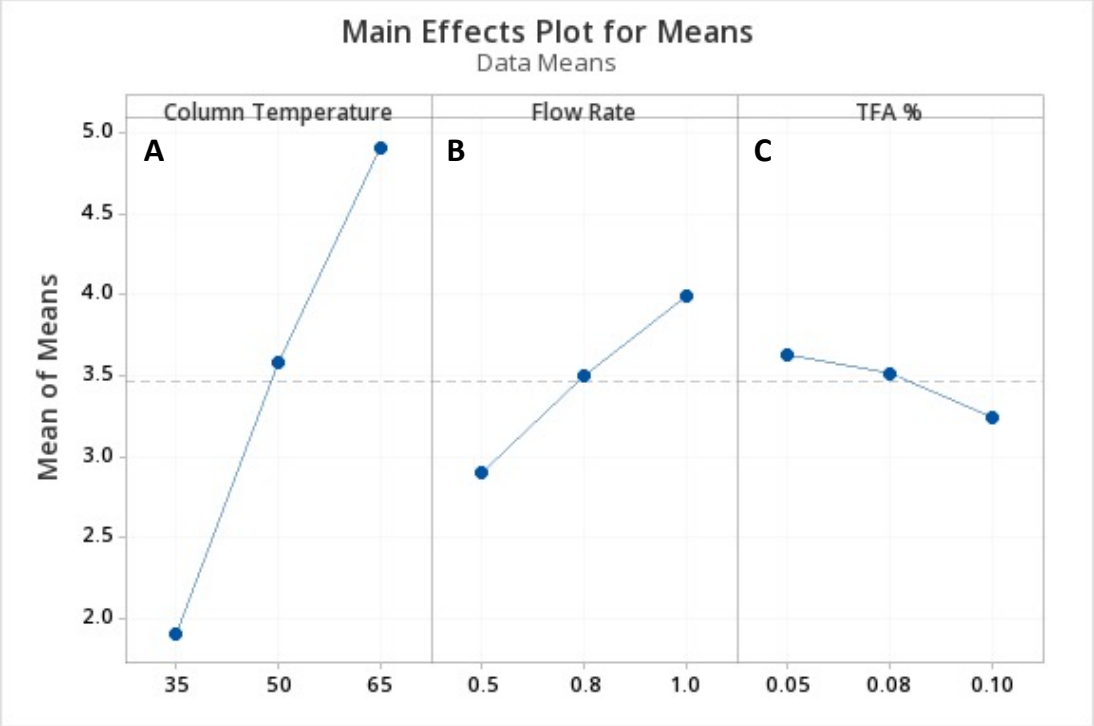

Figure 4.17. Main Effect plots for signal-to-noise ratios from TD. (A) column compartment temperature, (B) flow rate, (C) TFA percentage in the mobile phases.

As shown in Figure 4.18, the success of the HPLC optimisation study was demonstrated by analysis of a sample obtained from incubation of P006 in diluted serum for 30 min. Here, a notable a 5-fold increase in the R_s of the peaks between parent peptide and its main metabolite was obtained (from 1.13 to 5.65).

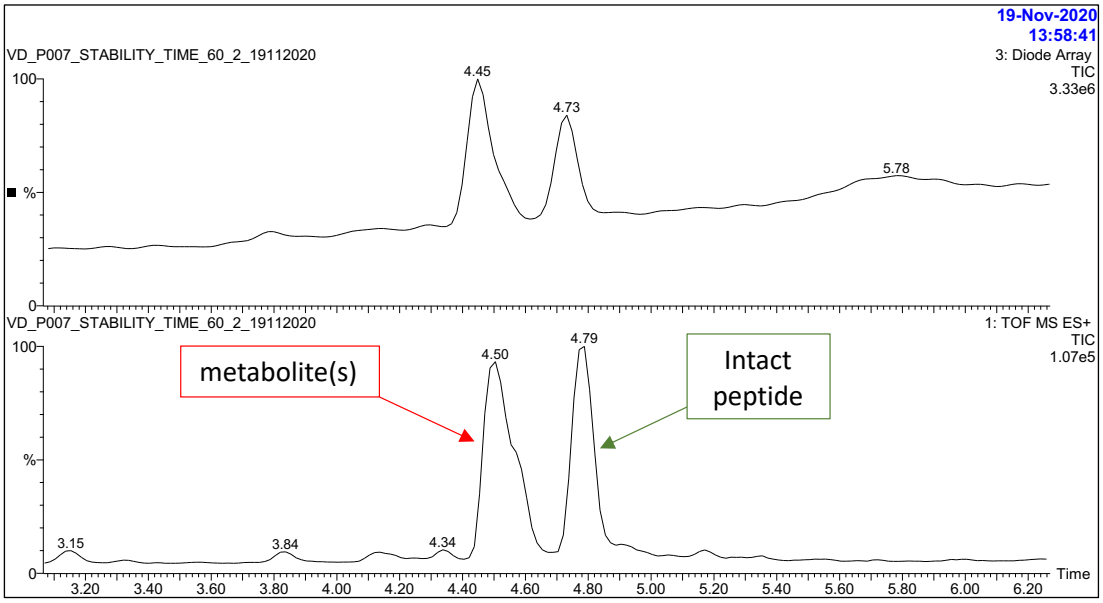

Figure 4.18. Example of DAD and TIC of LJMU019 after 30 min incubation in diluted serum.

4.4.2.4 HPLC method validation

The optimised analytical technique was validated in agreement with the ICH guidelines to prove its adequacy for the planned purpose [302]. P006 was taken as the reference peptide to carry out the validation of the analytical method, in which linearity, range, sensitivity, specificity, and robustness were evaluated.

The linearity study verified that the samples were in a concentration range in which the analyte response was linearly proportional to the concentrations. A standard curve (Figure 4.19) was obtained by plotting the mean peak area (n=3) against the concentration of the peptide. The slope, y-intercept and linearity of the curve were determined by linear regression analysis. The peak area of standard curve samples was a linear function of the peptide concentration over the concentration range of 5–1000 µg/mL. The regression coefficient (R^2) was 0.9999 and the y-intercept was not significantly different from zero.

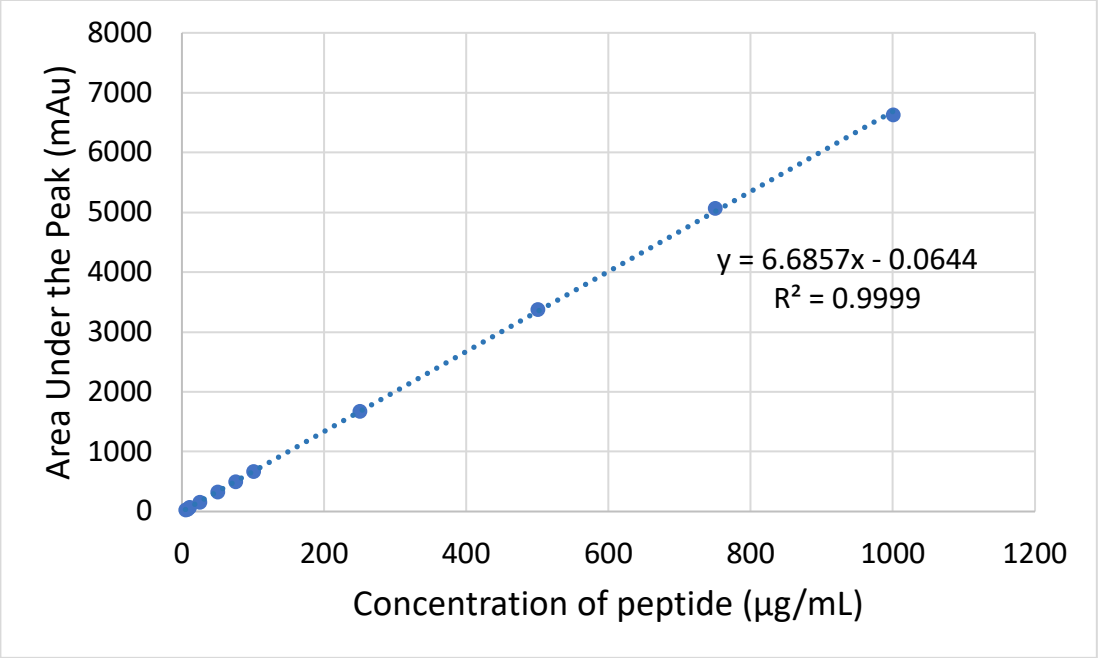

Figure 4.19. P006 calibration in H_2O; concentration range from 5 to 1000 mg/mL.

The specified range (5-1000 µg/mL) was derived from linearity studies and confirmed that the analytical procedure provided an acceptable degree of linearity, accuracy and precision when applied to samples containing amounts of analyte within or at the extremes of the specified range of the analytical procedure.

Precision of the analytical method was confirmed through intra-day repeatability testing, assessed using 9 determinations (3 concentrations/3 replicates each), and inter-day repeatability (assessed in 3 different days), as shown in Table 4.4.

Table 4.4. Intra-day and inter-day variation and accuracy tested using three different concentrations of peptide within the calibration range. Values are reported as means ± SD.

	Concentration of P006 (µg/mL)	Calculated concentration of P006 ± SD	Accuracy (%)
Intra-day	50	48.84 ± 0.42	99.02
	100	100.31 ± 0.26	99.70
	250	252.49 ± 2.25	102.38
Inter-day	50	48.92 ± 1.00	102.25
	100	99.53 ± 1.18	100.48
	250	253.51 ± 1.13	98.62

The repeatability of injection was demonstrated for the same concentrations and repeatedly injecting each sample five times. Results are shown in Table 4.5.

Table 4.5. Injection repeatability for three different concentrations. Values are represented as mean ± SD.

Concentration of P006 (µg/mL)	Number of replicates	Peak intensity ± SD (Height of peak)	RSD (%)
50	5	71.36 ± 0.79	1.11
100	5	146.44 ± 1.98	1.35
250	5	356.18 ± 4.20	1.18

Sensitivity, defined as "the ability of a method to detect small changes in analyte concentration" [352], was studied through two parameters: lower limit of quantification (LLOQ) and lower limit of detection (LLOD). These could be particularly affected by small changes in concentration, and, for this reason, their variability should be assessed. The LLOD, also called analytic sensitivity, was found to be 13.2357 µg/mL. This represents the smallest amount of an analyte that can reliably be detected. On the other hand, the LLOQ, defined as "the lowest calibration standard on the calibration curve where the detection response for the analyte should be at least five times over the blank", was found to be 40.1083 µg/mL [353].

The specificity test proved that, at the retention time of P006, there were no interferences between the peptide and other impurities (i.e., deionised H_2O with 5% DMSO and blank serum supernatant, for pharmacokinetic studies, and blank PLGA nanoparticles after ultracentrifugation, blank chitosan microparticles after centrifugation, for formulation studies explored in Chapter 5). This test was designed to prove that the analytical procedure was specific for P006, leading to complete discrimination from other impurities that may be expected to be present in the sample (e.g., human serum supernatant components in the stability study).

The robustness of the analytical technique was proven by changing flow rate, wavelength, and column compartment temperature during analysis of a solution of peptide 250 μg/mL. This test is an indication of the analytical procedure capacity to remain unaffected by small, but deliberate variations in method parameters and proves its reliability during routine use. Finally, storage stability was proved at 25°C ± 2°C up to 72 h. This test was essential to confirm that samples could be stored at room temperature for days before analysis without any major change occurring.

The validation of the analytical procedure showed that the method was adequate to quantify the peptide P006. This procedure should have been repeated for each peptide analogue tested for stability in human serum to confirm that the analytical technique was adequate, thus ensuring great accuracy. However, due to lack of time and resources (e.g., HPLC usage), we could not repeat the validation for each peptide analogue and had to assume that the procedure was suitable by only analysing solutions of known concentrations prepared for the calibration curve.

4.4.3 Blood stability of P006 and analogues

Peptides containing natural amino acids are prone to proteolysis due to blood peptidases acting on the amide bonds present in their structures [283]. For this reason, it is important to evaluate their stability in the systemic circulation and, if low, to attempt to improve this through structural modification strategies. In this study, P006 and its derivatives were incubated in diluted serum to evaluate their

stability. By doing so, it was possible to derive kinetic information (i.e., degradation profile and *in vitro* half-life) and to define the main degradation products.

Comparison of HPLC chromatograms derived from analysis of P006 samples after incubation in diluted serum for 0, 15, 30, 45, and 60 min showed a gradual decrease in parent peptide (RT 5.43 min) and an increase in other species forming over the time (RT 5.01 min), as shown in Figure 4.20.

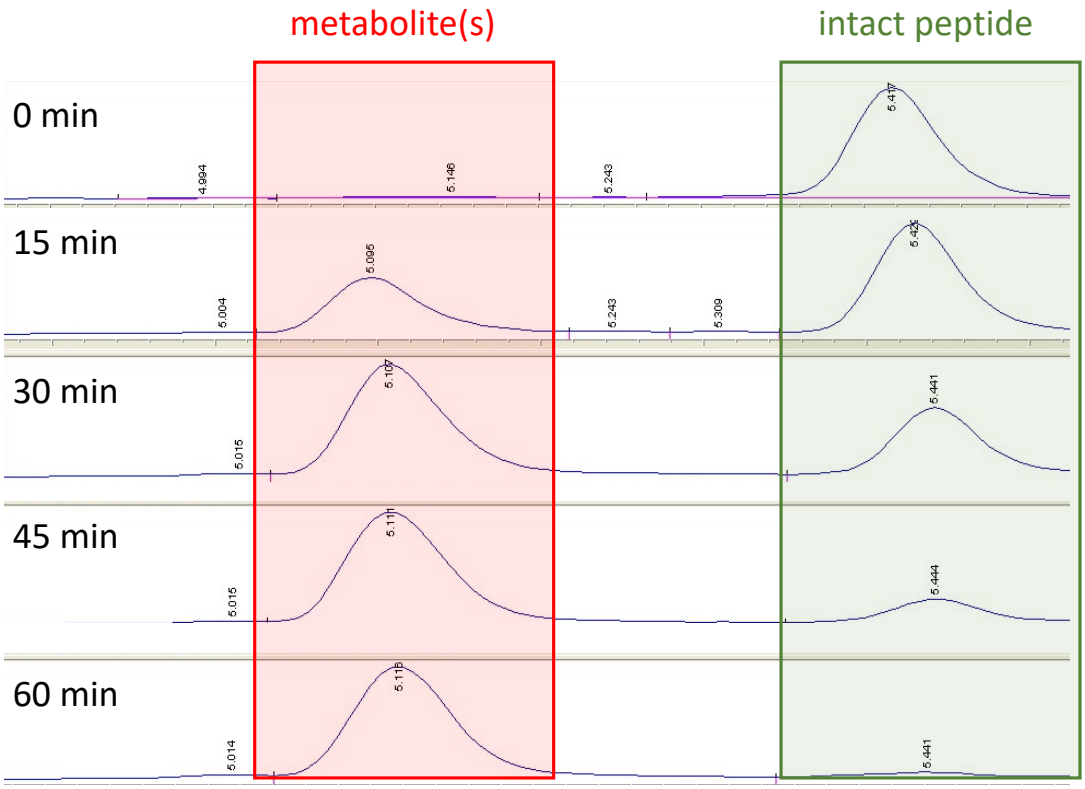

Figure 4.20. HPLC chromatograms showing the degradation of P006 (green) to its metabolite(s) (red) in diluted aq. serum over 60 min.

By measuring the area under the peak at the retention time corresponding to the elution of the parent peptide (i.e., 5.43 min for P006), it was possible to quantify the amount degraded over 60 min. The kinetic profile for P006 is shown in Figure 4.21, where the percentage of degraded peptide is plotted versus time, normalised on the concentration of intact peptide at time zero (taken as 100%).

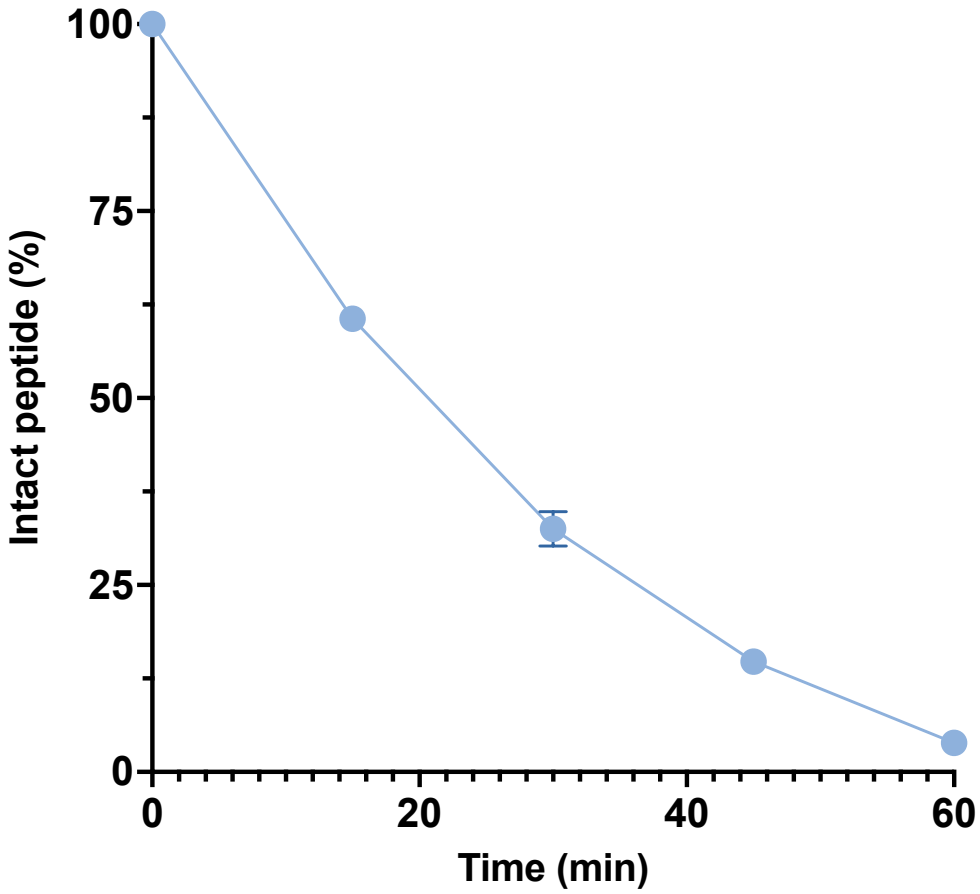

Figure 4.21. Degradation profile of P006 when incubated in diluted serum (25% v/v) over 60 min. Concentration of P006 at time zero was taken as 100%. Error bars not shown when smaller than the marker.

As shown in Figure 4.21, P006 underwent fast degradation in diluted serum, being almost completely digested after 60 min (remaining % of intact peptide 4.1 ± 0.1). Modifications performed on P006 structure were designed to improve the stability and, in general, the pharmacokinetic profile of the peptide.

4.4.3.1 Blood stability of fluorinated P006 analogues

The effects of P006 internal modifications with fluorinated amino acids (i.e., 4-F-Phe and F_5-Phe) on proteolytic stability were studied. Degradation profiles for fluorinated analogues, normalised using the peptide concentration at time zero as 100%, are reported in Figure 4.22. Similar digestion kinetics were observed for all the

modifications, aside from LJMU016, where the stability over time was significantly improved, yielding a percentage of intact peptide after 60 min of ~33%, a ~10-fold increase compared to P006.

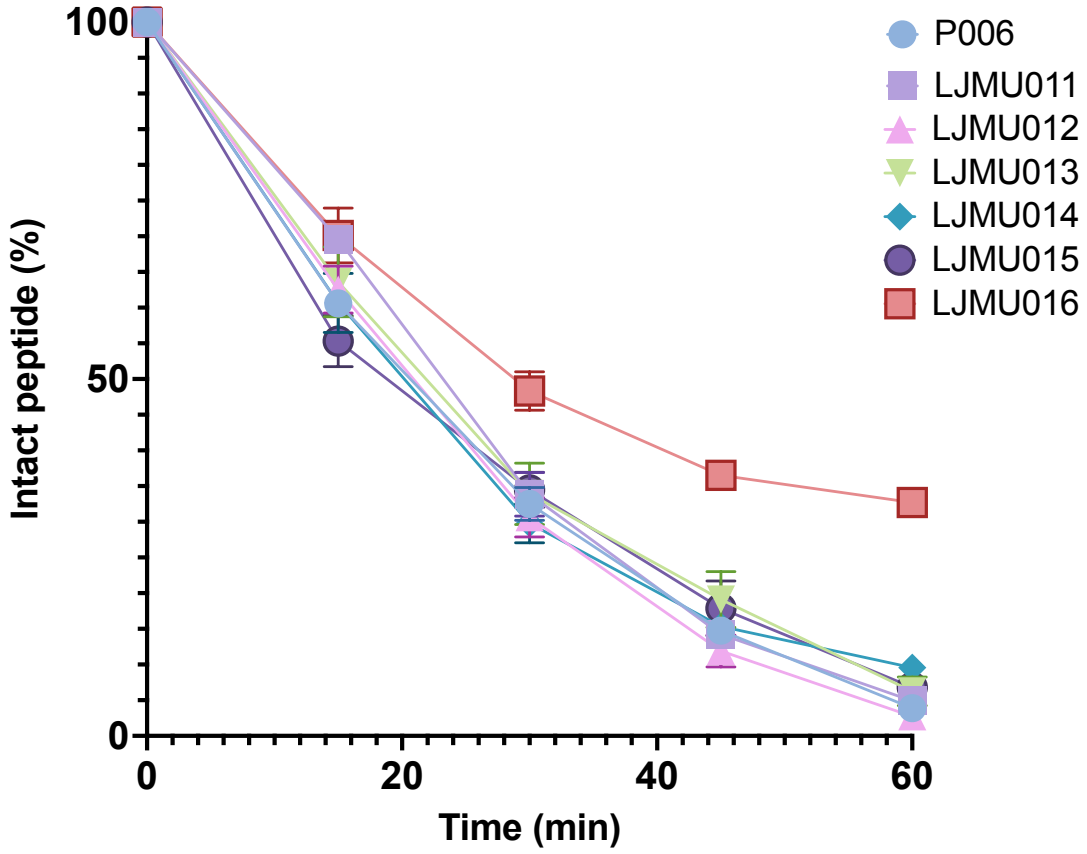

Figure 4.22. Degradation profile of P006 and fluorinated analogues when incubated in diluted serum (25% v/v) over 60 min. Concentration of peptide at time zero was taken as 100%.

Table 4.6 shows the modification performed for each analogue and the effect on the percentage of intact peptide after 60 min incubation in diluted serum.

Table 4.6. Fluorinated peptide analogues, modification performed on P006 sequence and percentage of intact peptide after 60 min incubation in diluted serum (25% v/v).

Entry	Modification	Intact peptide after 60 min (%)
LJMU011	Phe37 → 4-F-Phe	5.2 ± 1.0
LJMU012	Phe35 → 4-F-Phe	2.8 ± 1.2
LJMU013	Phe35 & Phe37 → 4-F-Phe	3.6 ± 3.3
LJMU014	Phe37 → F_5-Phe	9.5 ± 1.8
LJMU015	Phe35 → F_5-Phe	7.0 ± 0.6
LJMU016	Phe35 & Phe37 → F_5-Phe	32.8 ± 0.7

Ordinary one-way ANOVA analysis performed on the percentage of intact peptide after 60 min showed that, while the replacement of Phe-37 and/or Phe-35 with 4-F-Phe did not result in any significant improvement in proteolytic stability, the substitution of Phe-37 and/or Phe-35 with F_5-Phe resulted in a positive effect on stability, by increasing the percentage of intact peptide of around 6%, 3%, and 29% for LJMU014, LJMU015, and LJMU016, respectively (Figure 4.23). Protease protection may be due to steric occlusion of the fluorinated peptide from the enzyme active site, to the effect of increased local hydrophobicity, and/or to protection of peptide soft-spots susceptible to peptidase activity [200]. This could be further investigated with LC-MS analysis to identify the metabolites formed.

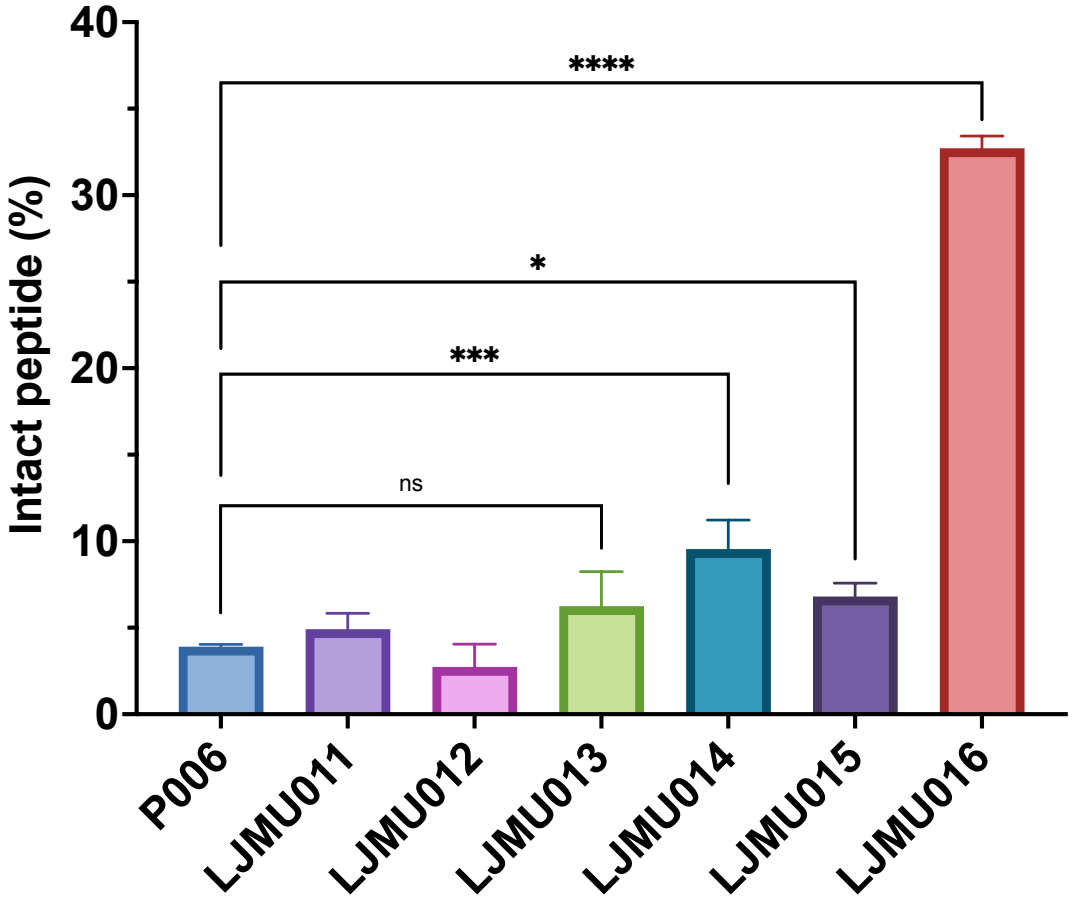

*Figure 4.23. Fluorinated analogues. Percentage of intact peptide after 60 min incubation in human serum compared to P006. Statistical significance is reported in the graph. ns mean p value > 0.05, * means p value ≤ 0.05, ** means p value ≤ 0.01, *** means p value ≤0.001, **** means p value ≤0.0001.*

4.4.3.2 Blood stability of peptide-peptoid hybrid analogues

Stability in human serum was also investigated for the peptide-peptoid hybrid analogues (LJMU019-LJMU024). Modification of the parent peptide with peptoid monomers was confirmed to be a successful strategy to protect from proteolytic degradation. Figure 4.24 shows the degradation profile of each peptide-peptoid hybrid, compared to P006.

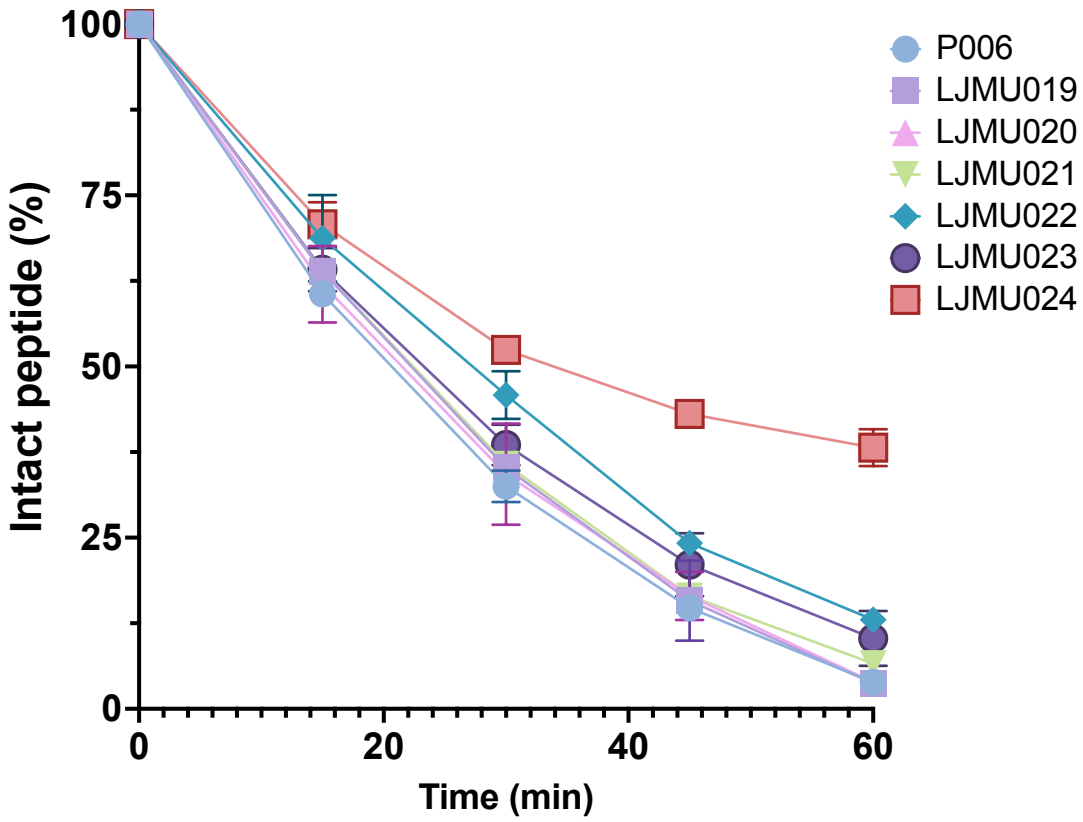

Figure 4.24. Degradation profile of P006 and peptide-peptoid hybrid analogues when incubated in diluted serum (25% v/v) over 60 min. Concentration of compound at time zero was taken as 100%.

This study showed similar degradation profiles for analogues containing peptoid monomers at positions 37, 36, or 35, with no significant effect on proteolytic stability. On the other hand, significant improvement was obtained when the replacement of the amino acid with peptoid monomer occurred in positions 32, 31, or 28. Table 4.7 sums up the peptoid replacement performed for each analogue and the effect on the percentage of intact peptide after 60 min incubation in diluted serum.

Table 4.7. Peptide-peptoid hybrid analogues, peptoid replacement performed on P006 sequence and percentage of intact peptide after 60 min incubation in diluted serum (25% v/v).

Entry	Modification	Intact peptide after 60 min (%)
LJMU019	Phe37 → NPhe	4.4 ± 1.7
LJMU020	Ala36 → Sar	4.0 ± 1.7
LJMU021	Phe35 → NPhe	6.7 ± 1.2
LJMU022	Val32 → NVal	13.0 ± 0.3
LJMU023	Asp31 → NAsp	10.4 ± 3.5
LJMU024	Val28 → NVal	38.0 ± 2.2

The percentage of intact peptide after 60 min and relative statistical analysis are shown in Figure 4.25. Therefore, as a result of peptoid scanning, it was possible to evaluate the role of each amino acid in stability and activity mechanisms; this study suggested that amino acids closer to the N-terminus were more prone to degradation as protection of the amide bond by relocation of the side chain on the nitrogen resulted in higher percentages of intact peptide after 60 min. In particular, outstanding improvement in stability was obtained when Val28 was replaced with its peptoid counterpart (LJMU024), implying a pivotal role of this amino acid in the proteolysis mechanism.

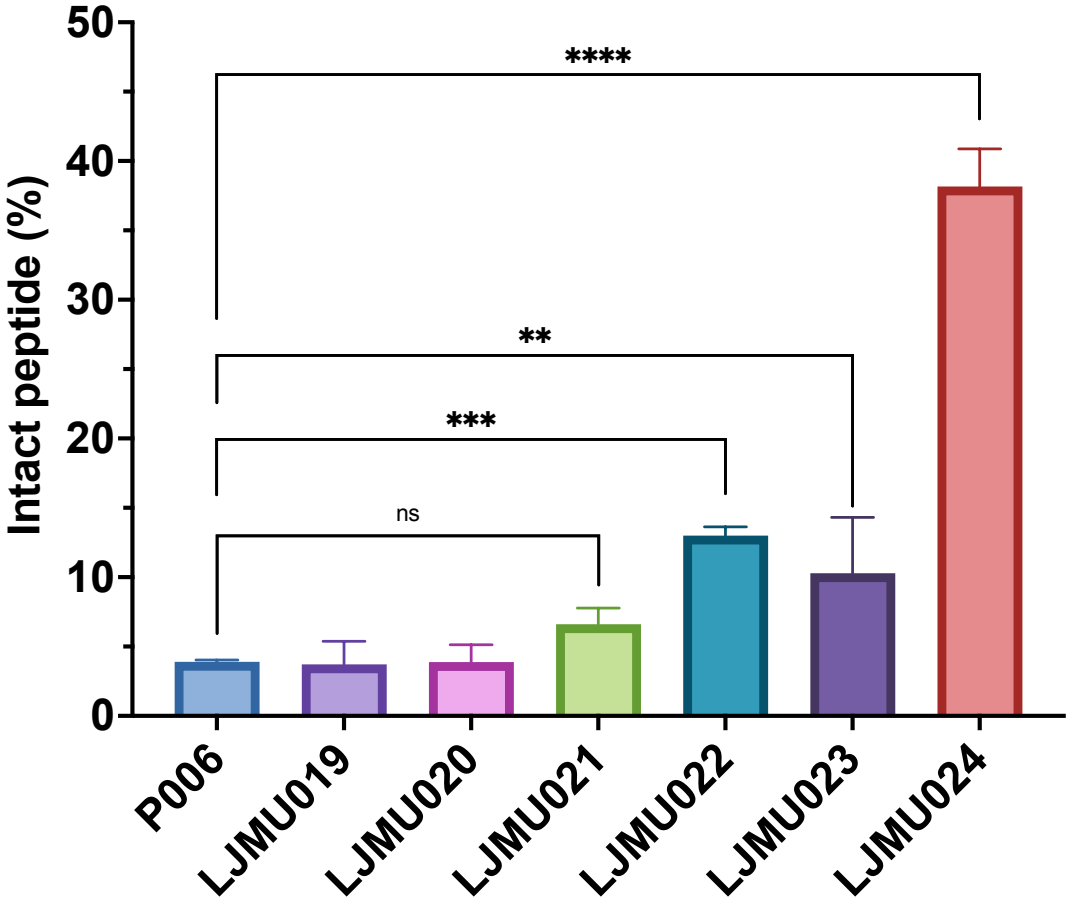

*Figure 4.25. Peptide-peptoid hybrid analogues. Percentage of intact peptide after 60 min incubation in human serum compared to P006. Statistical significance is reported in the graph. ns mean p value > 0.05, * means p value ≤0.05, ** means p value ≤ 0.01, *** means p value ≤0.001, **** means p value ≤0.0001.*

4.4.3.3 Blood stability of N-terminally modified analogues

Proteolytic stability of N-terminally modified analogues was tested over 60 min in diluted human serum. Table 4.8 reports the effect of N-terminal modification of P006 sequence on the percentage of intact peptide after incubation over 60 min in human serum. N-terminally modified analogues showed an extraordinary stability, yielding ~ 94%, 86%, and 75% of intact peptide for LJMU027, LJMU017, and LJMU018, respectively.

Table 4.8. N-terminally modified analogues, modification at the N-terminus, and percentage of intact peptide after 60 min incubation in diluted serum (25% v/v).

Entry	Modification	Intact peptide after 60 min (%)
LJMU027	N-terminal benzoyl	94.33 ± 3.27
LJMU017	N-terminal 4-F-benzoyl	85.50 ± 4.40
LJMU018	N-terminal F_5-benzoyl	74.95 ± 2.04

Figure 4.26 shows the percentages of intact peptide after 60 min and relative statistical analysis.

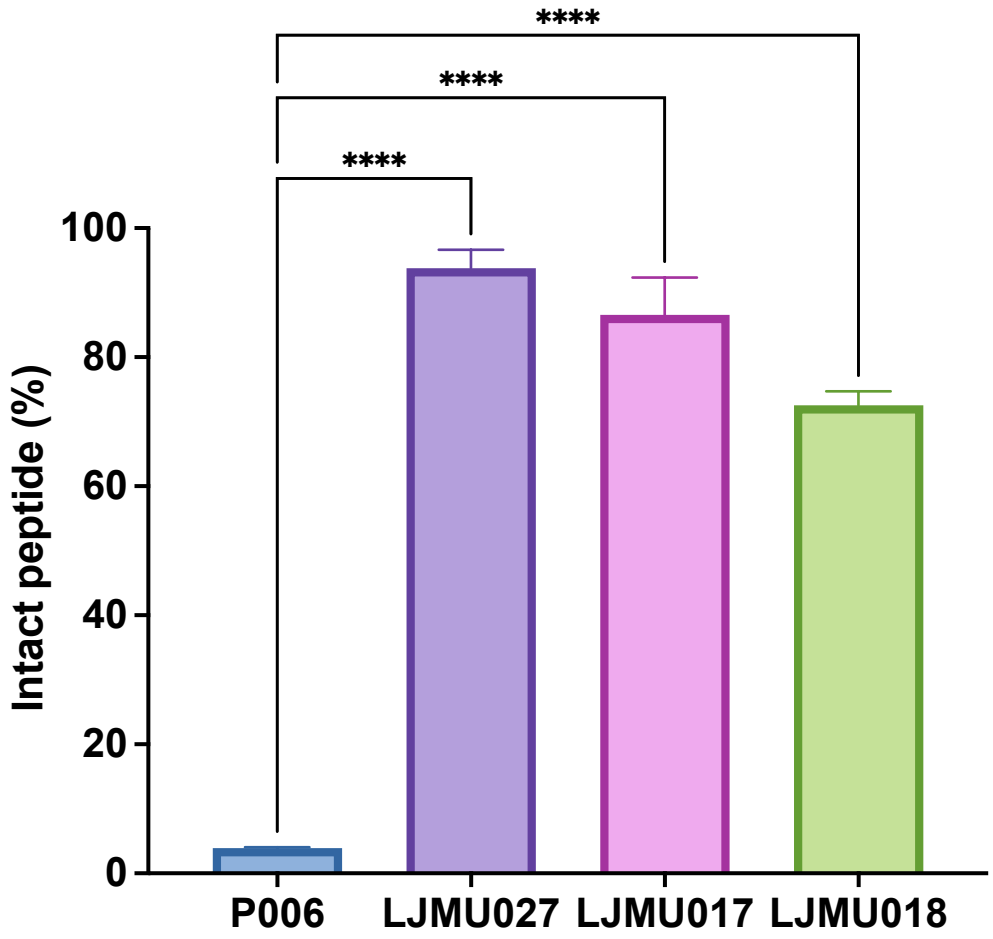

*Figure 4.26. N-terminally modified analogues. Percentage of intact peptide after 60 min incubation in human serum compared to P006. Statistical significance is reported in the graph. **** means p value ≤0.0001.*

As such, the modification of the N-terminus of the peptides appeared to be a promising strategy for single site modification providing stability to aminopeptidases without compromising receptor interaction. This approach was already successfully demonstrated in glucagon-like peptide-1 (GLP-1) analogues where attachment of N-acetyl or N-pyroglutamyl to GLP-1 conferred complete resistance to dipeptidyl peptidase IV while having potent effect in animal models [354]. Another relevant study involved N-terminal modifications of neurotensin(8-13), proving that N-terminal modifications prevented aminopeptidase cleavage in serum and, even though this modification caused a decrease in binding affinity at the receptor site, this could be countered by increased *in vivo* stability [236].

4.4.3.4 Plasma protein binding and MeOH as alternative quenching reagent to release the fraction bound

Analysis of serum stability data showed that, for some peptides, the concentration at time zero was significantly lower than expected (i.e., 0.083 mg/mL after addition of TCA aq. solution). Indeed, while for most peptides the decrease was < 20%, for LJMU016 and N-terminally modified analogues, this loss was greater than 60%.

The loss of peptide at time zero was hypothesised to be due to the effect that increased lipophilicity has on protein binding. It is well known that more lipophilic drugs have a greater tendency to bind to plasma proteins [355,356]. In this case, highly lipophilic peptides – the benzoyl-modified peptides (i.e., LJMU027, LJMU017, LJMU018) and the one presenting two F_5-Phe (i.e., LJMU016) – being tightly bound to plasma proteins, may precipitate together with them, when the denaturing agent is added to serum to stop the reaction. To check the correlation between lipophilicity and precipitation, the percentage of 'lost peptide' in this experiment was plotted against the lipophilicity index, expressed as HPLC retention time of the peptide, color-coding the categories of peptide modifications (Figure 4.27). From this graph, two main clusters of peptides could be identified, the less hydrophobic ones, where the percentage of lost peptide was lower than 20% and the more hydrophobic ones, for which the percentage of lost peptide at time zero of the stability study was

greater than 60%. The idea of binding to plasma protein was further investigated and is reported in section 4.4.4.

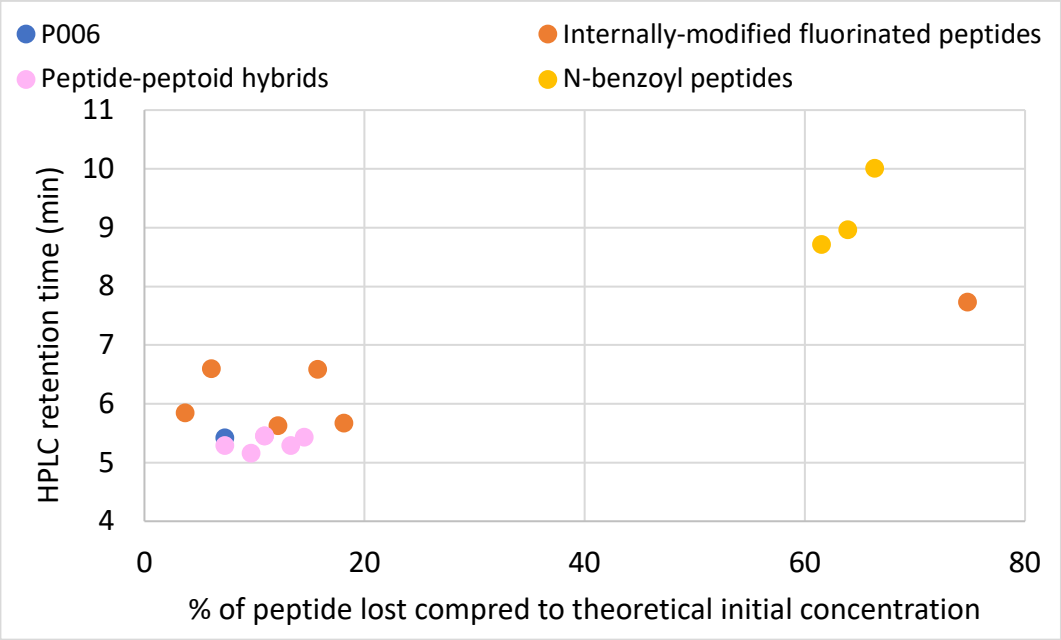

Figure 4.27. Correlation between peptide loss (%) at time zero of the stability study and lipophilicity expressed as HPLC retention time (min). Peptides and peptide-peptoid hybrids are color-coded based on the modification they are characterised by.

To ensure a full recovery of intact peptide, serum protein precipitation was attempted using MeOH in place of TCA. In the literature, a variety of methods are reported for protein removal, including extraction with organic solvents, ultrafiltration, and precipitation with different solvents; the choice of the method can influence the outcome of the experiment (e.g., metabolites and drug concentrations) [357]. Among the possible protein precipitation agents, MeOH was chosen because both P006 and the benzoyl derivatives were highly soluble in this solvent.

MeOH was determined to be a suitable protein precipitation agent, while ensuring full recovery of peptide. The difference between TCA quenching and MeOH quenching in recovery of peptide at time zero is best exemplified in Figure 4.28, where the concentration of intact peptide versus time graphs have been compared.

In both cases, N-terminal benzoyl compounds showed exceptional stability over 60 min compared to P006. However, when the reaction was stopped with TCA solution the initial concentration of benzoyl derivatives was significantly lower than for P006 (Figure 4.28A). This was not the case when the serum proteins were precipitated with MeOH (Figure 4.28B). Therefore, it was speculated that the peptide 'lost' during TCA quenching was probably bound to serum proteins and not released after precipitation. Moreover, the apparent degradation rate appeared to be slower in the MeOH experiment compared to the TCA experiment; assuming that the same enzymatic rate occurs, it is likely that, when MeOH is added, the peptide bound to proteins is released, yielding a higher amount of residual intact compound at the corresponding time points.

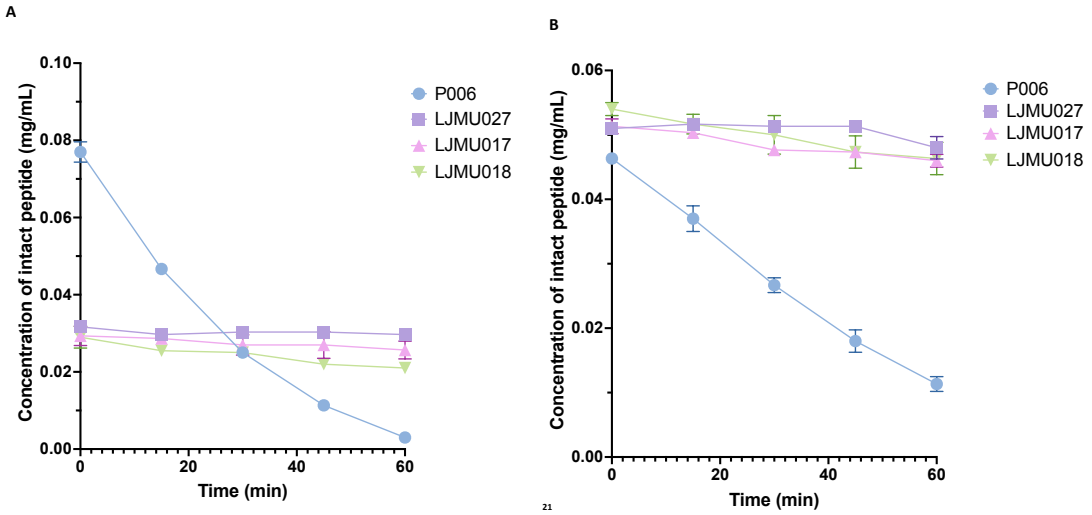

Figure 4.28. (A) Degradation profiles of P006, LJMU027, LJMU017, and LJMU018 using TCA as quenching reagent. (B) Degradation profiles of P006, LJMU027, LJMU017, and LJMU018 using MeOH as quenching reagents.

Figure 4.29 shows the percentages of intact peptide after 60 min incubation in diluted human serum when MeOH is used as quenching reagent. As shown on the bar chart, the amount of intact peptide for the benzoyl derivatives (LJMU027, LJMU017, and LJMU018) is significantly higher than that of P006.

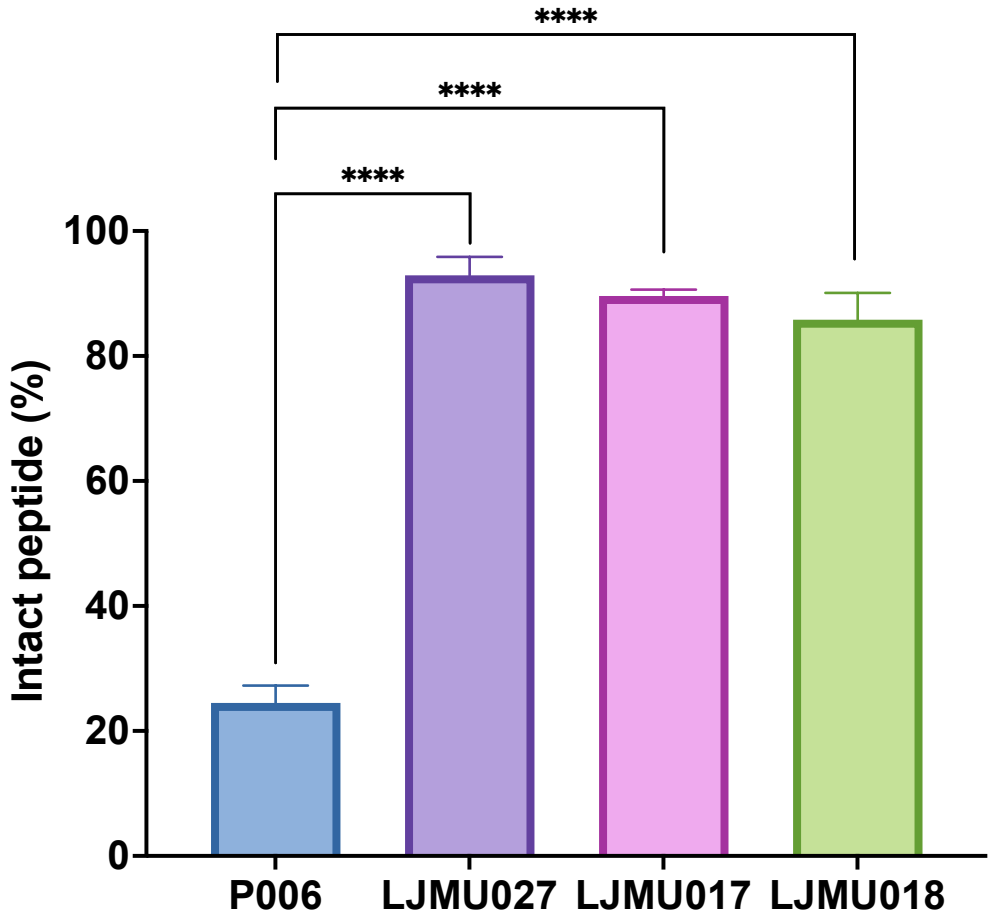

*Figure 4.29. Percentage of intact peptide after 60 min incubation in diluted serum, after protein quenching with MeOH. Statistical significance is reported in the graph. **** means p value ≤0.0001.*

4.4.3.5 In vitro half-life estimation

Once data on the degradation of each peptide/peptidomimetic was collected, it was possible to estimate the *in vitro* half-life in case of intravenous administration of P006 and derivatives. To prove that the degradation profile of P006 can be approximated to a first-order kinetic reaction, ln[P006] was plotted against the time (Figure 4.30), resulting in a straight line ($R^2 > 0.95$).

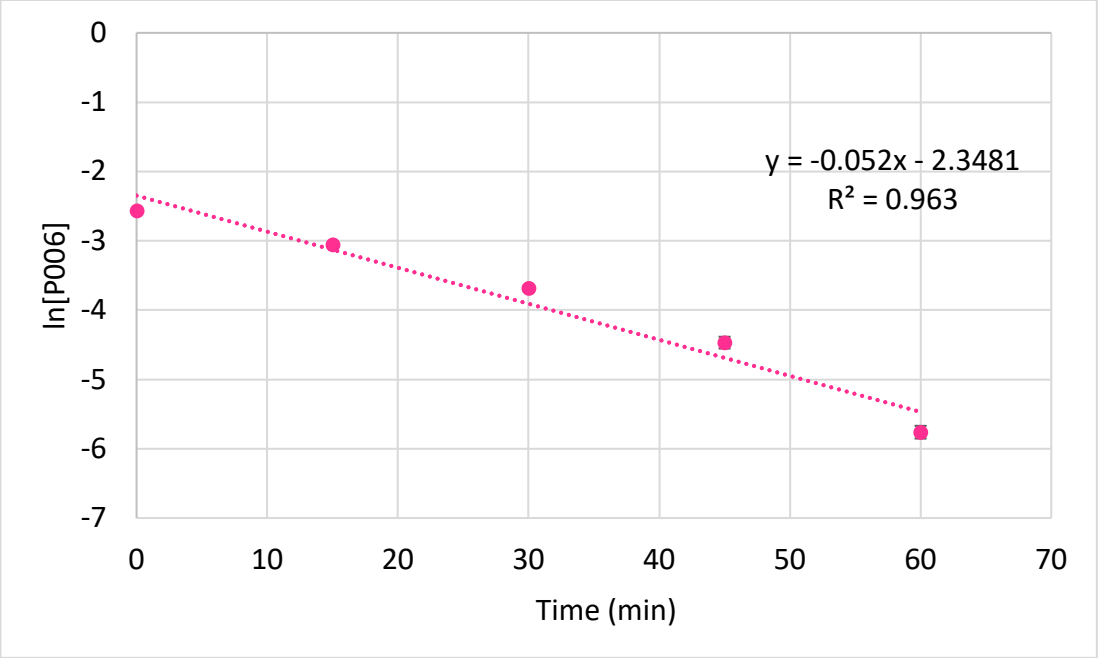

Figure 4.30. First-order reaction plot ln[P006] versus time (min) to determine the rate constant.

For first-order reactions, half-life can be calculated with Equation 4.4, and the slope of the plot of ln[A] versus t is -*k*. In the case of P006, *k* can be derived from the equation in Figure 4.30 (*k* = 0.052). Hence, $t_{1/2}$ for P006 can be obtained by $t_{1/2}$= 0.693/0.052 = 13.33 min.

The degradation profile for each peptide was approximated to a first-order reaction (R^2 > 0.9 in the ln[A] versus time curve, see Appendix) with a degradation profile comparable to an exponential decay graph, and the relative half-life was calculated from the slope of the ln[A] versus time graph, using Equation 4.4.

Equations derived from ln[A] versus time graphs, R^2 (> 0.9) of the curve, first-order rate constants (*k*), and derived half-lives ($t_{1/2}$) are shown in Table 4.9.

Table 4.9. First-order kinetic equations, R^2 of the equations, constants (k), and deriving half-lives for peptide degradation in diluted pooled human serum.

Peptide	Equation ln[peptide] versus time	R^2	*k*	$t_{1/2} = 0.693/k$ (min)
P006	y = -0.052x - 2.3481	0.9626	0.052	13.33
LJMU011	y = -0.0502x - 2.4558	0.9676	0.0502	13.80
LJMU012	y = -0.0598x - 2.3072	0.9516	0.0598	11.59
LJMU013	y = -0.0469x - 2.3453	0.9589	0.0451	15.37
LJMU014	y = -0.0409x - 2.6344	0.9957	0.0409	16.94
LJMU015	y = -0.043x - 2.4667	0.9833	0.043	16.12
LJMU016	y = -0.0192x - 2.7202	0.9666	0.0192	36.09
LJMU017	y = -0.0024x - 3.5276	0.9557	0.0024	288.75
LJMU018	y = -0.0037x - 3.5984	0.9904	0.0037	187.30
LJMU019	y = -0.0544x - 2.3515	0.9435	0.0544	12.74
LJMU020	y = -0.0527x - 2.3162	0.9478	0.0527	13.15
LJMU021	y = -0.0453x - 2.4871	0.9809	0.0453	15.30
LJMU022	y = -0.034x - 2.4976	0.9852	0.034	20.38
LJMU023	y = -0.0382x - 2.5103	0.9901	0.0382	18.14
LJMU024	y = -0.0163x - 2.6707	0.9662	0.0163	42.52
LJMU027	No degradation over 60 min	-	-	-

4.4.3.6 Metabolite identification via mass spectrometry

Metabolite identification (met ID) is commonly achieved through mass spectrometry [358]. LC-MS analysis was performed, for each peptide at each time point of the stability study in human serum, to gain a better insight of both the kinetics of the metabolic reactions occurring, and the metabolites originating from the compound under evaluation (see Appendix). This resulted in the discovery of the so-called 'soft-spots' of the peptides/peptomers, i.e. the sites more susceptible to undergoing

proteolytic cleavage. Metabolites derived from incubation of peptides and peptide-peptoid hybrids in serum and the corresponding putative sequences are listed in Table 4.10.

LC-MS chromatograms for parent peptide (or peptide-peptoid hybrid) and metabolites identified at time 60 min are included in the Appendix section.

Table 4.10. Peptide and peptide-peptoid hybrid sequences, m/z of metabolites forming at 60 min, and putative metabolite(s) sequence. Modifications from P006 sequence are colour-coded in green (internal fluorination), pink (peptoid), and orange (N-terminal modifications).

Entry	Sequence	*m/z* metabolites (time 60 min)	Putative metabolite(s) sequence(s)
P006	VPTDVGPFAF-NH_2	852.5534 751.5021	TDVGPFAF-NH_2 DVGPFAF-NH_2
LJMU011	VPTDVGPFA-4-F-Phe-NH_2	870.5958 769.5393	TDVGPFA-4-F-Phe-NH_2 DVGPFA-4-F-Phe-NH_2
LJMU012	VPTDVGP-4-F-Phe-AF-NH_2	870.5267 769.4744	TDVGP-4-F-Phe-AF-NH_2 DVGP-4-F-Phe-AF-NH_2
LJMU013	VPTDVGP-4-F-Phe-A-4-F-Phe-NH_2	888.5756 787.5142	TDVGP-4-F-Phe-A-4-F-Phe-NH_2 DVGP-4-F-Phe-A-4-F-Phe-NH_2
LJMU014	VPTDVGPFA-F_5-Phe-NH_2	942.6239 841.5548	TDVGPFA-F_5-Phe-NH_2 DVGPFA-F_5-Phe-NH_2
LJMU015	VPTDVGP-F_5-Phe-AF-NH_2	942.5518 841.4731	TDVGP-F_5-Phe-AF-NH_2 DVGP-F_5-Phe-AF-NH_2
LJMU016	VPTDVGP-F_5-Phe-A-F_5-Phe-NH_2	1032.4651 931.4290	TDVGP-F_5-Phe-A-F_5-Phe-NH_2 DVGP-F_5-Phe-A-F_5-Phe-NH_2

Entry	Sequence	*m/z* metabolites (time 60 min)	Putative metabolite(s) sequence(s)
LJMU017	4-F-Bz-VPTDVGPFAF-NH_2	1024.7659	4-F-Bz-VPTDVGPFA-COOH
LJMU018	F_5-Bz-VPTDVGPFAF-NH_2	1096.6792	F_5-Bz-VPTDVGPFA-COOH
LJMU019	VPTDVGPFA-Nphe-NH_2	852.5671 751.5406	TDVGPFA-Nphe-NH_2 DVGPFA-Nphe-NH_2
LJMU020	VPTDVGPF-Sar-F-NH_2	852.4849 751.4249	TDVGPF-Sar-F-NH_2 VPTDVGPF-Sar-F-NH_2
LJMU021	VPTDVGP-Nphe-AF-NH_2	852.4575 751.4120	TDVGP-Nphe-AF-NH_2 DVGP-Nphe-AF-NH_2
LJMU022	VPTD-NVal-GPFAF-NH_2	852.4849 753.4442	TD-NVal-GPFAF-NH_2 D-NVal-GPFAF-NH_2
LJMU023	VPT-NAsp-VGPFAF-NH_2	852.5123 751.4636	T-NAsp-VGPFAF-NH_2 NAsp-VGPFAF-NH_2
LJMU024	NVal-PTDVGPFAF-NH_2	852.5123 751.4636	TDVGPFAF-NH_2 DVGPFAF-NH_2
LJMU027	Bz-VPTDVGPFAF-NH_2	1006.4487	Bz-VPTDVGPFA-COOH

For P006 and all the internally modified analogues (both fluorinated amino acids and peptoid replacements), the main cleavage site was identified to be at the N-terminal side between Pro29 and Thr30, and subsequent cleavage occurred one amino acid further along the sequence (between Thr30 and Asp31). However, this metabolism was slower and the metabolite DVGPFAF-NH_2 (*m/z* 751.5021) and analogues were only detected after 45 min of incubation in serum. These reactions could be ascribed to the action of dipeptidyl-peptidases and tripeptidyl-peptidases, respectively.

When a lipophilic moiety was placed at the N-terminus near the main cleavage site (originating peptides LJMU027, LJMU017, LJMU018), a much greater peptidase resistance was observed and only a very minor metabolite was detected. This possibly resulted from the action of a carboxypeptidase, liberating a single amino acid at the C-terminus (Phe37), yielding the metabolite $(F)_n$-benzoyl-VPTDVGPFA-COOH (*m/z* 1006.4467, 1024.7808, 1096.6792, for LJMU027, LJMU017, and LJMU018, respectively). The diagram in Figure 4.31 shows the main cleavage sites for P006 and derivatives with free N-terminus compared to the main cleavage site for N-terminally modified analogues.

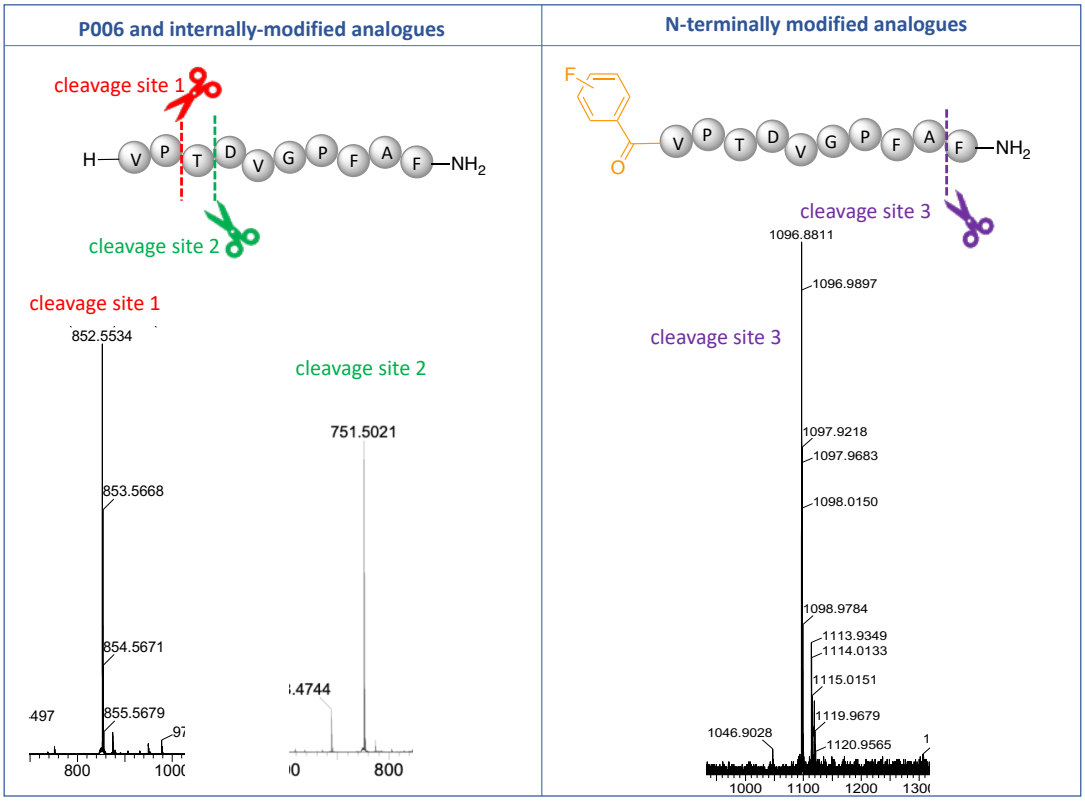

Figure 4.31. Main cleavage sites for P006 and derivatives. For P006 and internally modified analogues (free N-terminus), the main cleavage sites appeared to be near the N-terminus. As opposite, when the N-terminus was masked with a benzoyl group, the only metabolite detected was the benzoyl-peptide lacking the last amino acid at the C-terminus.

4.4.4 Plasma protein Binding (PPB)

As discussed in section 4.4.3.4, when benzoyl derivatives (i.e., LJMU027, LJMU017, LJMU018) were tested for stability in human serum, their concentration at time zero was unexpectedly low when quenched with TCA aq. solution. This did not happen when serum was quenched with MeOH – a solvent in which the N-benzoyl derivatives are highly soluble. This triggered the idea of possible binding to serum proteins, resulting in protection against peptidases (as observed for e.g. Liraglutide and Semaglutide, discussed earlier). Therefore, an assessment of plasma protein binding (PPB) for P006 and benzoyl derivatives was planned. Unfortunately, few clear and repeatable methods for peptide PPB are available in the literature, therefore, some method development was first required.

As a model, PPB was assessed using human serum albumin (HSA). The use of plasma or serum was not suitable for assessing peptides PPB as peptidases contained in plasma or serum would have caused peptide degradation before equilibrium between fraction bound and free peptide was achieved, particularly for peptides that proved to have a short serum half-life.

4.4.4.1 HSA precipitation method for protein binding estimation

It was considered that one way to efficiently and rapidly separate free and bound peptides would be to precipitate the protein(s) to which the peptide was bound and analyse the concentration of peptide in the residual supernatant solution. The idea underpinning this technique relies on the well-accepted concept that HSA removal from a solution can be achieved through precipitation with an aqueous acidic solution (e.g., TCA 15% *w/v* in H_2O) or an organic solvent (e.g., MeOH or acetone), followed by centrifugation [359].

The proposal was that, once the equilibrium between bound and unbound fraction was reached, HSA and HSA:peptide complex could be removed from the solution and the supernatant containing unbound peptide analysed by RP-HPLC. This could then be compared to an HSA-free control solution of peptide treated under the same conditions and protein binding estimated as the difference between the concentration of peptide in HSA-free solution and concentration of peptide in HSA-containing solution.

Initially, HSA was incubated with P006 and LJMU027 at the highest concentrations previously tested for physicochemical stability (500 μM). As described earlier, at this concentration, the more lipophilic peptide (LJMU027) suffered poor solubility, making quantitative analysis of protein binding a challenge. However, in the presence of HSA, LJMU027 appeared to have enhanced solubility and did not precipitate as observed in the buffer-only control, which afforded a visible opalescent precipitate. This indicated that HSA binding was indeed a likely competing process in the serum stability analysis.

To eliminate precipitation concerns, HSA binding was subsequently tested over 24 h using a 4-fold lower peptide concentration (125 μM) while keeping the HSA concentration at 80 μM. The experiment was repeated using both TCA aq. solution (15% *w/v*) and pure MeOH as quenching reagents. As expected from earlier observations, MeOH appeared to be efficient in the extraction of free and HSA-bound peptides and is hence inadequate for this purpose. TCA, however, appeared to precipitate both the protein and any bound peptide simultaneously (Figure 4.32) and may give an indication of the relative protein-bound fraction in blood.

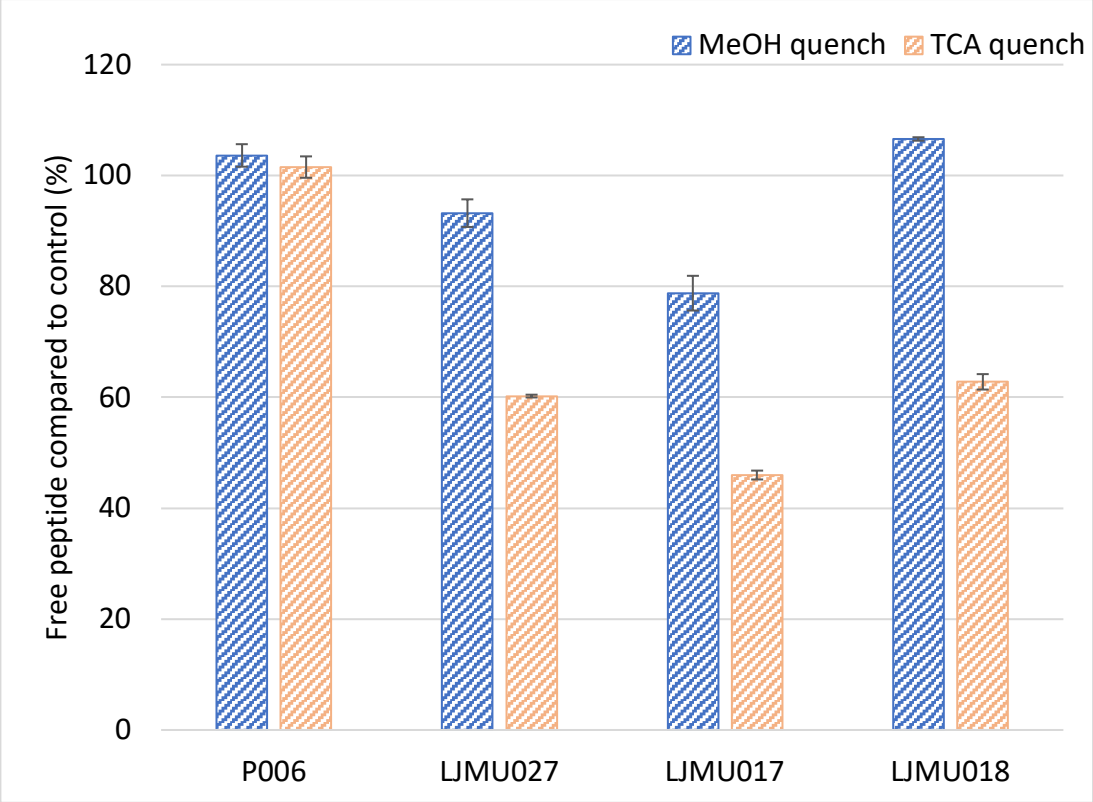

Figure 4.32. Comparison between HSA quenching obtained with MeOH (in blue) and aq. TCA solution (in orange), after incubation of peptides (125 mM) with HSA (80 mM) for 24 h.

To determine the time required to reach equilibrium between unbound and bound peptide, the experiment was repeated at different time points (i.e., 0, 15, 30, 60 min and 24 h). By definition, an equilibrium state does not vary with time. Thus, to

determine a binding equilibrium constant (i.e., K_D), it is important to prove that there is no change in the amount of bound complex over time [321].

As shown in Figure 4.33, while P006 did not show any significant binding to HSA over 24 h, LJMU027 showed binding to HSA and the equilibrium between unbound and bound fractions reached a stable position within 15 min. After this the percentage of hypothetical bound peptide remained constant up to 24 h. For this reason, 15 min was selected as the time to stop the reaction by precipitation of HSA.

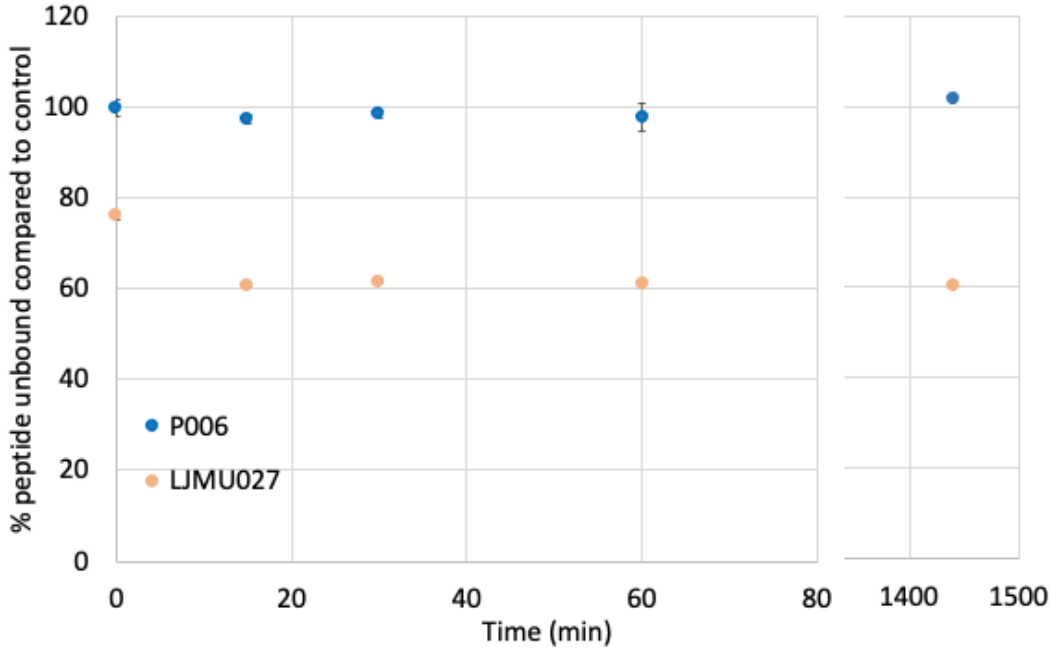

Figure 4.33. Time course experiment to assess the time necessary to reach equilibrium between unbound and bound peptide fractions.

At this point, an estimation of K_D was attempted. Here, a constant concentration of peptide (50 μM) was titrated against increasing concentrations of HSA (between 10 and 400 μM). Scaling down the concentration of peptide (from 125 to 50 μM) allowed the evaluation of a greater range of HSA concentrations without exceeding the maximal HSA solubility in H_2O (~50 mg/mL or 758 μM) and without overloading the HPLC with unprecipitated HSA. Moreover, using appropriately low concentrations of the limiting component is recommended as artifacts can arise

when the concentration of the limiting component is too high compared to the K_D [321]. An HSA-free solution of peptide (50 μM) was used as control (0% bound).

As clear from Figure 4.34, P006 showed the lowest binding affinity for HSA: by increasing the HSA concentration, the percentage of bound peptide fluctuated between 0 and 10%. On the contrary, the percentage of bound peptide for benzoyl derivatives (LJMU027, LJMU017, LJMU018) afforded a curve with increasing binding between 0% to ~80% when the curve began to plateau by 400 μM HSA. Moreover, there seemed to be a trend showing that the higher the number of fluorine atoms attached to the benzoyl ring, the greater the binding: LJMU018, presenting 5 fluorine atoms around the aromatic ring, is the tightest bound, followed by LJMU017 (one fluorine atom in position 4 of the benzoyl ring) and, finally, LJMU027 that does not present any fluorine.

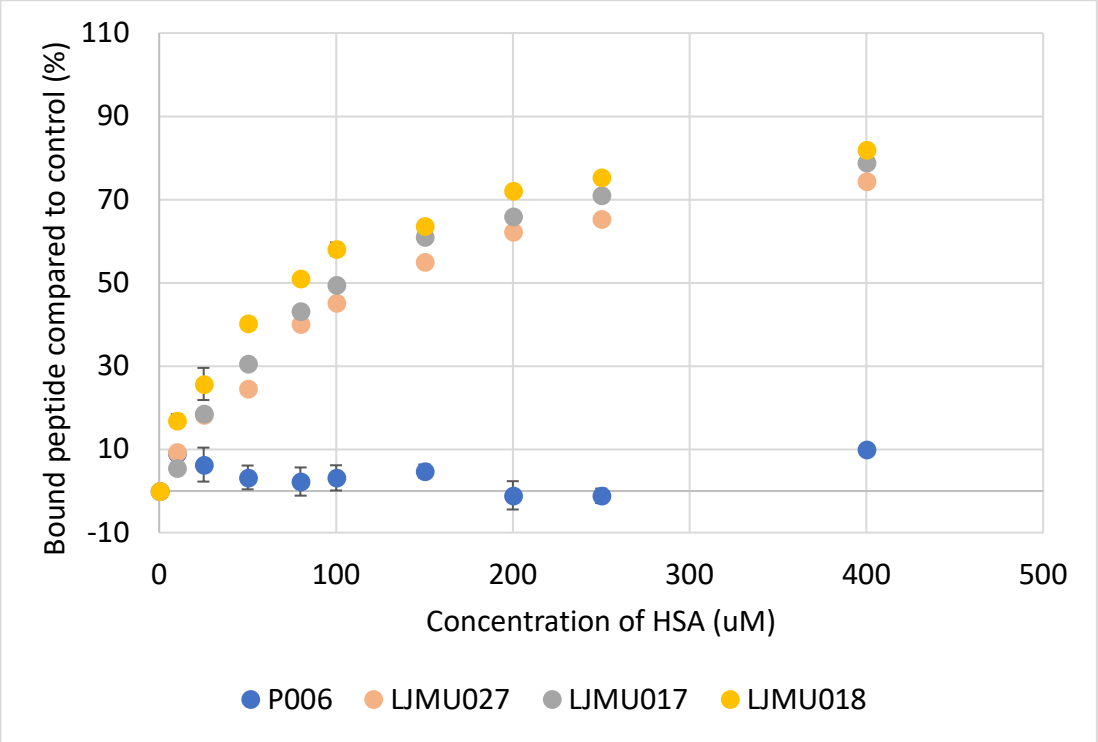

Figure 4.34. Percentage of bound peptide at increasing concentrations of HSA, compared to an HSA-free solution taken as control. Some errors bars not shown because smaller than the marker.

From the graph in Figure 4.34, K_D was estimated by graphically deriving the amount of HSA at which 50% of the peptide was bound.

Table 4.11. N-benzoyl analogues and estimated K_D values from HSA precipitation experiment. KD have been graphically estimated by considering K_D as the concentration of HSA at which 50% of the peptide is bound.

Entry	Modification	Estimated K_D (μM)
LJMU027	N-terminal benzoyl	~125
LJMU017	N-terminal 4-F-benzoyl	~ 100
LJMU018	N-terminal F_5-benzoyl	~ 80

This experiment confirmed the hypothesis that an increase in lipophilicity of P006, by addition of aromatic moieties at the N-terminus, significantly increases the plasma protein binding. This idea has literature precedent, where there exists a positive sigmoidal correlation between logD values and plasma protein binding (%) [355,356].

In conclusion, the HSA precipitation method described could be considered an inexpensive preliminary screening test for protein binding that does not require sophisticated instruments and could be useful to rank compounds within a library. However, it could be argued that the extent of plasma protein binding measured with this method could be an underestimation because the amount of peptide released from HSA upon denaturation by addition of acidic solution, cannot be quantified. Hence, the trends shown by HSA precipitation experiment should be confirmed by ED and/or UF.

4.4.4.2 Equilibrium Dialysis (ED)

For quantitative microdialysis, rapid equilibrium dialysis (RED) devices with MWCO of 8 kDa and 12 kDa (ThermoFisher Scientific) were employed. The initial optimisation of a dialysis experiment requires the assessment of the suitability of a compound for dialysis i.e. the ability and the time required to reach dynamic equilibrium between the two chambers in the absence of protein. If the compound

is involved in nonspecific binding towards the material of the chambers and/or the membrane, equilibrium may not be reached and the concentrations detected would be lower [329]. The concentrations in the two chambers should be measured against a calibration curve obtained by analysing compound solutions in a range of known concentrations prepared in the same medium (for this study, PBS, pH 7.4, 5% DMSO). Calibration curves were accepted only if the R^2 was greater than 0.999. An example of calibration curve for P006 is shown in Figure 4.35.

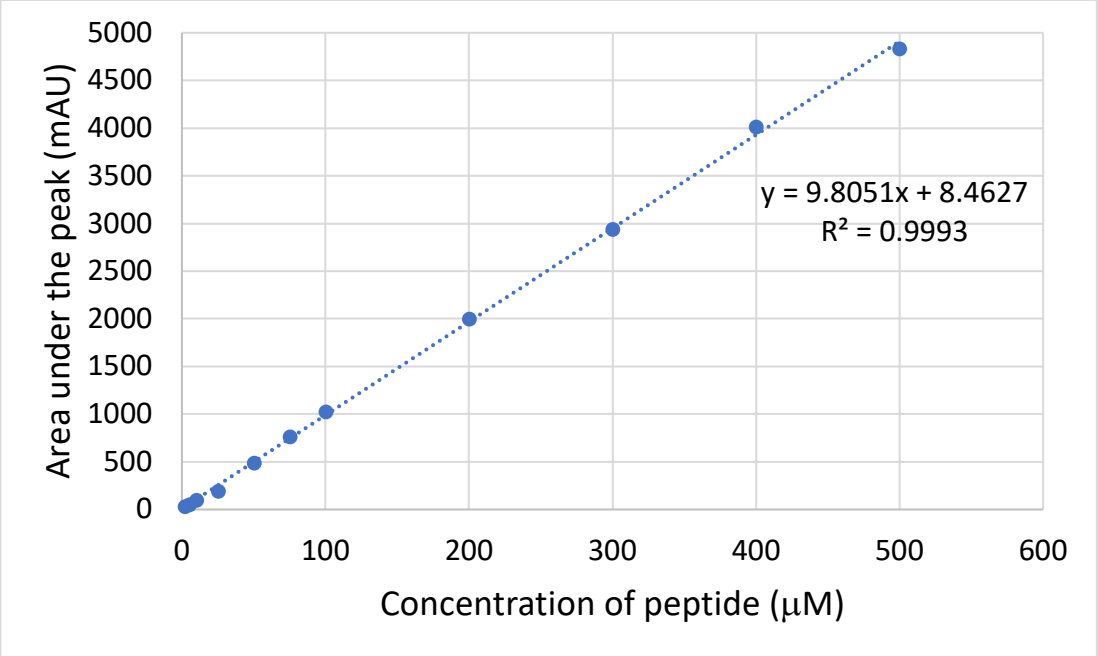

Figure 4.35. Calibration curve for P006 in PBS aq. solution (pH 7.4, 5% DMSO).

RED devices with MWCO of 8 kDa were initially evaluated for their suitability for peptide dialysis in the absence of protein under various conditions (room temperature and 37 °C, 4 and 24 h). The partition coefficient of the peptide in the absence of the protein (p_c) was considered suitable to proceed with protein binding experiments only if $0.9 < p_c < 1.1$ [329]. P006 was used to optimise the time and conditions required to reach equilibrium between the two chambers. Firstly, P006 dialysability was tested with 8 kDa MWCO RED devices at room temperature for 4 h and 24 h, which confirmed that equilibrium was not reached at this low temperature. Subsequently, the test was repeated for 24 h at 37 °C, affording a p_c value of ~1,

indicating that equilibrium was reached. For this reason, 24 h was chosen as the incubation time required for the peptide to equilibrate between the sample chamber and the adjacent chamber of the 8 kDa MWCO RED devices.

Given the relatively slow equilibration using the 8 kDa MWCO REDs, the analogous experiment using 12 kDa MWCO RED devices was only performed at 37 °C, over 4, 6, 8, 12, and 24 h. The graph in Figure 4.36 shows the partition coefficients (p_c) at different time points, converging on p_c = 1 after incubation times of 12 h and 24 h. Hence, 12 h was selected to reduce the time of experiment and avoid issues related to overnight incubation (e.g., precipitation of the sample due to long incubation times as well as short circuit or instrumental problems while the experiment was not monitored).

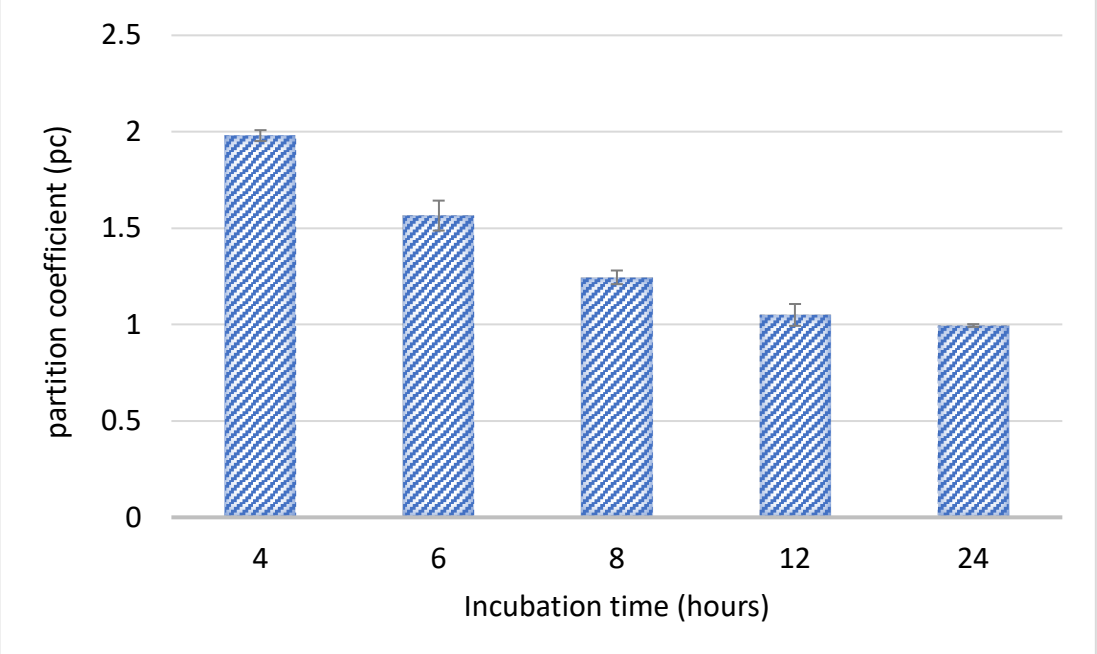

Figure 4.36. Partition coefficients obtained by incubating the peptide solution (P006) in the 12 kDa MWCO RED devices for various times (i.e., 4, 6, 8, 12, 24 h) at 37°C.

Both the 8 kDa and 12 kDa RED devices showed much slower equilibration compared to previously optimised and validated protocols (e.g., 12-24 h instead of 2-6 h) [329,331,360]. This is probably because these commercial devices have been

optimised for small molecules, whilst this work utilises larger peptides that evidently require a longer time to diffuse through the membrane. For this reason, the application of RED devices for peptides brought no significant advantages compared to the 'gold-standard' equilibrium dialysis method (e.g., no reduced equilibration times even though the cellulose membrane presents a high area-to-volume ratio) [330,331]. Moreover, the time required for equilibration with a higher cut-off membrane (12 kDa compared to 8 kDa) was expected to be lower; however, 12 h was the minimum time required to obtain an acceptable p_c value.

Peptides (LJMU027, LJMU017, and LJMU018) were evaluated for their dialysability under the above conditions (8 kDa MWCO: 24 h at 37°C; 12 kDa MWCO: 12 h at 37°C) prior to measuring HSA protein binding. p_c values calculated for each peptide and reported in Table 4.12 were all within the range of suitability ($0.9 < p_c < 1.1$).

Table 4.12. pc values assessed for each peptide using 8 kDa and 12 kDa MWCO RED devices.

Peptide	**8 kDa - p_c**	**12 kDa - p_c**
P006	1.01	1.05
LJMU027	0.99	1.13
LJMU017	1.05	1.11
LJMU018	1.04	1.13

Once the suitability of the compounds for dialysis was confirmed under the optimised conditions, peptide protein binding experiments were executed as reported in literature [329].

There are different ways to assess the extent of binding from the RED experiment, by using the measured concentration either in the sample chamber (red), in the buffer chamber (white) or a combination of both. The Excel workbook created by Shave and collaborators [329] allows the user to predict K_D values by simply entering the correct experimental conditions (i.e., concentration and volume of protein and peptide solutions) and values obtained from the experiment [329]. On the other

hand, Waters *et al.* suggested that it is possible to calculate the apparent affinity (log*K*) using the following equation:

$$logK = \log\left(\frac{1 - fu}{fu}\right)$$

Equation 4.15

where fu is the fraction unbound calculated from the ratio between the concentration in the buffer chamber and the concentration in the sample chamber [331]. Similarly, the instruction protocol from Thermo Fisher suggests calculating the percentage of free compound with Equation 4.10:

$$\%\ free\ compound = \frac{C_1}{C_2} * 100$$

and then deriving the percentage of bound compound by subtraction [330]. Similar data analysis was conducted by Greco and collaborators, who exploited the RED devices for assessment of protein binding of peptidomimetics [338].

Similarly, in this study, the percentage of bound peptide was calculated by taking into consideration the concentration in the sample chamber and in the buffer chamber in the protein experiment. Surprisingly, for both the 8 kDa and 12 kDa MWCO RED equilibrium dialysis experiments, the percentage of bound peptide for the benzoyl derivatives was not significantly different from the percentage of bound P006, as shown in Figure 4.37.

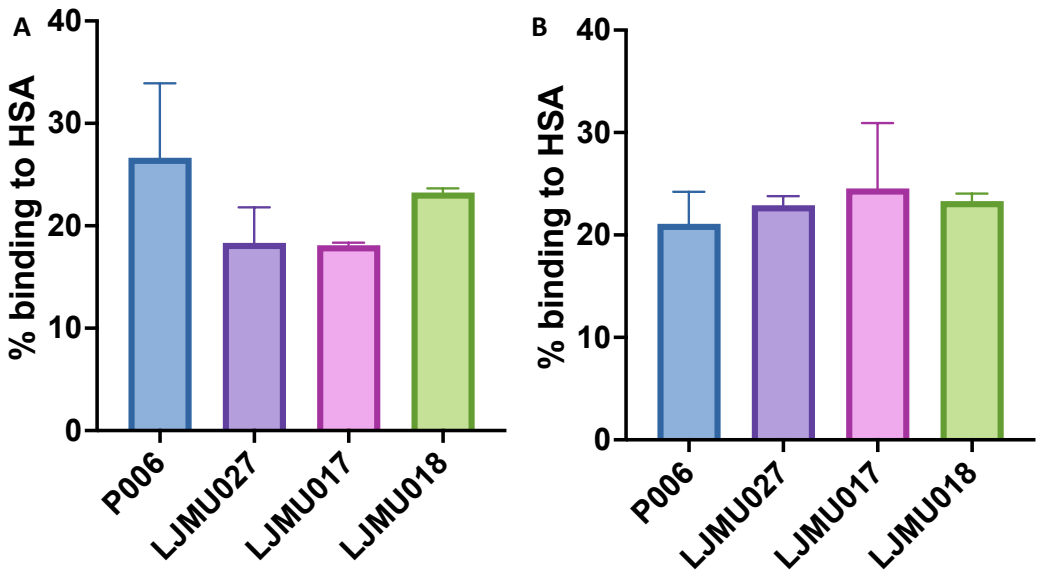

Figure 4.37. (A) Percentage of peptide bound to HSA measured with 8 kDa MWCO RED devices (B) Percentage of peptide bound to HSA measured with 12 kDa MWCO RED devices. Ordinary one-way ANOVA on GraphPad Prism was performed to assess the significance of the data. All data comparison showed no statistical significance (p value > 0.05).

The impact of protein leakage on the results obtained, previously described by van Liempd *et al.*, was excluded due to a control experiment carried out by the Lusby Research Group (Isis Middleton, PhD student at University of Edinburgh) where it was demonstrated that the amount of HSA leakage from the sample chamber (red) to the buffer chamber (white) over 48 h was lower than 3% (Middleton *et al.*, unpublished data) [361]. Hence, the unexpected percentage of bound peptide was not a result of HSA leakage in the buffer compartment. Moreover, even in the case of nonspecific binding and/or total recovery lower than 100%, this should not impact on the partition between bound and unbound, as concluded in the study carried out by the Pfizer Pharmacokinetics department [362]. However, the long incubation times required for reaching equilibrium (i.e., 12-24 h) could affect the solubility of the benzoylated peptides, thus bringing about misleading results. Hence, a third method to assess protein binding was investigated to conclude which method was the most reliable.

4.4.4.3 Ultrafiltration (UF)

Determination of the extent of plasma protein binding for P006 and LJMU027 was assessed using Sartorius Vivaspin 500 ultrafiltration devices. To allow a direct comparison with the RED 8 kDa MWCO devices experiment, initially, the same conditions were employed. In particular, the incubation time was kept at 24 h and the solutions of peptide and HSA-peptide were prepared according to the final concentrations reached after equilibration through the RED devices membrane (concentration of HSA 80 μM, concentration of peptide 125 μM). In this case, the separation between bound and unbound fractions was attempted by ultrafiltration and compared to the concentration of the peptide only solution. As shown in Figure 4.38, the percentage of unbound P006 after 24 h incubation with HSA was ~100%, while for LJMU027 this was around 70% (considering 100% the amount of peptide recovered in the absence of HSA). This data was in close agreement with the outcome of the HSA precipitation method (see section 4.4.4.1), where the percentage of free LJMU027 in solution after 24 h incubation with HSA was around 60%, while P006 was almost completely free in solution.

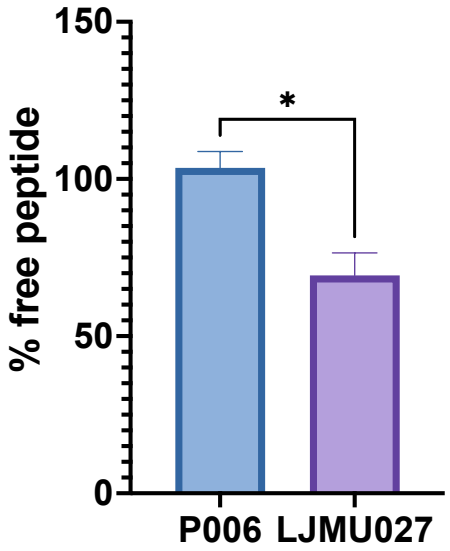

Figure 4.38. Percentage of free peptide (P006 and LJMU027) in HSA binding experiment using UF devices (24 h incubation). Statistical analysis (unpaired two-tailed t-test) showed significance of the results (p value < 0.05).

The dataset can be analysed by deriving peptide concentration after ultrafiltration from calibration curves obtained by preparing solutions of a range of concentrations in the same medium (i.e., PBS aq. solution, pH 7.4, 5% DMSO). In this experimental procedure the PES filters were washed twice with 100 μL of buffer, leading to a final maximal concentration of 53.6 μM, starting from 125 μM. Hence, if nonspecific binding did not occur, the concentration of the peptide buffer solution (HSA free) would be ~53.5 μM. As represented in Figure 4.39, this hypothesis was confirmed for P006 (concentration average 53.76 μM), while the concentration of LJMU027 was ~75% lower than the hypothetical value (~14 μM instead of 53.5 μM), providing the first evidence of nonspecific binding occurring.

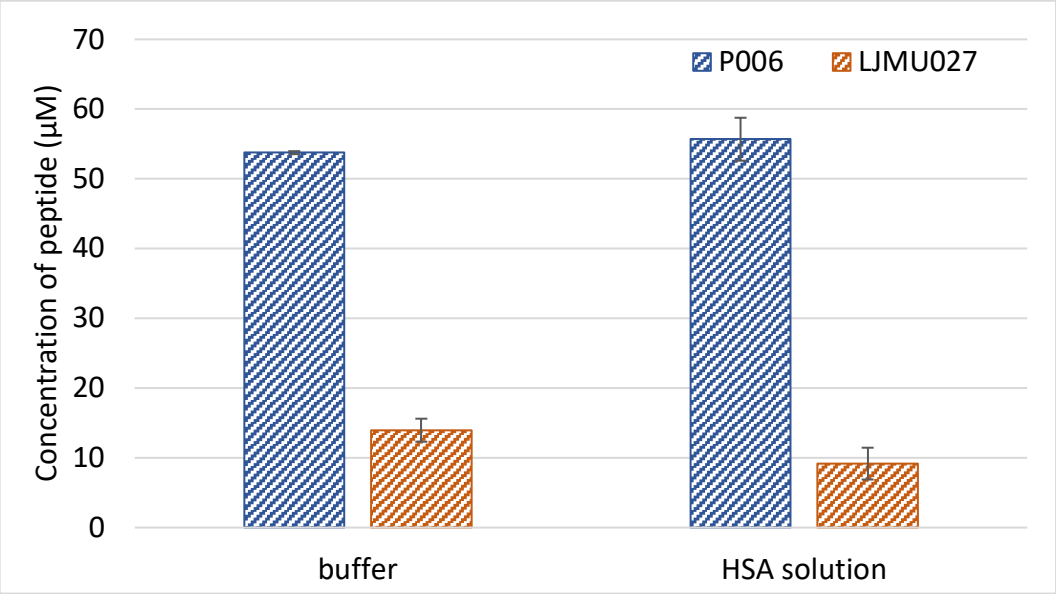

Figure 4.39. Comparison between concentration of peptide in PBS buffer solution after ultrafiltration and in HSA solution after ultrafiltration. Blue columns represent P006, while orange columns represent LJMU027.

At this point, when the K_D estimation for LJMU027 was attempted using the ultrafiltration method, an additional control to assess the extent of nonspecific binding was added to the experimental set-up, wherein the HSA-free peptide solution was treated under the same conditions but centrifuged without the use of the PES membrane. Moreover, the incubation time was reduced to 15 min as this

was sufficient to reach equilibrium between bound and unbound fractions (as previously shown in Figure 4.33). Finally, the concentration of peptide could not be reduced from 125 μM to 50 μM, as previously attempted with the RED experiment, as this would have led to quantification problems. A reduction of initial peptide concentration by 60% (50 μM) would lead to a final concentration after dilution with PBS aq. solution of 21.44 μM, with obvious detection issues in the case of peptide binding to HSA. This experiment showed that, by comparing the two solutions of LJMU027 – one centrifuged without the membrane and the other one filtered through the Vivaspin device containing a PES membrane – the recovery of the filtered solution was lower than 50% (Figure 4.40), proving that the extent of nonspecific binding to the PES membrane for LJMU027 was over 50%. The peptide, being around 10 times smaller than the MWCO of the UF device should easily penetrate the pores of the membrane. Hence, we can speculate that the benzoyl peptide analogue may interact with the material of the membrane (polyethersulfone, PES), struggling to permeate through. PES is a widely used membrane material with a highly hydrophobic core due to the presence of aromatic rings, but, at the same time, its structure facilitates hydrogen bonding with water molecules, allowing high permeation of water [336]. Though, being a fully aromatic polymer, PES may promote π interactions with the aromatic moiety of the benzoyl derivatives, preventing the permeation of the peptide through the membrane.

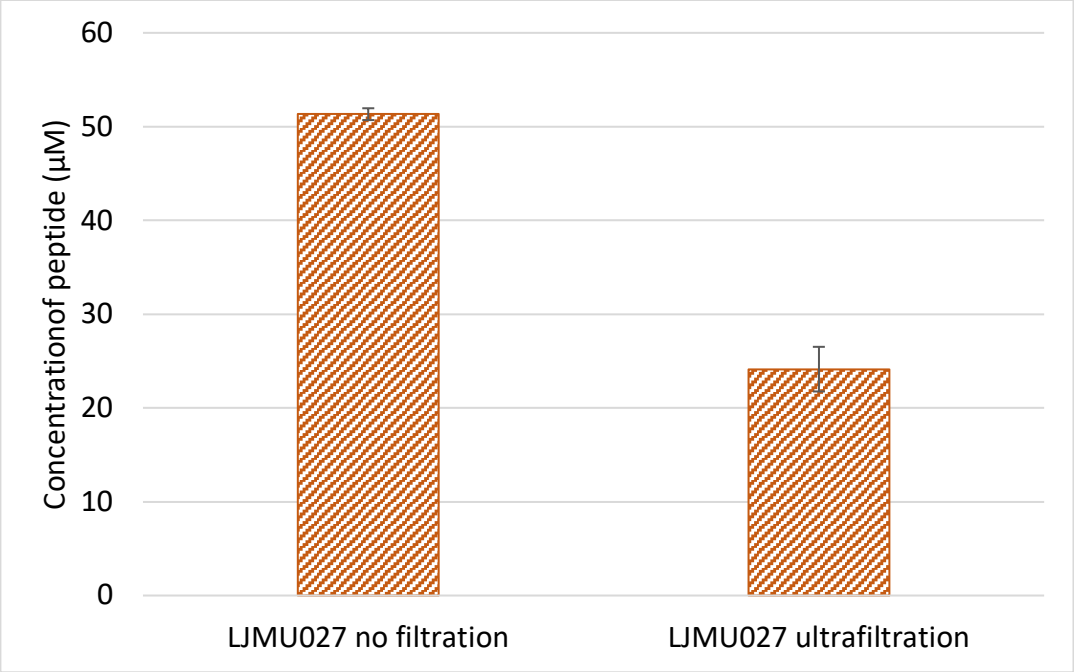

Figure 4.40. Extent of non-specific binding to PES membrane of the Vivaspin device, through comparison between non-filtered and filtered peptide solutions (in PBS aq. solution, 5% DMSO).

When approaching the analysis of the K_D estimation for LJMU027, the data were normalised by assuming the filtered HSA-free peptide solution to be 100%. Still, the high variability of the results did not show any significant difference at increasing concentrations of HSA (100, 200, 300, and 400 µM), as shown in Figure 4.41. The ultrafiltration method was deemed to be unreliable for the estimation of peptide-HSA interaction K_D.

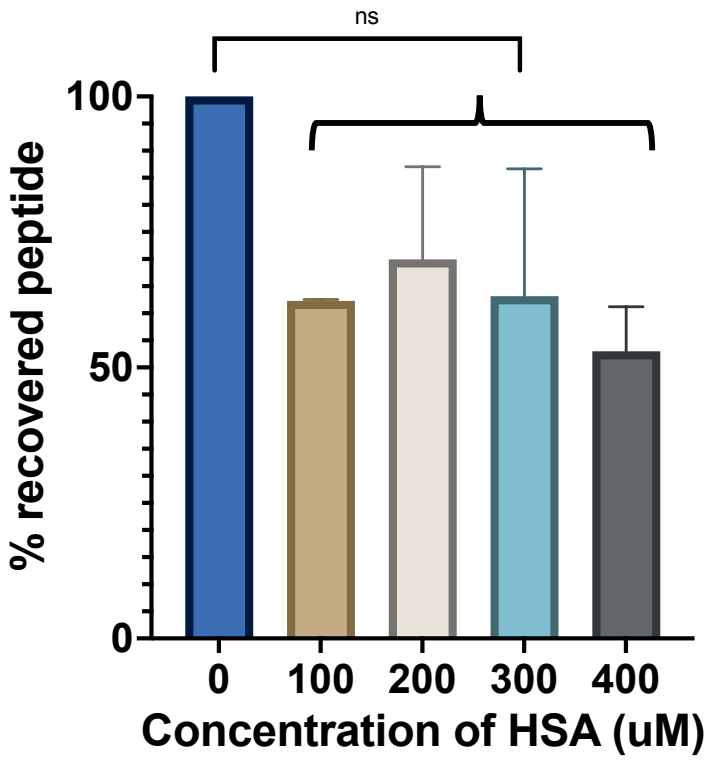

Figure 4.41. Extent of LJMU027 binding by titrating peptide solution (125 mM) with increasing concentrations of HSA (100, 200, 300, 400 mM). Data were normalised taking the HSA-free solution of peptide after filtration as 100%. Significance was assessed by ordinary one-way ANOVA on GraphPad Prism software. ns mean p value > 0.05.

4.5 Conclusions

The initial lead antagonist P006 exhibited potent antagonism of the CGRP-R, however, its low drug-likeness, due to very low stability in human serum and high aqueous solubility which made the formulation challenging, required structural optimisation. Three different strategies: fluorination, peptoid scanning, and N-terminal modification were examined. Firstly, stability in human serum was assessed, showing an impressive improvement in stability for the N-benzoyl modified peptides, while a smaller increase was obtained with fluorination and with peptoid scanning (with exception of LJMU016 and LJMU024). In particular, N-benzoylation likely precluded access to the cleavage site by a putative aminopeptidase, consequently affording a very high stability in blood serum (~75-94% intact after 60 min

incubation). On the other hand, peptoid replacements were effective only when the amino acid replaced was near to the cleavage site (i.e., Val28), and the further the replacement was from the cleavage site, the lower the effect on stability. Finally, fluorination of the two Phe residues in positions 37 and 35 was effective in improving stability only when Phe was replaced with F_5-Phe, with particular improvements noted with the doubly substituted compound (LJMU016), where the hydrophobicity was greatly increased, while 4-F-Phe substitution did not successfully yield more stable compounds.

Analysis of various strategies to assess plasma protein binding of peptide candidates brought to light issues related to commercially available kits, usually developed for small molecules. On the other hand, the in-house developed HSA precipitation strategy was successful in giving an estimated value of plasma protein binding, even though this may be, at worst, an underestimation due to difficulties in quantification of the peptide released when HSA is precipitated. Finally, the developed strategy suggested a putative binding related to the benzoyl derivatives, while the extent of binding of P006 was lower, yet not quantified with a degree of certainty.

In conclusion, N-benzoylated P006 analogues were identified as new lead compounds, showing an activity profile comparable (or better in the case of LJMU027) to that of P006, and exhibiting a significant improvement in pharmacokinetic profile, particular stability in serum. Hence, these were selected as the best compounds to bring forward to formulation, *in vivo* studies and future lead optimisation work.

5 Formulation and self-assembly of peptide CGRP-R antagonists

5.1 Introduction

5.1.1 Formulation and nasal delivery

When a pharmaceutically active agent is encapsulated in, or attached to a polymer, drug safety and efficacy can be significantly improved. Hence, there is great interest in studying delivery systems and approaches to transport drugs to the target tissue through different portals in the body [363]. Delivery of a drug to the site of action can be achieved *via* the use of technology platforms of various size, from micro- to nanoscale.

Since microencapsulation technology was first approached in the 1930s, a great number of studies has focused on drug encapsulation for drug delivery to reach the target site, and to release the drug in a controlled manner [364]. Polymeric microparticles (MPs) are ideal carriers for many controlled drug delivery applications, due to their biodegradability, biocompatibility, as well as the ability to encapsulate a variety of drugs [365].

More recently, nanotechnology, described as the 'technology on the nanoscale' [366], has greatly expanded, leading in 2005 to the FDA approval of the first medicine employing nanotechnology. Abraxane (Taxol-loaded protein nanoparticles), was proven to be less toxic and more effective compared to the free drug for the treatment of breast cancer [367]. Nowadays, a large number of medicines in clinical use or in clinical and pre-clinical trials involve the use of nanotechnology to deliver the active principle. Nanoparticles (NPs) can be defined as a solid colloidal particles ranging in size from 10 to 1000 nm [368].

A delivery system is usually chosen according to the route of administration. When a drug is required to act at the central nervous system (CNS) level, the blood brain barrier (BBB) is a major obstacle to the delivery of potential therapeutics to the brain [369,370]. Classically, to cross the BBB, drugs should have a molecular weight lower than 400 Da, be largely apolar, and not multicyclic [371]. However, most peptides do

not fit within these parameters. An alternative method to deliver molecules to the CNS is *via* the nose-to-brain route that enables transport of drugs directly into the brain *via* the trigeminal nerves or the olfactory neurons, which are in contact with both the nasal cavity and the central nervous system, creating a direct pathway to the brain [370–372]. The advantages of intranasal administration include not only circumventing the BBB, but also avoiding adverse events in the gastro-intestinal tract, first-pass metabolism and/or degradation in the blood compartment, ease of administration, large surface area available for drug targeting, and highly vascularised mucosa in close proximity to the portal entry [370,373,374].

For the nasal delivery route, the dosage form can be prepared as a liquid or a solid. Despite the fact that liquid dosage forms prevail in nasal drug delivery, powders containing active pharmaceutical ingredients are preferred since they offer a range of advantages over liquid forms demonstrated *in vitro*, *in vivo*, and in clinical trials – e.g., greater chemical stability, enhanced nasal absorption, small packaging size, and ease of handling [375,376].

Generally, nasal administration is achieved through nasal devices, primarily chosen according to the type of formulation e.g., being liquid or powder. Nasal drug delivery devices currently available for both liquid and powder formulations have been extensively reviewed by Djupesland *et al.* [374]. Briefly, the function of nasal powder devices is usually based on one of the following principles: i) powder sprayers presenting a compressible compartment which, when released, achieves a plume of powder particles; ii) breath-actuated inhalers, where the patient inhales the powder with his own breath; iii) devices comprising of a mouthpiece and a nosepiece fluidly connected (nasal insufflators), where the delivery occurs when the patient exhales into the mouthpiece and the airflow carries the particle powder into the nose [374]. Thus, nano- and micro-technology can be combined to create a technological platform in form of a powder suitable for nasal delivery of active peptides.

5.1.2 Peptide delivery

Due to unfavourable physicochemical properties and low bioavailability, most of peptide drugs are still delivered by injection [377]. Indeed, the therapeutic effect of a peptide drug can be hampered by fast elimination from the system through the kidneys, rapid degradation in blood, uptake by the reticuloendothelial system, and accumulation in nontargeted cells [370,378]. Various delivery systems and techniques have been developed to overcome these limitations, leading to the development of a wide range of drug carriers. According to the type of peptide drug, this can be physically encapsulated or chemically bound to a polymer. In the first case, encapsulation is dependent on the solubility of the drug, while in the second case the presence of a functional group allowing efficient reaction is required.

Various strategies have been pursued for the preparation of nose-to-brain delivery formulations of peptides. Most commonly, active pharmaceuticals (e.g., insulin or oxytocin) have been dissolved in aqueous media, and, in some cases, functional excipients or cell penetrating peptides have been added to the formulation to improve the delivery [379–384]. Another strategy included the preparation of nanoparticles (NPs) to enhance the penetration and/or to prolong the residence time in the nasal cavity. Nanosystems can be divided into NPs prepared from lipids (e.g., solid lipid NPs), NPs prepared from polymers (e.g., chitosan or poly(L-lactide-co-glycolide NPs), and NPs prepared from peptide self-assembly [372,385–387].

5.1.3 Polymeric nanoparticles

To overcome the limitations associated with degradation and poor adsorption of drugs, polymeric nanoparticles have been extensively studied to deliver peptides to the brain. Despite not being widely used in medicine, polymeric NPs offer the advantages of protecting the encapsulated drug from extracellular transport by P-glycoproteins as well as biological and/or chemical degradation [372,388]. Preclinical studies have shown promising results for the delivery of peptides through NPs [388,389].

5.1.3.1 Poly(D,L-lactic-co-glycolic acid) (PLGA) NPs preparation

In particular, poly(D,L-lactic-co-glycolic acid) (PLGA, **90**) is one of the most successful biodegradable and biocompatible polymers approved by the FDA and EMA for human use in various drug delivery systems [390]. Hydrolysis of PLGA leads to the formation of nontoxic oligomers and monomers of lactic and glycolic acid (**91** and **92**, respectively), easily metabolised by the body *via* the Krebs cycle, with subsequent minimal toxicity associated [390].

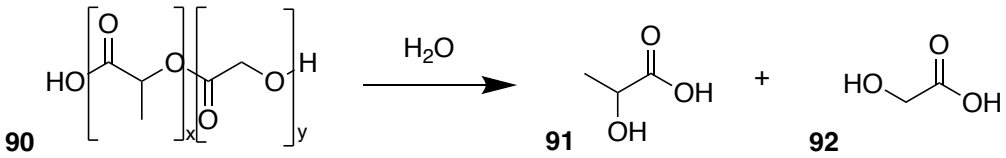

*Figure 5.1. Chemical structure of PLGA (90), yielding lactic acid (91) and glycolic acid (**92**) through hydrolysis.*

The use of PLGA to protect drugs from degradation in the nasal cavity has been previously explored. Olanzapine-loaded PLGA NPs (diameter size ~90 nm and drug entrapment of ~70%) resulted in a 10-fold increased delivery to the brain compared to olanzapine solution [372]. Moreover, oxcarbazepine-loaded PLGA NPs (diameter size ~250 nm and encapsulation efficiency >80%) have demonstrated a reduction in seizures in a rat seizure model [391]. Thus, peptide-loaded PLGA NPs can be considered a potential approach for effective and sustained nose-to-brain delivery.

Strategies explored to prepare PLGA NPs can be divided into bottom-up and top-down approaches [392]. The bottom-up techniques comprise the nanoprecipitation method, and the single and double emulsion techniques [391,393–398]. In the emulsion evaporation methods (Figure 5.2), an organic phase containing polymer is emulsified under high-shear stress with an aqueous phase containing a surfactant – e.g., anionic sodium dodecyl sulfate (SDS) or non-ionic polyvinyl alcohol (PVA). The emulsification process is followed by the evaporation of the organic solvent under stirring or vacuum. Single or double emulsions can be used to encapsulate drugs with different properties; in particular, the oil-in-water (o/w) emulsion is used for

hydrophobic compounds, while the water-in-oil-in-water (w/o/w) emulsion for hydrophilic compounds [392].

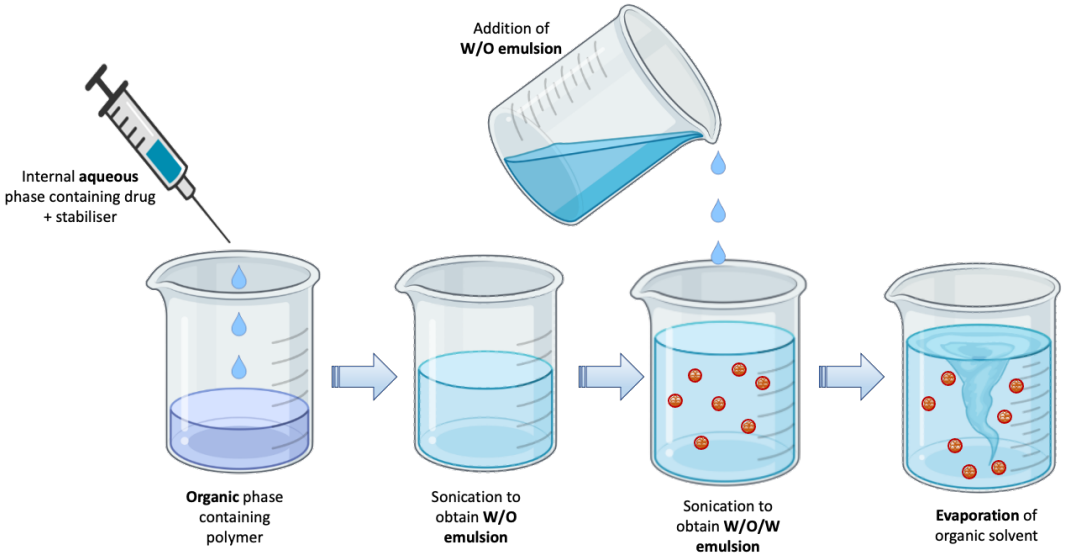

Figure 5.2. Preparation of nanoparticles by double emulsion solvent evaporation method.

Nanoprecipitation (Figure 5.3), patented by Fessi *et al.* in 1989, is a widely used technique based on formation of NPs due to polymer precipitation [399]. Polymer and drug are dissolved in a polar, water-miscible solvent (e.g., acetone); the solution is then added dropwise into an aqueous solution containing a surfactant (e.g., PVA) [392]. Polymeric NPs or aggregates are immediately formed by rapid solvent diffusion, in a four-step process including supersaturation, nucleation, growth by condensation, and growth by coagulation [392,399,400]. Nanoprecipitation has been successfully used to encapsulate both hydrophobic and hydrophilic drugs [401], but has shown more promising applications for hydrophobic compounds, soluble in ethanol or acetone, with limited solubility in water [401]. For example, Barichello and collaborators obtained encapsulation efficiencies close to 100% for hydrophobic drugs (i.e., indomethacin and cyclosporin A), but less than 15% for hydrophilic drugs (i.e., vancomycin and phenobarbital) [402].

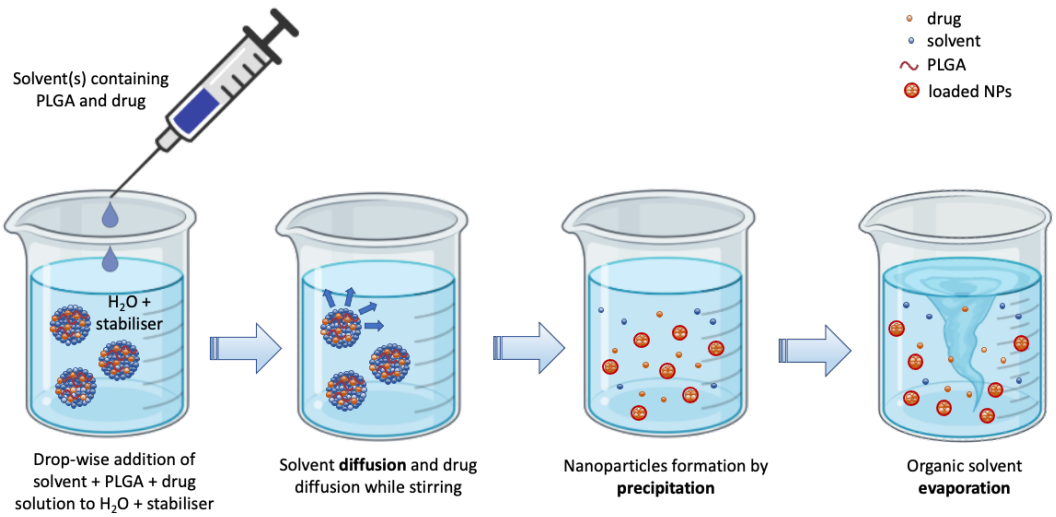

Figure 5.3. Representative scheme of a 4-step PLGA NPs production by nanoprecipitation method [403].

5.1.3.2 Encapsulation of peptides into polymeric nanoparticles

Encapsulation of various peptide molecules within PLGA NPs was successfully obtained by the double emulsion solvent evaporation method [398,404–408]. Chereddy and collaborators explored the double emulsion technique to prepare PLGA NPs loaded with the antimicrobial peptide LL37 (diameter size ~300 nm and encapsulation efficiency of ~70%) [407]. Another example of the use the of double emulsion method is represented by the encapsulation into PLGA NPs of 15-mer peptides active against canine parvovirus (diameter size of ~180-220 nm and encapsulation efficiency of ~80%) [406]. Silva *et al.* studied the effect of various parameters on the preparation of PLGA NPs loaded with a 24-amino acid peptide, eventually yielding 40% encapsulation efficiency and low burst release [405].

On the other hand, nanoprecipitation was seldom exploited for the preparation of peptide-loaded PLGA NPs. Bisht and collaborators employed this method to fabricate PLGA NPs for intravitreal delivery of a Connexin43 mimetic peptide. Here, the formulation was optimised by studying the influence of the amount of PLGA, acetone, and PVA on average particle size, polydispersity index (PDI), and zeta potential (ZP) and concluding that particle size (diameter size of the optimised

formulation ~100 nm) can be minimised by reducing the amount of polymer and increasing the organic phase volume. However, no information was given on the encapsulation efficiency and release profile of the formulations [397].

Finally, a comparison between nanoprecipitation and double emulsion techniques in the encapsulation of a hydrophilic short peptide (i.e., dalargin) was described by Chen *et al.*, who concluded that incorporation of the peptide in polymeric NPs is strongly influenced by the presence of ionic additives and by the preparation method, with the highest encapsulation efficiency (~69%) obtained by nanoprecipitation and by using sodium dodecyl sulphate (SDS) as ionic additive [398].

5.1.4 Peptide self-assembly

One of the most promising approaches to yield nanoscale technology systems is the bottom-up approach, which represents the self-assembly of atoms or molecules from basic chemical building blocks to yield nanomaterials or nanodevices [366].

Self-assembly is the process by which an organised structure spontaneously forms from individual components, as a consequence of specific interactions occurring between the components [409]. When the process involves biomolecules, self-assembly can be described as the ability to associate *via* noncovalent interactions into ordered architectures, following a bottom-up approach [410]. Therefore, this is a free energy-driven process that often originates from stimuli or conditions that trigger the formation of a range of noncovalent interactions (e.g., hydrogen bonding, electrostatic and/or hydrophobic interactions, $\pi-\pi$ stacking, and Van der Waals forces) between molecules in the system [367,411,412]. Molecular self-assembly occurs naturally in living systems; examples of its occurrence are protein folding in enzymes, formation of DNA double helix, and self-assembly of lipids to form cell membranes, to name but a few [410].

The field of peptide self-assembly has been studied since 1989, when the biochemist Shuguang Zhang, in Alexander Rich's laboratory at Massachusetts Institute of Technology, discovered the properties of the segment EAK16 (**93**) of the yeast

protein zuotin, which subsequently inspired the design of a large class of self-assembling peptides [413,414].

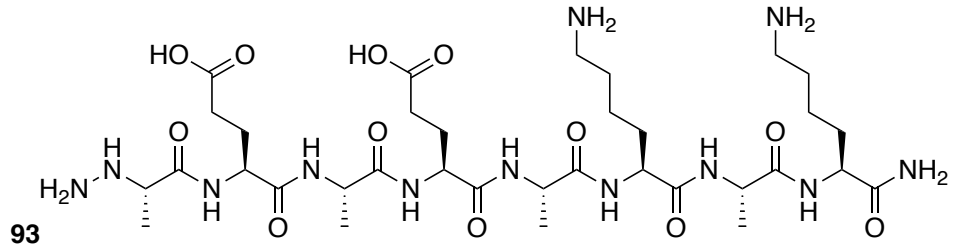

Figure 5.4. Chemical structure of the peptide EAK16, discovered by Zhang et. al [413,415].

Self-assembling peptides are generally naturally occurring or synthetic peptides, comprising 2 to 50 amino acid residues, that present the ability to form long-range ordered supramolecular architectures [411].

Nowadays, due to their intrinsic biocompatibility and biodegradability, self-assembling peptides have attracted great attention for various applications – e.g., cutting-edge nanotechnology (sustained releases and delivery of various molecules), 3D cell cultures, 3D tissue printing, wound healing acceleration, tissue regeneration, and membrane proteins stabilisation [367,413,416].

5.1.4.1 Different chemical structures of self-assembling peptides

Peptides with the ability to self-assemble comprise a variety of chemical structures (Table 5.1 and Figure 5.5) that form α-helices, β-sheet fibrils, surfactant-like assemblies, α-helical coiled coils, and/or collagen triple helices, which further organise into nanoarchitectures with a variety of different morphologies [410–412,415,417–422].

Table 5.1. Description of self-assembling peptide building blocks.

Peptide structure	Description	References
Peptide amphiphiles (**94**)	Peptides containing a hydrophobic building block (e.g., alkyl chain) and a hydrophilic functional region.	[367,422–424]
Surfactant-like peptides (**95**)	Amphiphilic peptides containing both hydrophobic and hydrophilic amino acids in their head and tail; alternatively, peptides that present repeated sequences of hydrophobic amino acids.	[425–427]
LMW peptides (**96**)	Simple di- or tri-peptides with or without N-terminal modifications (e.g., Fmoc and naphthyl).	[422,428,429]
Ionic-complementary peptides (**97**)	Peptides containing a hydrophobic tail that promotes self-assembly in water or a hydrophilic tail with charged amino acids that forms ionic bonds. They are classified by the number of repeated ion charges: type I (+-+-+-), type II (++-++-), type III (+++--+++), and type IV (++++----).	[430–433]
Bolaamphiphiles (**98**)	Peptides containing hydrophilic head and tail, connected by a hydrophobic region, generally composed of alkyl groups.	[411,418]
Cyclic peptides (**99**)	Peptides containing an even number of alternating D- and L- amino acids forming hydrogen bonding. Alternatively, peptides characterised by an amphiphilic cycle (e.g., one side of the cycle is hydrophilic, the other side is hydrophobic).	[434,435]

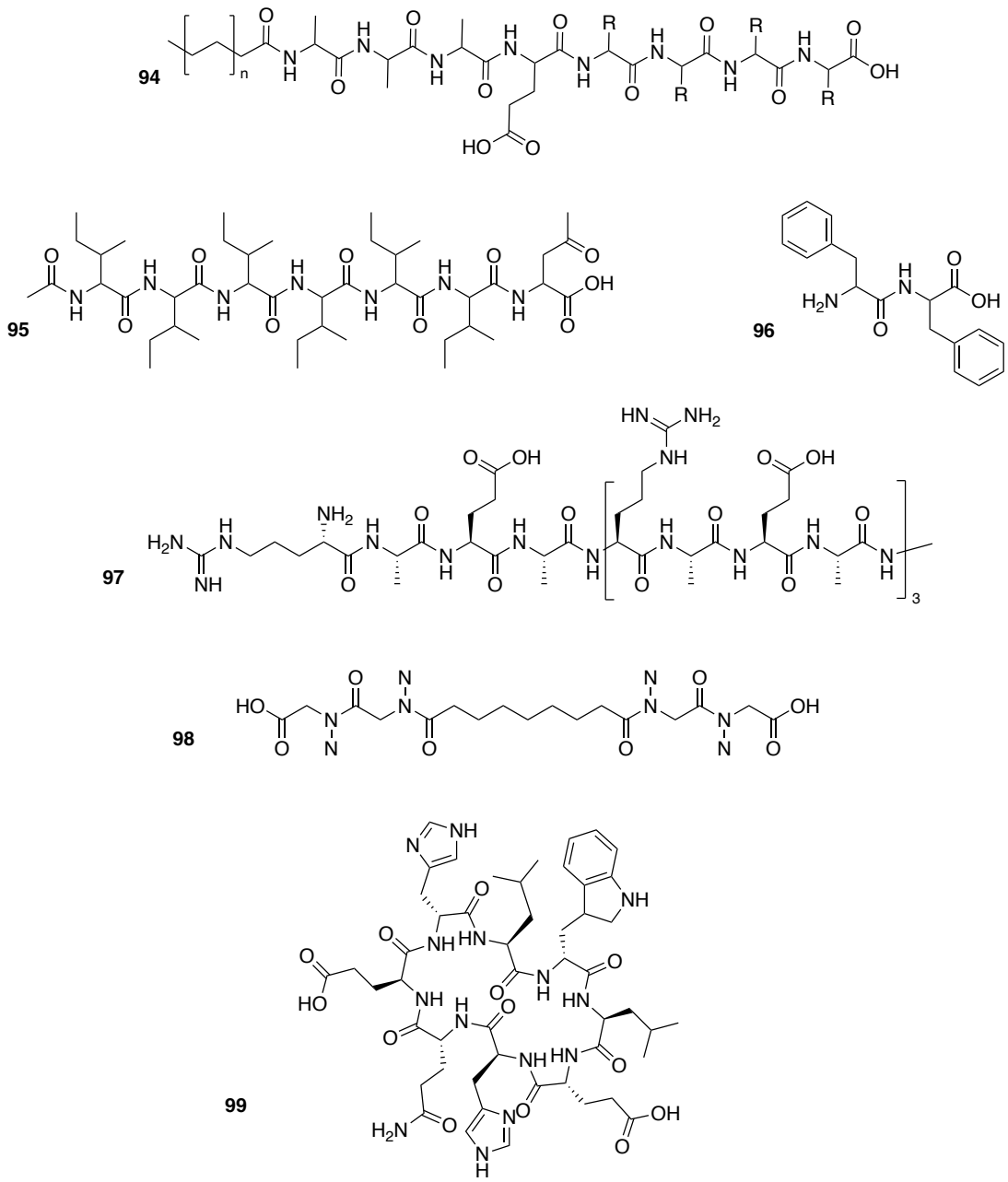

*Figure 5.5. Chemical structures of various self-assembling peptides and peptide-conjugates. (**94**) Representative structure of a peptide amphiphile. (**95**) Surfactant-like linear peptide structure (V6D1). (**96**) LMW peptide structure (diphenylalanine). (**97**) Ionic complementary peptide structure (RADA 16-I). (**98**) Linear structure of the bolaamphiphile peptide conjugate, bis(n-αamido-glycylglycine)-1,7-heptane dicarboxylate. (**99**) Cyclic structure of CPx peptide, (alternating D- and L- amino acids)* [422,430,434].

In particular, peptide amphiphiles (PAs, **94**) are a class of peptides which gained great attention for their ability to self-assemble into high-aspect-ratio nanostructures under specific conditions (i.e., pH, temperature, and ionic strength) [367,410].

Amphiphilic peptides can be divided into three classes: (i) peptides containing both polar and non-polar residues, (ii) hydrophilic peptides attached to short hydrophobic alkyl chains, (iii) peptide-based copolymers [367,410,424,436].

As shown in Figure 5.6, most commonly, PAs contain four key domains: (i) a hydrophobic tail that forms hydrophobic interactions, drive self-assembly, and induce secondary and tertiary conformations (orange), (ii) a peptide sequence capable of forming intermolecular hydrogen bonding (red), (iii) charged amino acids to enhance water solubility (purple), and (iv) a bioactive epitope that can interact with cells or proteins (light blue) [367,410,436].

94

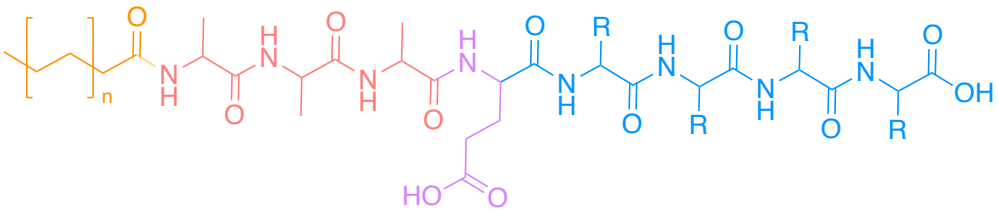

Figure 5.6. Molecular structure of a representative PA with four characteristic regions.

5.1.4.2 Nanostructures formed from self-assembling peptides

Depending on the building block design and the interactions with the aqueous solution, peptides can self-assemble into an array of different structures, including micelles, vesicles, nanofibers, nanotubes, nanotapes, monolayers, bilayers, and ribbons, to reduce unfavourable interactions with the surrounding aqueous environment [412,436,437].

Nanoparticles deriving from self-assembly of peptides can adopt various conformations, from micelles to vesicles [412]. Formation of micelles is common in

the self-assembly process of amphiphilic peptides; micelles can adopt a rod-like or worm-like shape, or a spherical conformation [438,439]. PAs and LMW peptides can also spontaneously form vesicular structures that may find applications as biodegradable drug delivery systems to encapsulate hydrophilic molecules, then released with a pH-dependent release profile [428,440–442].

PAs with an alkyl group at the N-terminus (e.g., **94**) as well as ionic complementary peptides (e.g., **97**) can assemble into nanofibers, with a diameter usually less than 100 nm [412]. Nanotubes present a similar architecture to that of nanofibers but differ for the presence of a hole in the inner side of the capillary. Cyclic peptides are the most commonly used building blocks to form nanotubes [434,435]. However, diphenylalanine-based peptides and lipid-like peptides (i.e., A_6D and A_6K) have been shown to self-assemble into nanotubes [428,443].

Various self-assembling peptides can form nanotapes, which often interact with each other forming double-layers; at high concentrations, peptides arranging into nanotapes can form hydrogels [438,444–446].

5.1.4.3 Mechanism of PAs self-assembly and strategies to control the process

Self-assembly of PAs in water is governed by driving forces deriving from at least three major energy contributions, two favouring self-assembly and one impeding it. Specifically, the hydrophobic interactions of the alkyl group and the hydrogen bonding capacity of the middle peptide segment promote aggregation of PAs, while the electrostatic repulsions between charged amino acids promote dissociation of PAs. The balance between each of these energy contributions results in the final assembly of the PA [367]. Manipulation of the molecular forces involved in the process of self-assembly results in control of the PA architectures formed.

5.1.4.4 Factors that influence peptide self-assembly

Numerous factors contribute to the overall behaviour of a self-assembling peptide in an aqueous environment. Among them, pH, temperature, peptide concentration, and incubation time should be carefully studied to govern the assembly.

5.1.4.4.1 Influence of pH on self-assembly

pH is a key factor in determining the peptide structure, as pH fluctuations result in changes in hydrogen bonds and salt bridges [412,429,447]. Sharp differences in pH-responsive behaviour have been reported by various research groups and some of them have exploited the pH-responsiveness to develop materials capable of reversible pH-triggered morphological changes. An example was reported by Ghosh and collaborators who studied the behaviour of PAs that assembled into nanofibers only when encountering acidic environment (pH 6.6) of the tumour vasculature, while existing as monomers or spherical micelles under normal physiological conditions (pH 7.4) [448]. Laverty and collaborators studied the formation of hydrogels from ultrashort peptides by initially suspending the peptide in H_2O, then dissolving it by addition of NaOH solution to achieve pH~9, and finally forming nanofibers and supramolecular hydrogels when the peptide solution is titrated with 0.5 M HCl to achieve pH 6-7 [429,447]. Moreover, pH can drive transition in peptide nanostructures, as demonstrated by Dehsorkhi and colleagues, who studied the behaviour of a PA with a cationic pentapeptide headgroup. In this study, transitions from micelles, to flat tape-like structures and, finally, twisted right-handed structures were observed at different pH values, from acidic to neutral [446]. Aggeli *et al.* showed the effect of pH on tuning the hierarchical self-assembly of an 11-mer peptide appropriately modified with acidic (i.e., glutamic acid) or basic (i.e., ornithine) residues. In the first case, the Glu-modified analogue can be switched from its nematic to its isotropic fluid state by increasing pH, while, in the second case, the Orn-modified analogue exhibits the inverse behaviour [449]. Another example is represented by the control of the self-assembly and subsequent hydrogelation of an amphiphilic β-hairpin peptide (MAX_1) by substituting lysine residues, eventually tuning the net charge of the peptide. Here, it was demonstrated that folding, self-

assembly, and properties of the resulting hydrogel are dependent not only on net charge of the peptide but also on the exact position of the Lys replacement [450]. Finally, self-assembling behaviour of peptide sequences made up of oppositely charged amino acids is strongly influence by environmental pH: pH that results in alternating positively and negatively charged peptide surface favours nanofibers formation, while pH that results in negatively charged peptide surface impedes the aggregation [451].

5.1.4.4.2 Influence of temperature on self-assembly

Some peptides exist as single molecules at room temperature but, when heated, they organise into nanostructures [412]. An example of temperature-dependent self-assembly behaviour is encountered in elastin-like polypeptides, which form spherical micelles only when heated slightly above body temperature (42 °C) [452]. Another study on self-assembly of short elastin-like peptides, carried out by Cao *et al.,* proved the temperature dependence of the self-assembly behaviour of these peptide class [453]. Moreover, an example of thermal transition of a peptide amphiphile is reported by Miravet and collaborators, who studied the behaviour of C_{16}-KTTKS self-assembly at different temperatures, proving, for the first time, that a PA behaves similarly to a conventional surfactant existing in three forms (monomers, insoluble fibrous aggregates, and micelles) with increasing temperatures [438]. Finally, it has been demonstrated that the diphenylalanine peptide forms nanofibers and organogel when heated at 90 °C and then cooled down to 25 °C, due to the effect of hydrogen bonding increase during the heating-cooling process [454].

5.1.4.4.3 Influence of peptide concentration on self-assembly and determination of critical aggregate concentration

Peptide concentration can influence the self-assembly process. Similarly to surfactants, peptides may exist in monomeric forms and assemble only upon reaching a certain initial absolute entropy, which is a function of the number of molecules and the volume [443,455]. This is mirrored in the critical aggregate concentration (CAC), described as the concentration at which the energetically

favourable release of water molecules around the hydrophobic portions of the peptide becomes more significant than the electrostatic repulsion of the head groups, resulting in peptide self-assembly to form micelles or other ordered architectures [443,456]. Moreover, even above the CAC, self-assembly behaviour may be different at different peptide concentrations. In these regards, Hong and colleagues found that the ionic-complementary peptide EAK16-II forms well-defined nanofibers at low peptide concentrations, while forms dense fibre-networks at high peptide concentrations [457]. In order to determine the CAC, it is possible to monitor the formation of nanostructures through a fluorescence method employing pyrene as a probe [458].

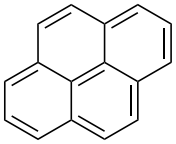

100

Figure 5.7. Pyrene chemical structure.

Pyrene (**100**) is a highly hydrophobic compound presenting very low solubility in water. However, in the presence of micelles and other aggregates, pyrene tends to solubilise into the inner hydrophobic regions of these assemblies [459]. This reflects on the fluorescence spectrum of the compound, which is strongly related to the polarity of the microenvironment. Hence, after excitation at a specific wavelength (~330-340 nm), the relative intensity of the third vibronic band, named I_3 (at 384 nm), increases with increased polarity of the environment (aggregated molecules). On the other hand, the relative intensity of the first vibronic band, named I_1 (at 373 nm), is not affected by increased polarity [460,461]. These features can be used to study the microenvironment of pyrene, eventually detecting formation of aggregates. To monitor changes in the polarity of the environment of aggregating molecules in water, the ratio between the two abovementioned vibronic bands (I_3/I_1), named pyrene 1:3 ratio, is used [459,462]. Above the critical aggregate concentration, the pyrene 1:3 ratio is roughly constant as the probe is incorporated into the hydrophobic region of the aggregates [462]. This fluorescence method has been widely used in literature to determine the critical micelle concentration for

surfactants and the critical aggregation concentration for self-assembling peptides [438,459,462–467]. A simple approach to treat the pyrene 1:3 ratio data has been illustrated by Aguiar and colleagues and is based on the assumption that pyrene 1:3 ratio data are suitably fitted by a decreasing Boltzmann-type sigmoid [462]. CAC can be analytically determined as shown in Figure 5.8, where A_1 and A_2 represent the upper and the lower limits of the sigmoid, and x_0 is the centre of the sigmoid.

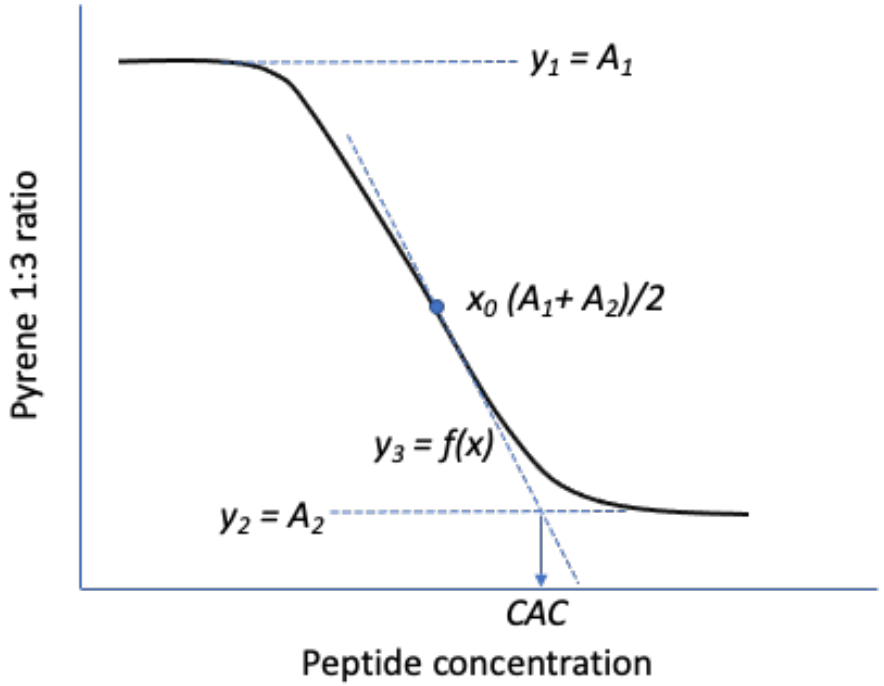

Figure 5.8. Decreasing Boltzmann type sigmoid graph. Characteristic parameters and CAC, deriving from intersection of the straight lines $y_2=A_2$ and $y_3= f(x)$, are shown in the graph [462].

5.1.4.4.4 Influence of incubation time

Incubation times of peptide solutions to allow self-assembly vary from seconds, as described by Wanzke's paper, to hours, as reported in majority of peptide self-assembly procedures, or weeks, as shown by Gordon *et al.* and Xu *et al.* [468–471]. Hence, understanding the time required for the peptide monomers to form organised structures is of pivotal importance.

5.1.4.5 *Peptide self-assembly as efficient system for delivery to the brain*

Aside from small lipophilic molecules presenting a molecular weight lower than 400 Da, with a polar surface area lower than 60-70 Å and a weak hydrogen bond potential, the majority of neuroactive drugs require specific carriers or receptors to cross the BBB [371,387]. Nose-to-brain delivery is a promising approach to directly reach the brain bypassing the obstacle of the BBB. However, various evidence has also suggested that small neuroactive peptides – e.g., enkephalin, luteinising hormone-releasing hormone, arginine-vasopressin – can permeate across the BBB through the so-called saturable peptide transporter systems (PTS) [387]. Finally, Yin and collaborators described the design of non-toxic peptide-based NPs, prepared with the amphiphilic peptide R_3V_6 for the combined delivery of the vascular endothelial growth factor-siRNA and the chemotherapeutic drug bis-chloroethylnitrosourea to treat glioblastoma in humans [472]. From this study, the evidence of the potential of using peptide-based NPs to deliver bioactive peptide to the brain has arisen.

5.1.4.6 *CGRP, P006 derivatives, and their potential to self-assemble*

The calcitonin family of peptides includes calcitonin (CT) itself, CGRP, adrenomedullin (AM), and amylin (AMY), which all share structural homologies [473]. Amylin is a 37-amino acid peptide co-secreted with insulin from pancreatic β-cells. It has been extensively demonstrated that amylin aggregates are responsible for islet-cells damage in type-2 diabetes mellitus [474–477]. The high structural homology of AMY and CGRP led to study the role of CGRP in the aggregation process in the islet cells [477]. Surprisingly, Gray *et al*. discovered that α-CGRP forms smaller oligomers than amylin and that CGRP is much less prone to extensive aggregation compared to amylin. Electron Microscopy imaging demonstrated that, while amylin formed distinct fibrils, CGRP formed neither observable aggregates nor fibrils under the same conditions [477]. However, while the aggregation behaviour of CGRP has been previously studied, this has not been explored for truncated versions of CGRP.

P006, the initial CGRP-R antagonist of this optimisation strategy, presents in its sequence an alternation of hydrophobic and hydrophilic amino acidic residues as well as a charged amino acid (Glu31). Notably, the N-terminally modified analogues present an additional hydrophobic building block at one end of the sequence, resembling the structure of a peptide amphiphile, as shown in Figure 5.9. In addition to this, the C-terminus of P006 and derivatives includes the Phe-Ala-Phe motif, which may have similar behaviour to the Phe-Phe motif, known to form supramolecular structures.

The ability to spontaneously self-assemble into vesicular/micellar nanostructures may confer resistance to proteolysis, supporting the observations in Chapter 4, and may favour the transport of these peptides across the BBB, while being used as drugs themselves [412,442,472].

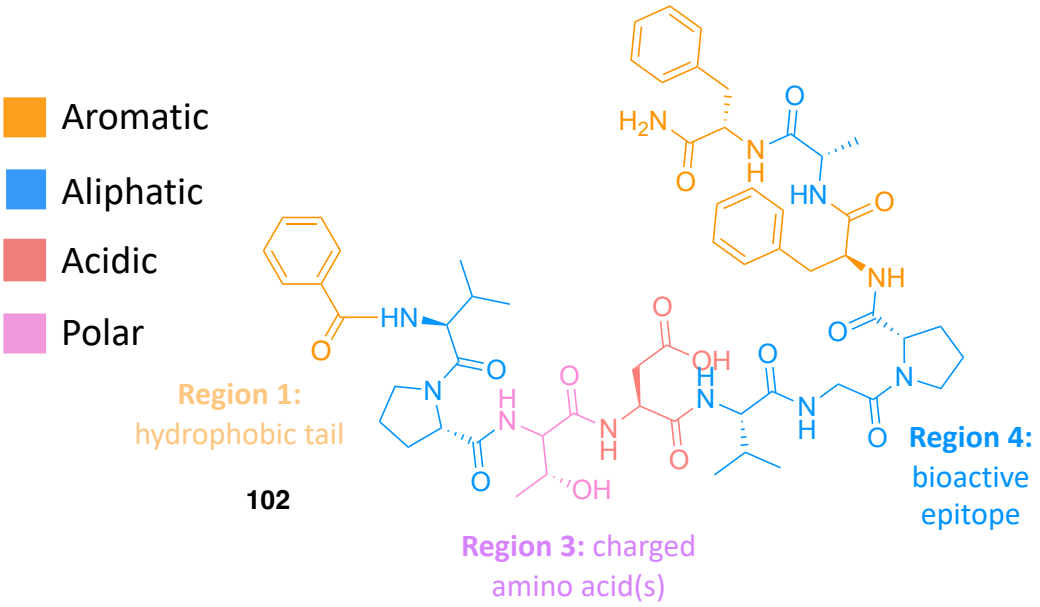

Figure 5.9. N-terminally benzoylated P006 (LJMU027) structure resembling a peptide amphiphile. The benzoyl moiety corresponds to region 1, while glutamic acid corresponds to region 3. The amino acids are colour-coded based on their nature: aromatic in orange, aliphatic in blue, acidic in red, and polar in pink.

5.1.5 *Mucoadhesive dry powders for efficient nose-to-brain delivery of peptides*

Peptide powder formulations require a micron-sized carrier for efficient nose-to-brain delivery. Nano-sized formulations, while being an interesting delivery strategy for peptides, are not directly suitable for nasal delivery, because they do not stick to the nasal mucosa, when inhaled. However, polymeric NPs or NPs deriving from peptide self-assembly can be incorporated into dry powder microparticles with an aerodynamic particle size greater than 10 μm, suitable for deposition primarily in the front part of the nasal cavity [373,376,478]. In fact, efficient filtration mechanisms in the nasal passages can be strategically used for nasal drug delivery, in particular when deposition of drug particles on the olfactory mucosa is necessary for nose-to-brain transport [373].

5.1.5.1 Spray-drying

Among various strategies to prepare mucoadhesive dry powders, spray-drying (SD) is the most efficiently employed [479]. Indeed, SD is widely used to prepare dry powders, granules, or agglomerates from solutions, emulsions, or suspensions containing a mixture of drug and excipients, while controlling particle size, morphology, and powder density [478–480]. In addition to this, SD is cheap and fast, which explains why it has been explored for numerous applications in pharmaceutics research [479].

The spray-drying process (Figure 5.10) begins with a solution of polymer and drug being pumped *via* a feed pump to an atomiser, which creates a fine mist, increasing the surface area of the solution. The mist is spray-dried into a chamber of air (drying chamber) at a temperature above the vaporisation temperature of the solution's solvent. At this point, when the mist comes into contact with hot air, the solvent vaporises, at a rate depending on several parameters (i.e., solution flow rate, temperature of solution, temperature of air, size of the mist droplets and total solid concentration). Both particles formed and vaporised solvent are removed from the chamber and a cyclone separates particles from humid air. Finally, particles are

forced to the bottom of the cyclone separator and the air is ejected to the atmosphere or is directed to a scrubber [480].

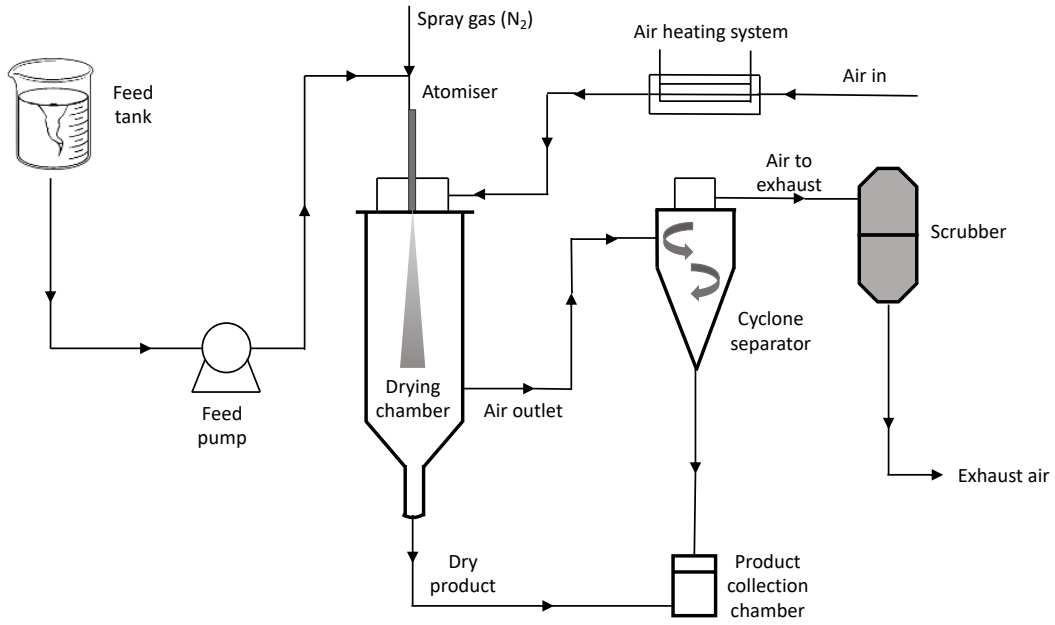

Figure 5.10. Schematic representation of spray-drying process.

For nasal delivery, spray-dried powders should be mucoadhesive so that they stick to the moist surface of the nasal mucosa before being dissolved and cleared. Effective brain uptake is rigorously related to the characteristics of the formulation, which should provide a prolonged residence time and maintain a high local drug concentration to allow drug diffusion [481]. Deposition and absorption of the dry powder for nasal delivery depends on moisture sensitivity, solubility, particle size, particle shape, and flow characteristics [481].

5.1.5.2 Chitosan

Chitosan (CHT, **101**) is a biodegradable natural polymer that, in the past 30 years, has played a key role in the development of novel effective therapeutic delivery systems, due to its biocompatibility, high charge density, nontoxicity, and mucoadhesiveness [482,483]. CHT is a polysaccharide derived from the partial alkaline deacetylation of chitin, which can be found in the exoskeleton of shellfish and crustaceans, and it

comprises randomly distributed deacetylated units (β-(1-4)-linked D-glucosamine) and acetylated units (N-acetyl-D-glucosamine) [481,483,484].

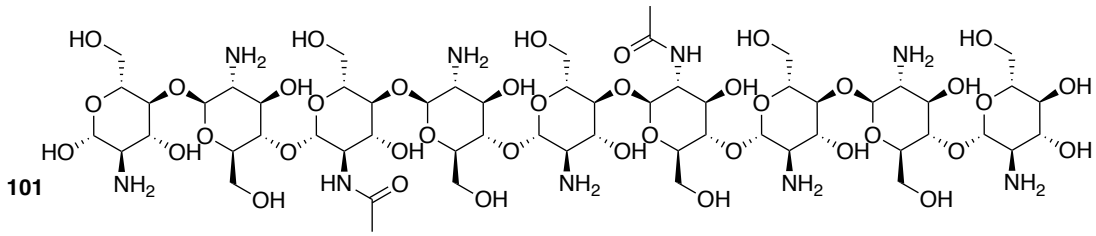

Figure 5.11. Chitosan chemical structure.

CHT is commercially available in a wide range of molecular masses (i.e., low: <50 kDa, medium: 50-150 kDa, and high: >150 kDa), degree of deacetylation (from 40 to 98%), and viscosities [481]. This polymer is soluble only at acidic pH, when the amino groups are protonated (pKa of the NH_3^+ form 6.3), thus increasing the solubility [485].

Due to a short local residence time, possibility to deliver only small volumes (25-200 μL), mucocillary clearance, enzymatic barriers, and high turnover rate of secretion in the nasal cavities, the bioavailability after nasal administration is usually low [482,486]. Thus, nowadays, chitosan is one of the most used excipients for preparation of nasal formulations, due to its intrinsic mucoadhesive, *in situ* gelling, and penetration enhancement properties resulting from its unique cationic character [481,482]. Mucoadhesive properties mainly derive from ionic interactions between the cationic primary amino groups of chitosan and the anionic substructures in the form of sialic acid and sulfonic acid characteristic of the mucus [482]. Moreover, chitosan is able to absorb water from the mucus layer in the nasal cavities, with subsequent swelling and formation of a gel-like layer that prolongs drug local residence time at the site of absorption, eventually increasing its bioavailability [481,483]. Finally, chitosan cationic charges are also responsible for its permeation enhancing effect: as demonstrated by Schipper and colleagues, chitosan interacts with the cell membrane resulting in a structural reorganisation of tight junction-

associated proteins, followed by enhanced transport through the paracellular pathway [487]. In the case of nose-to-brain delivery, the ability of chitosan to reversibly open the tight junctions can be translated into an increase of extracellular transport along olfactory and trigeminal nerve pathways into the CNS [481]. Hence, chitosan has been studied for its potential to carry neuroactive drugs into the brain by bypassing the BBB. In literature, various chitosan formulations – e.g., solutions, suspensions, in situ forming mucoadhesive gels, microemulsions, nanoparticles, and microspheres – have been proposed for nose-to-brain delivery of drugs [481].

In particular, chitosan microspheres obtained by spray drying were demonstrated to be a good carrier for poorly BBB-permeable drugs (e.g., methotrexate), with a higher brain uptake following nasal administration in animal models compared to a solution of methotrexate [488,489]. Though, this is proven by the use of intranasal chitosan formulations in a variety of clinical trials – e.g., the migraine drug Alniditan and the morphine derivative Rylomine, administered as a nasal chitosan solutions [490–492].

Recently, chitosan microspheres as a carrier for nasal delivery have been studied by our research group to prepare a dry powder containing a peptidic CGRP-R antagonist (Pro-34, Phe-35 CGRP 27-37). Here, an optimisation of spray-drying conditions through Design of Experiment led to the preparation of microspheres with a diameter of ~10 μm, required for nose-to-brain delivery [23].

5.1.6 Nano- and microstructure characterisation

Polymeric nano- and micro-particles as well as nanostructures deriving from peptide self-assembly have received enormous attention as promising target-specific drug delivery tools. Hence, finding adequate characterisation techniques with optimum capacity for studying their characteristics is of critical importance. These should involve both qualitative and quantitative techniques. The two main parameters studied in the characterisation of NPs and MPs are size and shape, as these, in turn, can affect the possible applications [493,494].

5.1.6.1 Dynamic Light Scattering

Characterisation of a population of particles can be performed by Dynamic Light Scattering (DLS). In this technique, light is scattered from a laser, which travels through the solution [493]. The size is determined through the measurement of the Brownian motion of the particles in suspension by relating its velocity, described as translational diffusion coefficient, to the size of the particles according to the Stokes-Einstein equation [495]. The diameter of a hypothetical hard sphere that diffuses at the same rate as the particle being measured is referred as hydrodynamic diameter and its value is derived from the time dependence of the scattering intensity measurement [493]. DLS also describes the homogeneity of the size distribution, expressed with a dimensionless value, named polydispersity index (PDI). PDI values between 0.1 and 0.25 indicate that the population of particles is relatively homogeneous, while PDI values greater than 0.5 denote a broad particles distribution [495].

5.1.6.2 Microscopy-based particle characterisation

Advanced imaging techniques, able to produce highly magnified images, are used to study size and shape of particles. The principles behind these techniques vary, depending on the technique used [493]. Electron microscopy (EM) is required for imaging particles in the nanoscale. Essentially, there are two types of EM, transmission electron microscopy (TEM) and scanning electron microscopy (SEM).

In TEM, an electron beam is transmitted through the sample, it interacts with the sample, and the transmitted electrons give rise to a “shadow image” of the sample, in which different areas are shown with different darkness according to their density [493,496]. However, the majority of particles are invisible to EM because the materials they are composed of do not deflect an electron beam adequately. In these cases, heavy-metal staining procedures are applied to the samples before imaging [497]. An exception to this has been reported by Sonzini et al., who described the possibility of introducing fluorinated moieties in peptides as a means to dissipate the beam current, allowing the sample to be imaged without staining [237].

In SEM analysis, a highly concentrated electron beam shot from an electron gun is directed toward the sample and, when it strikes the sample surface, it interacts with it. Metal materials already conduct electricity when bombarded with electrons, while nonmetal specimens need to be coated with a thin conducting material layer (e.g., gold) to be imaged [493].

5.2 Aims and Objectives

The aim of the research presented in this chapter was to formulate the CGRP-R peptide antagonists for future development of a nasal delivery system to the brain. This would be achieved either by first formulating nanoparticles and then encapsulating the nanoparticles into a dry powder, mucoadhesive chitosan microparticle carrier or by directly encapsulating peptide within chitosan microparticles. Two possible NPs formulations were explored; i) the development of peptide-containing polymeric nanoparticles; ii) peptide self-assembly into nanoparticles.

5.3 Materials and Methods

5.3.1 Materials

PLGA (Resomer RG 502 H, MW 7,000-17,000), Poly(vinyl alcohol) (PVA, MW 13,000-23,000), low molecular weight chitosan [CAS number 9012-76-4], pyrene puriss. for fluorescence (CAS 129-00-0), acetone, and trifluoroacetic acid (TFA) were purchased from Sigma Aldrich. Formvar/Carbon copper grids (400 mesh) for TEM and Aluminium pin stubs (13 mm) for SEM were purchased from Agar Scientific. HPLC-grade acetonitrile, methanol, and glacial acetic acid were purchased from Fisher Scientific.

5.3.2 High-performance liquid chromatography

Peptide solutions were analysed by RP-HPLC using the previously optimised method (see Section 4.4.2.3 in Chapter 4). Briefly, an Agilent 1100 system equipped with a Phenomenex Aeris 3.6 μm peptide XB-C18 LC Column (100 Å 150 x 4.6 mm), using a

linear gradient from 80% solution A (high purity water, 0.05% TFA) to 60% solution B (MeCN, 0.05% TFA) over 10 minutes was employed. A flow rate of 1 mL/min was used, the absorbance was detected at 215 nm and the analysis was performed at 65 °C.

5.3.3 Peptide centrifugation and ultracentrifugation feasibility

A solution of peptide (P006) in water (0.1 mg/mL) was tested to assess whether centrifuge and ultracentrifugation precipitated polymers while retaining the peptide in solution. Variable conditions – 30 and 60 min at 13,200 rpm and room temperature for centrifugation, and 30 and 60 min at 35,000 rpm and 20 °C for ultracentrifugation – were investigated. The resulting supernatants were analysed by RP-HPLC, as described in section 5.3.2. Each test was carried out in triplicate.

5.3.4 PLGA NPs optimisation (DoE) and peptide loading

5.3.4.1 Blank and loaded NPs preparation

For blank PLGA NP optimisation, a L9 3^3 Taguchi orthogonal array Design (TD) was constructed using Minitab software. Here, a nanoprecipitation-solvent evaporation method similar to that described by Chaudhary *et al.* was used [498]. In detail, 3 variables – quantity of PLGA, % of aqueous PVA, ratio between organic phase (OP) and aqueous phase (AP) –at 3 levels (low, medium, high) were studied (Table 5.2).

Table 5.2. L9 3^3 TD: independent variables under evaluation.

Factors	Used Levels		
	Low (1)	**Medium (2)**	**High (3)**
Quantity of PLGA (mg) (A)	10	20	30
Stabiliser concentration (% *w*/*v*) (B)	1	2.5	5
OP:AP ratio (C)	1:4	1:7	1:10

Optimisation of the particle size was performed using the Taguchi "smaller is better" criterion, considering both the average size of the NPs and the polydispersity index (PDI). Responses were analysed in terms of signal-to-noise ratio (SN ratio) of each trial and ANOVA statistical analysis was performed to determine the significance of each factor. The best optimal level for each factor obtained from TD analysis was used to prepare an optimised formulation for peptide loading. In detail, the polymer (10, 20 or 30 mg) and, in the case of loaded formulation, the peptide (peptide stock solution 10 mg/mL, 200 μL in total) were dissolved in acetone (5 mL) to form the organic phase (OP) and added dropwise via a syringe and a needle into different volumes (20 mL for 1:4 ratio, 35 mL for 1:7 ratio, or 50 mL for 1:10 ratio) of the aqueous phase (AP) containing 1, 2.5 or 5% of stabiliser (i.e., PVA), while stirring at 200 rpm. The nanoparticle suspension was kept under continuous stirring at 500 rpm for 3 h to allow for the complete evaporation of organic solvent. NPs were then collected by ultracentrifugation (Beckman Coulter Optima XPN Ultracentrifuge, 35,000 rpm, 20°C, 20 min). The pellet was washed with deionised water to remove unencapsulated peptide from the surface of NPs, then collected again by ultracentrifugation. Finally, supernatant was discarded, and NPs pellet was resuspended in water for further analysis. The experiment was performed in triplicate.

5.3.4.2 Dynamic Light Scattering and Zeta Potential

Hydrodynamic diameter and polydispersity index (PDI) of PLGA NPs were determined by DLS, using a Zetasizer instrument (Nano ZS, Malvern Ltd., United Kingdom). The zeta potential was measured by laser Doppler electrophoresis, using the same device. The analysis was performed at room temperature and data was reported as the mean and standard deviation obtained from 3 measurements. Samples were analysed directly after solvent evaporation.

5.3.4.3 Drug loading and encapsulation efficiency into PLGA NPs

The loading efficiency of the peptide in PLGA nanoparticles was determined as described below. The amount of peptide entrapped into the nanoparticles was

calculated as the difference between the total amount of peptide used to prepare the formulation and the amount of peptide detected in the supernatant after ultracentrifugation. The supernatant was directly injected into a HPLC system employing a method described in section 5.3.2. The concentration of peptide in the supernatant was obtained by measuring the area under the peak and relating it to a calibration curve of known peptide concentrations, ranging from 5 to 1000 μg/mL in H_2O (R^2>0.999).

Encapsulation efficiency (EE%) was calculated with the following equation:

$$EE\% = 100 - \frac{\text{concentration of peptide in supernatant} * 100}{\text{total concentration of peptide in formulation}}$$

Equation 5.1

5.3.4.4 In vitro drug release study from polymeric NPs

Blank and loaded NP pellets were resuspended into 1 mL of phosphate buffered saline (PBS) and mixed in a sample mixer (HulaMixer, orbital mixing at 20 rpm) at 37 °C for 72 h. Polymeric NPs were then pelleted by ultracentrifugation (Beckman Coulter Optima XPN Ultracentrifuge, 35,000 rpm, 20°C, 20 min) and the supernatant was analysed by RP-HPLC, with the analytical method described in section 5.3.2. The presence of peptide in the supernatant indicated release from NPs formulation. The study was carried out in triplicate.

5.3.5 Preparation of nanostructures from peptide self-assembly

5.3.5.1 Nanostructure optimisation via design of experiments

In the Plackett-Burman Design of experiment (12 runs, 1 middle point), five parameters were studied at two levels: concentration of peptide, pH, sonication time, incubation time, and incubation temperature (Table 4.1). The endpoint of the design was evaluated as the average size of the aggregates, where possible.

Table 5.3. Factors under evaluation in the Plackett-Burman Design.

Factor under evaluation	Level 1	Level 2
Concentration of peptide (mM)	0.01	2
pH	3	11
Sonication time (min)	0	60
Incubation time (h)	3	11
Incubation temperature (°C)	5	37

5.3.5.2 Dynamic Light Scattering (DLS)

Z-average and polydispersity index (PDI) of peptide aggregates were determined at room temperature by dynamic light scattering, using a Zetasizer instrument (Nano ZS, Malvern Ltd., United Kingdom).

5.3.5.3 Critical aggregate concentration (CAC) determination

Firstly, pyrene solution (10 mM, in MeOH) absorbance in the UV-Vis spectrum (range 200-600 nm) was analysed on a Nicolet Evolution 300 BB from Thermo Electron Corp. spectrophotometer equipped with Vision Pro software, using a 10 mm path length quartz cuvette to determine the excitation wavelength to use for further analysis.

For CAC determination a fluorescence method, similar to that employed by Miravet *et al*., was used [438]. Briefly, a dried film of pyrene was obtained by adding 100 μL of a MeOH solution of pyrene (0.25 mM) to a black-walled, transparent flat bottom 96-well plate, left evaporating overnight in the dark at room temperature. The pyrene dried film was then resuspended in aqueous peptide solutions of various concentrations (from 0.0005 to 1 mM or from 0.5 to 2 mM, 100 μL/well). The plate was covered with foil and incubated for 24 h at 37 °C on a Stuart microplate shaker (at 50 rpm). Finally, fluorescence emission spectra were recorded at 37 °C using a Tecan Spark 10M plate reader, using an excitation wavelength of 334 nm, and emission range from 360 to 400 nm (step size 1 nm). The ratio I_3/I_1 was plotted against concentration and the position of the *x* value corresponding to a significant and continuous decrease in ratio I_3/I_1 was taken as the CAC.

5.3.5.4 Preparation of optimised peptide nanostructures

A known amount of freeze-dried peptide powder was dissolved in DMSO, then deionised H_2O was added to reach a final concentration of 0.1 or 2 mM, with a final concentration of DMSO of ~5%. Samples were mixed for 5 min, then incubated at room temperature for 24 h or 7 days.

5.3.5.5 Transmission Electron Microscopy (TEM)

For P006 and LJMU027, data was collected on a FEI F20 microscope operating at 200 kV. Images were recorded on a Gatan Rio 3K CMOS detector with a nominal magnification of 19 kx – 50 kx, corresponding to a pixel size of 0.32 to 0.13 nm/pixel. A typical image dose was ~ 50 electrons/Å**2. For sample preparation, 10 μL of a peptide solution (prepared as described in section 5.3.5.4) was mixed with 10 μL of negative staining reagent (1% phosphotungstic acid solution). Then, 10 μL of this mixture was placed on the surface of a copper grid covered by perforated Formvar/Carbon film (400 mesh). The excess solution was removed by capillarity with a filter paper and, after drying in air for at least 15 min, the grid was analysed [419]. Images were analysed with ImageJ for particle measurements.

For fluorinated peptides (i.e., LJMU017 and LJMU018), TEM micrographs were obtained from a FEI Morgagni 268 microscope, operating at 100 kV and under high vacuum, with a magnification up to 140 kx. Images were recorded using iTEM FEI imaging software via a megaview II digital camera. Samples were prepared as described in section 5.3.5.4 at concentrations 0.5 mM and incubated for 24 h prior analysis. Grids stained with phosphotungstic acid were prepared as described above. Stain-free grids were prepared by placing 10 μL of the sample on the surface of a copper grid covered by perforated Formvar/Carbon film (400 mesh). The excess solution was removed by capillarity with a filter paper and the grid was left drying for at least 15 min before analysis.

5.3.6 Chitosan MPs formulation

5.3.6.1 Blank and loaded MPs

Blank and peptide-containing microcarriers were prepared by spray-drying low molecular weight (LWM) chitosan (2% *w/v*) and P006 (1% *w/w*, where appropriate), from a solution of 0.5% acetic acid (25 mL). A Büchi B-290 Mini spray dryer (Büchi Labortechnik AG, Postfach, Switzerland) equipped with a nozzle atomiser with a nozzle orifice diameter of 2.0 mm was used. Nitrogen was used as the atomising gas and dry particles were separated from the airstream by centrifugal forces using a high-performance cyclone (Büchi Labortechnik AG). Optimal operating parameters were previously determined as; constant spray gas flow (60) and feed flow rate (15% of pump capacity, just under 5 mL/min), aspirator capacity 95%, and inlet temperature 165 °C [23]. After spray-drying, the microspheres powder was harvested from the collector and kept at room temperature under vacuum. The experiments were carried out in triplicate for both blank and loaded MPs.

5.3.6.2 Release from chitosan MPs

MPs (10 mg) were suspended in buffer (1 mL) in a 1.5 mL centrifuge tube and mixed at 20 rpm and 37 °C, utilising the unloaded MPs as blanks [488]. Three samples for each replicate (three replicates in total) were prepared and, at each time point (5, 15, 30, 60 min, 4, 8 and 24 h), one sample was centrifuged at 13,200 rpm for 30 min (Eppendorf Centrifuge 5415 D). The supernatant solution was analysed by RP-HPLC, with analytical method described in section 5.3.2.

5.3.6.3 Scanning Electron Microscopy (SEM)

Microparticle morphology and diameter were studied through SEM analysis. A thin layer of powder was placed on top of an aluminium pin stub and coated with gold prior to analysis and an FEI Inspect S model with accelerating voltage of 0.1-30 kv range with a nominal magnification up to 100 kx was used. The average diameter of the particles was calculated with ImageJ 1.51 software, measuring 100 particles for each sample in a single image. Imaging and measurements for each sample were performed in triplicate.

5.3.6.4 Thermogravimetric Analysis (TGA)

Moisture content of blank chitosan microcarriers was determined by thermogravimetric analysis on a TGA Q5000 (TA Instruments, New Castle, DE, SAD). The spray-dried powder (10 mg) was loaded on a platinum TGA pan suspended from a microbalance and heated from 25 °C to 250 °C at 10 °C per min [479]. The water loss between 25 and 100 °C was analysed. The experiment was repeat three times.

5.3.7 Data Analysis and Statistical analysis

Data were visualised with Excel and GraphPad Prism (version 9.3.1). IBM SPSS Statistics Software (version 27) was used for statistical analysis of TD used for NPs optimisation.

5.4 Results and Discussion

5.4.1 Peptide centrifugation and ultracentrifugation suitability test

P006 was taken as a model peptide to assess whether the centrifugation and ultracentrifugation procedures would affect the supernatant peptide concentration. After centrifugation at room temperature, the peptide solution was analysed and compared to a control solution, which was not subjected to centrifugation. In both cases, after 30 and 60 min, the recovery of peptide was ~ 100%. On the other hand, when the solution of P006 was subject to 30- or 60-min ultracentrifugation, the recovery was 99.1%, indicating that <1% (within the standard error) of peptide was pelleted, confirming in any case the suitability of the techniques to separate polymer (i.e., PLGA or chitosan) from the peptide.

5.4.2 PLGA NPs optimisation (DoE) and peptide formulation

5.4.2.1 Blank PLGA NPs optimisation

For the preparation of polymeric NPs, PLGA was selected due to its biocompatibility, biodegradability, and sustained released properties [390,499]. Moreover, numerous studies have demonstrated the successful encapsulation of peptides, lipopeptides, and proteins in PLGA NPs [390]. Among the methods for preparation of PLGA NPs,

the most common are single emulsion, double emulsion, and nanoprecipitation techniques [390,402]. In this study, the nanoprecipitation-solvent evaporation method was chosen as an alternative to single and double emulsion procedures as preparation of P006-loaded PLGA NPs *via* double emulsion had already been explored by our research group. Previously, numerous variables were evaluated through design of experiments to increase the encapsulation efficiency – e.g., quantity of polymer, sonication time, volume of organic and aqueous phases, type and quantity of stabiliser, quantity of peptide, addition of salts to prevent diffusion of peptide in the external aqueous phase – however, the encapsulation efficiency was not significantly different from 0 and the results were highly variable, probably due to inefficient analytical methodologies for peptide detection and quantification (Capel *et al*., unpublished data).

In a comparative study carried out by Chen and collaborators, the nanoprecipitation method was selected as the most efficient method for encapsulation of the hydrophilic peptide dalargin (sequence: YaGFLR) [398]. Moreover, Bisht *et al*. chose the nanoprecipitation technique for encapsulation of a Connexin43 mimetic peptide (sequence: VDCFLSRPTEKT), although encapsulation efficiency and/or drug loading were not reported [397]. These peptides present structures and physicochemical properties similar to that of our 10-mer peptide P006 (sequence: VPTDVGPFAF), thus it was hypothesised that a similar approach could laed to successful encapsulation of the peptide.

Blank PLGA NP optimisation was carried out *via* TD (L9 3^3 array, Table 5.4), to study three parameters at three different levels, while reducing the total number of experiments performed.

Table 5.4. TD, run number and combination of independent variables. The experiments were performed in triplicates.

No. Exp. (n=3)	(A) PLGA (mg)	(B) PVA in AP (%)	(C) OP:AP ratio
1	10	1.0	1:4
2	10	2.5	1:7
3	10	5.0	1:10
4	20	1.0	1:7
5	20	2.5	1:10
6	20	5.0	1:4
7	30	1.0	1:10
8	30	2.5	1:4
9	30	5.0	1:7

NPs size ranged from 121.27 ± 10.21 to 578.00 ± 30.62 nm, while PDI values fluctuated between 0.07 ± 0.02 and 0.62 ± 0.09. Results were analysed by Minitab 19 Statistical Software and the main effect plot for signal-to-noise (SN) ratio is shown in Figure 5.12. According to the ranking calculated by the software, the parameter that had the highest influence on the NPs size was the amount of stabiliser in the aqueous phase: an increase in % of PVA over 1% significantly increased the size of the NPs, probably due to an excess aqueous phase viscosity [499]. Moreover, as previously observed, an increase in the polymer concentration positively affected the average particle size, while an increase in volume of the aqueous phase from 20 to 50 mL resulted in higher particle dispersion with consequent less interaction between them, yielding smaller size NPs [397].

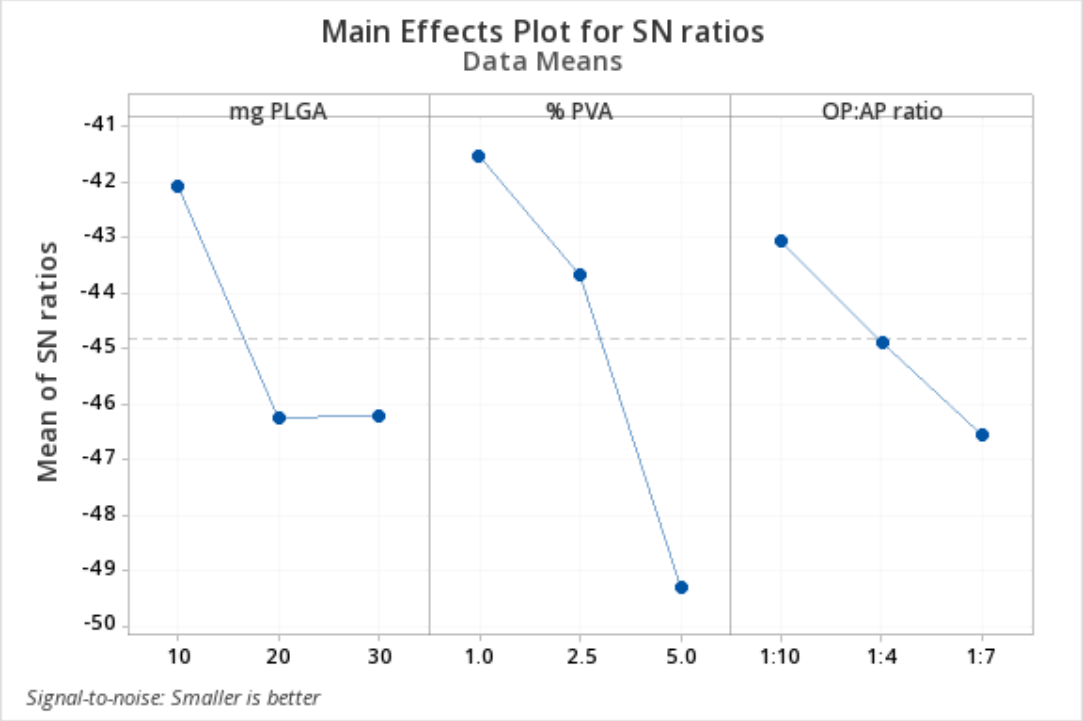

Figure 5.12. PLGA NPs optimisation via TD. Size and PDI main effects plot for signal-to-noise ratio (SN ratio). Ranking: mg PLGA (2), % PVA (1), OP:AP ratio (3).

Multiple linear regression analysis for particle size showed that the amount of PLGA (A), the % of PVA in the AP (B), and the OP:AP ratio (C) affected NPs size with statistical significance, as shown in Table 5.5. The R^2 value for the regression analysis resulted to be 0.862, thus the 86.2% of the variability of the dependent variable (output) is well represented by the independent factors of the model. Hence, to predict the NPs size, it is possible to solve the equation resulted from the regression analysis, using specific coefficients for each independent factor, as follow (Equation 5.2):

$$NPs\ size\ = -\ 10.413\ +\ 7.266 * (A)\ +\ 75.537 * (B) - 41.694 * (C)$$

Equation 5.2

Table 5.5. Linear regression analysis of NPs size versus NPs preparation variables. t value measures the ratio between the coefficient and its standard error; p value is a probability that measures the evidence against the null hypothesis (the lower the p value, the stronger the evidence against the null hypothesis).

	Particle size (nm)			
Predictor	Coefficients	Coefficients St. Err.	t	p
(Constant)	-10.413	47.291	- 0.220	0.828
mg PLGA	7.266	1.450	5.010	< 0.001 *
% PVA in AP	75.537	7.177	10.525	< 0.001 *
OP:AP ratio	- 41.694	14.503	- 2.875	0.009 *

Similarly, the multiple linear regression analysis performed for PDI values revealed that the amount of PLGA (A), the % of PVA in the AP (B), and the OP:AP ratio (C) affected the PDI with statistical significance, as reported in Table 5.6. The R^2 value was 0.808, meaning that 80.8% of the variability of the dependent variable (PDI, in this case) is explained by the independent factors of the model. Therefore, it is possible to predict the PDI value of the NPs by applying Equation 5.3:

$$PDI = 0.263 - 0.015 * (A) + 0.031 * (B) + 0.081 * (C)$$

Equation 5.3

Table 5.6. Linear regression analysis of PDI versus NPs preparation variables. t value measures the ratio between the coefficient and its standard error; p value is a probability that measures the evidence against the null hypothesis (the lower the p value, the stronger the evidence against the null hypothesis).

	PDI			
Predictor	Coefficients	Coefficients St. Err.	t	p
(Constant)	0.263	0.061	4.337	< 0.001 *
mg PLGA	- 0.015	0.002	- 8.133	< 0.001 *
% PVA in AP	0.031	0.009	3.388	0.003 *
OP:AP ratio	0.081	0.019	4.366	< 0.001 *

Table 5.7 shows F values, meaning the test statistic to define whether the term is associated with the response, obtained from ANOVA test performed on both the outcome of the TD (NPs size and PDI).

Table 5.7. ANOVA table of fitted model for PLGA NPs size and PDI. F values were obtained from ANOVA statistical analysis by dividing two mean squares to determine the ratio of explained variance to unexplained variance.

	Source	Degree of Freedom	Sum of Squares	Mean square	F	p
Particle size	Regression	3	545698.804	181899.601	48.044	< 0.001 *
	Residual error	23	87080.581	3786.112		
	Total	26	632779.385			
PDI	Regression	3	0.600	0.200	32.225	< 0.001 *
	Residual error	23	0.143	0.006		
	Total	26	0.743			

According to TD analysis using the 'smaller-is-better' criterion for size and PDI, the best formulation should be manufactured with the following parameters: 10 mg of PLGA, 1% PVA in the AP, OP:AP 1:10. The optimum formulation predicted from Minitab Software was manufactured in triplicate, yielding a size of 103.35 $\pm$ 1.77 nm and a PDI of 0.26 $\pm$ 0.01, confirming the success of the optimisation strategy employed. Nanoparticles with a diameter of around 100 nm or lower are thought to access the brain *via* the intra-axonal route because of their diameters being lower of that of the axons in the *filia olfactoria* [500].

Zeta potential analysis of the blank formulations showed that for all the combinations of parameters under evaluation, the charge of the NPs was almost neutral, oscillating between -0.10 and +1.29 mV. Hence, no significant effect was encountered for the different combinations of TD.

5.4.2.2 *Preparation of loaded PLGA NPs*

Following parameter optimisation, preparation of NPs loaded with P006 or LJMU027 was attempted. Here, the peptide was added to the OP containing PLGA and this solution was added dropwise to the AP. After evaporation of acetone, NP size was measured. Putative loaded NPs, both with P006 and LJMU027, showed an increase in average diameter (Figure 5.13), which may be attributed to the presence of peptide within the NPs or to increased particle aggregation when the peptide is present in solution.

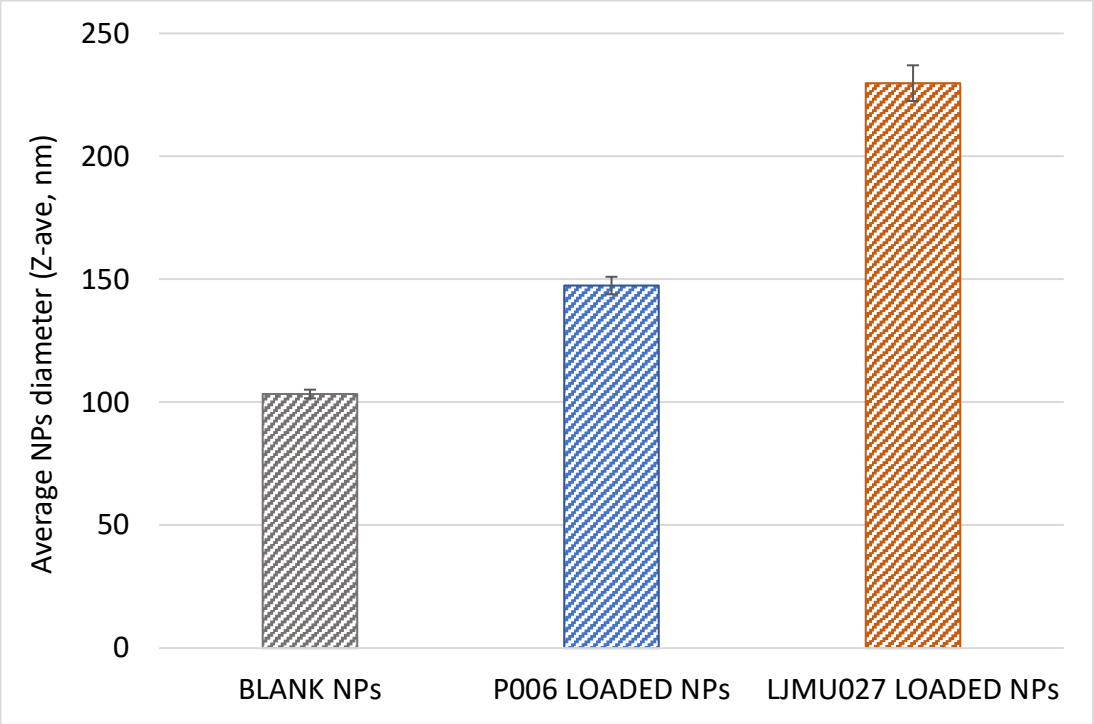

Figure 5.13. Blank and loaded PLGA NPs average size.

Calibration curves for determination of concentrations of P006 and LJMU027 were obtained by preparing serial dilutions of peptide from a stock solution in water and analysing them by HPLC. The area under the curve of the peak of interest was correlated to the concentration of peptide. Calibration curves were accepted only if $R^2 > 0.999$.

An indirect method, wherein the total amount of encapsulated drug was estimated by the difference between the drug in the supernatant after ultracentrifugation and the total drug initially added to the formulation, was used. The data obtained showed no encapsulation for either P006 or LJMU027, with the total amount of peptide in the supernatant comparable to that initially added to the acetone. Even though literature precedent reported examples of encapsulation of hydrophilic peptides within PLGA NPs through nanoprecipitation [397,398], this technique suffers the drawback of poor incorporation of water-soluble drugs, as reported by Govender *et al.* [396]. Hence, we speculated that the high water-solubility of P006 may impede its encapsulation. However, LJMU027 was expected to be encapsulated to some extent, due to its more hydrophobic nature, but surprisingly, these results indicated no encapsulation was achieved.

5.4.2.3 Release of peptide from polymeric NPs

To confirm the data obtained from indirect entrapment efficiency determination, NP pellets were resuspended in PBS and incubated for 72 h while mixing at 20 rpm. This study indicated that no peptide was released from the formulation after 72 h, corroborating the evidence that no peptide was loaded within NPs, and hence concluding that the nanoprecipitation technique is not appropriate for encapsulating either P006 or LJMU027.

An alternative approach to prepare NPs using peptide self-assembly to manufacture peptide-only nanostructures was explored. The increased proteolytic stability of P006 benzoylated derivatives may circumvent the need of a polymeric matrix to protect the peptide. Stable, self-assembled peptide structures could be delivered parentally or be loaded into chitosan microcarriers for nasal delivery.

5.4.3 Self-assembling peptides

P006 and its derivatives resemble the structure of amphiphile peptides with the potential to self-assemble. For this reason, a study on the self-assembly behaviour of these peptides was carried out with the aim of producing nano-sized particles

composed of peptide only in the form of vesicles or micelles. Characterisation of peptide nanostructures was performed through DLS, for particle size distribution assessment, TEM for particle imaging, and the pyrene test for critical aggregation concentration. Among the 19 peptides synthesised, P006, LJMU027, LJMU017, and LJMU018 were selected for this study. Briefly, P006 was chosen as the parent peptide of the library, LJMU027, was selected to study the effect of the benzoyl moiety and LJMU017 and LJMU018 were chosen to investigate the effect of fluorine addition on the aggregation and TEM imaging.

5.4.3.1 Design of Experiment for peptide self-assembly optimisation

To study the influence of various parameters on the self-assembly behaviour of P006, a Plackett-Burman Design (PBD) was constructed on Minitab Software (Table 5.8). As previously mentioned, PBD is a preliminary screening study useful to identify the independent variables that influence the most the outcome of the study, set to be the average size of the particles in solution measured by DLS.

Table 5.8. PBD combinations of independent variables, constructed using Minitab software.

Std Order	Run Order	Concentration of P006 (mM)	pH	Sonication time (min)	Time for assembly (h)	Temp. (°C)
3	1	0.01	11	60	1	37
12	2	0.01	3	0	1	5
5	3	2	11	0	48	37
8	4	0.01	3	60	48	37
4	5	2	3	60	48	5
2	6	2	11	0	48	5
9	7	0.01	3	0	48	37
7	8	0.01	11	60	48	5
6	9	2	11	60	1	37
11	10	0.01	11	0	1	5
10	11	2	3	0	1	37
1	12	2	3	60	1	5
13	13	1.005	7	30	24.5	21

As shown from the Pareto Chart in Figure 5.14, none of the factors under evaluation had a statistically significant effect (none of the representative bars in the chart crosses the reference line). However, the factor that had the greatest influence on the outcome was the concentration of peptide in solution, followed by temperature of incubation, sonication time, time for assembly, and, finally, pH. Hence, the main information gained from this study was that the concentration of peptide was the most influential factor although not significantly.

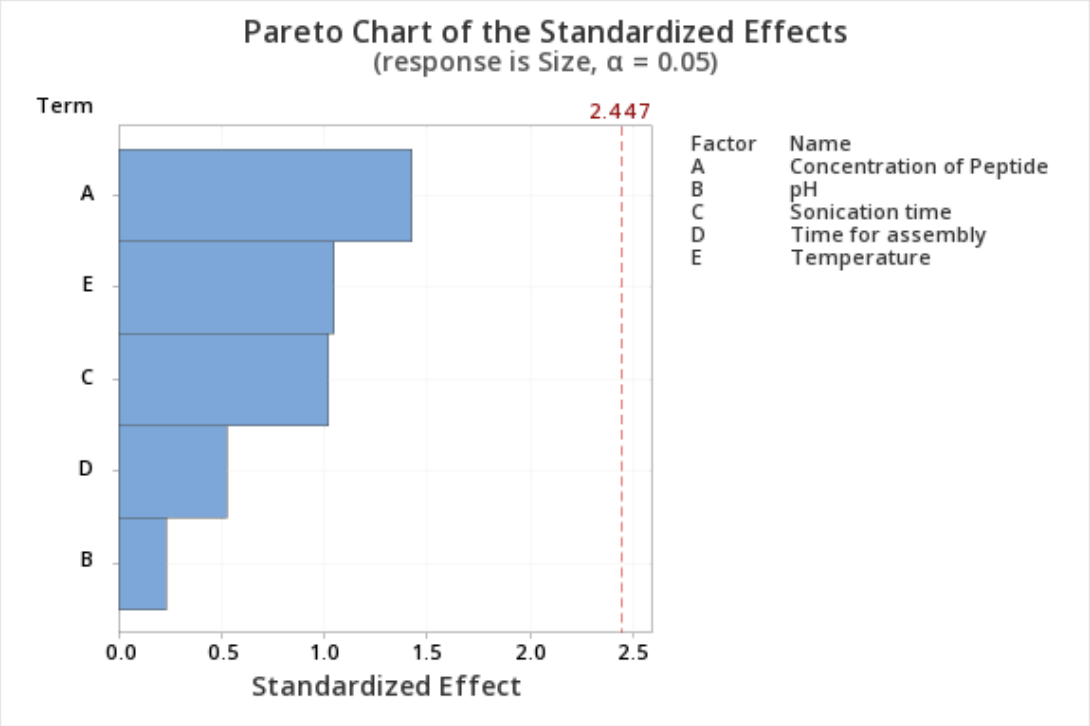

Figure 5.14. Standardised main effect Pareto chart derived from the Plackett-Burman Design experiment analysis. The vertical red line in the chart is the reference line that defines the 95% confidence level; bars that cross the reference line have a statistically significant effect.

At this point, samples from PBD were further studied by TEM imaging. By analysing the PBD samples, it emerged that, for P006 solution at concentrations as low as 0.01 mM there was an absence of nanostructures at any given condition of pH, temperature, sonication, and incubation time. On the other hand, for P006 solutions at high concentrations (i.e., 2 mM), nanostructures were visualised by TEM for any

combination of parameters. An example of the presence of micellar structures is shown in Figure 5.15. This confirmed the hypothesis that P006 is a peptide capable of self-assembly and 0.01 mM was probably below the CAC of P006.

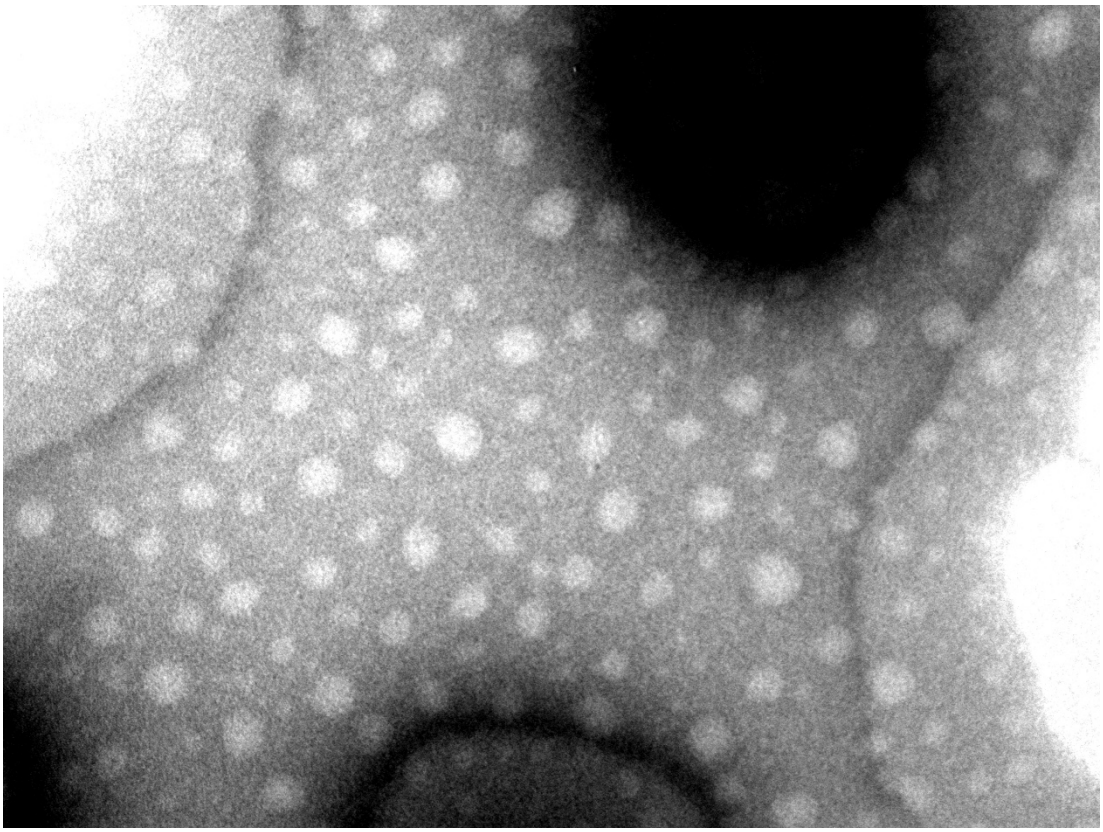

Figure 5.15. TEM micrograph taken from sample 6 from PBD. Micelles can be visualised on a grey background from the negative staining of the sample. Black spots are due to high concentrations of negative stain in some regions of the copper grid.

However, the PBD did not produce optimal conditions for assembly due to the fact that only results obtained from the high concentrations samples were reliable, while the combination of independent variables associated with low concentrations were not reliable, due to absence of nanostructures, as proven by TEM imaging.

5.4.3.2 Pyrene test for critical aggregation concentration determination

The critical aggregation concentration (CAC) of P006, LJMU027, LJMU017, and LJMU018 in water at 37 °C was determined *via* pyrene fluorescence spectroscopy. As previously mentioned, the fluorescence of pyrene is sensitive to the hydrophobicity

of the environment and, in this study, the concentration dependence of the ratio between the first and the third vibronic bands was analysed [438,460,461,501]. To empirically determine the excitation wavelength to use, a pyrene UV spectrum was recorded in pure MeOH (10 mM). The UV-Vis absorbance spectrum in Figure 5.16 shows the characteristic pyrene peak at 334 nm (λmax), confirming the adequacy of the previously determined optimal excitation wavelength (i.e., 335 nm) [462,502].

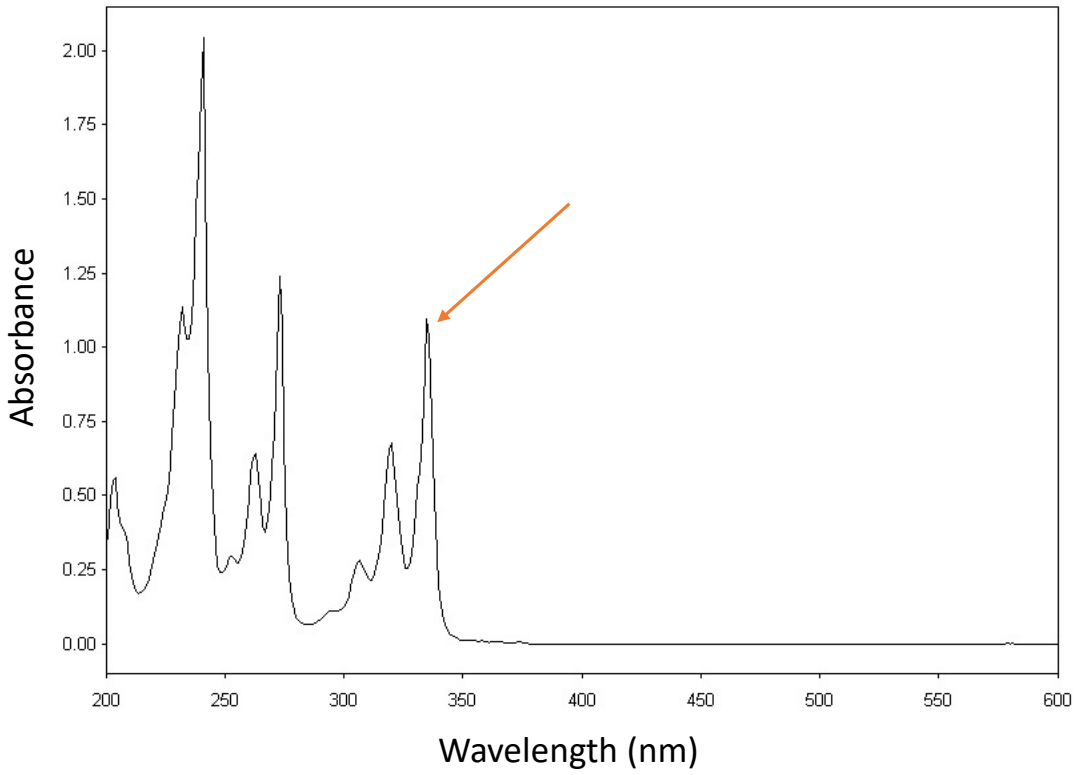

Figure 5.16. UV-Visible spectrum of pyrene (10 mM) in MeOH. Peak at 334 nm is indicated with orange arrow.

Similarly to the determination of the critical micelle concentration (CMC) for surfactants (Figure 5.17), peptide concentrations below the CAC result in a polar environment indicative of a high peak 1 to peak 3 ratio; as the peptide concentrations approach the CAC, the pyrene 1:3 ratio starts rapidly decreasing to reach a new lower constant value [503].

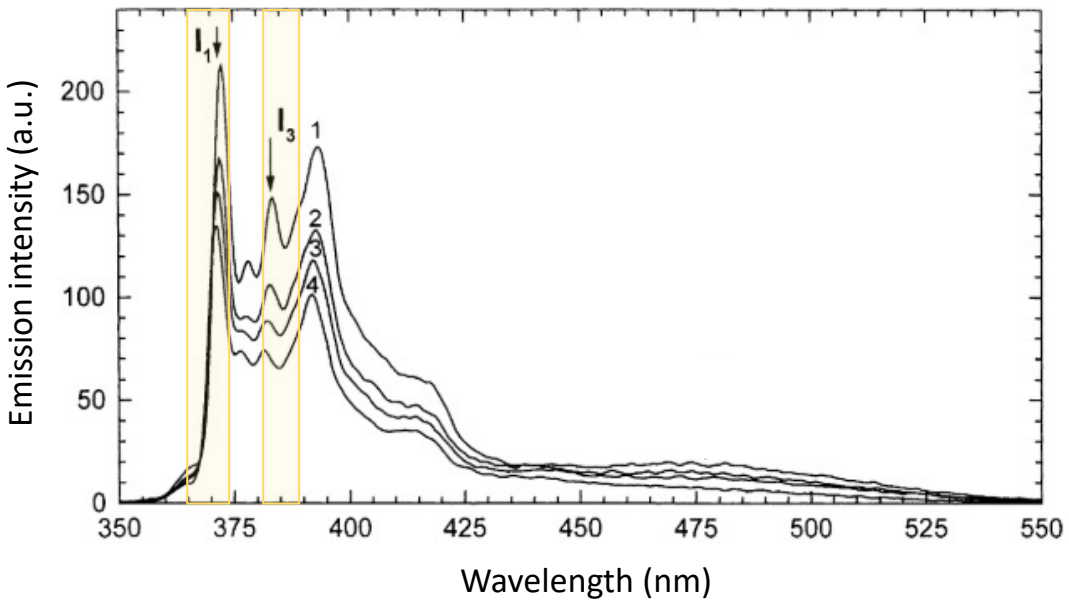

Figure 5.17. Fluorescence emission spectra of pyrene in aqueous solution of a surfactant (Triton X-165) at various concentrations as a representative spectra of pyrene fluorescence experiment for surfactants [503].

P006 I_1/I_3 ratio data showed no changes with increasing concentrations of peptide up to 1 mM, as shown in Figure 5.18A. Hence, P006 CAC determination *via* the pyrene assay was attempted at higher peptide concentrations (from 0.5 to 2 mM); still, no changes in the peak 1 to peak 3 ratio were registered, confirming the hypothesis that the pyrene was not sensing a change in microenvironment due to aggregate formation.

However, the LJMU027 I_1/I_3 ratio decreased when pyrene was titrated with increasing amounts of peptide, suggesting the formation of micellar structures, as represented in Figure 5.18B. The method employed by Aguiar *et al*. was not applicable for determination of CAC from LJMU027 pyrene 1:3 ratio data hereby obtained because the lower limit of the sigmoid was not reached [462]. Hence, similarly to the method employed by Islam *et al.*, CAC was approximated to the value of *x* corresponding to a significant and continuous decrease in the I_1/I_3 ratio, as shown in the graph B in Figure 5.18 [504]. Thus, CAC for LJMU027 was approximated to 100 μM (log [LJMU027] = ~2).

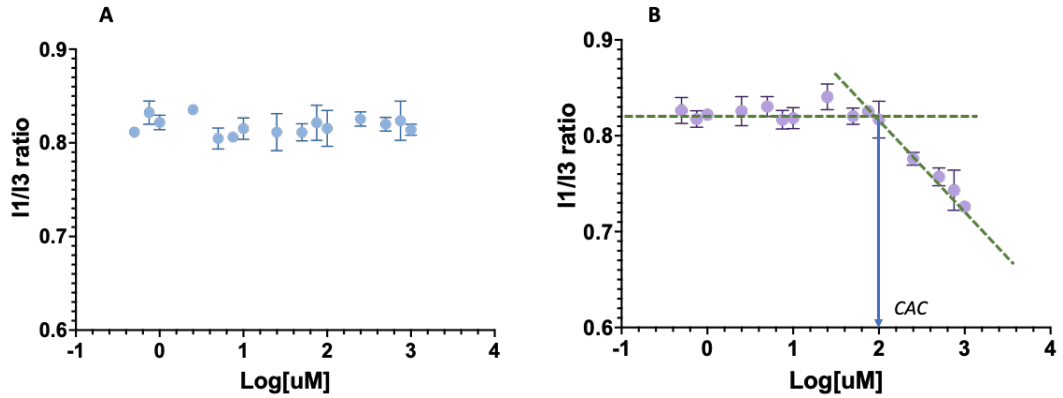

Figure 5.18. Pyrene 1:3 ratio versus logarithm of the peptide concentration graphs for P006 (A, in light blue) and LJMU027 (B, in lilac). CAC determination is indicated with a blue arrow in graph B.

Likewise, CAC was determined for LJMU017 and LJMU018 – presenting one fluorine atom in position 4 of the benzoyl ring and five fluorine atoms around the benzoyl ring, respectively – to investigate the effect of fluorine on the assembly. As shown in graphs A and B in Figure 5.19, the concentration at which the peptides assemble seemed to be affected by the presence of fluorine atoms, as the CAC values shifted to higher concentrations of peptide in both cases – ~500 μM for LJMU017 and ~250 μM for LJMU018. The influence of fluorine on self-assembly behaviour in this study was not in agreement with previous reports on Fmoc-Phe derivatives, showing that monofluorination or multiple fluorination of phenylalanine (i.e., 4-F-Phe and 3-F-Phe or F_5-Phe and 4-CF_3-Phe) did promote fast self-assembly/hydrogelation [505,506]. However, the significant structural differences between Phe-Phe dipeptide derivatives and these peptides may play a role on the influence of fluorine on the self-assembly behaviour.

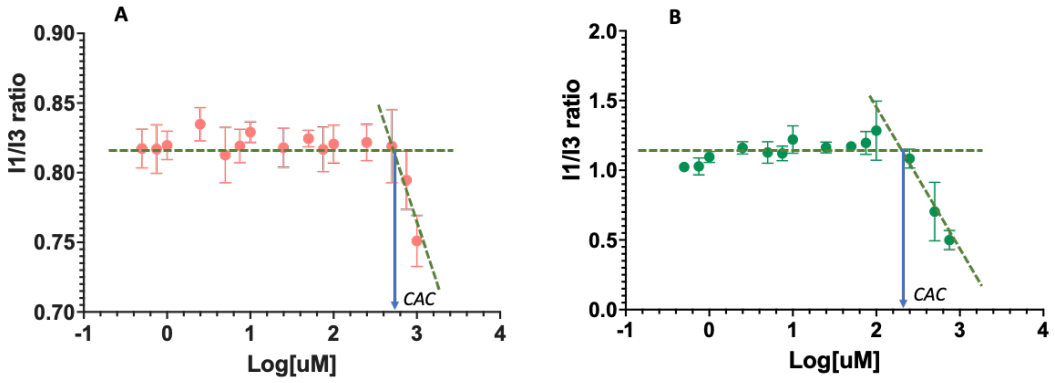

Figure 5.19. Pyrene 1:3 ratio versus logarithm of the concentration graphs for LJMU017 (A, in light orange) and LJMU018 (B, in green). CAC determination is indicated with a blue arrow in both the graphs.

5.4.3.3 Optimised self-assembly conditions: TEM and DLS analysis

P006 and LJMU027 were studied by TEM and DLS at two concentrations above the estimated CAC of LJMU027 (0.1 mM and 2 mM) to corroborate the results obtained from the pyrene fluorescence assay. Conditions employed for each sample are reported in Table 5.9.

Table 5.9. Conditions employed for P006 and LJMU027 self-assembled samples preparation.

Sample name	Peptide	Concentration (mM)	Incubation time
1	P006	2	24 h
2	P006	0.1	24 h
3	LJMU027	2	24 h
4	LJMU027	0.1	24 h
5	P006	2	1 week
6	P006	0.1	1 week
7	LJMU027	2	1 week
8	LJMU027	0.1	1 week

As shown in Figure 5.20, the average size of the population of particles was greater with higher concentrations of peptide (2 mM, samples 1, 3, 5, and 7) and longer incubation time (one week, samples 5-8). Moreover, the average size of LJMU027

particles was higher than that of P006 particles. However, the high variability of both average size and PDI confirmed the inadequacy of the DLS to quantify the peptide self-assembly process response under the conditions employed.

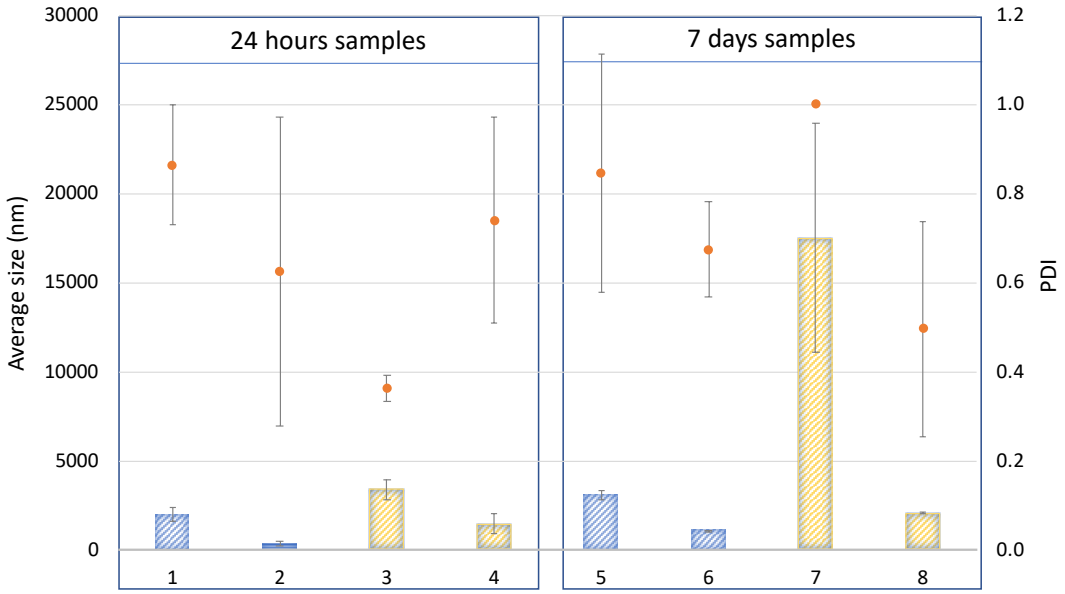

Figure 5.20. Average size (blue columns for P006 particles and yellow columns for LJMU027 particles) and PDI (orange dots) of self-assembling peptide particles measured by DLS.

At this point, TEM imaging was used to study the peptide self-assembly after one week incubation at room temperature (samples 5-8). Here, micelle formation was confirmed for each sample (P006 and LJMU027, both at 0.1 mM and 2 mM).

For P006 (2 mM), a homogenous population of spherical particles with an average particle diameter of ~26.5 nm (measured from 25 particles in a single image using ImageJ software) was visualised by electron microscopy imaging. Figure 5.21 shows two TEM micrographs, one at 200 nm and the other one with a zoom on a section of it (100 nm scale).

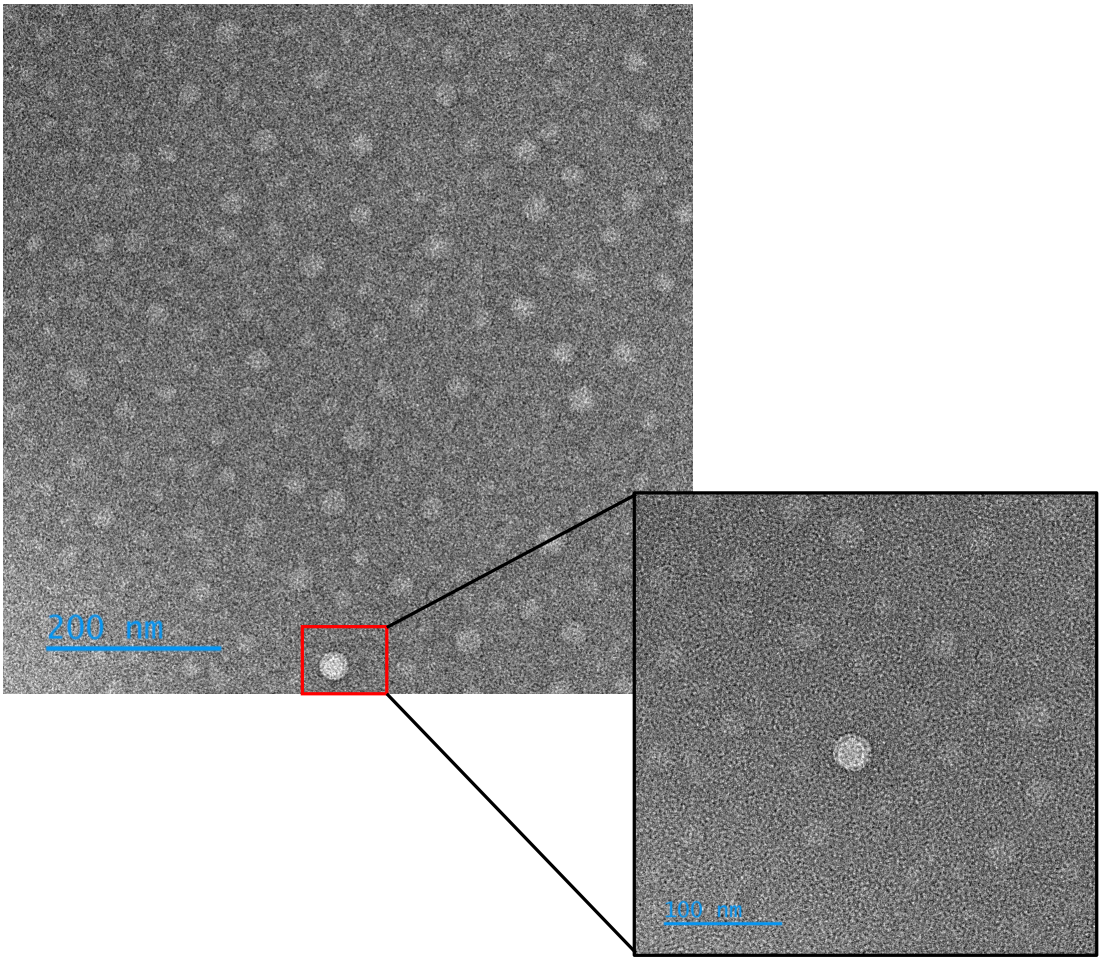

Figure 5.21. TEM micrographs of a population of particles deriving from self-assembly of P006 at concentration 2 mM. Main image 200 nm scale; inset 100 nm scale.

P006 samples at low concentrations (0.1 mM) were expected not to form particles, as suggested from CAC determination experiment. However, nanosized particles were visualised by TEM imaging. In particular, two different populations were imaged for this sample, one similar to that visualised at higher concentrations, but of smaller size (~14.1 nm, measured from 25 particles in a single image using ImageJ software) and with borders less clearly defined, and a second population of bigger and less uniform size (diameters ~30.7 nm, measured from 25 particles in a single image using ImageJ software), clearly showing micellar characteristics – a hydrophobic core surrounded by a darker region, supposed to be the hydrophilic head – as shown in Figure 5.22.

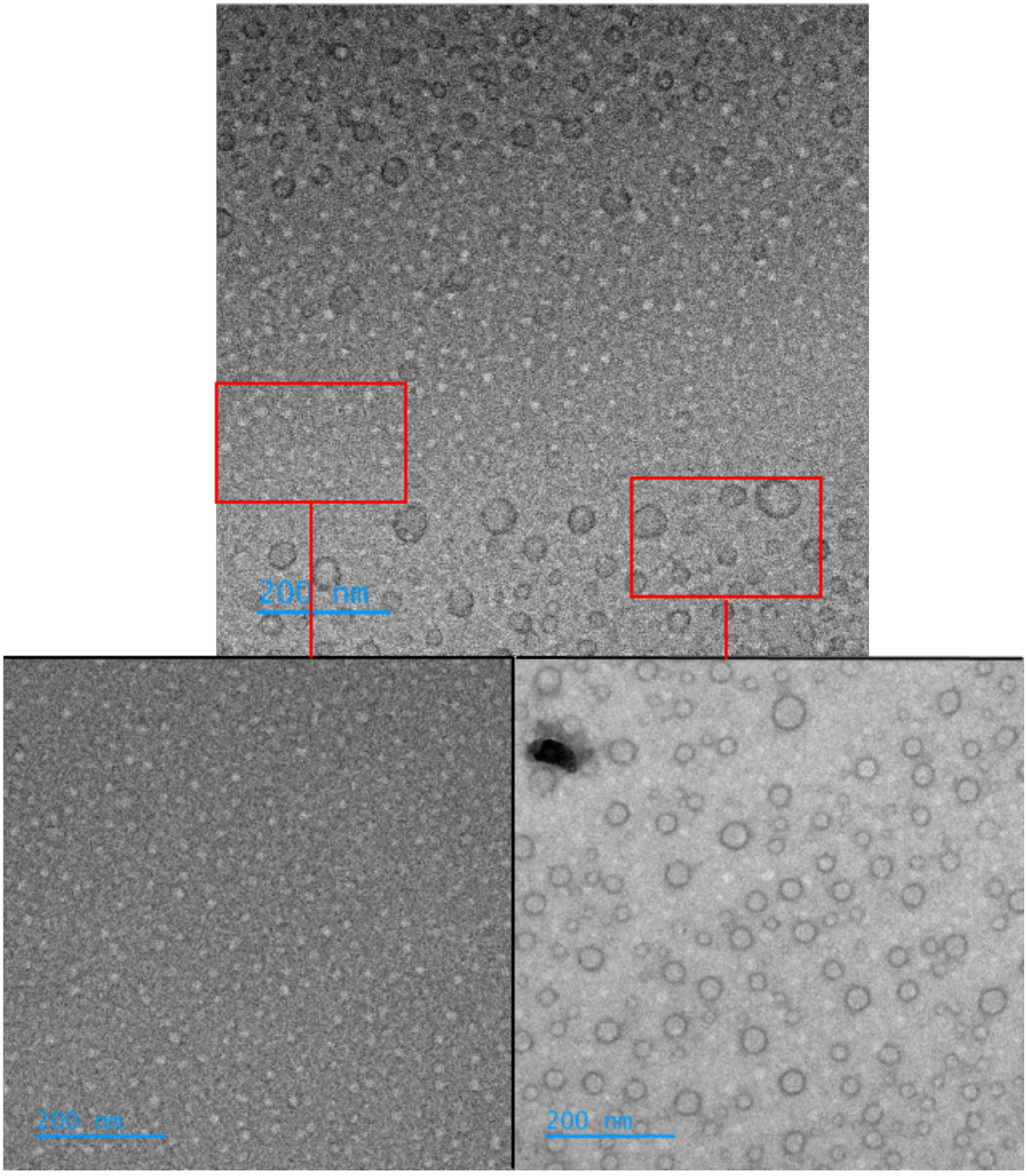

Figure 5.22. TEM micrographs of a population of particles deriving from self-assembly of P006 at concentration 0.1 mM. Upper image showing the co-presence of the two populations, while lower images showing on the left the population of smaller particle size and on the right the population of bigger particle size and clear micellar appearance. Scale of 200 nm is on all the pictures shown.

Solutions of LJMU027 (2 mM) after a week of incubation at room temperature showed some precipitate at the bottom of the glass vial presumably due to the low solubility of the peptide; here, spherical particles of homogeneous size (~18.7 nm,

measurement obtained from 25 particles in a single image using ImageJ software) were visualised, as shown in Figure 5.23.

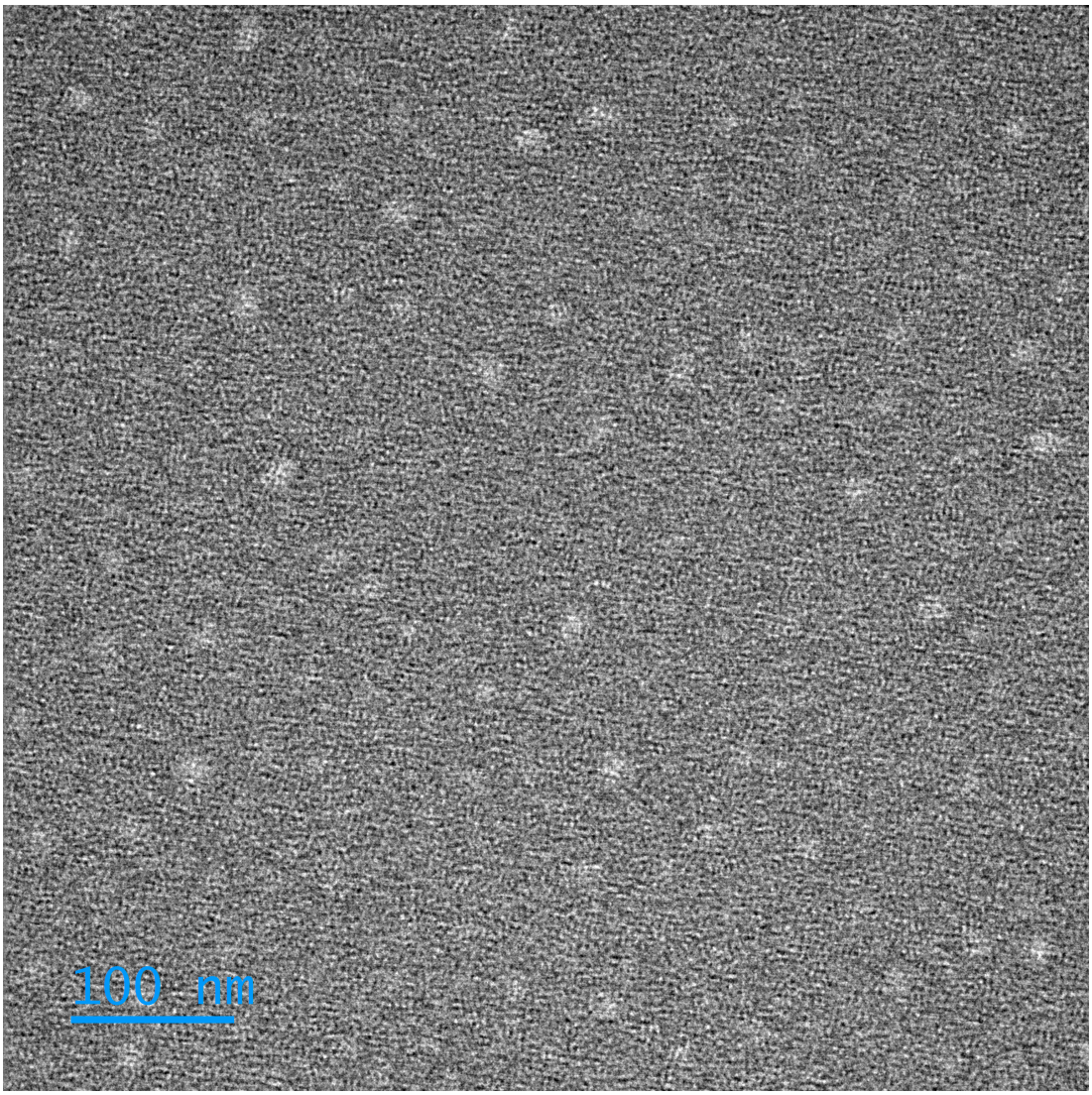

Figure 5.23. TEM micrograph of a population of particles deriving from self-assembly of LJMU027 solution (concentration 2 mM). Scale of 100 nm is shown at the bottom of the image.

Finally, particles deriving from the self-assembly of a solution of LJMU027 (0.1 mM) are shown in Figure 5.24. The population appeared to be uniform and showed an average particle size of ~14.4 nm, measured from 25 particles on a single image.

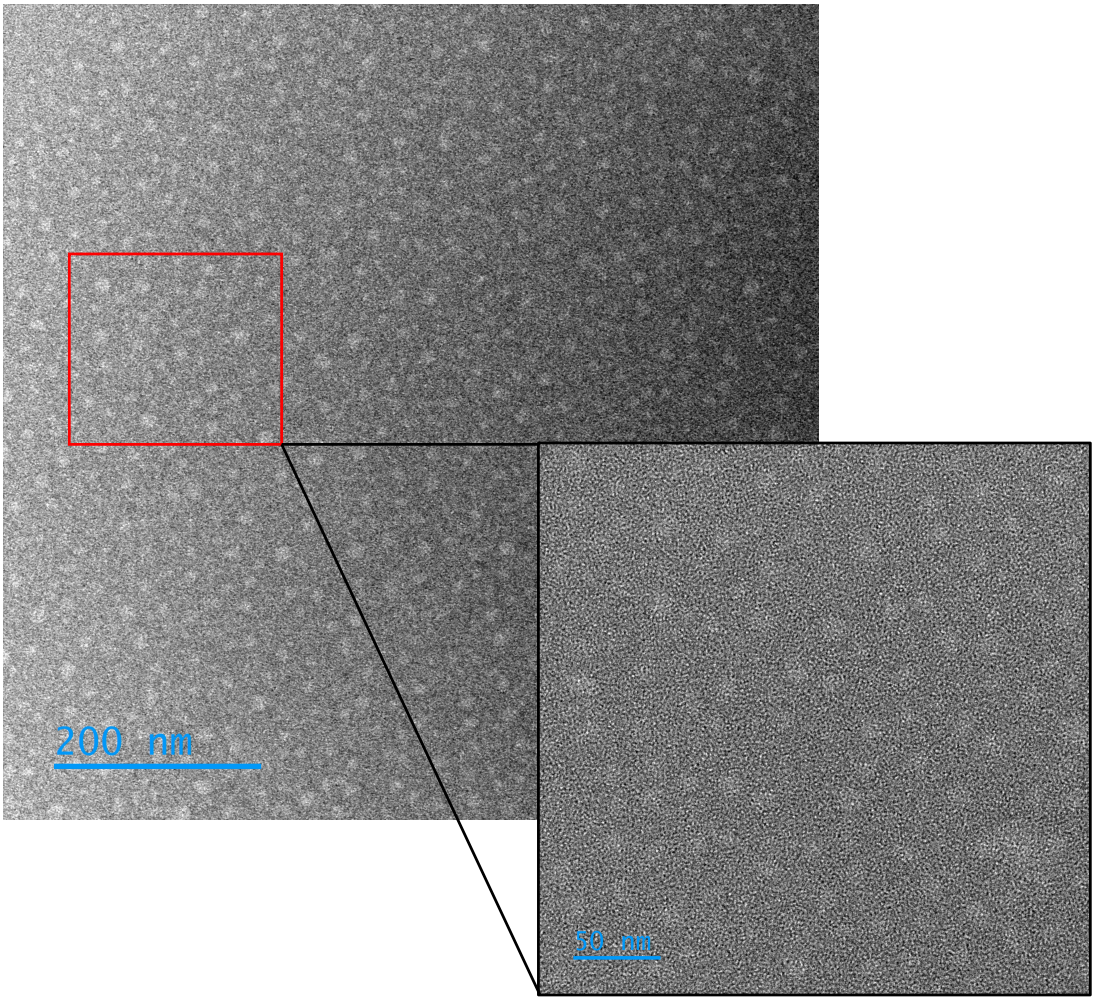

Figure 5.24. TEM micrograph of a population of particles deriving from self-assembly of LJMU027 at concentration of 0.1 mM. Main image 200 nm scale; inset 50 nm scale.

TEM imaging confirmed the hypothesis that P006 and derivatives are capable of forming nanostructures in aqueous solutions but did not corroborate the theory that the benzoyl derivatives are more prone to aggregation due to the hydrophobic moiety at the N-terminus. The CAC determination experiment showed no variability in the I_1/i_3 ratio for P006, suggesting that the peptide did not form micelles at the concentrations under evaluation. However, TEM imaging showed that P006 is capable of forming micellar nanostructures.

5.4.3.4 Stain-free TEM imaging for fluorinated peptides

For peptides containing fluorine atoms, stain-free TEM imaging was attempted. Fluorine building blocks can dissipate the beam current, allowing the samples to be imaged without any additional staining. This was previously proven for the N-terminal coupling of 3,5-bis(trifluoromethyl)-benzoic acid to a short Amyloid β sequence by Sonzini *et al.* [237]. However, stain-free imaging has never been explored for 4-F-benzoyl- and F_5-benzoyl- derivatives. Here, stain-free images were compared to images taken from stained samples (phosphotungstic acid hydrate solution, 1%) for LJMU017 and LJMU018, containing 4-F-benzoyl- and F_5-benzoyl- moieties at the N-terminus, respectively.

While for LJMU017 the quality of the images between the sample negatively stained and the sample analysed without any stain was not significantly improved, for LJMU018, fluorine atoms around the benzoyl moiety were able to dissipate the current beam and allowed visualisation of the particles at higher magnifications (up to 89 kx), as reported in Figure 5.25. Notably, visualisation of particles was improved when the sample was not pre-treated with stain as it avoided the presence of blobs of phosphotungstic acid solution that did not allow an increase in magnification above 11 kx to clearly visualise the particles. On the other hand, the absence of black spots of stain solution allowed an increase in magnification up to 89 kx and permitted clear particle visualisation.

Unfortunately, the FEI Morgagni 268 microscope at LJMU did not include the tool to measure the size of the aggregates formed; for this reason, scale bar of the micrographs and particles size are not reported, while magnification was annotated during the analysis.

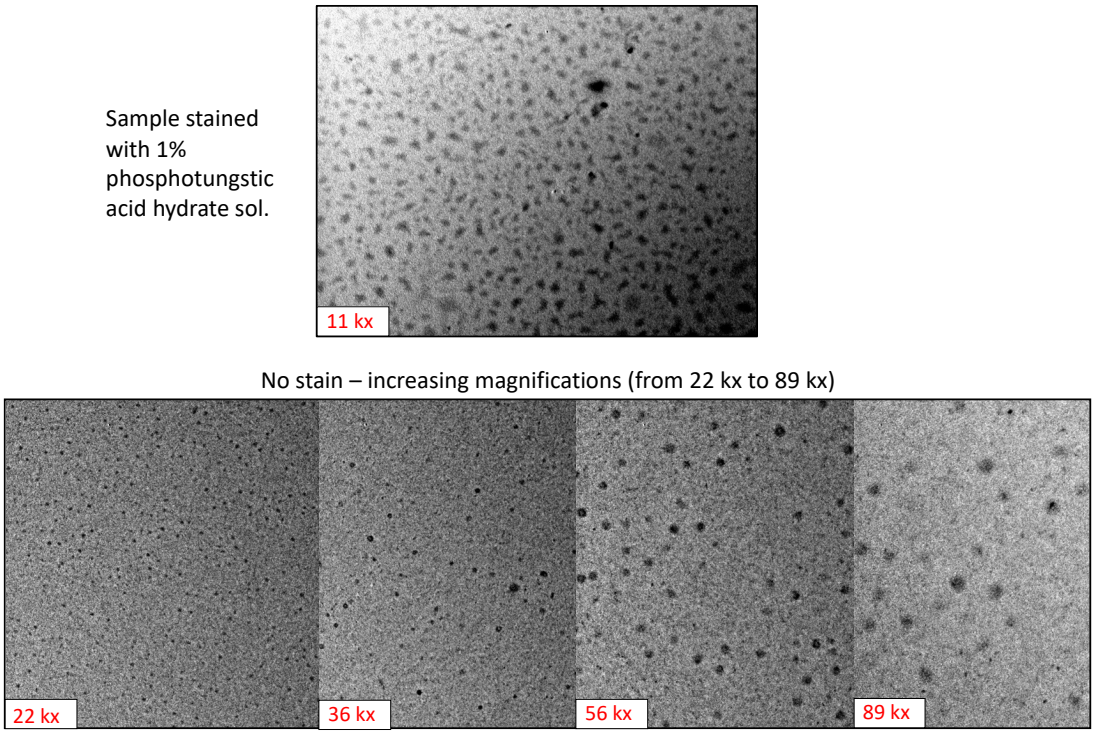

Figure 5.25. Comparison between TEM micrographs taken from a LJMU018 sample stained with phosphotungstic acid hydrate solution (upper image) and the same sample imaged without prior staining treatment (lower pictures).

5.4.4 Chitosan MPs formulation

5.4.4.1 Blank and loaded MPs

Nasal administration is a validated approach to deliver peptides as demonstrated by the approval of miacalcin nasal spray over two decades ago [507]. Nowadays, the use of chitosan as a transmucosal carrier for the delivery of peptides to the brain is a promising option [388,489,508–510]. The use of permeation enhancers and/or mucoadhesive carriers can provide prolonged contact between the mucosa and the drug formulation, enhancing the concentration that reaches the target tissue and the overall final drug effect [482]. In this study, microspheres were manufactured by spray-drying from a solution of low molecular weight chitosan (2% *w/v*). Chitosan was selected due to its mucoadhesive properties that would promote deposition on the nasal mucosa and increase the time of residence of the particles [483,508,510]. Moreover, the pre-clinical safety of intranasally administered chitosan has been widely proven and, in an extensive review published in 2014, Casettari *et al.* reported

that more than 3000 intranasal doses of chitosan have been administered to more than 1000 human subjects in clinical trials, and by now this will have significantly increased [508].

MPs based on chitosan are considered a viable option for use in *in vivo* studies in sheep: former research group members, undertook a feasibility study to nasally and intravenously administer a chitosan microsphere formulation of P006, without incurring toxicity in the sheep (Capel *et al*., unpublished data). However, the dose administered was too low (or it degraded too fast) to be detected *ex vivo*, requiring further studies to confirm the hypothesis before moving towards pre-clinical studies.

Parameters for the fabrication of chitosan MPs were previously optimised by our research group to yield particles with a diameter over 10 μm, necessary for avoiding deposition into the lungs [23,373]. Even though chitosan microspheres have the tendency to stick to the walls of the cyclone during spray-drying, in this study, blank and loaded chitosan MPs were obtained in high yields – 75% for the blank formulation and 68% for the loaded formulation (5 mg of peptide in 0.5 g of chitosan) – greater than previously assessed (~45%) [23].

For the MP formulations containing P006, it was assumed that there was an even dispersion of peptide through the MPs and that encapsulation was therefore 100%, as loading was directly related to the initial amount of peptide added (1% of LMWCh mass). Thus, the peptide was expected to be equally distributed between the recovered and unrecovered chitosan powder. The use of polysaccharide carriers is known to prevent peptide degradation during the spray-drying process, through e.g. water replacement and glassy immobilisation, leading to the formation of a protective coating around the peptide and eventually decreasing the effects of destructive factors [511]. The resistance of CGRP-R antagonist peptides to degradation during the spray-drying process was previously demonstrated by our research group using LC-MS analysis before and after spray drying [23].

5.4.4.2 Chitosan MPs characterisation (size and moisture content)

From Scanning Electron Microscopy (SEM) analysis of blank and loaded LMWCh chitosan MPs, information on the diameter and morphology was obtained. As shown in Figure 5.26, no significant difference was observed between the diameter of blank MPs (9.00 ± 0.74 μm) and that of loaded MPs (9.55 ± 0.91 μm).

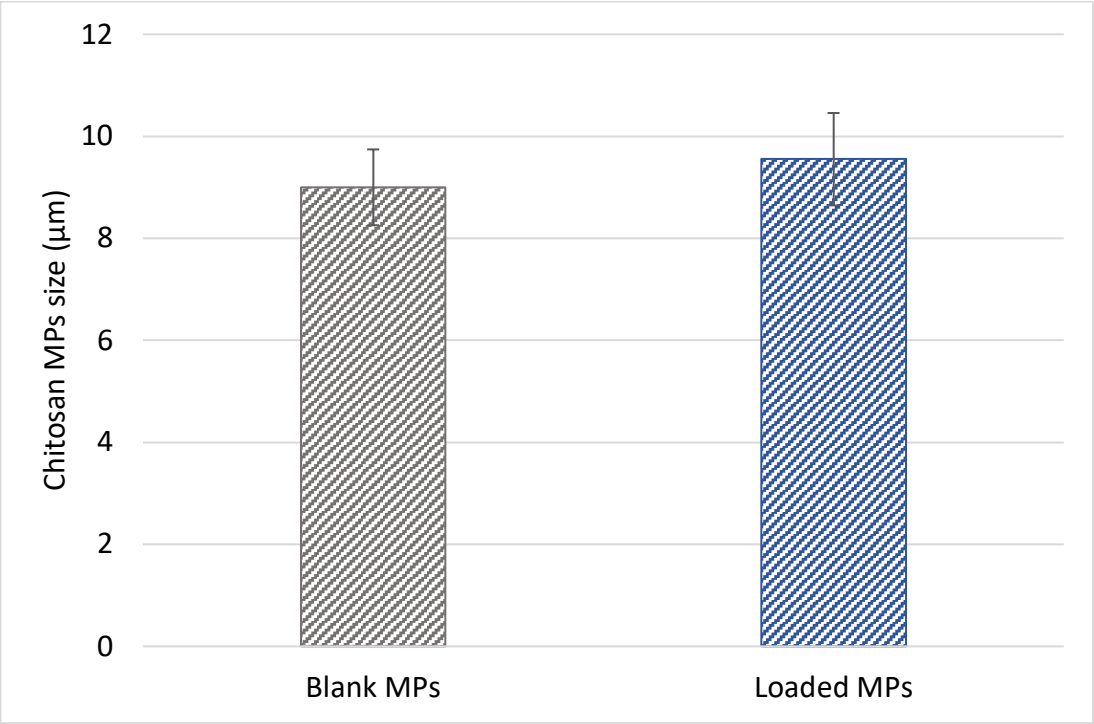

Figure 5.26. Size of blank and loaded LMW chitosan MPs measured by SEM images analysis (ImageJ software).

Variations in particle morphology was observed by microscopic analysis, with some particles having a rounded shape and some presenting a "cheesy rough wrinkled surface", in accordance with previous reports [480,512]. This is better visualised in Figure 5.27 and Figure 5.28, where blank and loaded MPs, respectively, are represented.

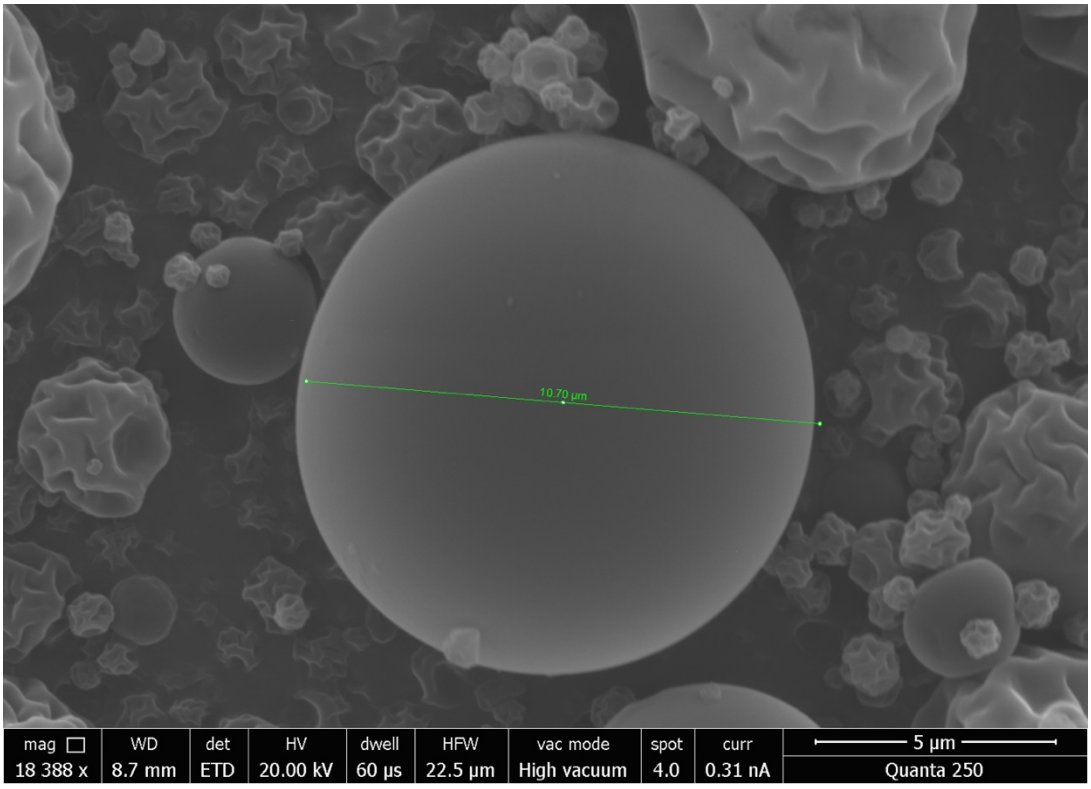

Figure 5.27. SEM micrograph from blank chitosan MPs sample. Diameter size is shown with a green line (10.70 µm).

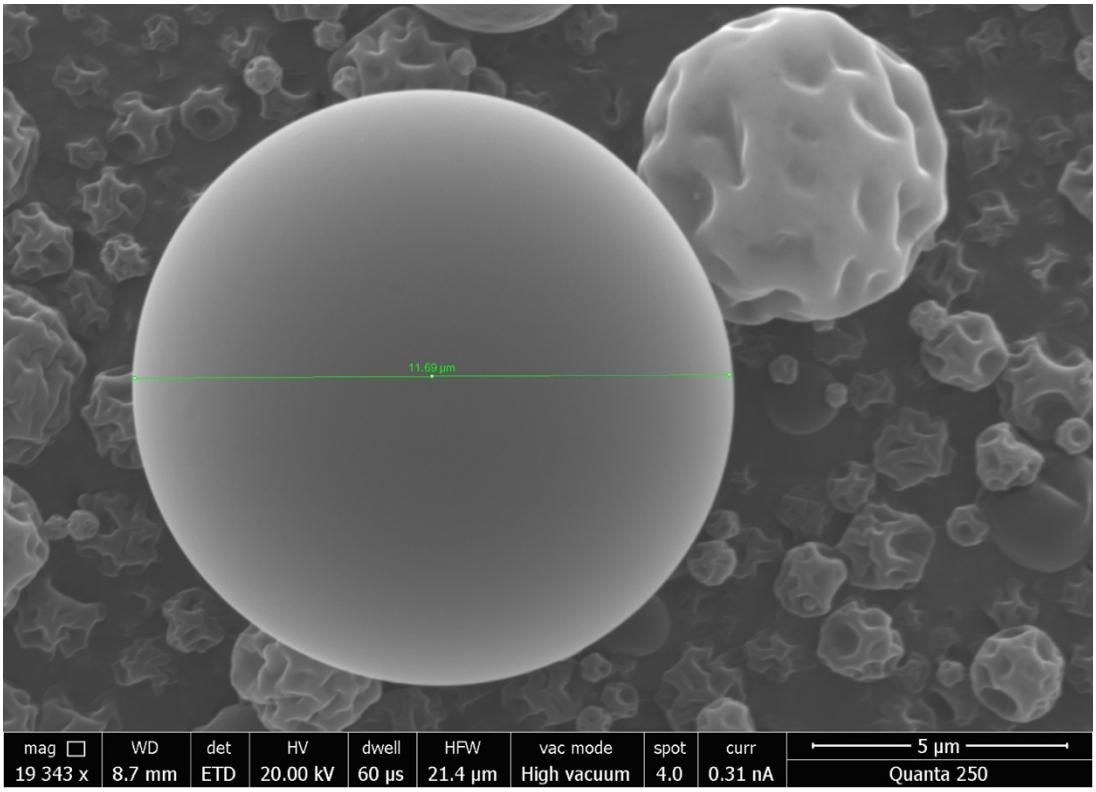

Figure 5.28. SEM micrograph from loaded chitosan MPs. Diameter size is shown with a green line (11.69 µm).

Blank chitosan microcarrier powder was tested by TGA and a weight loss of around 7.1 ± 1.28% was detected, meaning that the powder had a moisture content of around 7%, due to the hydrophilic nature of chitosan, and as previously described in literature [479].

5.4.4.3 Release study from chitosan MPs

In vitro release studies are often carried out using a dialysis method, where the formulation is dialysed against PBS buffer [480]. However, this technique implies that the peptide should readily equilibrate between the two chambers and that the sustained release is not due to delay in the passage and equilibration through the membrane, but due to the formulation itself. To avoid this artifact, described in Chapter 4 for plasma protein binding assessment through RED devices, the release study of P006-loaded chitosan MPs was performed by simply incubating the suspension of MPs in a 1.5 mL centrifuge tube and centrifuging the suspension after

various time points, up to 24 h, similar to the method reported by Sun *et al.* [488]. As shown in Figure 5.29, P006 was quickly released over the first 30 min, after which only a small increase in peptide released (~ an addition 6%) was detected over 24 h reaching a total drug release of ~74%. In general, the release rate depends on the degradation of the polymer and/or on the diffusion of the peptide from the microspheres, as well as on the size and the porosity of the particles [513]. The higher the particle size, the lower the contact surface, the slower the release. Moreover, when the drug is spray-dried with the polymer, the latter may simply become a powder without being encapsulated into the microspheres, and this would explain the burst release once in solution. This could possibly be resolved using, the complex-coacervation method, where chitosan microspheres are formed by interionic interaction between polymers of opposite charge, which would help trap the peptide, slowing the release from the MPs [483]. Another strategy would be to spray-dry self-assembled peptide nanostructures as a way to protect the peptide, control the release, while aiding retention in the nasal cavity, similar to the function of nanocomposite microparticles, previously explored by our research group [478].

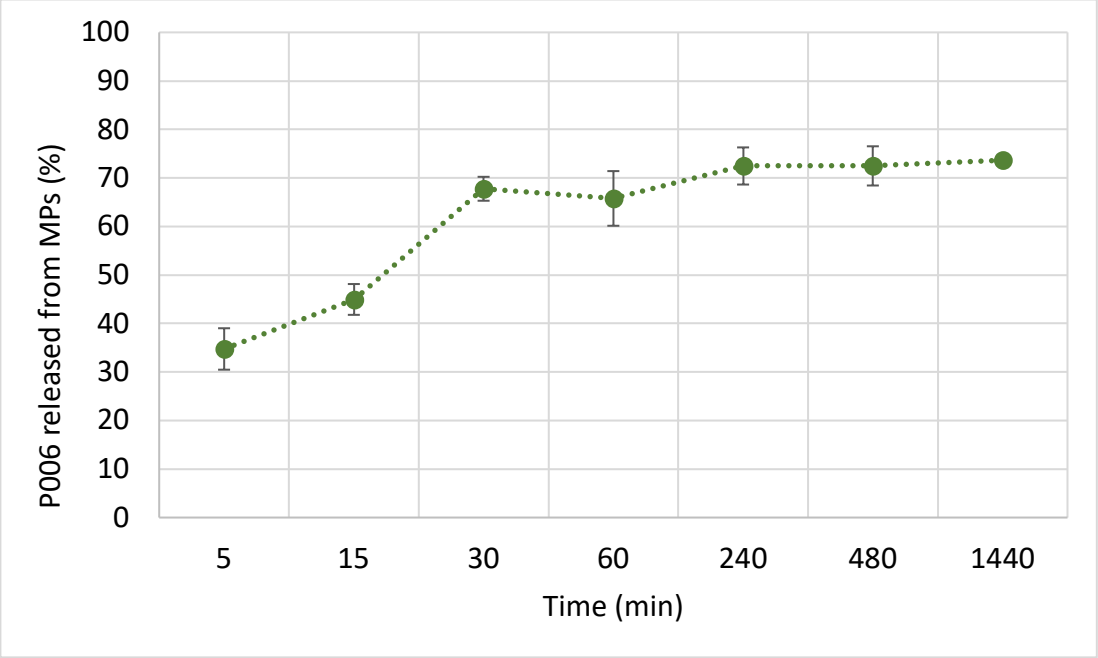

Figure 5.29. Release of P006 from chitosan microcarriers in PBS buffer solution over 24 h.

5.5 Conclusions

In this chapter, the formulation and self-assembly of an array of CGRP-antagonist peptides was explored. In particular, a nanoprecipitation method was successfully optimised for the preparation of PLGA nanoparticles through a TD. However, the attempt to encapsulate P006 or LJMU027 within optimised PLGA NPs failed and a release study confirmed that no peptide was liberated from the formulation.

P006 and benzoyl derivatives were then studied for their ability to form nanostructures. The peptide self-assembly behaviour was explored through a design of experiments approach (Plackett-Burman design) under various conditions. Dynamic light scattering, pyrene fluorescence method, and TEM were employed to study the influence of various conditions on the assembly. Here, TEM was taken as the only reliable technique to characterise the aggregates forming; moreover, stain-free images were obtained for fluorinated peptides, assessing the possibility of imaging aggregates deriving from fluorinated peptides without the use of stain. Hence, the potential of P006 and derivatives to self-assemble should be further investigated as micelles formation could prevent degradation, eventually becoming a viable option to nasally administer peptides without requiring a polymeric nanosized formulation (e.g., PLGA NPs) to protect it.

Finally, P006 was formulated into chitosan microparticles *via* spray-drying with parameters previously optimised by the author and former members of the research group prior to these thesis studies. Administration of chitosan formulations *via* nasal delivery is a well-recognised pathway to achieve brain delivery of drugs – the migraine drug Alniditan has been administered as a nasal chitosan solution in Phase I and II clinical trials and a morphine-chitosan solution (Rylomine) has undergone Phase III clinical trials in the US [490–492]. Here, spherical-shaped microspheres of ~9-10 μm diameter were obtained in high yields for both blank and loaded formulation and a burst release from loaded MPs (~ 68% after 30 min) was observed.

Chitosan MPs can be further explored to encapsulate self-assembled peptide nanostructures, as a way to prepare nanocomposite microparticles, which can prevent burst release, protect the peptide from degradation and aid retention in the nasal mucosa. Thus, chitosan microspheres can be considered a viable option for moving the project towards *in vivo* studies, pre-clinical and Phase I clinical trials, due to widely demonstrated safety of intranasal administered chitosan formulations.

6 General Discussion and Future Work

6.1 Overview of the project

Migraine is one of the most prevalent diseases in the world and it is associated with a substantial effect on the quality of life of migraineurs and their families [2]. However, medicines currently licenced for migraine therapy are only partially effective and present an important and worrying adverse event profile (e.g., coronary vasoconstriction, nausea, dizziness), preventing their use in numerous cases [514]. Hence, there is a pressing need to develop novel therapies to treat migraine and related symptoms.

Calcitonin gene-related peptide (CGRP) and its receptor (CGRP-R) have been recognised as key players in migraine pathophysiology, thus being important targets for novel anti-migraine medicines. Recently, CGRP-R has been targeted with small molecule antagonists (i.e., ubrogepant, rimegepant, atogepant) and monoclonal antibodies (i.e., erenumab), while the CGRP peptide itself has been targeted with monoclonal antibodies only (i.e., fremanezumab, galcanezumab, eptinezumab) [46,49,51,55,515]. In this work, we considered the potential of antagonising CGRP-R with peptides deriving from truncations and modifications of the natural hormone CGRP, to obtain a medicine that combines the advantages and overcome the limitations of the two abovementioned classes of drugs [139]. CGRP-R antagonism *via* peptide molecules has been previously explored by various research groups [66–68,180,181]. However, peptides containing natural amino acids typically suffer from unfavourable pharmacokinetic profiles that may preclude their use as medicines [516]. An established solution to this is to modify peptides to present non-native functional groups or features. However, there has been little exploration of this in CGRP peptide antagonists and some potential modifications have received little-to-no attention so far – e.g., *via* the use of fluorinated amino acids, peptoid monomers, and N-terminal benzoyl appendages, to increase their drug-like properties.

The aim of this multidisciplinary PhD project was to i) design, synthesise, and characterise peptides and peptidomimetics with putative antagonistic activity against the CGRP-R; ii) test their antagonistic activity against the CGRP-R and their cytotoxicity *in vitro*; iii) develop, optimise, and validate generally applicable techniques to study *in vitro* blood serum stability and plasma protein binding of peptides; and iv) develop delivery platforms suitable for nasal administration of future peptide therapeutics.

6.1.1 Discovery of potent peptide and peptidomimetic antagonists of the CGRP receptor

A library of 19 peptides and peptidomimetics was designed, synthesised, and characterised, based on the parent structure of P006, a potent CGRP-R antagonist designed by former members of our research group, in collaboration with PharmNovo AB.

The library included six analogues containing fluorinated amino acids (LJMU011-LJMU016), where one or both the Phe residues in position 35 and/or 37 of P006 were replaced with fluorinated counterparts (i.e., 4-F-Phe and F_5-Phe). These were designed to 1) study the conformation of the peptide through ^{19}F NMR and 2) to probe the effect of a local increase in hydrophobicity, without significantly altering the overall peptide structure. These modifications proved that fluorination of amino acid residues distal from the peptidylprolyl bond is a valuable tool to obtain information of the peptidylprolyl bond, without having a direct influence on it. However, the antagonist potency of the fluorinated analogues was slightly reduced in some cases (i.e., LJMU011, LJMU012, LJMU013, LJMU015) or severely affected in other cases (i.e., LJMU014 and LJMU016). Six peptide-peptoid hybrids (or peptomers) were prepared by replacing six amino acid residues of the parent P006 sequence with peptoid monomer counterparts to study 1) the tolerance of each position to the relocation of the side chain to the N_α position, and 2) to determine whether this could enhance the blood serum stability masking of peptidase-sensitive sites. This modification, even if small, was tolerated only in two positions (i.e., Phe37,

in the case of LJMU019, and Val28, in the case of LJMU024), while this was detrimental in every other position (i.e., LJMU020, LJMU021, LJMU022, and LJMU023).

As evidence emerged from mass spectrometric analysis of the products from cleavage, it became clear that masking of the major proteolysis site (i.e., between Pro29 and Thr30 at the peptide N-terminus) should provide a way to prolong serum stability. N-benzoylated analogues were designed to protect the peptide N-terminus and, at the same time, increase the overall hydrophobicity of the molecule. These resulted in increased (in the case of LJMU027) or comparable (in the case of LJMU017 and LJMU018) activity against the CGRP-R, affording promising compounds for further study in pharmacokinetic assays and future *in vivo* efficacy studies.

A summary of the modifications explored on P006 and the resulting outcomes for activity against the CGRP receptor is shown in Figure 6.1.

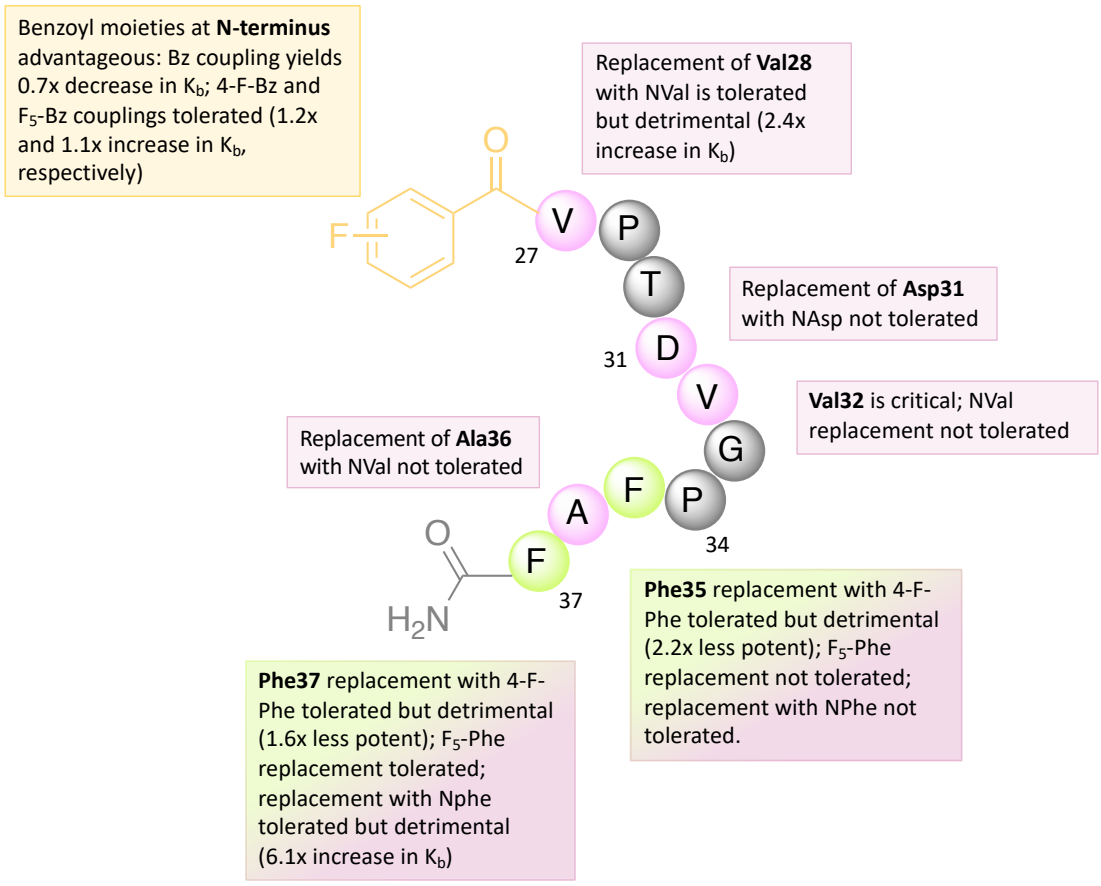

Figure 6.1. Summary of structure-activity relationship studies performed on P006 in this project. Modifications are color-coded as following: internal fluorine modifications in light green, peptoid replacements in pink, and N-terminal modifications in yellow. Amino acid residues not modified are coloured in grey.

6.1.2 Pharmacokinetic evaluation of P006 and derivatives

The potential of a peptide to become a drug may be hampered by the unfavourable pharmacokinetic profile characteristics typical of most peptide molecules. Among the pharmacokinetic properties, proteolytic stability and plasma protein binding were considered to be of high importance to the drug development. However, it became clear at the outset of this study, that *ex vivo* evaluation of peptide pharmacokinetics was limited by a lack of well-defined and generally applicable assays specifically tailored for peptides. Hence, a method for blood stability evaluation was optimised using Design of Experiments and validated following ICH guidelines. Peptides and peptidomimetics were tested in pooled human serum over

60 minutes and the major metabolites were identified through LC-MS analysis. While internally fluorinated peptides and peptide-peptoid hybrids showed minor improvements in proteolytic stability (with exception of LJMU016 and LJMU024), N-terminally modified peptides showed outstanding resistance to proteolysis, probably due to masking of the main cleavage site, identified between Pro29 and Thr30.

A peptide most likely to become a drug, should ideally exhibit prolonged stability to proteolysis in the biological fluids relevant to its route of administration e.g. blood serum, whilst retaining potent antagonism. Figure 6.2 compares the results from the stability and antagonism studies: the coloured background divides the graph in three main areas, from green (peptides with favourable drug-likeness properties) to red (peptides with unfavourable drug-likeness properties). Peptides that are in the top left of the chart are the most desirable. Clearly, the benzoylated peptides present the lowest K_b values (hence, the greatest antagonist potency) and the highest resistance to proteolysis activity.

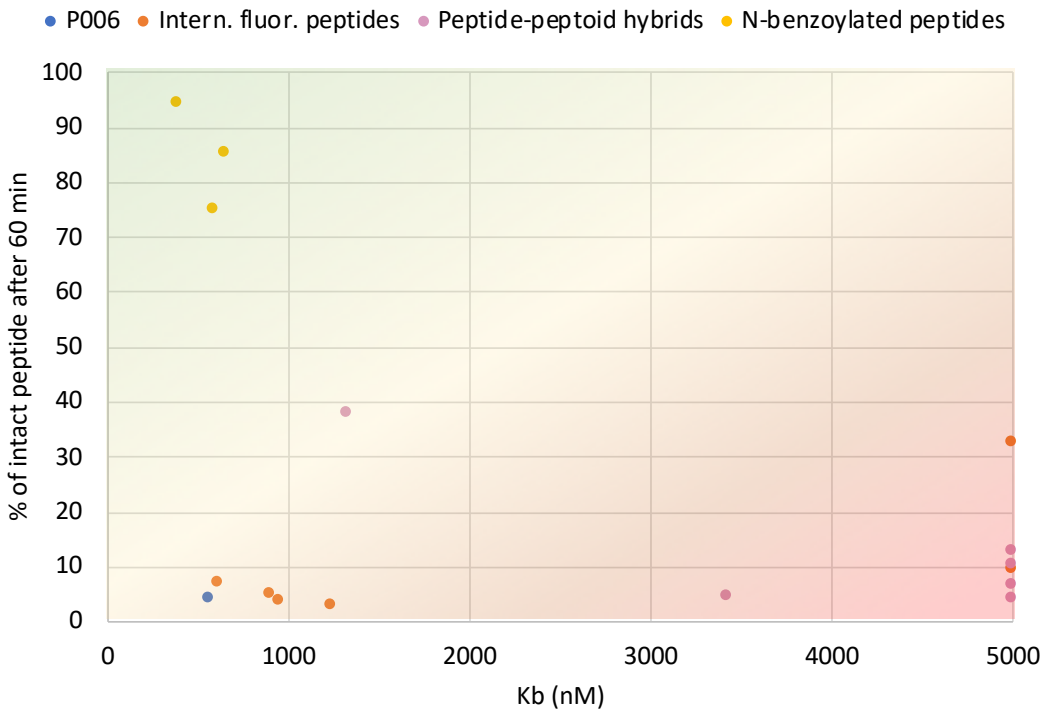

Figure 6.2. K_b versus percentage of intact peptide after 60 min incubation in diluted human serum. Peptides are colour-coded based on the modification they present. The gradient on the background divides the graph in areas, from green (more likely to become a drug) to red (less likely to become a drug). Inactive compounds have been deliberately assigned a K_b of 5000 nM.

Further information on the pharmacokinetic profile of P006 and benzoylated derivatives was obtained by plasma protein binding studies. An in-house method was initially developed based on observations from the blood stability method, wherein the plasma proteins were precipitated by the addition an acidic solution. In some cases, more hydrophobic peptides were found to remain bound to the precipitated proteins. This was exploited to test the propensity for P006 and the benzoyl derivatives to bind to HSA – a potential route to prolonging serum stability – by titrating constant concentrations of peptide (50 μM) against increasing concentrations of HSA (10-400 μM). Here, P006 showed a percentage of bound peptide between 0 and 10% for the highest concentrations of HSA, while LJMU027 and fluorinated analogues (i.e., LJMU017 and LJMU018) afforded increasing binding

percentages, ranging from 0 to 80% with increasing concentrations of HSA. To confirm the results obtained from HSA precipitation experiment, plasma protein binding was evaluated with various commercially available kits; however, their reliability seemed to be undermined by nonspecific binding, in the case of separation *via* ultrafiltration, and long incubation times required to reach equilibrium, in the case of equilibrium dialysis. Finally, the in-house developed method was found to be the most facile, reliable, and inexpensive, with the potential of becoming a widely used test for evaluation of peptide plasma protein binding.

6.1.3 Formulation and peptide self-assembly

To deliver drugs to the brain, it is necessary to cross or bypass the blood brain barrier (BBB). However, most peptides do not fit the parameters classically required to cross the BBB (i.e., molecular weight lower than 400 Da, be mainly apolar, and not multicyclic) [371]. Alternatively, it is theoretically possible to exploit the nose-to-brain route that enables transport of drugs directly into the brain *via* the trigeminal nerves or the olfactory neurons [370–372]. The advantages of intranasal administration include not only circumventing the BBB, but also avoiding first-pass metabolism and/or degradation in the blood compartment [370]. Numerous delivery systems and techniques have been developed to introduce peptides into the body and overcome their intrinsic limitations – i.e., fast elimination through the kidneys, rapid degradation in blood, uptake by the reticuloendothelial system, and accumulation in nontargeted cells [370,378]. Among them, polymeric nanoparticles containing peptide or nanoparticles deriving from peptide assembly can offer the advantage of protecting the peptide from biological and chemical degradation as well as extracellular transport by P-glycoproteins [372,388].

6.1.3.1 Polymeric nanoparticles

Poly(D,L-lactic-co-glycolic acid) (PLGA) was chosen for nanoparticle (NP) preparation due to its biodegradability, biocompatibility, and sustained released properties [390,499]. A nanoprecipitation-solvent evaporation method was selected as an alternative to the single and double emulsion methods, previously exploited with

limited success by our research group for the encapsulation of P006. Here, blank NPs were optimised *via* a Taguchi orthogonal array Design, to obtain NPs of ~100 nm, thought to be required to access to the brain *via* the intra-axonal route because of their diameters being lower of that of the axons in the *filia olfactoria* [500].

Once the parameters (i.e., amount of PLGA, percentage of stabiliser in the aqueous phase, and ratio between organic and aqueous phase) had been optimised, the predicted optimum formulation was manufactured, yielding an average NPs size of 103.35 ± 1.77 nm and a PDI of 0.26 ± 0.01, confirming the success of the optimisation strategy. Preparation of loaded NPs was attempted with P006 and LJMU027, the latter being highly hydrophilic, and the former being significantly more hydrophobic. Surprisingly, in both cases, through indirect determination of the total amount of encapsulated peptide, it appeared that nanoprecipitation techniques to prepare PLGA NPs did not succeed in encapsulating P006 and the benzoylated analogue. Thus, alternative strategies were explored.

6.1.3.2 Peptide self-assembly

Peptides of various structures, particularly if they are amphiphilic, may self-assemble in solution and form nanostructures (e.g., micelles, vesicles, or particles) composed of peptide only. This would potentially provide an increased blood plasma stability and a longer half-life than the monomeric form peptide. From the 19 peptides synthesised, four peptides were selected to study self-assembly: P006, as the parent peptide, LJMU027, to study the effect of the benzoyl moiety on the peptide behaviour, and the two fluorinated benzoyl derivatives (i.e., LJMU017 and LJMU018), to assess the influence of fluorine on the aggregation.

Plackett-Burman Design was used with P006 as preliminary screening study to identify the independent variables with the greatest influence on the average size of the particles in solution. Among the variables chosen (i.e., concentration of peptide, pH, sonication time, time for assembly, and temperature), the one that had the largest influence on the outcome was the concentration of peptide; however, none

had a statistically significant effect. Further evidence on the influence of the concentration on assembly was given by Transmission Electron Microscopy (TEM) imaging, showing that, for concentrations as low as 0.01 mM, there was an absence of nanostructures at any given condition of pH, temperature, sonication, and incubation time. On the other hand, at high concentrations (i.e., 2 mM), nanostructures were visualised for any combination of independent variables. At this point, it was hypothesised that a concentration of 0.01 mM was below the critical aggregate concentration (CAC). This was explored using a pyrene fluorescence spectroscopy assay with increasing concentrations of peptide (from 0.0005 to 1 mM). Pyrene is sensitive to the hydrophobicity of the environment, and this is mirrored in the ratio between the first (373 nm) and the third (384 nm) vibronic bands when pyrene is excited at 335 nm. Briefly, polar environments result in high pyrene 1:3 ratios, while hydrophobic environments result in low pyrene 1:3 ratios. Changes in pyrene 1:3 ratio were observed for LJMU027, LJMU017, and LJMU018, while no changes were detected for P006. Thus, CAC values for LJMU027, LJMU017, and LJMU018 were estimated to be around 100, 500, and 250 μM, respectively.

The self-assembly behaviour of P006 and LJMU027 in solution was studied at two concentrations (0.1 mM and 2 mm) and two incubation times (24 h and one week) using Dynamic Light Scattering (DLS) and TEM imaging. Here, the population of particles obtained was characterised in terms of appearance, size, and shape. Analysis of TEM images showed that, for any combination of concentration and incubation time, particles presented a spherical shape, some showing a characteristic micellar appearance, and were in the nanometre range (between 14 and 30 nm), thus theoretically capable of accessing the CNS *via* the intra-axonal route [500]. Hence, the idea of loading all-peptide nanoparticles into chitosan microspheres to provide protection, controlled release, and adhesion to the nasal mucosa may be a promising strategy to explore.

6.1.3.3 Chitosan microparticles

The use of chitosan as a biodegradable, biocompatible, and mucoadhesive carrier for nasal administration of peptides is a validated approach, as proven by the approval of miacalcin nasal spray [482,483,507]. In this study, low molecular weight chitosan was chosen for the preparation of microspheres *via* spray-drying, employing parameters previously optimised by our research group to yield particles with a diameter over 10 μm, necessary for avoiding deposition into the lungs [23]. Here, blank and loaded chitosan MPs were obtained in high yields – 75% and 68%, for the blank and loaded formulations, respectively. Scanning Electron Microscopy (SEM) imaging showed no significant difference between the diameter of blank MPs (9.00 ± 0.74 μm) and that of loaded MPs (9.55 ± 0.91 μm), yet being slightly lower than previously determined (10.7 ± 1.36 μm) [23]. Dissimilarities in particles morphology was observed by microscopic analysis, with some particles having a rounded shape and some presenting a wrinkled surface. The release study of P006 from chitosan microcarriers showed burst release over the first 30 min (~68% released) with only a small increase (~additional 6%) over the following 24 h. After hydration and swelling of the microspheres, the peptide was found to be free in solution as the chitosan was not crosslinked and the peptide was not entrapped in the nanospheres. The future possibility of loading the peptide into polymeric nanoparticles or preparing peptide-only nanostructures would slow down the release from the carriers.

6.2 Future work

In this project, important progress has been made towards the discovery of a potent peptide-based CGRP-R antagonist with drug-like properties. The lead candidate LJMU027 will be the subject of further lead-optimisation studies with the aim of reaching the pre-clinical and clinical stages of development for the treatment of migraine.

6.2.1.1 Optimisation of N-terminally modified analogues of P006

Strategies developed in this work to improve the drug-likeness of P006 brought to light the potential of N-terminal modifications to increase lipophilicity, proteolytic

stability, plasma protein binding, and self-assembly behaviour, without impacting on the activity against the CGRP-R. On this path, many strategies could be further explored to impact as little as possible on the overall structure while obtaining improved efficacy. N-terminal modifications which could be explored comprise smaller lipophilic alkyl appendages – e.g., N-acetylation (**103**), N-propylation (**104**), and N-isobutylation (**105**) – or other appendages – e.g., N-benzylurealation (**106**), N-dodecylurealation (**107**), N-aziridin-2-ol (**108**), N-3-(aziridine-2-yl)propanoylation (**109**), and cyclopentylurealation (**110**). These modifications are being currently explored by the Coxon Lab.

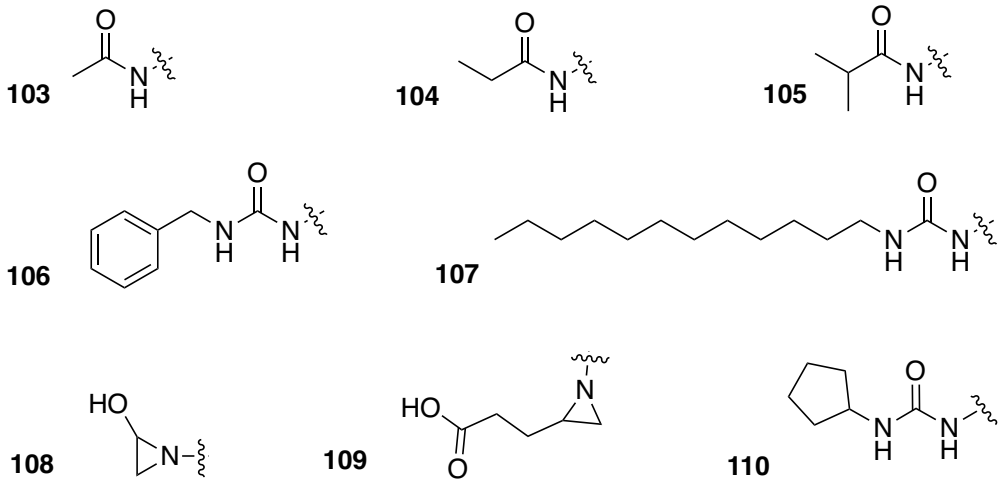

Figure 6.3. N-terminal modifications to explore in the future as alternatives to N-benzoylation of P006.

Moreover, as shown by LogD assessment, N-terminal appendages severely impact on the lipophilicity of the peptides, with possible solubility issues arising that may affect the feasibility of *in vivo* studies, as previously reported by Yan *et al.* [68]. Hence, these modifications could be moved to the side chain of a Lys coupled at the N-terminus, in place of Val28 (**111**), known to have little impact on the binding to the receptor. Leaving the N-terminus free would enhance water-solubility, while maintaining the moiety responsible for increased stability. However, the effect of these modifications should be carefully assessed as the relocation of the appendage

to the Lys side chain may not be efficacious in protecting the 'soft-spots' from aminopeptidases activity or may cause disruption to the receptor interactions.

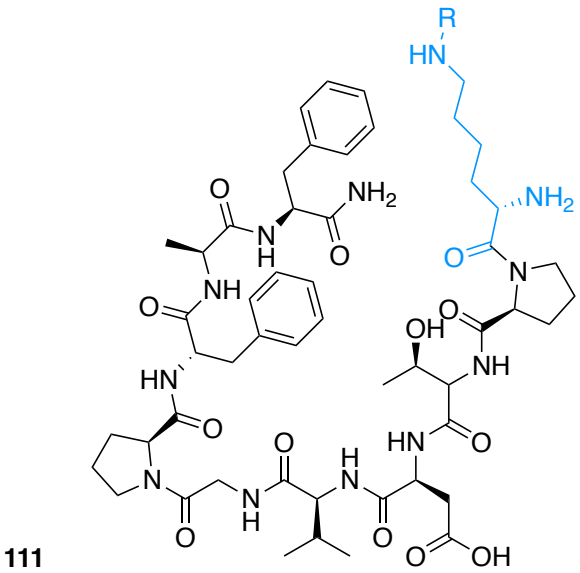

111

Figure 6.4. Chemical structure of P006 analogue with Lys in place of Val28. Lys is coloured in light blue.

6.2.1.2 Method development for peptide blood stability and plasma protein binding

The optimised methods described in Chapter 4 to assess blood stability and plasma protein binding of peptides could be validated by testing a library of approved peptide pharmaceuticals. In particular, for the determination of *in vitro* half-life, oxytocin (terminal half-life of 1-6 min), octreotide (terminal half-life of 1.5 hours), and liraglutide (terminal half-life of 13 hours) could be used to cover an array of peptides with different behaviours in *in vivo* metabolism studies. Moreover, plasma protein binding could be assessed *via* the in-house developed precipitation method for a small library of commercially available approved peptides with proven *in vivo* different extent of binding, such as bivalirudin (0%), eptifibatide (~25%), oxytocin (~30%), and liraglutide (>98%). If the values of estimated half-lives and plasma protein binding mirror the behaviour of these approved peptides *in vivo*, the methods would be recognised as reliable for pharmacokinetic properties evaluation of peptides.

6.2.1.3 Formulation and self-assembly

In this study, P006 and N-benzoyl derivatives have been observed to self-assemble into nanosized spherical structures in aqueous solutions. This could be exploited to prepare a delivery system composed by peptidic nanostructures loaded into chitosan microspheres. This should allow sufficient protection of the peptide from degradation (similarly to the role of polymeric NPs) as well as mucoadhesive properties and increased residence time in the nasal mucosa provided by the microcarrier.

6.2.1.4 In vivo studies

The *in vivo* activity of CGRP 27-37 derivatives was previously explored by our research group using a plasma protein extravasation (PPE) method in mouse models, showing a significant decrease in CGRP-induced PPE following CGRP 27-37 derivatives administration, indicative of decreased CGRP-induced vasodilation [23]. In addition, preliminary *in vivo* toxicity of P006 was examined in sheep through intravenous injection or nasal delivery of peptide-loaded chitosan microcarriers (Killoran *et al*., unpublished work). However, metabolites of the peptide were not detectable *ex vivo*, thus requiring further tests to confirm the hypothesis that the peptide is not toxic before moving to pre-clinical studies. Moreover, P006 could have incurred rapid degradation *in vivo*, explaining why this was not detectable in *ex vivo* blood samples. Hence, the administration of LJMU027, being more stable in blood, could be the next step of the *in vivo* testing. This peptide could be administered by IV injection, as highly stable to proteolytic digestion, as well as a dry powder for nasal delivery, composed by peptide nanoparticles in chitosan microspheres.

6.3 Conclusions

In this PhD thesis, common trends in approved peptide therapeutics and diagnostics have been explored. Among the successful strategies encountered, some of them were explored in our migraine drug discovery program.

In this work, novel peptide and peptidomimetic antagonists of the CGRP-R with improved drug-like properties have been developed, moving a big step towards the

discovery of novel therapies to treat migraine and conditions related to increase of CGRP levels in the body.

An inexpensive, fast, and facile method to assess blood stability of peptides was successfully optimised and validated. This method brought to light the liability of P006 (~5% intact after 60 min incubation in pooled aq. serum) and allowed the detection of the so-called 'soft-spots'. Here, the hypothesis was formed that judicious modifications could improve the proteolytic stability of the labile P006. Hence, our research was directed towards the discovery of potent serum-stable analogues of P006. Among them, the N-benzoylated analogue LJMU027 was found to be >90% intact after 60 min incubation in pooled aq. Serum.

Plasma protein binding of P006 and related analogues was studied with a range of commercially available kits and with an in-house method developed on the cast of the serum stability method. While commercially available kits suffered from drawbacks affecting the outcome, e.g., long incubation times required to reach equilibrium in the case of the dialysis method and nonspecific binding to the ultrafiltration membrane, the method developed in our lab did not require a membrane to separate bound and unbound fractions, and proved to be fast, facile, and reliable. This was used to compare the extent of binding of P006 and benzoylated analogues, discovering that, while P006 estimated binding capacity is <10%, even at high concentrations of HSA, the benzoylated analogues showed estimated binding affinity up to 80%, confirming the potential of the N-terminal moiety to improve binding to plasma proteins, expected to increase the *in vivo* efficacy of the drug.

Methods developed in this work could be generally applicable techniques for assessing the pharmacokinetic profile of peptides. The importance of efficient, fast, and accessible methods to assess blood stability and plasma protein binding is stressed by the increasing number of peptide drugs approvals together with the lack of methods tailored on peptides available in literature.

Finally, the discovery of the self-assembly behaviour of P006 and derivatives has opened the path of developing an all-peptide nano-formulation, which could be explored to protect the active peptide from degradation as well as to yield a

controlled release when administered *in vivo*. This could be then loaded into a polymeric microcarrier to obtain a dry powder administrable *via* a nasal device to increase patient compliance and reduce peripheral cardiovascular toxicity of the peptide medicine.

References

1 Yeh, W.Z., Blizzard, L. and Taylor, B. V. (2018) What Is the Actual Prevalence of Migraine? *Brain Behav.*, 8, e00950. https://doi.org/10.1002/BRB3.950.

2 Agosti, R. (2018) Migraine Burden of Disease: From the Patient's Experience to a Socio-Economic View. *Headache J. Head Face Pain*, 58, 17–32. https://doi.org/10.1111/HEAD.13301.

3 Goadsby, P.J., Lipton, R.B. and Ferrari, M.D. (2002) Migraine — Current Understanding and Treatment. Wood, A.J.J., Ed., *N. Engl. J. Med.*, 346, 257–270. https://doi.org/10.1056/NEJMra010917.

4 Stovner, L.J. (2018) Global, Regional, and National Burden of Migraine and Tension-Type Headache, 1990–2016: A Systematic Analysis for the Global Burden of Disease Study 2016. *Lancet Neurol.*, 17, 954–976. https://doi.org/10.1016/S1474-4422(18)30322-3.

5 Goadsby, P.J., Holland, P.R., Martins-Oliveira, M., Hoffmann, J., Schankin, C. and Akerman, S. (2017) Pathophysiology of Migraine: A Disorder of Sensory Processing. *Physiol. Rev.*, 97, 553–622. https://doi.org/10.1152/physrev.00034.2015.

6 Steiner, T.J., Stovner, L.J., Vos, T., Jensen, R. and Katsarava, Z. (2018) Migraine Is First Cause of Disability in under 50s: Will Health Politicians Now Take Notice? *J. Headache Pain*, 19, 1–4. https://doi.org/10.1186/S10194-018-0846-2/TABLES/2.

7 Buse, D.C., Fanning, K.M., Reed, M.L., Murray, S., Dumas, P.K., Adams, A.M. and Lipton, R.B. (2019) Life With Migraine: Effects on Relationships, Career, and Finances From the Chronic Migraine Epidemiology and Outcomes (CaMEO) Study. *Headache J. Head Face Pain*, 59, 1286–1299. https://doi.org/10.1111/HEAD.13613.

8 Leonardi, M. and Raggi, A. (2019) A Narrative Review on the Burden of Migraine: When the Burden Is the Impact on People's Life. *J. Headache Pain*, 20, 1–11. https://doi.org/10.1186/S10194-019-0993-0/FIGURES/2.

9 Bloudek, L.M., Stokes, M., Buse, D.C., Wilcox, T.K., Lipton, R.B., Goadsby, P.J., Varon, S.F., Blumenfeld, A.M., Katsarava, Z., Pascual, J., Lanteri-Minet, M.,

Cortelli, P., Martelletti, P., Varon, S.F., Stokes, M., Wilcox, Á.T.K., Buse, D.C., Lipton, Á.R.B., Goadsby, P.J., Blumenfeld, A.M., Katsarava, Z., Pascual, J., Lanteri-Minet, M., Cortelli, P. and Martelletti, P. (2012) Cost of Healthcare for Patients with Migraine in Five European Countries: Results from the International Burden of Migraine Study (IBMS). *J Headache Pain*, 13, 361–378. https://doi.org/10.1007/s10194-012-0460-7.

10 Kernick, D. (2020) Monoclonal Antibodies for Migraine Prevention: Hope, Hype, and Health Economy Challenge. *Br. J. Gen. Pract.*, 70, e523–e524. https://doi.org/10.3399/BJGP20X711833.

11 Steiner, T.J., Scher, A.I., Stewart, W.F., Kolodner, K., Liberman, J. and Lipton, R.B. (2003) The Prevalence and Disability Burden of Adult Migraine in England and Their Relationships to Age, Gender and Ethnicity. *Cephalalgia*, 23, 519–527. https://doi.org/10.1046/j.1468-2982.2003.00568.x.

12 Charles, A. (2018) The Pathophysiology of Migraine: Implications for Clinical Management. *Lancet Neurol.*, 17, 174–182. https://doi.org/10.1016/S1474-4422(17)30435-0.

13 Dodick, D.W. (2018) A Phase-by-Phase Review of Migraine Pathophysiology. *Headache J. Head Face Pain*, 58, 4–16. https://doi.org/10.1111/HEAD.13300.

14 Viana, M., Sprenger, T., Andelova, M. and Goadsby, P.J. (2013) The Typical Duration of Migraine Aura: A Systematic Review. *Cephalalgia*, 33, 483–490. https://doi.org/10.1177/0333102413479834.

15 Solomon, G.D. and Price, K.L. (1997) Burden of Migraine. *Pharmacoeconomics*, 11, 1–10. https://doi.org/10.2165/00019053-199700111-00003.

16 Olesen, J., Bousser, M.G., Diener, H.C., Dodick, D., First, M., Goadsby, P.J., Göbel, H., Lainez, M.J.A., Lance, J.W., Lipton, R.B., Nappi, G., Sakai, F., Schoenen, J., Silberstein, S.D. and Steiner, T.J. (2006) New Appendix Criteria Open for a Broader Concept of Chronic Migraine. *Cephalalgia*, 26, 742–746. https://doi.org/10.1111/j.1468-2982.2006.01172.x.

17 Silberstein, S.D. (2005) Chronic Daily Headache. *J. Osteopath. Med.*, 105, 23–29. https://doi.org/10.7556/JAOA.2005.20011.

18 Kelman, L. (2006) The Postdrome of the Acute Migraine Attack. *Cephalalgia*,

26, 214–220. https://doi.org/10.1111/J.1468-2982.2005.01026.X.

19 Buse, D.C., Greisman, J.D., Baigi, K. and Lipton, R.B. (2019) Migraine Progression: A Systematic Review. *Headache J. Head Face Pain*, 59, 306–338. https://doi.org/10.1111/HEAD.13459.

20 Hay, D.L., Garelja, M.L., Poyner, D.R. and Walker, C.S. (2018) Update on the Pharmacology of Calcitonin/CGRP Family of Peptides: IUPHAR Review 25. *Br. J. Pharmacol.*, 175, 3–17. https://doi.org/10.1111/bph.14075.

21 Ma, H. (2017) Calcitonin Gene-Related Peptide (CGRP).

22 Lang, M., De Pol, S., Baldauf, C., Hofmann, H.-J., Reiser, O. and Beck-Sickinger, A.G. (2006) Identification of the Key Residue of Calcitonin Gene Related Peptide (CGRP) 27-37 to Obtain Antagonists with Picomolar Affinity at the CGRP Receptor. https://doi.org/10.1021/jm050613s.

23 von Mentzer, B., Russo, A.F., Zhang, Z., Kuburas, A., Killoran, P.M., D'Aloisio, V., Nizic, L., Capel, V., Kendall, D.A., Coxon, C.R. and Hutcheon, G.A. (2020) A CGRP Receptor Antagonist Peptide Formulated for Nasal Administration to Treat Migraine. *J. Pharm. Pharmacol.*, 72, jphp.13317. https://doi.org/10.1111/jphp.13317.

24 Cottrell, G.S. (2018) CGRP Receptor Signalling Pathways. *Handb. Exp. Pharmacol.*, 255, 37–64. https://doi.org/10.1007/164_2018_130.

25 Walker, C.S., Raddant, A.C., Woolley, M.J., Russo, A.F. and Hay, D.L. (2018) CGRP Receptor Antagonist Activity of Olcegepant Depends on the Signalling Pathway Measured. *Cephalalgia*, 38, 437–451. https://doi.org/10.1177/0333102417691762.

26 McLatchie, L.M., Fraser, N.J., Main, M.J., Wise, A., Brown, J., Thompson, N., Solari, R., Lee, M.G. and Foord, S.M. (1998) RAMPS Regulate the Transport and Ligand Specificity of the Calcitonin- Receptor-like Receptor. *Nature*, 393, 333–339. https://doi.org/10.1038/30666.

27 Aiyar, N., Disa, J., Stadel, J.M. and Lysko, P.G. (1999) Calcitonin Gene-Related Peptide Receptor Independently Stimulates 3',5'-Cyclic Adenosine Monophosphate and Ca2+ Signaling Pathways. *Mol. Cell. Biochem. 1999 1971*, 197, 179–185. https://doi.org/10.1023/A:1006962221332.

28 Goadsby, P.J., Edvinsson, L. and Ekman, R. (1988) Release of Vasoactive Peptides in the Extracerebral Circulation of Humans and the Cat during Activation of the Trigeminovascular System. *Ann. Neurol.*, 23, 193–196. https://doi.org/10.1002/ana.410230214.

29 Lassen, L., Haderslev, P., Jacobsen, V., Iversen, H., Sperling, B. and Olesen, J. (2002) Cgrp May Play A Causative Role in Migraine. *Cephalalgia*, 22, 54–61. https://doi.org/10.1046/j.1468-2982.2002.00310.x.

30 Bellamy, J.L., Cady, R.K. and Durham, P.L. (2006) Salivary Levels of CGRP and VIP in Rhinosinusitis and Migraine Patients. *Headache*, 46, 24–33. https://doi.org/10.1111/j.1526-4610.2006.00294.x.

31 Cady, R.K., Vause, C. V., Ho, T.W., Bigal, M.E. and Durham, P.L. (2009) Elevated Saliva Calcitonin Gene-Related Peptide Levels during Acute Migraine Predict Therapeutic Response to Rizatriptan. *Headache*, 49, 1258–1266. https://doi.org/10.1111/j.1526-4610.2009.01523.x.

32 Jang, M.U., Park, J.W., Kho, H.S., Chung, S.C. and Chung, J.W. (2011) Plasma and Saliva Levels of Nerve Growth Factor and Neuropeptides in Chronic Migraine Patients. *Oral Dis.*, 17, 187–193. https://doi.org/10.1111/j.1601-0825.2010.01717.x.

33 Van Dongen, R.M., Zielman, R., Noga, M., Dekkers, O.M., Hankemeier, T., Van Den Maagdenberg, A.M.J.M., Terwindt, G.M. and Ferrari, M.D. (2017) Migraine Biomarkers in Cerebrospinal Fluid: A Systematic Review and Meta-Analysis. *Cephalalgia*, 37, 49–63. https://doi.org/10.1177/0333102415625614.

34 Kamm, K., Straube, A. and Ruscheweyh, R. (2019) Calcitonin Gene-Related Peptide Levels in Tear Fluid Are Elevated in Migraine Patients Compared to Healthy Controls. *Cephalalgia*, 39, 1535–1543. https://doi.org/10.1177/0333102419856640.

35 Hansen, J.M., Hauge, A.W., Olesen, J. and Ashina, M. (2010) Calcitonin Gene-Related Peptide Triggers Migraine-like Attacks in Patients with Migraine with Aura. *Cephalalgia*, 30, 1179–1186. https://doi.org/10.1177/0333102410368444.

36 Fahrenkrug, J. (2009) VIP and PACAP. *Results Probl. Cell Differ.*, 50, 1–20. https://doi.org/10.1007/400_2009_24.

37 Schytz, H.W., Olesen, J. and Ashina, M. (2010) The PACAP Receptor: A Novel Target for Migraine Treatment. *Neurotherapeutics*, 7, 191–196. https://doi.org/10.1016/J.NURT.2010.02.003.

38 Edvinsson, L., Tajti, J., Szalárdy, L. and Vécsei, L. (2018) PACAP and Its Role in Primary Headaches. *J. Headache Pain*, 19, 1–7. https://doi.org/10.1186/S10194-018-0852-4/FIGURES/1.

39 Amin, F.M., Hougaard, A., Schytz, H.W., Asghar, M.S., Lundholm, E., Parvaiz, A.I., De Koning, P.J.H., Andersen, M.R., Larsson, H.B.W., Fahrenkrug, J., Olesen, J. and Ashina, M. (2014) Investigation of the Pathophysiological Mechanisms of Migraine Attacks Induced by Pituitary Adenylate Cyclase-Activating Polypeptide-38. *Brain*, 137, 779–794. https://doi.org/10.1093/BRAIN/AWT369.

40 Schytz, H.W., Birk, S., Wienecke, T., Kruuse, C., Olesen, J. and Ashina, M. (2009) PACAP38 Induces Migraine-like Attacks in Patients with Migraine without Aura. *Brain*, 132, 16–25. https://doi.org/10.1093/BRAIN/AWN307.

41 Zagami, A.S., Edvinsson, L. and Goadsby, P.J. (2014) Pituitary Adenylate Cyclase Activating Polypeptide and Migraine. *Ann. Clin. Transl. Neurol.*, 1, 1036–1040. https://doi.org/10.1002/ACN3.113.

42 Wang, J., Song, X., Zhang, D., Chen, X., Li, X., Sun, Y., Li, C., Song, Y., Ding, Y., Ren, R., Harrington, E.H., Hu, L.A., Zhong, W., Xu, C., Huang, X., Wang, H.W. and Ma, Y. (2020) Cryo-EM Structures of PAC1 Receptor Reveal Ligand Binding Mechanism. *Cell Res. 2020 305*, 30, 436–445. https://doi.org/10.1038/s41422-020-0280-2.

43 Edvinsson, L. (2015) PACAP and Its Receptors in Migraine Pathophysiology: Commentary on Walker et Al., Br J Pharmacol 171: 1521–1533. *Br. J. Pharmacol.*, 172, 4782. https://doi.org/10.1111/BPH.12772.

44 Edvinsson, L., Haanes, K.A., Warfvinge, K. and Krause, Di.N. (2018) CGRP as the Target of New Migraine Therapies - Successful Translation from Bench to Clinic. *Nat. Rev. Neurol.*, 14, 338–350. https://doi.org/10.1038/s41582-018-

0003-1.

45 Charles, A. and Pozo-Rosich, P. (2019) Targeting Calcitonin Gene-Related Peptide: A New Era in Migraine Therapy. *Lancet*, 394, 1765–1774. https://doi.org/10.1016/S0140-6736(19)32504-8.

46 Andreou, A.P., Fuccaro, M. and Lambru, G. (2020) The Role of Erenumab in the Treatment of Migraine. *Ther. Adv. Neurol. Disord.*, 13, 1756286420927119. https://doi.org/10.1177/1756286420927119.

47 Tso, A.R. and Goadsby, P.J. (2017) Anti-CGRP Monoclonal Antibodies: The Next Era of Migraine Prevention? *Curr Treat Options Neurol*, 19, 27. https://doi.org/10.1007/s11940-017-0463-4.

48 Diener, H.-C., Förderreuther, S., Gaul, C., Giese, F., Hamann, T., Holle-Lee, D., Jürgens, T.P., Kamm, K., Kraya, T., Lampl, C., May, A., Reuter, U., Scheffler, A. and Tfelt-Hansen, P. (2020) Prevention of Migraine with Monoclonal Antibodies against CGRP or the CGRP Receptor. *Neurol. Res. Pract. 2020 21*, 2, 1–6. https://doi.org/10.1186/S42466-020-00057-1.

49 Negro, A. and Martelletti, P. (2019) Gepants for the Treatment of Migraine. *https://doi.org/10.1080/13543784.2019.1618830*, 28, 555–567. https://doi.org/10.1080/13543784.2019.1618830.

50 Cooper, W., Doty, E.G., Hochstetler, H., Hake, A. and Martin, V. (2020) The Current State of Acute Treatment for Migraine in Adults in the United States. *https://doi.org/10.1080/00325481.2020.1767402*, 132, 581–589. https://doi.org/10.1080/00325481.2020.1767402.

51 Sparrow, A.M. and Searles, J.W. (2019) The Market for Migraine Drugs. *Nat. Rev. Drug Discov.*, 18. https://doi.org/10.1038/d41573-018-00014-3.

52 Ramadan, N.M. and Buchanan, T.M. (2006) New and Future Migraine Therapy. *Pharmacol. Ther.*, 112, 199–212. https://doi.org/10.1016/J.PHARMTHERA.2005.04.010.

53 Ong, J.J.Y. and De Felice, M. (2017) Migraine Treatment: Current Acute Medications and Their Potential Mechanisms of Action. *Neurother. 2017 152*, 15, 274–290. https://doi.org/10.1007/S13311-017-0592-1.

54 Saper, J.R. and Silberstein, S. (2006) Pharmacology of Dihydroergotamine and

Evidence for Efficacy and Safety in Migraine. *Headache J. Head Face Pain*, 46, S171–S181. https://doi.org/10.1111/J.1526-4610.2006.00601.X.

55 Antonaci, F., Ghiotto, N., Wu, S., Pucci, E. and Costa, A. (2016) Recent Advances in Migraine Therapy. *Springerplus*, 5, 1–14. https://doi.org/10.1186/S40064-016-2211-8/TABLES/6.

56 Loder, E., Rizzoli, P., Loder, E. and Rizzoli, P. (2018) Pharmacologic Prevention of Migraine: A Narrative Review of the State of the Art in 2018. *Headache J. Head Face Pain*, 58, 218–229. https://doi.org/10.1111/HEAD.13375.

57 Schwedt, T.J. (2018) Preventive Therapy of Migraine. *Contin. Lifelong Learn. Neurol.*, 24, 1052–1065. https://doi.org/10.1212/CON.0000000000000635.

58 Ha, H., Gonzalez, A. and Rosa, S. (2019) Migraine Headache Prophylaxis. *Am. Fam. Physician*, 99, 17–24. www.aafp.org/afpAmericanFamilyPhysician17https://familydoctor.org/condition/migraines/.

59 Danesh, A. and Gottschalk, P.C.H. (2019) Beta-Blockers for Migraine Prevention: A Review Article. *Curr. Treat. Options Neurol.*, 21, 1–13. https://doi.org/10.1007/S11940-019-0556-3/TABLES/2.

60 Bagnato, F. and Good, J. (2016) The Use of Antiepileptics in Migraine Prophylaxis. *Headache J. Head Face Pain*, 56, 603–615. https://doi.org/10.1111/HEAD.12781.

61 Becker, W.J. (2015) Acute Migraine Treatment in Adults. *Headache J. Head Face Pain*, 55, 778–793. https://doi.org/10.1111/HEAD.12550.

62 Modi, S., Lowder, D.M. and Brody, P.S. (2006) Medications for Migraine Prophylaxis. *Am. Fam. Physician*, 73, 72–78. www.aafp.org/afp.

63 Lambru, G., Andreou, A.P., Guglielmetti, M. and Martelletti, P. (2018) Emerging Drugs for Migraine Treatment: An Update. *Expert Opin. Emerg. Drugs*, 23, 301–318. https://doi.org/10.1080/14728214.2018.1552939.

64 Mavridis, T., Deligianni, C.I., Karagiorgis, G., Daponte, A., Breza, M. and Mitsikostas, D.D. (2021) Monoclonal Antibodies Targeting CGRP: From Clinical Studies to Real-World Evidence—What Do We Know So Far? *Pharm. 2021, Vol. 14, Page 700*, 14, 700. https://doi.org/10.3390/PH14070700.

65 Schuster, N.M. and Rapoport, A.M. (2017) Calcitonin Gene-Related Peptide-Targeted Therapies for Migraine and Cluster Headache: A Review. *Clin. Neuropharmacol.*, 40, 169–174. https://doi.org/10.1097/WNF.0000000000000227.

66 Rist, B., Entzeroth, M. and Beck-Sickinger, A.G. (1998) From Micromolar to Nanomolar Affinity: A Systematic Approach To Identify the Binding Site of CGRP at the Human Calcitonin Gene-Related Peptide 1 Receptor†. https://doi.org/10.1021/JM970533R.

67 Rist, B., Lacroix, J.S., Entzeroth, M., Doods, H.N. and Beck-Sickinger, A.G. (1999) CGRP 27–37 Analogues with High Affinity to the CGRP1 Receptor Show Antagonistic Properties in a Rat Blood Flow Assay. *Regul. Pept.*, 79, 153–158. https://doi.org/10.1016/S0167-0115(98)00159-1.

68 Yan, L.Z., Johnson, K.W., Rothstein, E., Flora, D., Edwards, P., Li, B., Li, J., Lynch, R., Vaughn, R., Clemens-Smith, A., McCarty, D., Chow, C., McKnight, K.L., Lu, J., Nisenbaum, E.S. and Mayer, J.P. (2011) Discovery of Potent, Cyclic Calcitonin Gene-Related Peptide Receptor Antagonists. *J. Pept. Sci.*, 17, 383–386. https://doi.org/10.1002/psc.1358.

69 Rapoport, A. and Winner, P. (2006) Nasal Delivery of Antimigraine Drugs: Clinical Rationale and Evidence Base. *Headache J. Head Face Pain*, 46, S192–S201. https://doi.org/10.1111/J.1526-4610.2006.00603.X.

70 Vlieghe, P., Lisowski, V., Martinez, J. and Khrestchatisky, M. (2010) Synthetic Therapeutic Peptides: Science and Market. *Drug Discov. Today*, 15, 40–56. https://doi.org/10.1016/j.drudis.2009.10.009.

71 Craik, D.J., Fairlie, D.P., Liras, S. and Price, D. (2013) The Future of Peptide-Based Drugs. *Chem. Biol. Drug Des.*, 81, 136–147. https://doi.org/10.1111/cbdd.12055.

72 D'Hondt, M., Bracke, N., Taevernier, L., Gevaert, B., Verbeke, F., Wynendaele, E. and De Spiegeleer, B. (2014) Related Impurities in Peptide Medicines. *J. Pharm. Biomed. Anal.*, 101, 2–30. https://doi.org/10.1016/j.jpba.2014.06.012.

73 Erak, M., Bellmann-Sickert, K., Els-Heindl, S. and Beck-Sickinger, A.G. (2018) Peptide Chemistry Toolbox – Transforming Natural Peptides into Peptide

Therapeutics. *Bioorganic Med. Chem.*, 26, 2759–2765. https://doi.org/10.1016/j.bmc.2018.01.012.

74 Henninot, A., Collins, J.C. and Nuss, J.M. (2018) The Current State of Peptide Drug Discovery: Back to the Future? *J. Med. Chem.*, 61, 1382–1414. https://doi.org/10.1021/acs.jmedchem.7b00318.

75 Lau, J.L. and Dunn, M.K. (2018) Therapeutic Peptides: Historical Perspectives, Current Development Trends, and Future Directions. *Bioorganic Med. Chem.*, 26, 2700–2707. https://doi.org/10.1016/j.bmc.2017.06.052.

76 FDA.Gov. https://www.fda.gov/drugs/regulatory-science-action/impact-story-developing-tools-evaluate-complex-drug-products-peptides.

77 EMA-European Medicines Agency. https://www.ema.europa.eu/en.

78 PMDA - Pharmaceuticals and Medical Devices Agency. https://www.pmda.go.jp/english/index.html.

79 Tsomaia, N. (2015) European Journal of Medicinal Chemistry Peptide Therapeutics: Targeting the Undruggable Space. *Eur. J. Med. Chem.*, 94, 459–470.

80 Baig, M.H., Ahmad, K., Rabbani, G. and Choi, I. (2018) Use of Peptides for the Management of Alzheimer's Disease: Diagnosis and Inhibition. *Front. Aging Neurosci.*, 0, 21. https://doi.org/10.3389/FNAGI.2018.00021.

81 Ferlay, J., Soerjomataram, I., Dikshit, R., Eser, S., Mathers, C., Rebelo, M., Parkin, D.M., Forman, D. and Bray, F. (2015) Cancer Incidence and Mortality Worldwide: Sources, Methods and Major Patterns in GLOBOCAN 2012. *Int. J. Cancer*, 136, E359–E386. https://doi.org/10.1002/ijc.29210.

82 Daviglus, M.L., Lloyd-Jones, D.M. and Pirzada, A. (2006, September 20) Preventing Cardiovascular Disease in the 21st Century: Therapeutic and Preventive Implications of Current Evidence. American Journal of Cardiovascular Drugs, 87–101. https://doi.org/10.2165/00129784-200606020-00003.

83 Zimmet, P.Z., Magliano, D.J., Herman, W.H. and Shaw, J.E. (2014, January 1) Diabetes: A 21st Century Challenge. The Lancet Diabetes and Endocrinology, 56–64. https://doi.org/10.1016/S2213-8587(13)70112-8.

84 Peptide Therapeutics Market | Growth, Trends, COVID-19 Impact, and Forecasts (2021 - 2026) - Mordor Intelligence. https://www.mordorintelligence.com/industry-reports/peptide-therapeutics-market.

85 Nirmatrelvir: Uses, Interactions, Mechanism of Action | DrugBank Online. https://go.drugbank.com/drugs/DB16691.

86 Coronavirus (COVID-19) Update: FDA Authorizes First Oral Antiviral for Treatment of COVID-19 | FDA. https://www.fda.gov/news-events/press-announcements/coronavirus-covid-19-update-fda-authorizes-first-oral-antiviral-treatment-covid-19.

87 ClinicalTrials.Gov. https://www.clinicaltrials.gov/.

88 Global Peptide Therapeutics Market (2021 to 2025) - by Type, Synthesis Technology, Manufacturing Type, Application and Region - ResearchAndMarkets.Com | Business Wire. https://www.businesswire.com/news/home/20210813005281/en/Global-Peptide-Therapeutics-Market-2021-to-2025---by-Type-Synthesis-Technology-Manufacturing-Type-Application-and-Region---ResearchAndMarkets.com.

89 Reubsaet, J.L.E., Beijnen, J.H., Bult, A., Van Maanen, R.J., Marchal, J.A.D. and Underberg, W.J.M. (1998) Analytical Techniques Used to Study the Degradation of Proteins and Peptides: Chemical Instability. *J. Pharm. Biomed. Anal.*, 17, 955–978. https://doi.org/10.1016/S0731-7085(98)00063-6.

90 Maher, S. and Brayden, D.J. (2012) Overcoming Poor Permeability: Translating Permeation Enhancers for Oral Peptide Delivery. *Drug Discov. Today Technol.*, 9, e113–e119. https://doi.org/10.1016/J.DDTEC.2011.11.006.

91 McNaught, A.D. and A. Wilkinson. (1997) IUPAC. Compendium of Chemical Terminology, 2nd Ed. (the “Gold Book”). . . Blackwell Scientific Publications, Oxford. https://goldbook.iupac.org/terms/view/P04479.

92 IUPAC-IUB Joint Commission on Biochemical Nomenclature (JCBN). (1984) Nomenclature and Symbolism for Amino Acids and Peptides: Recommendations 1983. *Eur. J. Biochem.*, 138, 9–37. https://doi.org/10.1111/j.1432-1033.1984.tb07877.x.

93 Wu, L.C. (2013) Regulatory Considerations for Peptide Drug Products. 1–30.

94 Uhlig, T., Kyprianou, T., Martinelli, F.G., Oppici, C.A., Heiligers, D., Hills, D., Calvo, X.R. and Verhaert, P. (2014) The Emergence of Peptides in the Pharmaceutical Business: From Exploration to Exploitation. *EuPA Open Proteomics*, 4, 58–69. https://doi.org/10.1016/j.euprot.2014.05.003.

95 Mathur, D., Prakash, S., Anand, P., Kaur, H., Agrawal, P., Mehta, A., Kumar, R., Singh, S. and Raghava, G.P.S. (2016) PEPlife : A Repository of the Half- Life of Peptides. *Sci. Rep.*, 1–7.

96 Usmani, S.S., Bedi, G., Samuel, J.S., Singh, S., Kalra, S., Kumar, P., Ahuja, A.A., Sharma, M., Gautam, A. and Raghava, G.P.S. (2017) THPdb: Database of FDA-Approved Peptide and Protein Therapeutics. *PLoS One*, 12, 1–12. https://doi.org/10.1371/journal.pone.0181748.

97 Davenport, A.P., Scully, C.C.G., de Graaf, C., Brown, A.J.H. and Maguire, J.J. (2020) Advances in Therapeutic Peptides Targeting G Protein-Coupled Receptors. *Nat. Rev. Drug Discov.*, 19, 389–413. https://doi.org/10.1038/s41573-020-0062-z.

98 Lipinski, C.A., Lombardo, F., Dominy, B.W. and Feeney, P.J. (1997) Experimental and Computational Approaches to Estimate Solubility and Permeability in Drug Discovery and Development Settings. *Adv. Drug Deliv. Rev.*, 3–25.

99 Wager, T.T., Hou, X., Verhoest, P.R. and Villalobos, A. (2016) Central Nervous System Multiparameter Optimization Desirability: Application in Drug Discovery. *ACS Chem. Neurosci.*, 7, 767–775. https://doi.org/10.1021/acschemneuro.6b00029.

100 Tyagi, M., Begnini, F., Poongavanam, V., Doak, B.C. and Kihlberg, J. (2020) Drug Syntheses Beyond the Rule of 5. *Chem. - A Eur. J.*, 26, 49–88. https://doi.org/10.1002/chem.201902716.

101 Wager, T.T., Chandrasekaran, R.Y., Hou, X., Troutman, M.D., Verhoest, P.R., Villalobos, A. and Will, Y. (2010) Defining Desirable Central Nervous System Drug Space through the Alignment of Molecular Properties, in Vitro ADME, and Safety Attributes. *ACS Chem. Neurosci.*, 1, 420–434.

https://doi.org/10.1021/CN100007X.

102 Hansch, C. and Clayton, J.M. (1973) Lipophilic Character and Biological Activity of Drugs II: The Parabolic Case. *J. Pharm. Sci.*, 62, 1–21. https://doi.org/10.1002/JPS.2600620102.

103 Di, L. and Kerns, E.H. (2016) Lipophilicity. *Drug-Like Prop.*, 39–50. https://doi.org/10.1016/B978-0-12-801076-1.00005-8.

104 Knudsen, L.B. and Lau, J. (2019) The Discovery and Development of Liraglutide and Semaglutide. *Front. Endocrinol. (Lausanne).*, 0, 155. https://doi.org/10.3389/FENDO.2019.00155.

105 Mannhold, R., Poda, G.I., Ostermann, C. and Tetko, I. V. (2009) Calculation of Molecular Lipophilicity: State-of-the-Art and Comparison of Log P Methods on More than 96,000 Compounds. *J. Pharm. Sci.*, 98, 861–893. https://doi.org/10.1002/JPS.21494.

106 Viswanadhan, V.N., Ghose, A.K., Revankar, G.R. and Robins, R.K. (1989) Atomic Physicochemical Parameters for Three Dimensional Structure Directed Quantitative Structure-Activity Relationships. 4. Additional Parameters for Hydrophobic and Dispersive Interactions and Their Application for an Automated Superposition of Certain Naturally Occurring Nucleoside Antibiotics. *J. Chem. Inf. Comput. Sci.*, 29, 163–172. https://doi.org/10.1021/CI00063A006.

107 LogP Plugin | ChemAxon Docs. https://docs.chemaxon.com/display/docs/logp-plugin.md.

108 Tan, N.C., Yu, P., Kwon, Y.U. and Kodadek, T. (2008) High-Throughput Evaluation of Relative Cell Permeability between Peptoids and Peptides. *Bioorganic Med. Chem.*, 16, 5853–5861. https://doi.org/10.1016/j.bmc.2008.04.074.

109 BioByte. http://www.biobyte.com/.

110 N.A. (1999) ClogP Manual Section 1: Tutorials Introduction to ClogP. *BioByte Corp.*

111 Go.DrugBank. https://go.drugbank.com/.

112 Drug Central. http://drugcentral.org.

113 National Center for Advancing Translational Sciences NIH. https://drugs.ncats.io.

114 Drugs.Com. https://www.drugs.com.

115 Lehninger, A.L., Cox, M.M. and Nelson, D.L. (2000) Lehninger Principles of Biochemistry.

116 Chemicalize. https://chemicalize.com/.

117 ACD/I-Lab. https://ilab.acdlabs.com/iLab2/.

118 PubChem. https://pubchem.ncbi.nlm.nih.gov/.

119 Thomas, A., Deshayes, S., Decaffmeyer, M., Van Eyck, M.H., Charloteaux, B. and Brasseur, R. (2006) Prediction of Peptide Structure: How Far Are We? *Proteins Struct. Funct. Genet.*, 65, 889–897. https://doi.org/10.1002/PROT.21151.

120 Chen, C.H. and Lu, T.K. (2020) Development and Challenges of Antimicrobial Peptides for Therapeutic Applications. *Antibiot. 2020, Vol. 9, Page 24*, 9, 24. https://doi.org/10.3390/ANTIBIOTICS9010024.

121 Walther, F.J., Gordon, L.M. and Waring, A.J. (2016) Design of Surfactant Protein B Peptide Mimics Based on the Saposin Fold for Synthetic Lung Surfactants. *Biomed. Hub*, 1, 1–21. https://doi.org/10.1159/000451076.

122 Yin, N., Brimble, M.A., Harris, P.W. and Wen, J. (2014) Enhancing the Oral Bioavailability of Peptide Drugs by Using Chemical Modification and Other Approaches. *Med. Chem. (Los. Angeles).*, 4, 763–769. https://doi.org/10.4172/2161-0444.1000227.

123 Chanson, P., Tiit, J. and Harris, A.G. (1993) Clinical Pharmacokinetics of Octreotide: Therapeutic Applications in Patients with Pituitary Tumours. Clinical Pharmacokinetics, 375–391. https://doi.org/10.2165/00003088-199325050-00004.

124 O'Toole, T.J. and Sharma, S. (2019) Physiology, Somatostatin. StatPearls. http://www.ncbi.nlm.nih.gov/pubmed/30855911.

125 Hodgson, D.R.W. and Sanderson, J.M. (2004) The Synthesis of Peptides and Proteins Containing Non-Natural Amino Acids. *Chem. Soc. Rev.*, 33, 422–430. https://doi.org/10.1039/b312953p.

126 Hohsaka, T. and Sisido, M. (2002, December 1) Incorporation of Non-Natural Amino Acids into Proteins. Current Opinion in Chemical Biology, 809–815. https://doi.org/10.1016/S1367-5931(02)00376-9.

127 Pollegioni, L. and Servi, S. (2012) Unnatural Amino Acids. Methods in Molecular Biology.

128 Mant, C.T., Jiang, Z., Gera, L., Davis, T., Nelson, K.L., Bevers, S. and Hodges, R.S. (2019) De Novo Designed Amphipathic α-Helical Antimicrobial Peptides Incorporating Dab and Dap Residues on the Polar Face to Treat the Gram-Negative Pathogen, Acinetobacter Baumannii. *J. Med. Chem.*, 62, 3354–3366. https://doi.org/10.1021/acs.jmedchem.8b01785.

129 Lu, J., Xu, H., Xia, J., Ma, J., Xu, J., Li, Y. and Feng, J. (2020) D- and Unnatural Amino Acid Substituted Antimicrobial Peptides With Improved Proteolytic Resistance and Their Proteolytic Degradation Characteristics. *Front. Microbiol.*, 11, 563030. https://doi.org/10.3389/fmicb.2020.563030.

130 Witkowska, E., Orłowska, A., Sagan, B., Smoluch, M. and Izdebski, J. (2001) Tryptic Hydrolysis of HGH-RH(1-29)-NH2 Analogues Containing Lys or Orn in Positions 12 and 21. *J. Pept. Sci.*, 7, 166–172. https://doi.org/10.1002/psc.316.

131 Inouy, K., Sakakibara, S. and Prockop, D.J. (1976) Effects of the Stereo-Configuration of the Hydroxyl Group in 4-Hydroxyproline on the Triple-Helical Structures Formed by Homogeneous Peptides Resembling Collagen. *BBA - Protein Struct.*, 420, 133–141. https://doi.org/10.1016/0005-2795(76)90352-4.

132 Meyer, D., Mutschler, C., Robertson, I., Batt, A. and Tatko, C. (2013) Aromatic Interactions with Naphthylalanine in a *β* -Hairpin Peptide. *J. Pept. Sci.*, 19, 277–282. https://doi.org/10.1002/psc.2496.

133 Sidransky, H., Verney, E. and Kurl, R. (1990) Comparison of Effects of L-Tryptophan and a Tryptophan Analog, D,L-β-(1-Naphthyl)Alanine, on Processes Relating to Hepatic Protein Synthesis in Rats. *J. Nutr.*, 120, 1157–1162. https://doi.org/10.1093/jn/120.10.1157.

134 Sidransky, H. and Verney, E. (1996) Influence of L-Alanine on Effects Induced by L-Tryptophan on Rat Liver. *J. Nutr. Biochem.*, 7, 200–206.

https://doi.org/10.1016/0955-2863(96)00010-1.

135 Rodriguez, M., Bernad, N., Galas, M., Lignon, M., Laur, J., Aumelas, A. and Martinez, J. (1991) Synthesis and Biological Activities of Cholecystokinin Analogues Substituted in Position 30 by 3-(1-Naphthyl)-l-Alanine [Nal(1)] or 3-(2-Naphthyl)-l-Alanine [Nal(2)]. *Eur. J. Med. Chem.*, 26, 245–253. https://doi.org/10.1016/0223-5234(91)90056-S.

136 Zhang, L. and Bulaj, G. (2012) Converting Peptides into Drug Leads by Lipidation. *Curr. Med. Chem.*, 19, 1602–1618. https://doi.org/10.2174/092986712799945003.

137 Moradi, S.V., Hussein, W.M., Varamini, P., Simerska, P. and Toth, I. (2016, April 1) Glycosylation, an Effective Synthetic Strategy to Improve the Bioavailability of Therapeutic Peptides. Chemical Science, 2492–2500. https://doi.org/10.1039/c5sc04392a.

138 Hui, H., Farilla, L., Merkel, P. and Perfetti, R. (2002) The Short Half-Life of Glucagon-like Peptide-1 in Plasma Does Not Reflect Its Long-Lasting Beneficial Effects. *Eur. J. Endocrinol.*, 146, 863–869. https://doi.org/10.1530/EJE.0.1460863.

139 D'Aloisio, V., Dognini, P., Hutcheon, G.A. and Coxon, C.R. (2021) PepTherDia: Database and Structural Composition Analysis of Approved Peptide Therapeutics and Diagnostics. *Drug Discov. Today*, 26, 1409–1419. https://doi.org/10.1016/J.DRUDIS.2021.02.019.

140 DeFrees, S. (2007, July 23) Glycosylation of Peptides via O-Linked Glycosylation Sequences.

141 Akhilesh Kumar and Anand K. Bachhawat. (2012) Pyroglutamic Acid: Throwing Light on a Lightly Studied Metabolite on JSTOR. *Curr. Sci.*, 102, 288–297. https://www.jstor.org/stable/24083854?seq=1.

142 Garden, R.W., Moroz, T.P., Gleeson, J.M., Floyd, P.D., Li, L., Rubakhin, S.S. and Sweedler, J. V. (1999) Formation of N-Pyroglutamyl Peptides from N-Glu and N-Gln Precursors in Aplysia Neurons. *J. Neurochem.*, 72, 676–681. https://doi.org/10.1046/j.1471-4159.1999.0720676.x.

143 Kehlen, A., Haegele, M., Böhme, L., Cynis, H., Hoffmann, T. and Demuth, H.U.

(2017) N-Terminal Pyroglutamate Formation in CX3CL1 Is Essential for Its Full Biologic Activity. *Biosci. Rep.*, 37, 20170712. https://doi.org/10.1042/BSR20170712.

144 Shah, P. and Westwell, A.D. (2007) The Role of Fluorine in Medicinal Chemistry. *J. Enzyme Inhib. Med. Chem.*, 22, 527–540. https://doi.org/10.1080/14756360701425014.

145 Faulds, D., Goa, K.L. and Benfield, P. (1993) Cyclosporin: A Review of Its Pharmacodynamic and Pharmacokinetic Properties, and Therapeutic Use in Immunoregulatory Disorders. *Drugs*, 45, 953–1040. https://doi.org/10.2165/00003495-199345060-00007.

146 Novartis. (1988) Sandimmune. Intensive Therapy and Clinical Monitoring, 172.

147 Thorstholm, L. and Craik, D.J. (2012) Discovery and Applications of Naturally Occurring Cyclic Peptides. *Drug Discov. Today Technol.*, 9, e13–e21. https://doi.org/10.1016/j.ddtec.2011.07.005.

148 Qvit, N., Rubin, S.J.S., Urban, T.J., Mochly-Rosen, D. and Gross, E.R. (2017) Peptidomimetic Therapeutics: Scientific Approaches and Opportunities. *Drug Discov. Today*. https://doi.org/10.1016/j.drudis.2016.11.003.

149 Hill, T.A., Shepherd, N.E., Diness, F. and Fairlie, D.P. (2014) Constraining Cyclic Peptides to Mimic Protein Structure Motifs. *Angew. Chemie - Int. Ed.*, 53, 13020–13041. https://doi.org/10.1002/anie.201401058.

150 Lenci, E. and Trabocchi, A. (2020) Peptidomimetic Toolbox for Drug Discovery. *Chem. Soc. Rev.*, 49, 3262–3277. https://doi.org/10.1039/d0cs00102c.

151 Lambert, J.N., Mitchell, J.P. and Roberts, K.D. (2001) The Synthesis of Cyclic Peptides. *J. Chem. Soc. Perkin 1*, 471–484. https://doi.org/10.1039/b001942i.

152 Tapeinou, A., Matsoukas, M.-T., Simal, C. and Tselios, T. (2015) Review Cyclic Peptides on a Merry-Go-Round; towards Drug Design. *Biopolymers*, 104, 453–461. https://doi.org/10.1002/bip.22669.

153 Botti, P., Pallin, T.D. and Tam, J.P. (1996) Cyclic Peptides from Linear Unprotected Peptide Precursors through Thiazolidine Formation. *J. Am. Chem. Soc.*, 118, 10018–10024. https://doi.org/10.1021/ja954278g.

154 Jing, X. and Jin, K. (2020) A Gold Mine for Drug Discovery: Strategies to Develop

Cyclic Peptides into Therapies. *Med. Res. Rev.*, 40, 753–810. https://doi.org/10.1002/med.21639.

155 Wallace, R.J. (1992) Acetylation of Peptides Inhibits Their Degradation by Rumen Micro-Organisms. *Br. J. Nutr.*, 68, 365–372. https://doi.org/10.1079/bjn19920095.

156 Lee, A.C.L., Harris, J.L., Khanna, K.K. and Hong, J.H. (2019, May 2) A Comprehensive Review on Current Advances in Peptide Drug Development and Design. International Journal of Molecular Sciences. https://doi.org/10.3390/ijms20102383.

157 Kim, K. and Seong, B.L. (2001) Peptide Amidation: Production of Peptide Hormones in Vivo and in Vitro. *Biotechnol. Bioprocess Eng.*, 6, 244–251.

158 Curtius, T. (1882) Ueber Einige Neue Der Hippursäure Analog Constituirte, Synthetisch Dargestellte Amidosäuren. *J. für Prakt. Chemie*, 26, 145–208. https://doi.org/10.1002/PRAC.18820260112.

159 Fischer, E. and Fourneau, E. (1906) Über Einige Derivate Des Glykocolls. *Untersuchungen über Amin. Polypept. und Proteïne*, 279–289. https://doi.org/10.1007/978-3-642-99499-9_21.

160 Mäde, V., Els-Heindl, S. and Beck-Sickinger, A.G. (2014) Automated Solid-Phase Peptide Synthesis to Obtain Therapeutic Peptides. *Beilstein J. Org. Chem. 10118*, 10, 1197–1212. https://doi.org/10.3762/BJOC.10.118.

161 Merrifield, R.B. (1963) Solid Phase Peptide Synthesis. I. The Synthesis of a Tetrapeptide. *J. Am. Chem. Soc.*, 85, 2149–2154. https://doi.org/10.1021/ja00897a025.

162 Stawikowski, M. and Fields, G.B. (2002) Introduction to Peptide Synthesis. *Curr. Protoc. Protein Sci.*, CHAPTER, Unit. https://doi.org/10.1002/0471140864.PS1801S26.

163 Bruce Merrifield – Biographical - NobelPrize.Org. https://www.nobelprize.org/prizes/chemistry/1984/merrifield/biographical/.

164 Merrifield, R.B. (1985) Solid Phase Synthesis (Nobel Lecture). *Angew. Chemie Int. Ed. English*, 24, 799–810. https://doi.org/10.1002/ANIE.198507993/FORMAT/PDF.

165 Pires, D.A.T., Bemquerer, M.P. and Nascimento, C.J. do. (2014) Some Mechanistic Aspects on Fmoc Solid Phase Peptide Synthesis. *Int. J. Pept. Res. Ther.*, 20, 53–69. https://doi.org/10.1007/s10989-013-9366-8.

166 Harris, P.W.R. and Brimble, M.A. (2013) A Comparison of Boc and Fmoc SPPS Strategies for the Preparation of C-Terminal Peptide α-Thiolesters: NY-ESO-1 ^{39}Cys-^{68}Ala-COSR. *Biopolymers*, 100, 356–365. https://doi.org/10.1002/BIP.22223.

167 Behrendt, R., White, P. and Offer, J. (2016) Advances in Fmoc Solid-Phase Peptide Synthesis. *J. Pept. Sci.*, 22, 4–27. https://doi.org/10.1002/PSC.2836.

168 Merrifield, R.B. (1965) Automated Synthesis of Peptides. *Science (80-.).*, 150, 178–184. https://doi.org/10.1126/SCIENCE.150.3693.178.

169 Højlys-Larsen, K.B. and Jensen, K.J. (2013) Peptide Synthesis and Applications: Linkers, Resins, and General Procedures for SPPS. *Methods Mol. Biol.*, 1047, 191–199. https://doi.org/10.1007/978-1-62703-544-6.

170 Bacsa, B., Desai, B., Dibó, G. and Kappe, C.O. (2006) Rapid Solid-Phase Peptide Synthesis Using Thermal and Controlled Microwave Irradiation. *J. Pept. Sci.*, 12, 633–638. https://doi.org/10.1002/PSC.771.

171 Erdélyi, M. and Gogoll, A. (2002) Rapid Microwave-Assisted Solid Phase Peptide Synthesis. *Synthesis (Stuttg).*, 2002, 1592–1596. https://doi.org/10.1055/S-2002-33348.

172 L. Pedersen, S., Pernille Tofteng, A., Leila Malik and J. Jensen, K. (2012) Microwave Heating in Solid-Phase Peptide Synthesis. *Chem. Soc. Rev.*, 41, 1826–1844. https://doi.org/10.1039/C1CS15214A.

173 Vanier, G.S. (2013) Microwave-Assisted Solid-Phase Peptide Synthesis Based on the Fmoc Protecting Group Strategy (CEM). *Pept. Synth. Appl. Methods Mol. Biol.*, 1047, 235–249. https://doi.org/10.1007/978-1-62703-544-6_17.

174 Olesen, J., Diener, H.C., Husstedt, I.W., Goadsby, P.J., Hall, D., Meier, U., Pollentier, S. and Lesko, L.M. (2004) Calcitonin Gene-Related Peptide Receptor Antagonist BIBN 4096 BS for the Acute Treatment of Migraine. *N. Engl. J. Med.*, 350, 1104–1110. https://doi.org/10.1056/NEJMoa030505.

175 Dennis, T., Fournier, A., St. Pierre, S. and Quirion, R. (1989) Structure-Activity

Profile of Calcitonin Gene-Related Peptide in Peripheral and Brain Tissues. Evidence for Receptor Multiplicity. *J. Pharmacol. Exp. Ther.*, 251, 718–725. https://citeseerx.ist.psu.edu/viewdoc/download?doi=10.1.1.960.5346&rep=rep1&type=pdf.

176 Chiba, T., Yamaguchi, A., Yamatani, T., Nakamura, A., Morishita, T., Inui, T., Fukase, M., Noda, T. and Fujita, T. (1989) Calcitonin Gene-Related Peptide Receptor Antagonist Human CGRP-(8-37). *Rapid Commun. - Am. Physiol. Soc.*, 256. https://doi.org/10.1152/AJPENDO.1989.256.2.E331.

177 Rovero, P., Giuliani, S. and Maggi, C.A. (1992) CGRP Antagonist Activity of Short C-Terminal Fragments of Human ACGRP, CGRP(23-37) and CGRP(19-37). *Peptides*, 13, 1025–1027. https://doi.org/10.1016/0196-9781(92)90067-D.

178 Maton, P.N., Pradhan, T., Zhou, Z.C., Gardner, J.D. and Jensen, R.T. (1990) Activities of Calcitonin Gene-Related Peptide (CGRP) and Related Peptides at the CGRP Receptor. *Peptides*, 11, 485–489. https://doi.org/10.1016/0196-9781(90)90047-9.

179 Chakder, S. and Rattan, S. (1990) [Tyr]-Calcitonin Gene-Related Peptide 28-37 (Rat) as a Putative Antagonist of Calcitonin Gene-Related Peptide Responses on Opossum Internal Anal Sphincter Smooth Muscle1. *J. Pharmacol. Exp. Ther.*, 253.

180 Carpenter, K.A., Schmidt, R., Von Mentzer, B., Haglund, U., Roberts, E. and Walpole, C. (2001) Turn Structures in CGRP C-Terminal Analogues Promote Stable Arrangements of Key Residue Side Chains. *Biochemistry*, 40, 8317–8325. https://doi.org/10.1021/bi0102860.

181 Lang, M., Pol, S. De, Baldauf, C., Hofmann, H.-J., Reiser, O. and Beck-Sickinger, A.G. (2005) Identification of the Key Residue of Calcitonin Gene Related Peptide (CGRP) 27−37 to Obtain Antagonists with Picomolar Affinity at the CGRP Receptor. *J. Med. Chem.*, 49, 616–624. https://doi.org/10.1021/JM050613S.

182 Russell, F.A., King, R., Smillie, S.-J., Kodji, X. and Brain, S.D. (2014) Calcitonin Gene-Related Peptide: Physiology and Pathophysiology. *Physiol. Rev.*, 94, 1099. https://doi.org/10.1152/PHYSREV.00034.2013.

183 Fried, J. and Sabo, E.F. (1954) 9a-Fluoro Derivatives of Cortisone and Hydrocortisone. *J. Am. Chem. Soc.*, 76, 1455–1456. https://pubs.acs.org/sharingguidelines.

184 O'Hagan, D. (2010) Fluorine in Health Care: Organofluorine Containing Blockbuster Drugs. *J. Fluor. Chem.*, 131, 1071–1081. https://doi.org/10.1016/J.JFLUCHEM.2010.03.003.

185 Wang, J., Sánchez-Roselló, M., Aceña, J.L., Pozo, C. del, Sorochinsky, A.E., Fustero, S., Soloshonok, V.A. and Liu, H. (2013) Fluorine in Pharmaceutical Industry: Fluorine-Containing Drugs Introduced to the Market in the Last Decade (2001–2011). *Chem. Rev.*, 114, 2432–2506. https://doi.org/10.1021/CR4002879.

186 Purser, S., R. Moore, P., Swallow, S. and Véronique Gouverneur. (2008) Fluorine in Medicinal Chemistry. *Chem. Soc. Rev.*, 37, 320–330. https://doi.org/10.1039/B610213C.

187 Huhmann, S., Nyakatura, E.K., Rohrhofer, A., Moschner, J., Schmidt, B., Eichler, J., Roth, C. and Koksch, B. (2021) Systematic Evaluation of Fluorination as Modification for Peptide-Based Fusion Inhibitors against HIV-1 Infection. *ChemBioChem*. https://doi.org/10.1002/CBIC.202100417.

188 Mei, H., Han, J., Klika, K., Fustero, S., Medio-Simon, M., Sedgwick, D.M., Santi, C., Renzor,] and Soloshonok, V.A. (2019) Fluorine-Containing Drugs Approved by the FDA in 2018. *Artic. Eur. J. Med. Chem.*, 25. https://doi.org/10.1016/j.ejmech.2019.111826.

189 Zhou, Y., Wang, J., Gu, Z., Wang, S., Zhu, W., Aceña, J.L., Soloshonok, V.A., Izawa, K., Liu, H., Acenã, J.L., Soloshonok, V.A., Izawa, K. and Liu, H. (2016) Next Generation of Fluorine-Containing Pharmaceuticals, Compounds Currently in Phase II–III Clinical Trials of Major Pharmaceutical Companies: New Structural Trends and Therapeutic Areas. *Chem. Rev.*, 116, 422–518. https://doi.org/10.1021/ACS.CHEMREV.5B00392.

190 Zhuang, C., Wu, Y., Zhang, W. and Miao, Z. (2020) Fluorine-Containing Drugs and Drug Candidates Derived from Natural Products. In: Atta-ur-Rahman, Anjum, S. and El-Seedi, H., Eds., Natural Products in Clinical Trials, 123–129.

191 Mei, H., Remete, A.M., Zou, Y., Moriwaki, H., Fustero, S., Kiss, L., Soloshonok, V.A. and Han, J. (2020) Fluorine-Containing Drugs Approved by the FDA in 2019. *Chinese Chem. Lett.*, 31, 2401–2413. https://doi.org/10.1016/j.cclet.2020.03.050.

192 Edvinsson, L. and Linde, M. (2010) New Drugs in Migraine Treatment and Prophylaxis: Telcagepant and Topiramate. *Lancet*, 376, 645–655. https://doi.org/10.1016/S0140-6736(10)60323-6.

193 Tepper, S.J. and Cleves, C. (2009) Telcagepant, a Calcitonin Gene-Related Peptide Antagonist for the Treatment of Migraine. *Curr. Opin. Investig. Drugs*, 10, 711–720. https://europepmc.org/article/med/19579177.

194 Bell, I.M., Stump, C.A., Gallicchio, S.N., Staas, D.D., Zartman, C.B., Moore, E.L., Sain, N., Urban, M., Bruno, J.G., Calamari, A., Kemmerer, A.L., Mosser, S.D., Fandozzi, C., White, R.B., Zrada, M.M., Selnick, H.G., Graham, S.L., Vacca, J.P., Kane, S.A. and Salvatore, C.A. (2012) MK-8825: A Potent and Selective CGRP Receptor Antagonist with Good Oral Activity in Rats. *Bioorg. Med. Chem. Lett.*, 22, 3941–3945. https://doi.org/10.1016/J.BMCL.2012.04.105.

195 Feistel, S., Albrecht, S. and Messlinger, K. (2013) The Calcitonin Gene-Related Peptide Receptor Antagonist MK-8825 Decreases Spinal Trigeminal Activity during Nitroglycerin Infusion. *J. Headache Pain*, 14, 93. https://doi.org/10.1186/1129-2377-14-93/FIGURES/2.

196 QULIPTA Label. www.fda.gov/medwatch.

197 Mei, H., Han, J., Klika, K.D., Izawa, K., Sato, T., Meanwell, N.A. and Soloshonok, V.A. (2020) Applications of Fluorine-Containing Amino Acids for Drug Design. *Eur. J. Med. Chem.*, 186, 111826. https://doi.org/10.1016/J.EJMECH.2019.111826.

198 Asante, V., Mortier, J., Schlüter, H. and Koksch, B. (2013) Impact of Fluorination on Proteolytic Stability of Peptides in Human Blood Plasma. *Bioorg. Med. Chem.*, 21, 3542–3546. https://doi.org/10.1016/J.BMC.2013.03.051.

199 Huhmann, S., Stegemann, A.-K., Folmert, K., Klemczak, D., Moschner, J., Kube, M. and Koksch, B. (2017) Position-Dependent Impact of Hexafluoroleucine and

Trifluoroisoleucine on Protease Digestion. *Beilstein J. Org. Chem.*, 13, 2869. https://doi.org/10.3762/BJOC.13.279.

200 Huhmann, S. and Koksch, B. (2018) Fine-Tuning the Proteolytic Stability of Peptides with Fluorinated Amino Acids. *European J. Org. Chem.*, 2018, 3667–3679. https://doi.org/10.1002/EJOC.201800803.

201 Meng, H., Krishnaji, S.T., Beinborn, M. and Kumar, K. (2008) Influence of Selective Fluorination on the Biological Activity and Proteolytic Stability of Glucagon-like Peptide-1. *J. Med. Chem.*, 51, 7303–7307. https://doi.org/10.1021/JM8008579/SUPPL_FILE/JM8008579_SI_001.PDF.

202 Welte, H., Zhou, T., Mihajlenko, X., Mayans, O. and Kovermann, M. (2020) What Does Fluorine Do to a Protein? Thermodynamic, and Highly-Resolved Structural Insights into Fluorine-Labelled Variants of the Cold Shock Protein. *Sci. Reports 2020 101*, 10, 1–12. https://doi.org/10.1038/s41598-020-59446-w.

203 Verhoork, S.J.M., Killoran, P.M. and Coxon, C.R. (2018) Fluorinated Prolines as Conformational Tools and Reporters for Peptide and Protein Chemistry. *Biochemistry*, 57, 6132–6143. https://doi.org/10.1021/acs.biochem.8b00787.

204 Salwiczek, M., Nyakatura, E.K., Gerling, U.I.M., Ye, S. and Koksch, B. (2012) Fluorinated Amino Acids: Compatibility with Native Protein Structures and Effects on Protein–Protein Interactions. *Chem. Soc. Rev.*, 41, 2135–2171. https://doi.org/10.1039/c1cs15241f.

205 Awad, L.F. and Ayoup, M.S. (2020) Fluorinated Phenylalanines: Synthesis and Pharmaceutical Applications. *Beilstein J. Org. Chem. 1691*, 16, 1022–1050. https://doi.org/10.3762/BJOC.16.91.

206 O'Hagan, D. and Young, R.J. (2016) Accurate Lipophilicity (Log P) Measurements Inform on Subtle Stereoelectronic Effects in Fluorine Chemistry. *Angew. Chemie Int. Ed.*, 55, 3858–3860. https://doi.org/10.1002/ANIE.201511055.

207 Arias, M., Aramini, J.M., Riopel, N.D. and Vogel, H.J. (2020) Fluorine-19 NMR Spectroscopy of Fluorinated Analogs of Tritrpticin Highlights a Distinct Role for Tyr Residues in Antimicrobial Peptides. *Biochim. Biophys. Acta - Biomembr.*,

1862, 183260. https://doi.org/10.1016/J.BBAMEM.2020.183260.

208 Butterfield, S.M., Paresma, R.P. and Waters, M.L. (2002) Contribution of Aromatic Interactions to α-Helix Stability. *J. Am. Chem. Soc.*, 124, 9751–9755. https://doi.org/10.1021/JA026668Q.

209 Geurink, P.P., Liu, N., Spaans, M.P., Downey, S.L., van den Nieuwendijk, A.M.C.H., van der Marel, G.A., Kisselev, A.F., Florea, B.I., Overkleeft, H.S., Nieuwendijk, A.M.C.H. van den, Marel, G.A. van der, Kisselev, A.F., Florea, B.I. and Overkleeft, H.S. (2010) Incorporation of Fluorinated Phenylalanine Generates Highly Specific Inhibitor of Proteasome's Chymotrypsin-like Sites. *J. Med. Chem.*, 53, 2319–2323. https://pubs.acs.org/doi/abs/10.1021/jm9015685.

210 Senguen, T.F., Lee, N.R., Gu, X., Ryan, D.M., MDoran, T.M., Anderson, E.A. and LNilsson, B.L. (2011) Probing Aromatic, Hydrophobic, and Steric Effects on the Self-Assembly of an Amyloid-β Fragment Peptide. *Mol. Biosyst.*, 7, 486–496. https://doi.org/10.1039/C0MB00080A.

211 Tantry, S., Ding, F.-X., Dumont, M., Becker, J.M. and Naider, F. (2010) Binding of Fluorinated Phenylalanine α-Factor Analogues to Ste2p: Evidence for a Cation−π Binding Interaction between a Peptide Ligand and Its Cognate G Protein-Coupled Receptor. *Biochemistry*, 49, 5007–5015. https://doi.org/10.1021/BI100280F.

212 Russo, A.F. and Recober, A. (2007) Olcegepant, a Non-Peptide CGRP1 Antagonist for Migraine Treatment Drug Profile: Olcegepant, a Non-Peptide CGRP1 Antagonist for Migraine Treatment. *IDrugs*, 10, 566–574. https://www.researchgate.net/publication/6174500.

213 Recio, C., Maione, F., Iqbal, A.J., Mascolo, N. and De Feo, V. (2017) The Potential Therapeutic Application of Peptides and Peptidomimetics in Cardiovascular Disease. *Front. Pharmacol.*, 7, 1–11. https://doi.org/10.3389/fphar.2016.00526.

214 Culf, A.S. and Ouellette, R.J. (2010) Solid-Phase Synthesis of N-Substituted Glycine Oligomers (α-Peptoids) and Derivatives. *Molecules*, 15, 5282–5335. https://doi.org/10.3390/molecules15085282.

215 Miller, S.M., Simon, R.J., Ng, S., Zuckermann, R.N., Kerr, J.M. and Moos, W.H. (1994) Proteolytic Studies of Homologous Peptide and N-Substituted Glycine Peptoid Oligomers. *Bioorganic Med. Chem. Lett.*, 4, 2657–2662. https://doi.org/10.1016/S0960-894X(01)80691-0.

216 Kessler, H. (1993) Peptoids—A New Approach to the Development of Pharmaceuticals. *Angew. Chemie Int. Ed. English*, 32, 543–544. https://doi.org/10.1002/anie.199305431.

217 Kapoor, R., Wadman, M.W., Dohm, M.T., Czyzewski, A.M., Spormann, A.M. and Barron, A.E. (2011) Antimicrobial Peptoids Are Effective against Pseudomonas Aeruginosa Biofilms. *Antimicrob. Agents Chemother.*, 55, 3054–3057. https://doi.org/10.1128/AAC.01516-10.

218 Kapoor, R., Eimerman, P.R., Hardy, J.W., Cirillo, J.D., Contag, C.H. and Barron, A.E. (2011) Efficacy of Antimicrobial Peptoids against Mycobacterium Tuberculosis. *Antimicrob. Agents Chemother.*, 55, 3058–3062. https://doi.org/10.1128/AAC.01667-10.

219 Mojsoska, B., Carretero, G., Larsen, S., Mateiu, R.V. and Jenssen, H. (2017) Peptoids Successfully Inhibit the Growth of Gram Negative E. Coli Causing Substantial Membrane Damage. *Sci. Rep.*, 7, 1–12. https://doi.org/10.1038/srep42332.

220 Servoss, S. and Moss, M. (2012, October 19) Peptoids and Methods for Treating Alzheimer's Disease.

221 Singh, L., Field, M.J., Hill, D.R., Horwell, D.C., McKnight, A.T., Roberts, E., Tang, K.W. and Woodruff, G.N. (1995) Peptoid CCK Receptor Antagonists: Pharmacological Evaluation of CCKA, CCKB and Mixed CCKA B Receptor Antagonists. *Eur. J. Pharmacol.*, 286, 185–191. https://doi.org/10.1016/0014-2999(95)00445-Q.

222 Villoslada, P., Vila, G., Colafrancesco, V., Moreno, B., Fernandez-Diez, B., Vazquez, R., Pertsovskaya, I., Zubizarreta, I., Pulido-Valdeolivas, I., Messeguer, J., Vendrell-Navarro, G., Frade, J.M., López-Sánchez, N., Teixido, M., Giralt, E., Masso, M., Dugas, J.C., Leonoudakis, D., Lariosa-Willingham, K.D., Steinman, L. and Messeguer, A. (2019) Axonal and Myelin Neuroprotection by the

Peptoid BN201 in Brain Inflammation. *Neurotherapeutics*, 16, 808–827. https://doi.org/10.1007/s13311-019-00717-4.

223 Bhowmik, A., Basu, M. and Ghosh, M.K. (2017) Design, Synthesis and Use of Peptoids in the Diagnosis and Treatment of Cancer. *Front. Biosci. (Elite Ed).*, 9, 101–108. https://doi.org/10.2741/e789.

224 Sun, J. and Zuckermann, R.N. (2013) Peptoid Polymers: A Highly Designable Bioinspired Material. *ACS Nano*, 7, 4715–4732. https://doi.org/10.1021/NN4015714.

225 Simon, R.J., Kania, R.S., Zuckermann, R.N., Huebner, V.D., Jewell, D.A., Banville, S., Ng, S., Wang, L., Rosenberg, S., Marlowe, C.K., Spellmeyer, D.C., Tan, R., Frankel, A.D., Santi, D. V., Cohen, F.E. and Bartlett, P.A. (1992) Peptoids: A Modular Approach to Drug Discovery. *Proc. Natl. Acad. Sci. U. S. A.*, 89, 9367–9371. https://doi.org/10.1073/pnas.89.20.9367.

226 Zuckermann, R.N. (2011) Peptoid Origins. *Biopolymers*, 96, 545–555. https://doi.org/10.1002/bip.21573.

227 Robertson, E.J., Battigelli, A., Proulx, C., Mannige, R. V., Haxton, T.K., Yun, L., Whitelam, S. and Zuckermann, R.N. (2016) Design, Synthesis, Assembly, and Engineering of Peptoid Nanosheets. *Acc. Chem. Res.*, 49, 379–389. https://doi.org/10.1021/acs.accounts.5b00439.

228 Saini, A. and Verma, G. (2017) Chapter 10 - Peptoids: Tomorrow's Therapeutics. Nanostructures for Novel Therapy. https://doi.org/10.1016/B978-0-323-46142-9/00010-4.

229 Chen, D., M. Disotuar, M., Xiong, X., Yuanxiang Wang and Hung-Chieh Chou, D. (2017) Selective N-Terminal Functionalization of Native Peptides and Proteins. *Chem. Sci.*, 8, 2717–2722. https://doi.org/10.1039/C6SC04744K.

230 Adessi, C. and Soto, C. (2002) Converting a Peptide into a Drug: Strategies to Improve Stability and Bioavailability. *Curr. Med. Chem.*, 9, 963–978. https://doi.org/10.2174/0929867024606731.

231 Zupančič, O. and Bernkop-Schnürch, A. (2017) Lipophilic Peptide Character – What Oral Barriers Fear the Most. *J. Control. Release*, 255, 242–257. https://doi.org/10.1016/J.JCONREL.2017.04.038.

232 Ray, A., Jatana, N. and Thukral, L. (2017) Lipidated Proteins: Spotlight on Protein-Membrane Binding Interfaces. *Prog. Biophys. Mol. Biol.*, 128, 74–84. https://doi.org/10.1016/J.PBIOMOLBIO.2017.01.002.

233 Ward, B.P., Ottaway, N.L., Perez-Tilve, D., Ma, D., Gelfanov, V.M., Tschöp, M.H. and DiMarchi, R.D. (2013) Peptide Lipidation Stabilizes Structure to Enhance Biological Function. *Mol. Metab.*, 2, 468–479. https://doi.org/10.1016/j.molmet.2013.08.008.

234 Rosen, C.B. and Francis, M.B. (2017) Targeting the N Terminus for Site-Selective Protein Modification. *Nat. Chem. Biol. 2017 137*, 13, 697–705. https://doi.org/10.1038/nchembio.2416.

235 Judd, A.K., Kaushanskaya, A., Tuttle, D.J., Sanchez, A., Khroyan, T., Polgar, W. and Toll, L. (2003) N-Terminal Modifications Leading to Peptide ORL1 Partial Agonists and Antagonists. *J. Pept. Res.*, 62, 191–198. https://doi.org/10.1034/J.1399-3011.2003.00077.X.

236 Orwig, K.S., Lassetter, M.R., Hadden, M.K. and Dix, T.A. (2009) Comparison of N-Terminal Modifications on Neurotensin(8−13) Analogues Correlates Peptide Stability but Not Binding Affinity with in Vivo Efficacy. *J. Med. Chem.*, 52, 1803–1813. https://doi.org/10.1021/JM801072V.

237 Sonzini, S., T. Jones, S., Zarah Walsh and A. Scherman, O. (2015) Simple Fluorinated Moiety Insertion on Aβ 16–23 Peptide for Stain-Free TEM Imaging. *Analyst*, 140, 2735–2740. https://doi.org/10.1039/C4AN02278E.

238 Julka, S. and Regnier, F.E. (2004) Benzoyl Derivatization as a Method To Improve Retention of Hydrophilic Peptides in Tryptic Peptide Mapping. *Anal. Chem.*, 76, 5799–5806. https://doi.org/10.1021/AC049688E.

239 Corry, A.J., Mooney, Á., O'Sullivan, D. and Kenny, P.T.M. (2009) Synthesis, Characterization and in Vitro Anti-Cancer Activity of N-(Ferrocenyl)Benzoyl Tri- and Tetrapeptide Esters. *Inorganica Chim. Acta*, 362, 2957–2961. https://doi.org/10.1016/J.ICA.2009.01.021.

240 Smith, D.D., Saha, S., Fang, G., Schaffert, C., Waugh, D.J.J., Zeng, W., Toth, G., Hulce, M. and Abel, P.W. (2003) Modifications to the N-Terminus but Not the C-Terminus of Calcitonin Gene-Related Peptide(8-37) Produce Antagonists

with Increased Affinity. *J. Med. Chem.*, 46, 2427–2435. https://doi.org/10.1021/jm020507f.

241 Hay, D.L. and Walker, C.S. (2017) CGRP and Its Receptors. *Headache J. Head Face Pain*, 57, 625–636. https://doi.org/10.1111/HEAD.13064.

242 Liang, Y.L., Khoshouei, M., Deganutti, G., Glukhova, A., Koole, C., Peat, T.S., Radjainia, M., Plitzko, J.M., Baumeister, W., Miller, L.J., Hay, D.L., Christopoulos, A., Reynolds, C.A., Wootten, D. and Sexton, P.M. (2018) Cryo-EM Structure of the Active, G s -Protein Complexed, Human CGRP Receptor. *Nature*, 561, 492–497. https://doi.org/10.1038/s41586-018-0535-y.

243 Moore, E.L. and Salvatore, C.A. (2012) Targeting a Family B GPCR/RAMP Receptor Complex: CGRP Receptor Antagonists and Migraine. *Br. J. Pharmacol.*, 166, 66–78. https://doi.org/10.1111/J.1476-5381.2011.01633.X.

244 Cyclic AMP Assays - Eurofins - DiscoverX. https://www.discoverx.com/products-applications/camp-assays.

245 CAMP Accumulation Assay - Creative BioMart. https://www.creativebiomart.net/cAMP-Accumulation-Assay.htm.

246 CAMP - Gs Dynamic HTRF Kit | Cisbio. https://www.cisbio.eu/camp-gs-dynamic-kit-40361.

247 Bradley, J. and McLoughlin, D. (2009) Use of the DiscoveRx Hithunter CAMPII Assay for Direct Measurement of CAMP in Gs and Gi GPCRs. *Methods Mol. Biol.*, 552, 171–179. https://doi.org/10.1007/978-1-60327-317-6_12.

248 O'Brien, J., Wilson, I., Orton, T. and Pognan, F. (2000) Investigation of the Alamar Blue (Resazurin) Fluorescent Dye for the Assessment of Mammalian Cell Cytotoxicity. *Eur. J. Biochem.*, 267, 5421–5426. https://doi.org/10.1046/J.1432-1327.2000.01606.X.

249 Hamid, R., Rotshteyn, Y., Rabadi, L., Parikh, R. and Bullock, P. (2004) Comparison of Alamar Blue and MTT Assays for High Through-Put Screening. *Toxicol. Vitr.*, 18, 703–710. https://doi.org/10.1016/J.TIV.2004.03.012.

250 Rampersad, S.N. (2012) Multiple Applications of Alamar Blue as an Indicator of Metabolic Function and Cellular Health in Cell Viability Bioassays. *Sensors 2012, Vol. 12, Pages 12347-12360*, 12, 12347–12360.

https://doi.org/10.3390/S120912347.

251 Candeias, L.P., Macfarlane, D.P.S., Mcwhinnie, S.L.W., Maidwell, N.L., Roeschlaub, C.A., Sammes, P.G. and Whittlesey, R. (1998) The Catalysed NADH Reduction of Resazurin to Resorufin. *J. Chem. Soc., Perkin Trans. 2*, 2333–2334.

252 (2017) Automated Synthesis of Peptoids and Peptoid-Peptide Hybrids. *CEM Appl. Note ap0116*, 1–3.

253 Sarin, V.K., Kent, S.B.H., Tam, J.P. and Merrifield, R.B. (1981) Quantitative Monitoring of Solid-Phase Peptide Synthesis by the Ninhydrin Reaction. *Anal. Biochem.*, 117, 147–157. https://doi.org/10.1016/0003-2697(81)90704-1.

254 Wood, C.W., Ibarra, A.A., Bartlett, G.J., Wilson, A.J., Wilson, A.J., Woolfson, D.N., Woolfson, D.N., Woolfson, D.N., Sessions, R.B. and Sessions, R.B. (2020) BAlaS: Fast, Interactive and Accessible Computational Alanine-Scanning Using BudeAlaScan. *Bioinformatics*, 36, 2917–2919. https://doi.org/10.1093/BIOINFORMATICS/BTAA026.

255 McIntosh-Smith, S., Wilson, T., Ibarra, A.Á., Crisp, J. and Sessions, R.B. (2012) Benchmarking Energy Efficiency, Power Costs and Carbon Emissions on Heterogeneous Systems. *Comput. J.*, 55, 192–205. https://doi.org/10.1093/COMJNL/BXR091.

256 Schild, H.O. (1949) PAx and Competitive Drug Antagonism. *Br. J. Pharmacol. Chemother.*, 4, 277. https://doi.org/10.1111/J.1476-5381.1949.TB00548.X.

257 Arunlakshana, O. and Schild, H.O. (1959) Some Quantitative Uses of Drug Antagonists. *Br. J. Pharmacol. Chemother.*, 14, 48. https://doi.org/10.1111/J.1476-5381.1959.TB00928.X.

258 Gorske, B.C., Jewell, S.A., Guerard, E.J. and Blackwell, H.E. (2005) Expedient Synthesis and Design Strategies for New Peptoid Construction. *Org. Lett.*, 7, 1521–1524. https://doi.org/10.1021/ol0502984.

259 Olivos, H.J., Alluri, P.G., Reddy, M.M., Salony, D. and Kodadek, T. (2002) Microwave-Assisted Solid-Phase Synthesis of Peptoids. *Org. Lett.*, 4, 4057–4058. https://doi.org/10.1021/ol0267578.

260 Maggi, C.A., Chiba, T. and Giuliani, S. (1991) Human α-Calcitonin Gene-Related Peptide-(8-37) as an Antagonist of Exogenous and Endogenous Calcitonin

Gene-Related Peptide. *Eur. J. Pharmacol.*, 192, 85–88. https://doi.org/10.1016/0014-2999(91)90072-X.

261 Woolley, M.J., Simms, J., Uddin, S., Poyner, D.R. and Conner, A.C. (2017) Relative Antagonism of Mutants of the CGRP Receptor Extracellular Loop 2 Domain (ECL2) Using a Truncated Competitive Antagonist (CGRP8–37): Evidence for the Dual Involvement of ECL2 in the Two-Domain Binding Model. *Biochemistry*, 56, 3877–3880. https://doi.org/10.1021/ACS.BIOCHEM.7B00077.

262 Shelton, P.T. and Jensen, K.J. (2013) Linkers, Resins, and General Procedures for Solid-Phase Peptide Synthesis. *Methods Mol. Biol.*, 1047, 23–41. https://doi.org/10.1007/978-1-62703-544-6_2.

263 Park, M., Wetzler, M., Jardetzky, T.S. and Barron, A.E. (2013) A Readily Applicable Strategy to Convert Peptides to Peptoid-Based Therapeutics. *PLoS One*, 8, 1–7. https://doi.org/10.1371/journal.pone.0058874.

264 Mora, P., Masip, I., Cortés, N., Marquina, R., Merino, R., Merino, J., Carbonell, T., Mingarro, I., Messeguer, A. and Pérez-Payá, E. (2005) Identification from a Positional Scanning Peptoid Library of in Vivo Active Compounds That Neutralize Bacterial Endotoxins. *J. Med. Chem.*, 48, 1265–1268. https://doi.org/10.1021/JM040834I.

265 Masip, I., Cortés, N., Abad, M.J., Guardiola, M., Pérez-Payá, E., Ferragut, J., Ferrer-Montiel, A. and Messeguer, A. (2005) Design and Synthesis of an Optimized Positional Scanning Library of Peptoids: Identification of Novel Multidrug Resistance Reversal Agents. *Bioorg. Med. Chem.*, 13, 1923–1929. https://doi.org/10.1016/J.BMC.2005.01.024.

266 Vendrell-Navarro, G., Rúa, F., Bujons, J., Brockmeyer, A., Janning, P., Ziegler, S., Messeguer, A. and Waldmann, H. (2015) Positional Scanning Synthesis of a Peptoid Library Yields New Inducers of Apoptosis That Target Karyopherins and Tubulin. *ChemBioChem*, 16, 1580–1587. https://doi.org/10.1002/CBIC.201500169.

267 Zuckermann, R.N., Kerr, J.M., Moosf, W.H. and Kent, S.B.H. (1992) Efficient Method for the Preparation of Peptoids [Oligo(N-Substituted Glycines)] by

Submonomer Solid-Phase Synthesis. *J. Am. Chem. Soc.*, 114, 10646–10647. https://doi.org/10.1021/ja00052a076.

268 Bolt, H.L., Denny, P.W. and Cobb, S.L. (2016) An Efficient Method for the Synthesis of Peptoids with Mixed Lysine-Type/ Arginine-Type Monomers and Evaluation of Their Anti-Leishmanial Activity. *J. Vis. Exp.* https://doi.org/10.3791/54750.

269 Jobin, S., Vézina-Dawod, S., Herby, C., Derson, A. and Biron, E. (2015) Preparation of N-Substituted N-Arylsulfonylglycines and Their Use in Peptoid Synthesis. *Org. Lett.*, 17, 5626–5629. https://doi.org/10.1021/ACS.ORGLETT.5B02862.

270 Ruijtenbeek, R., Kruijtzer, J.A.W., Van De Wiel, W., Fischer, M.J.E., Flück, M., Redegeld, F.A.M., Liskamp, R.M.J. and Nijkamp, F.P. (2001) Peptoid-Peptide Hybrids That Bind Syk SH2 Domains Involved in Signal Transduction. *CHEMBIOCHEM*, 2, 171–179. https://doi.org/10.1002/1439-7633.

271 Streuli, A., Coxon, C.R. and Steuer, C. (2021) Simultaneous Quantification of Commonly Used Counter Ions in Peptides and Active Pharmaceutical Ingredients by Mixed Mode Chromatography and Evaporative Light Scattering Detection. *J. Pharm. Sci.*, 110, 2997–3003. https://doi.org/10.1016/J.XPHS.2021.04.008.

272 D'Aloisio, V. and Coxon, C.R. (2021) Reversed Phase Flash Chromatography Purification of Peptide-Peptoid Hybrids. *Teledyne Isco - Appl. Note AN 115*.

273 Andrés, A., Rosés, M., Ràfols, C., Bosch, E., Espinosa, S., Segarra, V. and Huerta, J.M. (2015) Setup and Validation of Shake-Flask Procedures for the Determination of Partition Coefficients (Log D) from Low Drug Amounts. *Eur. J. Pharm. Sci.*, 76, 181–191. https://doi.org/10.1016/J.EJPS.2015.05.008.

274 Xing, L. and Glen, R.C. (2002) Novel Methods for the Prediction of LogP, PKa, and LogD. *J. Chem. Inf. Comput. Sci.*, 42, 796–805. https://doi.org/10.1021/CI010315D.

275 Tetko, I. V. and Bruneau, P. (2004) Application of ALOGPS to Predict 1-octanol/Water Distribution Coefficients, LogP, and LogD, of AstraZeneca In-house Database. *J. Pharm. Sci.*, 93, 3103–3110.

https://doi.org/10.1002/JPS.20217.

276 Eddershaw, P.J., Beresford, A.P. and Bayliss, M.K. (2000) ADME/PK as Part of a Rational Approach to Drug Discovery. *Drug Discov. Today*, 5, 409–414. https://doi.org/10.1016/S1359-6446(00)01540-3.

277 van de Waterbeemd, H., Karajiannis, H. and El Tayar, N. (1994) Lipophilicity of Amino Acids. *Amin. Acids 1994 72*, 7, 129–145. https://doi.org/10.1007/BF00814156.

278 Bolt, H.L., Williams, C.E.J., Brooks, R. V., Zuckermann, R.N., Cobb, S.L. and Bromley, E.H.C. (2017) Log D versus HPLC Derived Hydrophobicity: The Development of Predictive Tools to Aid in the Rational Design of Bioactive Peptoids. *Pept. Sci.*, 108, e23014. https://doi.org/10.1002/BIP.23014.

279 Leo, A., Hansch, C. and Elkins, D. (1971) Partition Coefficients and Their Uses. *Chem. Rev.*, 71, 525–616. https://doi.org/10.1021/cr60274a001.

280 Ligor, M., Kováčová, J., Gadzała-Kopciuch, R.M., Studzin, S., Bocian, S., Lehotay, J. and Buszewski, B. (2014) Study of RP HPLC Retention Behaviours in Analysis of Carotenoids. *Chromatographia*, 77, 1047–1057. https://doi.org/10.1007/s10337-014-2657-1.

281 Yamaguchi, A., Chiba, T., Okimura, Y., Yamatani, T., Morishita, T., Nakamura, A., Inui, T., Noda, T. and Fujita, T. (1988) Receptors for Calcitonin Gene-Related Peptide on the Rat Liver Plasma Membranes. *Biochem. Biophys. Res. Commun.*, 152, 383–391. https://doi.org/10.1016/S0006-291X(88)80725-3.

282 Chiba, T., Yamaguchi, A., Yamatani, T., Nakamura, A., Morishita, T., Inui, T., Fukase, M., Noda, T. and Medicine, I. (1989) Calcitonin Antagonist Gene-Related Peptide Receptor. *Am. J. Physiol.*, 331–335.

283 Di, L. (2014) Strategic Approaches to Optimizing Peptide ADME Properties. *AAPS J.*, 17, 134–143. https://doi.org/10.1208/s12248-014-9687-3.

284 Werle, M. and Bernkop-Schnürch, A. (2006) Strategies to Improve Plasma Half Life Time of Peptide and Protein Drugs. *Amin. Acids 2006 304*, 30, 351–367. https://doi.org/10.1007/S00726-005-0289-3.

285 Rawlings, N.D. and Barrett, A.J. (2014) Peptidases. *eLS*. https://doi.org/10.1002/9780470015902.A0000670.PUB3.

286 Jensen, K.J. (2013) Solid-Phase Peptide Synthesis: An Introduction. *Methods Mol. Biol.*, 1047, 1–21. https://doi.org/10.1007/978-1-62703-544-6_1.

287 Powell, M.F., Stewart, T., Otvos, Jr, L., Urge, L., Gaeta, F.C.A., Sette, A., Arrhenius, T., Thomson, D., Soda, K. and Colon, S.M. (1993) Peptide Stability in Drug Development. II. Effect of Single Amino Acid Substitution and Glycosylation on Peptide Reactivity in Human Serum. *Pharm. Res.*, 10, 1268–1273. https://doi.org/10.1023/A:1018953309913.

288 Demidov, V. V., Potaman, V.N., Frank-Kamenetskil, M.D., Egholm, M., Buchard, O., Sönnichsen, S.H. and Nlelsen, P.E. (1994) Stability of Peptide Nucleic Acids in Human Serum and Cellular Extracts. *Biochem. Pharmacol.* https://doi.org/10.1016/0006-2952(94)90171-6.

289 Hong, S.Y., Oh, J.E. and Lee, K.H. (1999) Effect of D-Amino Acid Substitution on the Stability, the Secondary Structure, and the Activity of Membrane-Active Peptide. *Biochem. Pharmacol.*, 58, 1775–1780. https://doi.org/10.1016/S0006-2952(99)00259-2.

290 Tamamura, H., Omagari, A., Hiramatsu, K., Gotoh, K., Kanamoto, T., Xu, Y., Kodama, E., Matsuoka, M., Hattori, T., Yamamoto, N., Nakashima, H., Otaka, A. and Fujii, N. (2001) Development of Specific CXCR4 Inhibitors Possessing High Selectivity Indexes as Well as Complete Stability in Serum Based on an Anti-HIV Peptide T140. *Bioorganic Med. Chem. Lett.*, 11, 1897–1902. https://doi.org/10.1016/S0960-894X(01)00323-7.

291 Cudic, M., Condie, B.A., Weiner, D.J., Lysenko, E.S., Xiang, Z.Q., Insug, O., Bulet, P. and Otvos, L. (2002) Development of Novel Antibacterial Peptides That Kill Resistant Isolates. *Peptides*, 23, 2071–2083. https://doi.org/10.1016/S0196-9781(02)00244-9.

292 Bracci, L., Falciani, C., Lelli, B., Lozzi, L., Runci, Y., Pini, A., De Montis, M.G., Tagliamonte, A. and Neri, P. (2003) Synthetic Peptides in the Form of Dendrimers Become Resistant to Protease Activity *. *J. Biol. Chem.*, 278, 46590–46595. https://doi.org/10.1074/JBC.M308615200.

293 Youngblood, D.S., Hatlevig, S.A., Hassinger, J.N., Iversen, P.L. and Moulton, H.M. (2006) Stability of Cell-Penetrating Peptide−Morpholino Oligomer

Conjugates in Human Serum and in Cells. *Bioconjug. Chem.*, 18, 50–60. https://doi.org/10.1021/BC060138S.

294 Nguyen, L.T., Chau, J.K., Perry, N.A., de Boer, L., Zaat, S.A.J. and Vogel, H.J. (2010) Serum Stabilities of Short Tryptophan- and Arginine-Rich Antimicrobial Peptide Analogs. Vij, N., Ed., *PLoS One*, 5, e12684. https://doi.org/10.1371/journal.pone.0012684.

295 Chen, Y., Mant, C.T. and Hodges, R.S. (2004) Selectivity Differences in the Separation of Amphipathic α-Helical Peptides during Reversed-Phase Liquid Chromatography at PHs 2.0 and 7.0: Effects of Different Packings, Mobile Phase Conditions and Temperature. *J. Chromatogr. A*, 1043, 99–111. https://doi.org/10.1016/j.chroma.2004.04.028.

296 Ferreira, I.M.P.L.V.O., Eça, R., Pinho, O., Tavares, P., Pereira, A. and Roque, A.C. (2007) Development and Validation of an HPLC/UV Method for Quantification of Bioactive Peptides in Fermented Milks. *J. Liq. Chromatogr. Relat. Technol.*, 30, 2139–2147. https://doi.org/10.1080/10826070701435145.

297 Billot, P. and Pitard, B. (1992) Taguchi Design Experiments for Optimizing the Gas Chromatographic Analysis of Residual Solvents in Bulk Pharmaceuticals. *J. Chromatogr. A*, 623, 305–313. https://doi.org/10.1016/0021-9673(92)80370-A.

298 Brubaker, J. (2020) The Differences Between HPLC & GC. https://sciencing.com/differences-between-hplc-gc-7456786.html.

299 Hibbert, D.B. (2012) Experimental Design in Chromatography: A Tutorial Review. *J. Chromatogr. B Anal. Technol. Biomed. Life Sci.*, 910, 2–13. https://doi.org/10.1016/j.jchromb.2012.01.020.

300 Sahu, P.K., Ramisetti, N.R., Cecchi, T., Swain, S., Patro, C.S. and Panda, J. (2018) An Overview of Experimental Designs in HPLC Method Development and Validation. *J. Pharm. Biomed. Anal.*, 147, 590–611. https://doi.org/10.1016/j.jpba.2017.05.006.

301 Lourenço, D., Sarraguça, M., Alves, G., Coutinho, P., Araujo, A.R.T.S. and Rodrigues, M. (2017) A Novel HPLC Method for the Determination of Zonisamide in Human Plasma Using Microextraction by Packed Sorbent

Optimised by Experimental Design. *Anal. Methods*, 9, 5910–5919. https://doi.org/10.1039/c7ay01912b.

302 n.a. (2005) International Conference on Harmonisation of Technical Requirements for Registration of Pharmaceuticals for Human Use - Validation of Analytical Procedures: Text and Methodology Q2(R1).

303 Wilson, S.F., Li, H., Rose, M.J., Xiao, J., Holder, J.R. and James, C.A. (2010) Development and Validation of a Method for the Determination of a Therapeutic Peptide with Affinity for the Human B1 Receptor in Human Plasma Using HPLC-MS/MS. *J. Chromatogr. B*, 878, 749–757. https://doi.org/10.1016/J.JCHROMB.2010.01.018.

304 Egusquiaguirre, S.P., Manguán-García, C., Perona, R., Pedraz, J.L., Hernández, R.M. and Igartua, M. (2014) Development and Validation of a Rapid HPLC Method for the Quantification of GSE4 Peptide in Biodegradable PEI-PLGA Nanoparticles. *J. Chromatogr. B Anal. Technol. Biomed. Life Sci.*, 972, 95–101. https://doi.org/10.1016/j.jchromb.2014.09.041.

305 Smith, D.A., Beaumont, K., Maurer, T.S. and Di, L. (2017) Relevance of Half-Life in Drug Design. *J. Med. Chem.*, 61, 4273–4282. https://doi.org/10.1021/ACS.JMEDCHEM.7B00969.

306 Toutain, P.L. and Bousquet-Mélou, A. (2004) Plasma Terminal Half-Life. *J. Vet. Pharmacol. Ther.*, 27, 427–439. https://doi.org/10.1111/J.1365-2885.2004.00600.X.

307 Harris, A.G. (1994) Somatostatin and Somatostatin Analogues: Pharmacokinetics and Pharmacodynamic Effects. *Gut*, 35, S1–S4. https://doi.org/10.1136/GUT.35.3_SUPPL.S1.

308 Stewart, W., Wood, C., Reed, M., Roy, J. and Lipton, R. (2008) Cumulative Lifetime Migraine Incidence in Women and Men. *Cephalalgia*, 28, 1170–1178. https://doi.org/10.1111/j.1468-2982.2008.01666.x.

309 Beaudry, F., Coutu, M. and Brown, N.K. (1999) Determination of Drug±plasma Protein Binding Using Human Serum Albumin Chromatographic Column and Multiple Linear Regression Model. https://doi.org/10.1002/(SICI)1099-0801(199910)13:6.

310 Belpaire, F.M. and Bogaert, M.G. (1990) Binding of Diltiazem to Albumin, A1-Acid Glycoprotein and to Serum in Man. *J. Clin. Pharmacol.*, 30, 311–317. https://doi.org/10.1002/J.1552-4604.1990.TB03599.X.

311 Howard, M.L., Hill, J.J., Galluppi, G.R. and McLean, M.A. (2010) Plasma Protein Binding in Drug Discovery and Development. *Comb. Chem. High Throughput Screen.*, 13, 170–187. https://doi.org/10.2174/138620710790596745.

312 Pollaro, L. and Heinis, C. (2010) Strategies to Prolong the Plasma Residence Time of Peptidedrugs. *Medchemcomm*, 1, 319–324. https://doi.org/10.1039/C0MD00111B.

313 Di Masi, A., Trezza, V., Leboffe, L. and Ascenzi, P. (2016) Human Plasma Lipocalins and Serum Albumin: Plasma Alternative Carriers? *J. Control. Release*, 228, 191–205. https://doi.org/10.1016/J.JCONREL.2016.02.049.

314 Fanali, G., Di Masi, A., Trezza, V., Marino, M., Fasano, M. and Ascenzi, P. (2012) Human Serum Albumin: From Bench to Bedside. *Mol. Aspects Med.*, 33, 209–290. https://doi.org/10.1016/J.MAM.2011.12.002.

315 Fasano, M., Curry, S., Terreno, E., Galliano, M., Fanali, G., Narciso, P., Notari, S. and Ascenzi, P. (2005) The Extraordinary Ligand Binding Properties of Human Serum Albumin. *IUBMB Life*, 57, 787–796. https://doi.org/10.1080/15216540500404093.

316 Yang, F., Zhang, Y. and Liang, H. (2014) Interactive Association of Drugs Binding to Human Serum Albumin. *Int. J. Mol. Sci. 2014, Vol. 15, Pages 3580-3595*, 15, 3580–3595. https://doi.org/10.3390/IJMS15033580.

317 Sugio, S., Kashima, A., Mochizuki, S., Noda, M. and Kobayashi, K. (1999) Crystal Structure of Human Serum Albumin at 2.5 Å Resolution. *Protein Eng. Des. Sel.*, 12, 439–446. https://doi.org/10.1093/PROTEIN/12.6.439.

318 Pollard, T.D. and De La Cruz, E.M. (2013) Take Advantage of Time in Your Experiments: A Guide to Simple, Informative Kinetics Assays. *Mol. Biol. Cell*, 24, 1103–1110. https://doi.org/10.1091/mbc.E13-01-0030.

319 Pollard, T.D. (2010) MBOC Technical Perspective: A Guide to Simple and Informative Binding Assays. *Mol. Biol. Cell*, 21, 4061–4067. https://doi.org/10.1091/mbc.E10-08-0683.

320 Hulme, E.C. and Trevethick, M.A. (2010) Ligand Binding Assays at Equilibrium: Validation and Interpretation. *Br. J. Pharmacol.*, 161, 1219. https://doi.org/10.1111/J.1476-5381.2009.00604.X.

321 Jarmoskaite, I., Alsadhan, I., Vaidyanathan, P.P. and Herschlag, D. (2020) How to Measure and Evaluate Binding Affinities. *Elife*, 9, 1–34. https://doi.org/10.7554/ELIFE.57264.

322 Toma, C.M., Imre, S., Vari, C.E., Muntean, D.L. and Tero-Vescan, A. (2021) Ultrafiltration Method for Plasma Protein Binding Studies and Its Limitations. *Process. 2021, Vol. 9, Page 382*, 9, 382. https://doi.org/10.3390/PR9020382.

323 Nakai, D., Kumamoto, K., Sakikawa, C., Kosaka, T. and Tokui, T. (2004) Evaluation of the Protein Binding Ratio of Drugs by a Micro-Scale Ultracentrifugation Method. *J. Pharm. Sci.*, 93, 847–854. https://doi.org/10.1002/JPS.20012.

324 Sipilä, H., Näntö, V., Kangas, L., Anttila, M. and Halme, T. (1988) Binding of Toremifene to Human Serum Proteins. *Pharmacol. Toxicol.*, 63, 62–64. https://doi.org/10.1111/J.1600-0773.1988.TB00911.X.

325 Barre, J., Chamouard, J.M., Houin, G. and Tillement, J.P. (1985) Equilibrium Dialysis, Ultrafiltration, and Ultracentrifugation Compared for Determining the Plasma-Protein-Binding Characteristics of Valproic Acid. *Clin. Chem.*, 31, 60–64. https://doi.org/10.1093/CLINCHEM/31.1.60.

326 Kariv, I., Cao, H. and Oldenburg, K.R. (2001) Development of a High Throughput Equilibrium Dialysis Method. *J. Pharm. Sci.*, 90, 580–587. https://doi.org/10.1002/1520-6017(200105)90:5<580::aid-jps1014>3.0.co;2-4.

327 Tasker, R.A.R. and Nakatsu, K. (1982) Factors Affecting Ultrafiltration - Assessed Values for Drug Binding. *Clin. Chem.*, 28, 1244–1246.

328 Lima, J.J., MacKichan, J.J., Libertin, N. and Sabino, J. (1983) Influence of Volume Shifts on Drug Binding during Equilibrium Dialysis: Correction and Attenuation. *J. Pharmacokinet. Biopharm. 1983 115*, 11, 483–498. https://doi.org/10.1007/BF01062207.

329 Shave, S., Pham, N.T., Śmieja, C.B. and Auer, M. (2020) Quantitative

Microdialysis: Experimental Protocol and Software for Small Molecule Protein Affinity Determination and for Exclusion of Compounds with Poor Physicochemical Properties. *Methods Protoc. 2020, Vol. 3, Page 55*, 3, 55. https://doi.org/10.3390/MPS3030055.

330 (2017) Single-Use RED Plate with Inserts - Instructions.

331 Waters, N.J., Jones, R., Williams, G. and Sohal, B. (2008) Validation of a Rapid Equilibrium Dialysis Approach for the Measurement of Plasma Protein Binding. *J. Pharm. Sci.*, 97, 4586–4595. https://doi.org/10.1002/JPS.21317.

332 Whitlam, J.B. and Brown, K.F. (1981) Ultrafiltration in Serum Protein Binding Determinations. *J. Pharm. Sci.*, 70, 146–150. https://doi.org/10.1002/JPS.2600700208.

333 Volpp, M. and Holzgrabe, U. (2019) Determination of Plasma Protein Binding for Sympathomimetic Drugs by Means of Ultrafiltration. *Eur. J. Pharm. Sci.*, 127, 175–184. https://doi.org/10.1016/J.EJPS.2018.10.027.

334 Tang, Y., Zhu, H., Zhang, Y. and Huang, C. (2006) Determination of Human Plasma Protein Binding of Baicalin by Ultrafiltration and High-Performance Liquid Chromatography. *Biomed. Chromatogr.*, 20, 1116–1119. https://doi.org/10.1002/BMC.655.

335 Vivaspin 500 Centrifugal Concentrators MWCO 5 KDa | Sigma-Aldrich. https://www.sigmaaldrich.com/GB/en/product/sigma/z614009?gclid=EAIaIQobChMIg_euoujo9AIVi-3tCh0mwg5oEAAYAyAAEgJOoPD_BwE.

336 Mohammad, A.W., Teow, Y.H., Chong, W.C. and Ho, K.C. (2019) Hybrid Processes: Membrane Bioreactor. *Membr. Sep. Princ. Appl. From Mater. Sel. to Mech. Ind. Uses*, 401–470. https://doi.org/10.1016/B978-0-12-812815-2.00013-2.

337 Plum, A., Jensen, L.B. and Kristensen, J.B. (2013) In Vitro Protein Binding of Liraglutide in Human Plasma Determined by Reiterated Stepwise Equilibrium Dialysis. *J. Pharm. Sci.*, 102, 2882–2888. https://doi.org/10.1002/JPS.23648.

338 Greco, I., Hummel, B.D., Vasir, J., Watts, J.L., Koch, J., Hansen, J.E., Nielsen, H.M., Damborg, P. and Hansen, P.R. (2018) In Vitro ADME Properties of Two Novel Antimicrobial Peptoid-Based Compounds as Potential Agents against

Canine Pyoderma. *Mol. 2018, Vol. 23, Page 630*, 23, 630. https://doi.org/10.3390/MOLECULES23030630.

339 Kurtzhals, P., Havelund, S., Jonassen, I., Kiehr, B., Larsen, U.D., Ribel, U. and Markussen, J. (1995) Albumin Binding of Insulins Acylated with Fatty Acids: Characterization of the Ligand-Protein Interaction and Correlation between Binding Affinity and Timing of the Insulin Effect in Vivo. *Biochem. J.*, 312, 725–731. https://doi.org/10.1042/BJ3120725.

340 Trüssel, S., Dumelin, C., Frey, K., Villa, A., Buller, F. and Neri, D. (2009) New Strategy for the Extension of the Serum Half-Life of Antibody Fragments. *Bioconjug. Chem.*, 20, 2286–2292. https://doi.org/10.1021/BC9002772/SUPPL_FILE/BC9002772_SI_001.PDF.

341 Dumelin, C.E., Trüssel, S., Buller, F., Trachsel, E., Bootz, F., Zhang, Y., Mannocci, L., Beck, S.C., Drumea-Mirancea, M., Seeliger, M.W., Baltes, C., Müggler, T., Kranz, F., Rudin, M., Melkko, S., Scheuermann, J., Neri, D., Trüssel, S., Buller, F., Bootz, F., Zhang, Y., Mannocci, L., Scheuermann, J., Neri, D., Beck, S.C., Drumea-Mirancea, M., Seeliger, M.W., Baltes, C., Müggler, T., Kranz, F. and Rudin, M. (2008) A Portable Albumin Binder from a DNA-Encoded Chemical Library. *Angew. Chemie*, 120, 3240–3245. https://doi.org/10.1002/ANGE.200704936.

342 Middendorp, S.J., Wilbs, J., Quarroz, C., Calzavarini, S., Angelillo-Scherrer, A. and Heinis, C. (2017) Peptide Macrocycle Inhibitor of Coagulation Factor XII with Subnanomolar Affinity and High Target Selectivity. *J. Med. Chem.*, 60, 1151–1158. https://doi.org/10.1021/ACS.JMEDCHEM.6B01548/SUPPL_FILE/JM6B01548_SI_002.PDB.

343 Wolf, L.M., Servossz, S.L. and Moss, M.A. (2017) Peptoids: Emerging Therapeutics for Neurodegeneration. *J. Neurol. Neuromedicine*, 2, 1–5. https://doi.org/10.29245/2572.942x/2017/7.1135.

344 Luo, Y., Bolt, H.L., Eggimann, G.A., McAuley, D.F., McMullan, R., Curran, T., Zhou, M., Jahoda, P.C.A.B., Cobb, S.L. and Lundy, F.T. (2017) Peptoid Efficacy against Polymicrobial Biofilms Determined by Using Propidium Monoazide-

Modified Quantitative PCR. *Chembiochem*, 18, 111. https://doi.org/10.1002/CBIC.201600381.

345 Jain, D. and Basniwal, P.K. (2013) ICH Guideline Practice: Application of Validated RP-HPLC-DAD Method for Determination of Tapentadol Hydrochloride in Dosage Form. *J. Anal. Sci. Technol.*, 4, 1–7. https://doi.org/10.1186/2093-3371-4-9/TABLES/3.

346 Boöttger, R., Hoffmann, R. and Knappe, D. (2017) Differential Stability of Therapeutic Peptides with Different Proteolytic Cleavage Sites in Blood, Plasma and Serum. *PLoS One*, 12, e0178943. https://doi.org/10.1371/JOURNAL.PONE.0178943.

347 Jenssen, H. and Aspmo, S.I. (2008) Serum Stability of Peptides. Methods in Molecular Biology, 177–186. https://doi.org/10.1007/978-1-59745-419-3_10.

348 Mant, C.T. and Hodges, R.S. (1991) High-Performance Liquid Chromatography of Peptides and Proteins: Separation, Analysis, and Conformation . Mant, C.T. and Hodges, R.S., Eds. https://books.google.it/books?hl=en&lr=&id=yksPEAAAQBAJ&oi=fnd&pg=PP1&dq=peptide+separation+hplc+method&ots=dZWDLyQnMr&sig=Ys8QBwfx28MIzDvggaDRZxB0ji4&redir_esc=y#v=onepage&q=peptide separation hplc method&f=false.

349 Factors Affecting Resolution in HPLC. https://www.sigmaaldrich.com/GB/en/technical-documents/technical-article/analytical-chemistry/small-molecule-hplc/factors-affecting-resolution-in-hplc#improve-resolution.

350 Ujah, C.O., Popoola, A.P.I., Popoola, O.M. and Aigbodion, V.S. (2018) Optimisation of Spark Plasma Sintering Parameters of Al-CNTs-Nb Nano-Composite Using Taguchi Design of Experiment. *Int. J. Adv. Manuf. Technol. 2018 1005*, 100, 1563–1573. https://doi.org/10.1007/S00170-018-2705-3.

351 Dash, R.N., Mohammed, H. and Humaira, T. (2016) An Integrated Taguchi and Response Surface Methodological Approach for the Optimization of an HPLC Method to Determine Glimepiride in a Supersaturatable Self-Nanoemulsifying Formulation. *Saudi Pharm. J.*, 24, 92–103.

https://doi.org/10.1016/J.JSPS.2015.03.004.

352 (1994) Reviewer Guidance - Validation of Chromatographic Methods. *Cent. Drug Eval. Res.* .

353 Vashist, S.K. and Luong, J.H.T. (2018) Bioanalytical Requirements and Regulatory Guidelines for Immunoassays. *Handb. Immunoass. Technol. Approaches, Performances, Appl.*, 81–95. https://doi.org/10.1016/B978-0-12-811762-0.00004-9.

354 Green, B.D., Mooney, M.H., Gault, V., Irwin, N., Bailey, C., Harriott, P., Greer, B., O'Harte, F.P.M. and Flatt, P.R. (2004) N-Terminal His(7)-Modification of Glucagon-like Peptide-1(7-36) Amide Generates Dipeptidyl Peptidase IV-Stable Analogues with Potent Antihyperglycaemic Activity. *J. Endocrinol.*, 180, 379–388. https://doi.org/10.1677/joe.0.1800379.

355 Arnott, J.A. and Planey, S.L. (2012) The Influence of Lipophilicity in Drug Discovery and Design. *http://dx.doi.org/10.1517/17460441.2012.714363*, 7, 863–875. https://doi.org/10.1517/17460441.2012.714363.

356 van de Waterbeemd, H., Smith, D.A. and Jones, B.C. (2001) Lipophilicity in PK Design: Methyl, Ethyl, Futile. *J. Comput. Mol. Des. 2001 153*, 15, 273–286. https://doi.org/10.1023/A:1008192010023.

357 McHugh, C.E., Flott, T.L., Schooff, C.R., Smiley, Z., Puskarich, M.A., Myers, D.D., Younger, J.G., Jones, A.E. and Stringer, K.A. (2018) Rapid, Reproducible, Quantifiable NMR Metabolomics: Methanol and Methanol: Chloroform Precipitation for Removal of Macromolecules in Serum and Whole Blood. *Metab. 2018, Vol. 8, Page 93*, 8, 93. https://doi.org/10.3390/METABO8040093.

358 Xiao, J.F., Zhou, B. and Ressom, H.W. (2012) Metabolite Identification and Quantitation in LC-MS/MS-Based Metabolomics. *TrAC Trends Anal. Chem.*, 32, 1–14. https://doi.org/10.1016/J.TRAC.2011.08.009.

359 Greenough, C., Jenkins, R.E., Kitteringham, N.R., Pirmohamed, M., Park, B.K. and Pennington, S.R. (2004) A Method for the Rapid Depletion of Albumin and Immunoglobulin from Human Plasma. *Proteomics*, 4, 3107–3111. https://doi.org/10.1002/PMIC.200300815.

360 Ye, Z., Zetterberg, C. and Gao, H. (2017) Automation of Plasma Protein Binding Assay Using Rapid Equilibrium Dialysis Device and Tecan Workstation. *J. Pharm. Biomed. Anal.*, 140, 210–214. https://doi.org/10.1016/J.JPBA.2017.03.019.

361 van Liempd, S., Morrison, D., Sysmans, L., Nelis, P. and Mortishire-Smith, R. (2011) Development and Validation of a Higher-Throughput Equilibrium Dialysis Assay for Plasma Protein Binding: *https://doi.org/10.1016/j.jala.2010.06.002*, 16, 56–67. https://doi.org/10.1016/J.JALA.2010.06.002.

362 Di, L., Umland, J.P., Trapa, P.E. and Maurer, T.S. (2012) Impact of Recovery on Fraction Unbound Using Equilibrium Dialysis. *J. Pharm. Sci.*, 101, 1327–1335. https://doi.org/10.1002/JPS.23013.

363 Langer, R. (1998) Drug Delivery and Targeting. *Nature*, 392, 5–10. https://doi.org/10.1016/s0378-5173(02)00260-0.

364 Tran, V.T., Benoît, J.P. and Venier-Julienne, M.C. (2011) Why and How to Prepare Biodegradable, Monodispersed, Polymeric Microparticles in the Field of Pharmacy? *Int. J. Pharm.*, 407, 1–11. https://doi.org/10.1016/J.IJPHARM.2011.01.027.

365 Varde, N.K. and Pack, D.W. (2005) Microspheres for Controlled Release Drug Delivery. *Expert Opin. Biol. Ther.*, 4, 35–51. https://doi.org/10.1517/14712598.4.1.35.

366 Nasrollahzadeh, M., Sajadi, S.M., Sajjadi, M. and Issaabadi, Z. (2019) An Introduction to Nanotechnology. *Interface Sci. Technol.*, 28, 1–27. https://doi.org/10.1016/B978-0-12-813586-0.00001-8.

367 Cui, H., Webber, M.J. and Stupp, S.I. (2010) Self-Assembly of Peptide Amphiphiles: From Molecules to Nanostructures to Biomaterials. *Pept. Sci.*, 94, 1–18. https://doi.org/10.1002/BIP.21328.

368 Kreuter, J. (2007) Nanoparticles—a Historical Perspective. *Int. J. Pharm.*, 331, 1–10. https://doi.org/10.1016/J.IJPHARM.2006.10.021.

369 Banks, W.A. (2008) Delivery of Peptides to the Brain: Emphasis on Therapeutic Development. *Pept. Sci.*, 90, 589–594. https://doi.org/10.1002/BIP.20980.

370 Dufes, C., Olivier, J.C., Gaillard, F., Gaillard, A., Couet, W. and Muller, J.M. (2003) Brain Delivery of Vasoactive Intestinal Peptide (VIP) Following Nasal Administration to Rats. *Int. J. Pharm.*, 255, 87–97. https://doi.org/10.1016/S0378-5173(03)00039-5.

371 Wang, Z., Xiong, G., Tsang, W.C., Schätzlein, A.G. and Uchegbu, I.F. (2019) Nose-to-Brain Delivery. *J. Pharmacol. Exp. Ther.*, 370, 593–601. https://doi.org/10.1124/JPET.119.258152.

372 Seju, U., Kumar, A. and Sawant, K.K. (2011) Development and Evaluation of Olanzapine-Loaded PLGA Nanoparticles for Nose-to-Brain Delivery: In Vitro and in Vivo Studies. *Acta Biomater.*, 7, 4169–4176. https://doi.org/10.1016/J.ACTBIO.2011.07.025.

373 Schroeter, J.D., Kimbell, J.S. and Asgharian, B. (2006) Analysis of Particle Deposition in the Turbinate and Olfactory Regions Using a Human Nasal Computational Fluid Dynamics Model. *http://www.liebertpub.com/jam*, 19, 301–313. https://doi.org/10.1089/JAM.2006.19.301.

374 Djupesland, P.G. (2013) Nasal Drug Delivery Devices: Characteristics and Performance in a Clinical Perspective-a Review. *Drug Deliv. Transl. Res.*, 3, 42–62. https://doi.org/10.1007/S13346-012-0108-9/FIGURES/4.

375 Cho, W., Kim, M.-S.S., Jung, M.-S.S., Park, J., Cha, K.-H.H., Kim, J.-S.S., Park, H.J., Alhalaweh, A., Velaga, S.P. and Hwang, S.-J.J. (2015) Design of Salmon Calcitonin Particles for Nasal Delivery Using Spray-Drying and Novel Supercritical Fluid-Assisted Spray-Drying Processes. *Int. J. Pharm.*, 478, 288–296. https://doi.org/10.1016/J.IJPHARM.2014.11.051.

376 Giuliani, A., Balducci, A.G., Zironi, E., Colombo, G., Bortolotti, F., Lorenzini, L., Galligioni, V., Pagliuca, G., Scagliarini, A., Calzà, L. and Sonvico, F. (2018) In Vivo Nose-to-Brain Delivery of the Hydrophilic Antiviral Ribavirin by Microparticle Agglomerates. *Drug Deliv.*, 25, 376–387. https://doi.org/10.1080/10717544.2018.1428242/SUPPL_FILE/IDRD_A_1428242_SM7572.DOCX.

377 Antosova, Z., Mackova, M., Kral, V. and Macek, T. (2009) Therapeutic Application of Peptides and Proteins: Parenteral Forever? *Trends Biotechnol.*,

27, 628–635. https://doi.org/10.1016/J.TIBTECH.2009.07.009.

378 Du, A.W. and Stenzel, M.H. (2014) Drug Carriers for the Delivery of Therapeutic Peptides. *Biomacromolecules*, 15, 1097–1114. https://doi.org/10.1021/BM500169P.

379 Craft, S., Baker, L.D., Montine, T.J., Minoshima, S., Watson, G.S., Claxton, A., Arbuckle, M., Callaghan, M., Tsai, E., Plymate, S.R., Green, P.S., Leverenz, J., Cross, D. and Gerton, B. (2012) Intranasal Insulin Therapy for Alzheimer Disease and Amnestic Mild Cognitive Impairment: A Pilot Clinical Trial. *Arch. Neurol.*, 69, 29–38. https://doi.org/10.1001/ARCHNEUROL.2011.233.

380 Born, J., Lange, T., Kern, W., McGregor, G.P., Bickel, U. and Fehm, H.L. (2002) Sniffing Neuropeptides: A Transnasal Approach to the Human Brain. *Nat. Neurosci. 2002 56*, 5, 514–516. https://doi.org/10.1038/nn0602-849.

381 Thorne, R.G., Hanson, L.R., Ross, T.M., Tung, D. and Frey, W.H. (2008) Delivery of Interferon-β to the Monkey Nervous System Following Intranasal Administration. *Neuroscience*, 152, 785–797. https://doi.org/10.1016/J.NEUROSCIENCE.2008.01.013.

382 Parker, K.J., Oztan, O., Libove, R.A., Sumiyoshi, R.D., Jackson, L.P., Karhson, D.S., Summers, J.E., Hinman, K.E., Motonaga, K.S., Phillips, J.M., Carson, D.S., Garner, J.P. and Hardan, A.Y. (2017) Intranasal Oxytocin Treatment for Social Deficits and Biomarkers of Response in Children with Autism. *Proc. Natl. Acad. Sci. U. S. A.*, 114, 8119–8124. https://doi.org/10.1073/PNAS.1705521114/-/DCSUPPLEMENTAL.

383 Buchthal, B., Weiss, U. and Bading, H. (2018) Post-Injury Nose-to-Brain Delivery of Activin A and SerpinB2 Reduces Brain Damage in a Mouse Stroke Model. *Mol. Ther.*, 26, 2357–2365. https://doi.org/10.1016/J.YMTHE.2018.07.018.

384 Lin, W., Xie, X., Deng, J., Liu, H., Chen, Y., Fu, X., Liu, H. and Yang, Y. (2015) Cell-Penetrating Peptide-Doxorubicin Conjugate Loaded NGR-Modified Nanobubbles for Ultrasound Triggered Drug Delivery. *http://dx.doi.org/10.3109/1061186X.2015.1058802*, 24, 134–146. https://doi.org/10.3109/1061186X.2015.1058802.

385 Godfrey, L., Iannitelli, A., Garrett, N.L., Moger, J., Imbert, I., King, T., Porreca, F., Soundararajan, R., Lalatsa, A., Schätzlein, A.G. and Uchegbu, I.F. (2018) Nanoparticulate Peptide Delivery Exclusively to the Brain Produces Tolerance Free Analgesia. *J. Control. Release*, 270, 135–144. https://doi.org/10.1016/j.jconrel.2017.11.041.

386 Van Woensel, M., Mathivet, T., Wauthoz, N., Rosière, R., Garg, A.D., Agostinis, P., Mathieu, V., Kiss, R., Lefranc, F., Boon, L., Belmans, J., Van Gool, S.W., Gerhardt, H., Amighi, K. and De Vleeschouwer, S. (2017) Sensitization of Glioblastoma Tumor Micro-Environment to Chemo- and Immunotherapy by Galectin-1 Intranasal Knock-down Strategy. *Sci. Reports 2017 71*, 7, 1–14. https://doi.org/10.1038/s41598-017-01279-1.

387 Duro-Castano, A., Moreira Leite, D., Forth, J., Deng, Y., Matias, D., Noble Jesus, C. and Battaglia, G. (2020) Designing Peptide Nanoparticles for Efficient Brain Delivery. *Adv. Drug Deliv. Rev.*, 160, 52–77. https://doi.org/10.1016/J.ADDR.2020.10.001.

388 Lalatsa, A., Schatzlein, A.G. and Uchegbu, I.F. (2014) Strategies To Deliver Peptide Drugs to the Brain. *Mol. Pharm.*, 11, 1081–1093. https://doi.org/10.1021/MP400680D.

389 Lalatsa, A., Schatzlein, A.G. and Uchegbu, I.F. (2012) Nanostructured Biomaterials for Overcoming Biological Barriers: Physiological Considerations and Mechanistic Issues. Alonso, M.J. and Csaba, N.S., Eds. https://books.google.it/books?hl=en&lr=&id=4BveZLfcDVMC&oi=fnd&pg=PA329&dq=Lalatsa,+A.%3B+Schatzlein,+A.+G.%3B+Uchegbu,+I.+F.+Nanostructures+Overcoming+the+Blood-Brain+Barrier:+Physiological+Considerations+and+Mechanistic+Issues.+In+Nanostructured+Biomaterials+for+Overcoming+Biological+Barriers%3B+Alonso,+M.+J.,+Csaba,+N.,+Eds.%3B+Royal+&ots=Sg4mk17mCc&sig=fdJRS9z_So2Phv5cdUxv1J3pGxo&redir_esc=y#v=onepage&q&f=false.

390 Danhier, F., Ansorena, E., Silva, J.M., Coco, R., Le Breton, A. and Préat, V. (2012) PLGA-Based Nanoparticles: An Overview of Biomedical Applications. *J. Control. Release*, 161, 505–522.

https://doi.org/10.1016/J.JCONREL.2012.01.043.

391 Musumeci, T., Serapide, M.F., Pellitteri, R., Dalpiaz, A., Ferraro, L., Dal Magro, R., Bonaccorso, A., Carbone, C., Veiga, F., Sancini, G. and Puglisi, G. (2018) Oxcarbazepine Free or Loaded PLGA Nanoparticles as Effective Intranasal Approach to Control Epileptic Seizures in Rodents. *Eur. J. Pharm. Biopharm.*, 133, 309–320. https://doi.org/10.1016/J.EJPB.2018.11.002.

392 Astete, C.E. and Sabliov, C.M. (2012) Synthesis and Characterization of PLGA Nanoparticles. *http://dx.doi.org/10.1163/156856206775997322*, 17, 247–289. https://doi.org/10.1163/156856206775997322.

393 McCall, R.L. and Sirianni, R.W. (2013) PLGA Nanoparticles Formed by Single- or Double-Emulsion with Vitamin E-TPGS. *J. Vis. Exp.*, 82, 51015. https://doi.org/10.3791/51015.

394 Kizilbey, K. (2019) Optimization of Rutin-Loaded PLGA Nanoparticles Synthesized by Single-Emulsion Solvent Evaporation Method. *ACS Omega*, 4, 555–562. https://doi.org/10.1021/ACSOMEGA.8B02767.

395 Alshamsan, A. (2014) Nanoprecipitation Is More Efficient than Emulsion Solvent Evaporation Method to Encapsulate Cucurbitacin I in PLGA Nanoparticles. *Saudi Pharm. J.*, 22, 219–222. https://doi.org/10.1016/J.JSPS.2013.12.002.

396 Govender, T., Stolnik, S., Garnett, M.C., Illum, L. and Davis, S.S. (1999) PLGA Nanoparticles Prepared by Nanoprecipitation: Drug Loading and Release Studies of a Water Soluble Drug. *J. Control. Release*, 57, 171–185. https://doi.org/10.1016/S0168-3659(98)00116-3.

397 Bisht, R. and Rupenthal, I.D. (2016) PLGA Nanoparticles for Intravitreal Peptide Delivery: Statistical Optimization, Characterization and Toxicity Evaluation. *https://doi.org/10.1080/10837450.2016.1240184*, 23, 324–333. https://doi.org/10.1080/10837450.2016.1240184.

398 Chen, Y., Wang, F. and Benson, H.A.E. (2008) Effect of Formulation Factors on Incorporation of the Hydrophilic Peptide Dalargin into PLGA and MPEG-PLGA Nanoparticles. *Pept. Sci.*, 90, 644–650. https://doi.org/10.1002/BIP.21013.

399 Fessi, H., Puisieux, F., Devissaguet, J.P., Ammoury, N. and Benita, S. (1989)

Nanocapsule Formation by Interfacial Polymer Deposition Following Solvent Displacement. *Int. J. Pharm.*, 55, R1–R4. https://doi.org/10.1016/0378-5173(89)90281-0.

400 Martínez Rivas, C.J., Tarhini, M., Badri, W., Miladi, K., Greige-Gerges, H., Nazari, Q.A., Galindo Rodríguez, S.A., Román, R.Á., Fessi, H. and Elaissari, A. (2017) Nanoprecipitation Process: From Encapsulation to Drug Delivery. *Int. J. Pharm.*, 532, 66–81. https://doi.org/10.1016/J.IJPHARM.2017.08.064.

401 Morales-Cruz, M., Flores-Fernández, G.M., Morales-Cruz, M., Orellano, E.A., Rodriguez-Martinez, J.A., Ruiz, M. and Griebenow, K. (2012) Two-Step Nanoprecipitation for the Production of Protein-Loaded PLGA Nanospheres. *Results Pharma Sci.*, 2, 79–85. https://doi.org/10.1016/J.RINPHS.2012.11.001.

402 Barichello, J.M., Morishita, M., Takayama, K. and Nagai, T. (1999) Encapsulation of Hydrophilic and Lipophilic Drugs in PLGA Nanoparticles by the Nanoprecipitation Method. *http://dx.doi.org/10.1081/DDC-100102197*, 25, 471–476. https://doi.org/10.1081/DDC-100102197.

403 Lancheros, R., Guerrero, C.A. and Godoy-Silva, R.D. (2018) Improvement of N-Acetylcysteine Loaded in PLGA Nanoparticles by Nanoprecipitation Method. *J. Nanotechnol.*, 2018. https://doi.org/10.1155/2018/3620373.

404 Varypataki, E.M., Silva, A.L., Barnier-Quer, C., Collin, N., Ossendorp, F. and Jiskoot, W. (2016) Synthetic Long Peptide-Based Vaccine Formulations for Induction of Cell Mediated Immunity: A Comparative Study of Cationic Liposomes and PLGA Nanoparticles. *J. Control. Release*, 226, 98–106. https://doi.org/10.1016/J.JCONREL.2016.02.018.

405 Silva, A.L., Rosalia, R.A., Sazak, A., Carstens, M.G., Ossendorp, F., Oostendorp, J. and Jiskoot, W. (2013) Optimization of Encapsulation of a Synthetic Long Peptide in PLGA Nanoparticles: Low-Burst Release Is Crucial for Efficient CD8+ T Cell Activation. *Eur. J. Pharm. Biopharm.*, 83, 338–345. https://doi.org/10.1016/J.EJPB.2012.11.006.

406 Derman, S., Mustafaeva, Z.A., Abamor, E.S., Bagirova, M. and Allahverdiyev, A. (2015) Preparation, Characterization and Immunological Evaluation: Canine Parvovirus Synthetic Peptide Loaded Plga Nanoparticles. *J. Biomed. Sci.*, 22, 1–

12. https://doi.org/10.1186/S12929-015-0195-2/FIGURES/9.

407 Chereddy, K.K., Her, C.H., Comune, M., Moia, C., Lopes, A., Porporato, P.E., Vanacker, J., Lam, M.C., Steinstraesser, L., Sonveaux, P., Zhu, H., Ferreira, L.S., Vandermeulen, G. and Préat, V. (2014) PLGA Nanoparticles Loaded with Host Defense Peptide LL37 Promote Wound Healing. *J. Control. Release*, 194, 138–147. https://doi.org/10.1016/J.JCONREL.2014.08.016.

408 Dos Reis, L.G., Lee, W.H., Svolos, M., Moir, L.M., Jaber, R., Windhab, N., Young, P.M. and Traini, D. (2019) Nanotoxicologic Effects of PLGA Nanoparticles Formulated with a Cell-Penetrating Peptide: Searching for a Safe PDNA Delivery System for the Lungs. *Pharm. 2019, Vol. 11, Page 12*, 11, 12. https://doi.org/10.3390/PHARMACEUTICS11010012.

409 Self-Assembly. Nature Portfolio. https://doi.org/10.1038/s41557-021-00864-2.

410 Dehsorkhi, A., Castelletto, V. and Hamley, I.W. (2014) Self-Assembling Amphiphilic Peptides. *J. Pept. Sci.*, 20, 453–467. https://doi.org/10.1002/PSC.2633.

411 Dognini, P., Coxon, C.R., Alves, W.A., Giuntini, F., Neves, S., Amparo, M., Faustino, F. and Moura, N.M.M. (2021) Peptide-Tetrapyrrole Supramolecular Self-Assemblies: State of the Art. *Mol. 2021, Vol. 26, Page 693*, 26, 693. https://doi.org/10.3390/MOLECULES26030693.

412 Lee, S., Trinh, T.H.T., Yoo, M., Shin, J., Lee, H., Kim, J., Hwang, E., Lim, Y.B. and Ryou, C. (2019) Self-Assembling Peptides and Their Application in the Treatment of Diseases. *Int. J. Mol. Sci. 2019, Vol. 20, Page 5850*, 20, 5850. https://doi.org/10.3390/IJMS20235850.

413 Zhang, S. (2017) Discovery and Design of Self-Assembling Peptides. *Interface Focus*, 7. https://doi.org/10.1098/RSFS.2017.0028.

414 Zhao, X., Pan, F. and Lu, J.R. (2008) Recent Development of Peptide Self-Assembly. *Prog. Nat. Sci.*, 18, 653–660. https://doi.org/10.1016/J.PNSC.2008.01.012.

415 Raymond, D.M. and Nilsson, B.L. (2018) Multicomponent Peptide Assemblies. *Chem. Soc. Rev.*, 47, 3659–3720. https://doi.org/10.1039/C8CS00115D.

416 Wang, J., Liu, K., Xing, R. and Yan, X. (2016) Peptide Self-Assembly: Thermodynamics and Kinetics. *Chem. Soc. Rev.*, 45, 5589–5604. https://doi.org/10.1039/C6CS00176A.

417 Gupta, S., Singh, I., Sharma, A.K. and Kumar, P. (2020) Ultrashort Peptide Self-Assembly: Front-Runners to Transport Drug and Gene Cargos. *Front. Bioeng. Biotechnol.*, 8, 504. https://doi.org/10.3389/FBIOE.2020.00504/BIBTEX.

418 Claussen, R.C., Rabatic, B.M. and Stupp, S.I. (2003) Aqueous Self-Assembly of Unsymmetric Peptide Bolaamphiphiles into Nanofibers with Hydrophilic Cores and Surfaces. *J. Am. Chem. Soc.*, 125, 12680–12681. https://doi.org/10.1021/JA035882R/SUPPL_FILE/JA035882RSI20030726_111934.PDF.

419 Qiu, F., Chen, Y., Tang, C., Zhou, Q., Wang, C., Shi, Y.K. and Zhao, X. (2008) De Novo Design of a Bolaamphiphilic Peptide with Only Natural Amino Acids. *Macromol. Biosci.*, 8, 1053–1059. https://doi.org/10.1002/MABI.200800180.

420 Hamley, I.W. and Hamley, I.W. (2014) Peptide Nanotubes. *Angew. Chemie Int. Ed.*, 53, 6866–6881. https://doi.org/10.1002/ANIE.201310006.

421 Gottlieb, D., Morin, S.A., Jin, S. and Raines, R.T. (2008) Self-Assembled Collagen-like Peptide Fibers as Templates for Metallic Nanowires. *J. Mater. Chem.*, 18, 3865–3870. https://doi.org/10.1039/B807150K.

422 Reches, M. and Gazit, E. (2006) Molecular Self-Assembly of Peptide Nanostructures: Mechanism of Association and Potential Uses. *Curr. Nanosci.*, 2, 105–111. https://doi.org/10.2174/157341306776875802.

423 Hamley, I.W. (2011) Self-Assembly of Amphiphilic Peptides. *Soft Matter*, 7, 4122–4138. https://doi.org/10.1039/c0sm01218a.

424 Löwik, D.W.P.M. and van Hest, J.C.M. (2004) Peptide Based Amphiphiles. *Chem. Soc. Rev.*, 33, 234–245. https://doi.org/10.1039/B212638A.

425 Zhao, X. (2009) Design of Self-Assembling Surfactant-like Peptides and Their Applications. *Curr. Opin. Colloid Interface Sci.*, 14, 340–348. https://doi.org/10.1016/J.COCIS.2009.07.002.

426 Vauthey, S., Santoso, S., Gong, H., Watson, N. and Zhang, S. (2002) Molecular Self-Assembly of Surfactant-like Peptides to Form Nanotubes and

Nanovesicles. *Proc. Natl. Acad. Sci.*, 99, 5355–5360. https://doi.org/10.1073/PNAS.072089599.

427 Wang, J., Han, S., Meng, G., Xu, H., Xia, D., Zhao, X., Schweins, R. and Lu, J.R. (2009) Dynamic Self-Assembly of Surfactant-like Peptides A6K and A9K. *Soft Matter*, 5, 3870–3878. https://doi.org/10.1039/B901653H.

428 Guo, C., Luo, Y., Zhou, R. and Wei, G. (2012) Probing the Self-Assembly Mechanism of Diphenylalanine-Based Peptide Nanovesicles and Nanotubes. *ACS Nano*, 6, 3907–3918. https://doi.org/10.1021/NN300015G/SUPPL_FILE/NN300015G_SI_003.AVI.

429 McCloskey, A.P., Draper, E.R., Gilmore, B.F. and Laverty, G. (2017) Ultrashort Self-Assembling Fmoc-Peptide Gelators for Anti-Infective Biomaterial Applications. *J. Pept. Sci.*, 23, 131–140. https://doi.org/10.1002/PSC.2951.

430 Chen, P. (2005) Self-Assembly of Ionic-Complementary Peptides: A Physicochemical Viewpoint. *Colloids Surfaces A Physicochem. Eng. Asp.*, 261, 3–24. https://doi.org/10.1016/J.COLSURFA.2004.12.048.

431 D'Auria, G., Vacatello, M., Falcigno, L., Paduano, L., Mangiapia, G., Calvanese, L., Gambaretto, R., Dettin, M. and Paolillo, L. (2009) Self-Assembling Properties of Ionic-Complementary Peptides. *J. Pept. Sci.*, 15, 210–219. https://doi.org/10.1002/PSC.1083.

432 Zhang, H., Park, J., Jiang, Y. and Woodrow, K.A. (2017) Rational Design of Charged Peptides That Self-Assemble into Robust Nanofibers as Immune-Functional Scaffolds. *Acta Biomater.*, 55, 183–193. https://doi.org/10.1016/J.ACTBIO.2017.03.041.

433 Kabiri, M., Bushnak, I., McDermot, M.T. and Unsworth, L.D. (2013) Toward a Mechanistic Understanding of Ionic Self-Complementary Peptide Self-Assembly: Role of Water Molecules and Ions. *Biomacromolecules*, 14, 3943–3950. https://doi.org/10.1021/BM401077B.

434 Insua, I. and Montenegro, J. (2020) 1D to 2D Self Assembly of Cyclic Peptides. *J. Am. Chem. Soc.*, 142, 300–307. https://doi.org/10.1021/JACS.9B10582/SUPPL_FILE/JA9B10582_SI_002.XYZ.

435 Song, Q., Cheng, Z., Kariuki, M., Hall, S.C.L., Hill, S.K., Rho, J.Y. and Perrier, S.

(2021) Molecular Self-Assembly and Supramolecular Chemistry of Cyclic Peptides. *Chem. Rev.*, 121, 13936–13995. https://doi.org/10.1021/ACS.CHEMREV.0C01291.

436 Kokkoli, E., Mardilovich, A., Wedekind, A., Rexeisen, E.L., Garg, A. and Craig, J.A. (2006) Self-Assembly and Applications of Biomimetic and Bioactive Peptide - Amphiphiles. *Soft Matter*, 2, 1015–1024. https://doi.org/10.1039/B608929A.

437 Israelachvili, J.N. (2011) Intermolecular and Surface Forces. https://books.google.it/books?hl=en&lr=&id=vgyBJbtNOcoC&oi=fnd&pg=PP1&dq=J.+N.+Israelachvili,+Intermolecular+and+surface+forces,+1992,+San+Diego,+Academic+Press.&ots=_QRl5qx4Pa&sig=2nQMpsuGnnRTWku2k-0llyfhnUY&redir_esc=y#v=onepage&q&f=false.

438 Miravet, J.F., Escuder, B., Segarra-Maset, M.D., Tena-Solsona, M., Hamley, I.W., Dehsorkhi, A. and Castelletto, V. (2013) Self-Assembly of a Peptide Amphiphile: Transition from Nanotape Fibrils to Micelles. *Soft Matter*, 9, 3558–3564. https://doi.org/10.1039/C3SM27899A.

439 Shimada, T., Sakamoto, N., Motokawa, R., Koizumi, S. and Tirrell, M. (2011) Self-Assembly Process of Peptide Amphiphile Worm-Like Micelles. *J. Phys. Chem. B*, 116, 240–243. https://doi.org/10.1021/JP209105Z.

440 van Hell, A.J., Costa, C.I.C.A., Flesch, F.M., Sutter, M., Jiskoot, W., Crommelin, D.J.A., Hennink, W.E. and Mastrobattista, E. (2007) Self-Assembly of Recombinant Amphiphilic Oligopeptides into Vesicles. *Biomacromolecules*, 8, 2753–2761. https://doi.org/10.1021/BM0704267/SUPPL_FILE/BM0704267-FILE002.PDF.

441 Gudlur, S., Sukthankar, P., Gao, J., Avila, L.A., Hiromasa, Y., Chen, J., Iwamoto, T. and Tomich, J.M. (2012) Peptide Nanovesicles Formed by the Self-Assembly of Branched Amphiphilic Peptides. *PLoS One*, 7, e45374. https://doi.org/10.1371/JOURNAL.PONE.0045374.

442 Mishra, A., Panda, J.J., Basu, A. and Chauhan, V.S. (2008) Nanovesicles Based on Self-Assembly of Conformationally Constrained Aromatic Residue Containing Amphiphilic Dipeptides. *Langmuir*, 24, 4571–4576.

https://doi.org/10.1021/LA7034533/SUPPL_FILE/LA7034533-FILE002.PDF.

443 Nagai, A., Nagai, Y., Qu, H. and Zhang, S. (2007) Dynamic Behaviors of Lipid-like Self-Assembling Peptide A6D and A6K Nanotubes. *J. Nanosci. Nanotechnol.*, 7, 2246–2252. https://doi.org/10.1166/JNN.2007.647.

444 Hamley, I.W., Dehsorkhi, A., Jauregi, P., Seitsonen, J., Ruokolainen, J., Coutte, F., Chataigné, G. and Jacques, P. (2013) Self-Assembly of Three Bacterially-Derived Bioactive Lipopeptides. *Soft Matter*, 9, 9572–9578. https://doi.org/10.1039/C3SM51514A.

445 Amalia Aggeli, Mark Bell, Neville Boden, Keen, J.N., McLeish, T.C.B., Irina Nyrkova, SheenaE. Radford and Alexander Semenov. (1997) Engineering of Peptide β-Sheet Nanotapes. *J. Mater. Chem.*, 7, 1135–1145. https://doi.org/10.1039/A701088E.

446 Dehsorkhi, A., Castelletto, V., Hamley, I.W., Adamcik, J. and Mezzenga, R. (2013) The Effect of PH on the Self-Assembly of a Collagen Derived Peptide Amphiphile. *Soft Matter*, 9, 6033–6036. https://doi.org/10.1039/C3SM51029H.

447 Laverty, G., McCloskey, A.P., Gilmore, B.F., Jones, D.S., Zhou, J. and Xu, B. (2014) Ultrashort Cationic Naphthalene-Derived Self-Assembled Peptides as Antimicrobial Nanomaterials. *Biomacromolecules*, 15, 3429–3439. https://doi.org/10.1021/BM500981Y/SUPPL_FILE/BM500981Y_SI_001.PDF.

448 Ghosh, A., Haverick, M., Stump, K., Yang, X., Tweedle, M.F. and Goldberger, J.E. (2012) Fine-Tuning the PH Trigger of Self-Assembly. *J. Am. Chem. Soc.*, 134, 3647–3650.
https://doi.org/10.1021/JA211113N/SUPPL_FILE/JA211113N_SI_001.PDF.

449 Aggeli, A., Bell, M., Carrick, L.M., Fishwick, C.W.G., Harding, R., Mawer, P.J., Radford, S.E., Strong, A.E. and Boden, N. (2003) PH as a Trigger of Peptide β-Sheet Self-Assembly and Reversible Switching between Nematic and Isotropic Phases. *J. Am. Chem. Soc.*, 125, 9619–9628. https://doi.org/10.1021/JA021047I.

450 Rajagopal, K., Lamm, M.S., Haines-Butterick, L.A., Pochan, D.J. and Schneider, J.P. (2009) Tuning the PH Responsiveness of β-Hairpin Peptide Folding, Self-

Assembly, and Hydrogel Material Formation. *Biomacromolecules*, 10, 2619–2625. https://doi.org/10.1021/BM900544E/SUPPL_FILE/BM900544E_SI_001.PDF.

451 Chen, Y., Gan, H.X. and Tong, Y.W. (2015) PH-Controlled Hierarchical Self-Assembly of Peptide Amphiphile. *Macromolecules*, 48, 2647–2653. https://doi.org/10.1021/MA502572W/SUPPL_FILE/MA502572W_SI_001.PDF.

452 Dreher, M.R., Simnick, A.J., Fischer, K., Smith, R.J., Patel, A., Schmidt, M. and Chilkoti, A. (2008) Temperature Triggered Self-Assembly of Polypeptides into Multivalent Spherical Micelles. *J. Am. Chem. Soc.*, 130, 687–694. https://doi.org/10.1021/JA0764862/SUPPL_FILE/JA0764862-FILE003.PDF.

453 Cao, M., Shen, Y., Wang, Y., Wang, X. and Li, D. (2019) Self-Assembly of Short Elastin-like Amphiphilic Peptides: Effects of Temperature, Molecular Hydrophobicity and Charge Distribution. *Mol. 2019, Vol. 24, Page 202*, 24, 202. https://doi.org/10.3390/MOLECULES24010202.

454 Huang, R., Wang, Y., Qi, W., Su, R. and He, Z. (2014) Temperature-Induced Reversible Self-Assembly of Diphenylalanine Peptide and the Structural Transition from Organogel to Crystalline Nanowires. *Nanoscale Res. Lett.*, 9, 1–9. https://doi.org/10.1186/1556-276X-9-653/TABLES/1.

455 Palma, C.A., Cecchini, M. and Samorí, P. (2012) Predicting Self-Assembly : From Empirism to Determinism. *Chem. Soc. Rev.*, 41, 3713–3730. https://doi.org/10.1039/C2CS15302E.

456 Mandal, D., Nasrolahi Shirazi, A. and Parang, K. (2014) Self-Assembly of Peptides to Nanostructures. *Org. Biomol. Chem.*, 12, 3544–3561. https://doi.org/10.1039/C4OB00447G.

457 Hong, Y., Pritzker, M.D., Legge, R.L. and Chen, P. (2005) Effect of NaCl and Peptide Concentration on the Self-Assembly of an Ionic-Complementary Peptide EAK16-II. *Colloids Surfaces B Biointerfaces*, 46, 152–161. https://doi.org/10.1016/J.COLSURFB.2005.11.004.

458 Fan, Q., Ji, Y., Wang, J., Wu, L., Li, W., Chen, R. and Chen, Z. (2018) Self-Assembly Behaviours of Peptide–Drug Conjugates: Influence of Multiple

Factors on Aggregate Morphology and Potential Self-Assembly Mechanism. *R. Soc. Open Sci.*, 5. https://doi.org/10.1098/RSOS.172040.

459 Martari, M. and Sanderson, R.D. (2008) Critical Self-Assembly Concentration of Bolaamphiphilic Peptides and Peptide Hybrids Determined by Fluorescence Measurements. *South African J. Chem.*, 61, 47–52. http://www.scielo.org.za/scielo.php?script=sci_arttext&pid=S0379-43502008000100010.

460 Dong, D.C. and Winnik, M.A. (1982) THE Py SCALE OF SOLVENT POLARITIES. SOLVENT EFFECTS ON THE VIBRONIC FINE STRUCTURE OF PYRENE FLUORESCENCE and EMPIRICAL CORRELATIONS WITH ET and Y VALUES. *Photochem. Photobiol.*, 35, 17–21. https://doi.org/10.1111/J.1751-1097.1982.TB03805.X.

461 Kalyanasundaram, K. and Thomas, J.K. (1977) Environmental Effects on Vibronic Band Intensities in Pyrene Monomer Fluorescence and Their Application in Studies of Micellar Systems. *J. Am. Chem. Soc.*, 99, 2039–2044. https://doi.org/10.1021/JA00449A004.

462 Aguiar, J., Carpena, P., Molina-Bolívar, J.A. and Carnero Ruiz, C. (2003) On the Determination of the Critical Micelle Concentration by the Pyrene 1:3 Ratio Method. *J. Colloid Interface Sci.*, 258, 116–122. https://doi.org/10.1016/S0021-9797(02)00082-6.

463 Hutchinson, J.A., Hamley, I.W., Torras, J., Alemán, C., Seitsonen, J. and Ruokolainen, J. (2019) Self-Assembly of Lipopeptides Containing Short Peptide Fragments Derived from the Gastrointestinal Hormone PYY 3-36 : From Micelles to Amyloid Fibrils. *J. Phys. Chem. B*, 123, 614–621. https://doi.org/10.1021/ACS.JPCB.8B11097/SUPPL_FILE/JP8B11097_SI_001.PDF.

464 Mohr, A., Talbiersky, P., Korth, H.G., Sustmann, R., Boese, R., Bläser, D. and Rehage, H. (2007) A New Pyrene-Based Fluorescent Probe for the Determination of Critical Micelle Concentrations. *J. Phys. Chem. B*, 111, 12985–12992. https://doi.org/10.1021/JP0731497/SUPPL_FILE/JP0731497SI20070731_052

551.PDF.

465 Regev, O. and Zana, R. (1999) Aggregation Behavior of Tyloxapol, a Nonionic Surfactant Oligomer, in Aqueous Solution. *J. Colloid Interface Sci.*, 210, 8–17. https://doi.org/10.1006/JCIS.1998.5776.

466 Basu Ray, G., Chakraborty, I. and Moulik, S.P. (2006) Pyrene Absorption Can Be a Convenient Method for Probing Critical Micellar Concentration (Cmc) and Indexing Micellar Polarity. *J. Colloid Interface Sci.*, 294, 248–254. https://doi.org/10.1016/J.JCIS.2005.07.006.

467 Zana, R., Lévy, H. and Kwetkat, K. (1998) Mixed Micellization of Dimeric (Gemini) Surfactants and Conventional Surfactants. I. Mixtures of an Anionic Dimeric Surfactant and of the Nonionic Surfactants C12E5and C12E8. *J. Colloid Interface Sci.*, 197, 370–376. https://doi.org/10.1006/JCIS.1997.5248.

468 Wanzke, C., Jussupow, A., Kohler, F., Dietz, H., Kaila, V.R.I. and Boekhoven, J. (2019) Dynamic Vesicles Formed By Dissipative Self-Assembly. https://doi.org/10.1002/syst.201900044.

469 Doran, T.M., Kamens, A.J., Byrnes, N.K. and Nilsson, B.L. (2012) Role of Amino Acid Hydrophobicity, Aromaticity, and Molecular Volume on IAPP(20–29) Amyloid Self-Assembly. *Proteins Struct. Funct. Bioinforma.*, 80, 1053–1065. https://doi.org/10.1002/PROT.24007.

470 Xu, H., Wang, J., Han, S., Wang, J., Yu, D., Zhang, H., Xia, D., Zhao, X., Waigh, T.A. and Lu, J.R. (2009) Hydrophobic-Region-Induced Transitions in Self-Assembled Peptide Nanostructures. *Langmuir*, 25, 4115–4123. https://doi.org/10.1021/LA802499N/SUPPL_FILE/LA802499N_SI_001.PDF.

471 Gordon, D.J., Balbach, J.J., Tycko, R. and Meredith, S.C. (2004) Increasing the Amphiphilicity of an Amyloidogenic Peptide Changes the β-Sheet Structure in the Fibrils from Antiparallel to Parallel. *Biophys. J.*, 86, 428–434. https://doi.org/10.1016/S0006-3495(04)74119-3.

472 Yi, N., Oh, B., Kim, H.A. and Lee, M. (2014) Combined Delivery of BCNU and VEGF SiRNA Using Amphiphilic Peptides for Glioblastoma. *http://dx.doi.org/10.3109/1061186X.2013.850502*, 22, 156–164. https://doi.org/10.3109/1061186X.2013.850502.

473 Edvinsson, L., Grell, A.S. and Warfvinge, K. (2020) Expression of the CGRP Family of Neuropeptides and Their Receptors in the Trigeminal Ganglion. *J. Mol. Neurosci.*, 70, 930–944. https://doi.org/10.1007/S12031-020-01493-Z/FIGURES/9.

474 Paulsson, J.F., Andersson, A., Westermark, P. and Westermark, G.T. (2006) Intracellular Amyloid-like Deposits Contain Unprocessed pro-Islet Amyloid Polypeptide (ProIAPP) in Beta Cells of Transgenic Mice Overexpressing the Gene for Human IAPP and Transplanted Human Islets. *Diabetologia*, 49, 1237–1246. https://doi.org/10.1007/S00125-006-0206-7/FIGURES/8.

475 Kiriyama, Y. and Nochi, H. (2018) Role and Cytotoxicity of Amylin and Protection of Pancreatic Islet β-Cells from Amylin Cytotoxicity. *Cells*, 7. https://doi.org/10.3390/CELLS7080095.

476 Ritzel, R.A., Meier, J.J., Lin, C.Y., Veldhuis, J.D. and Butler, P.C. (2007) Human Islet Amyloid Polypeptide Oligomers Disrupt Cell Coupling, Induce Apoptosis, and Impair Insulin Secretion in Isolated Human Islets. *Diabetes*, 56, 65–71. https://doi.org/10.2337/DB06-0734.

477 Gray, A.L.H., Antevska, A., Link, B.A., Bogin, B., Burke, S.J., Dupuy, S.D., Collier, J.J., Levine, Z.A., Karlstad, M.D. and Do, T.D. (2021) α-CGRP Disrupts Amylin Fibrillization and Regulates Insulin Secretion: Implications on Diabetes and Migraine. *Chem. Sci.*, 12, 5853–5864. https://doi.org/10.1039/D1SC01167G.

478 Mohamed, A., Pekoz, A.Y., Ross, K., Hutcheon, G.A. and Saleem, I.Y. (2019) Pulmonary Delivery of Nanocomposite Microparticles (NCMPs) Incorporating MiR-146a for Treatment of COPD. *Int. J. Pharm.*, 569, 118524. https://doi.org/10.1016/J.IJPHARM.2019.118524.

479 Alhalaweh, A., Andersson, S. and Velaga, S.P. (2009) Preparation of Zolmitriptan–Chitosan Microparticles by Spray Drying for Nasal Delivery. *Eur. J. Pharm. Sci.*, 38, 206–214. https://doi.org/10.1016/J.EJPS.2009.07.003.

480 Desai, K.G.H. and Park, H.J. (2008) Encapsulation of Vitamin C in Tripolyphosphate Cross-Linked Chitosan Microspheres by Spray Drying. *http://dx.doi.org/10.1080/02652040400026533*, 22, 179–192. https://doi.org/10.1080/02652040400026533.

481 Rassu, G., Soddu, E., Cossu, M., Gavini, E., Giunchedi, P. and Dalpiaz, A. (2016) Particulate Formulations Based on Chitosan for Nose-to-Brain Delivery of Drugs. A Review. *J. Drug Deliv. Sci. Technol.*, 32, 77–87. https://doi.org/10.1016/J.JDDST.2015.05.002.

482 Bernkop-Schnürch, A. and Dünnhaupt, S. (2012) Chitosan-Based Drug Delivery Systems. *Eur. J. Pharm. Biopharm.*, 81, 463–469. https://doi.org/10.1016/J.EJPB.2012.04.007.

483 Sinha, V.R., Singla, A.K., Wadhawan, S., Kaushik, R., Kumria, R., Bansal, K. and Dhawan, S. (2004) Chitosan Microspheres as a Potential Carrier for Drugs. *Int. J. Pharm.*, 274, 1–33. https://doi.org/10.1016/J.IJPHARM.2003.12.026.

484 Garcia-Fuentes, M. and Alonso, M.J. (2012) Chitosan-Based Drug Nanocarriers: Where Do We Stand? *J. Control. Release*, 161, 496–504. https://doi.org/10.1016/J.JCONREL.2012.03.017.

485 Luppi, B., Bigucci, F., Cerchiara, T. and Zecchi, V. (2010) Chitosan-Based Hydrogels for Nasal Drug Delivery: From Inserts to Nanoparticles. *https://doi.org/10.1517/17425247.2010.495981*, 7, 811–828. https://doi.org/10.1517/17425247.2010.495981.

486 Arora, P., Sharma, S. and Garg, S. (2002) Permeability Issues in Nasal Drug Delivery. *Drug Discov. Today*, 7, 967–975. https://doi.org/10.1016/S1359-6446(02)02452-2.

487 Schipper, N.G.M., Olsson, S., Hoogstraate, J.A., DeBoer, A.G., Vårum, K.M. and Artursson, P. (1997) Chitosans as Absorption Enhancers for Poorly Absorbable Drugs 2: Mechanism of Absorption Enhancement. *Pharm. Res. 1997 147*, 14, 923–929. https://doi.org/10.1023/A:1012160102740.

488 Sun, Y., Shi, K., Wan, F. and Cui, F. De. (2012) Methotrexate-Loaded Microspheres for Nose to Brain Delivery: In Vitro/in Vivo Evaluation. *J. Drug Deliv. Sci. Technol.*, 22, 167–174. https://doi.org/10.1016/S1773-2247(12)50022-5.

489 Sun, Y., Cui, F., Shi, K., Wang, J., Niu, M. and Ma, R. (2009) The Effect of Chitosan Molecular Weight on the Characteristics of Spray-Dried Methotrexate-Loaded Chitosan Microspheres for Nasal Administration.

http://dx.doi.org/10.1080/03639040802395185, 35, 379–386. https://doi.org/10.1080/03639040802395185.

490 Roon, K.I., Soons, P.A., Uitendaal, M.P., De Beukelaar, F. and Ferrari, M.D. (1999) Pharmacokinetic Profile of Alniditan Nasal Spray during and Outside Migraine Attacks. *Br. J. Clin. Pharmacol.*, 47, 285–290. https://doi.org/10.1046/J.1365-2125.1999.00894.X.

491 Stoker, D.G., Reber, K.R., Waltzman, L.S., Ernst, C., Hamilton, D., Gawarecki, D., Mermelstein, F., McNicol, E., Wright, C. and Carr, D.B. (2008) Analgesic Efficacy and Safety of Morphine-Chitosan Nasal Solution in Patients with Moderate to Severe Pain Following Orthopedic Surgery. *Pain Med.*, 9, 3–12. https://doi.org/10.1111/J.1526-4637.2007.00300.X/2/PME_300_F5.JPEG.

492 Christensen, K.S., Cohen, A.E., Mermelstein, F.H., Hamilton, D.A., McNicol, E., Babul, N. and Carr, D.B. (2008) The Analgesic Efficacy and Safety of a Novel Intranasal Morphine Formulation (Morphine plus Chitosan), Immediate Release Oral Morphine, Intravenous Morphine, and Placebo in a Postsurgical Dental Pain Model. *Anesth. Analg.*, 107, 2018–2024. https://doi.org/10.1213/ANE.0B013E318187B952.

493 Titus, D., James Jebaseelan Samuel, E. and Roopan, S.M. (2019) Nanoparticle Characterization Techniques. Green Synthesis, Characterization and Applications of Nanoparticles. https://doi.org/10.1016/B978-0-08-102579-6.00012-5.

494 Mourdikoudis, S., Pallares, R.M. and Thanh, N.T.K. (2018) Characterization Techniques for Nanoparticles: Comparison and Complementarity upon Studying Nanoparticle Properties. *Nanoscale*, 10, 12871–12934. https://doi.org/10.1039/C8NR02278J.

495 Cho, E.J., Holback, H., Liu, K.C., Abouelmagd, S.A., Park, J. and Yeo, Y. (2013) Nanoparticle Characterization: State of the Art, Challenges, and Emerging Technologies. *Mol. Pharm.*, 10, 2093–2110. https://doi.org/10.1021/MP300697H.

496 Nagashima, K., Zheng, J., Parmiter, D. and Patri, A.K. (2011) Biological Tissue and Cell Culture Specimen Preparation for TEM Nanoparticle Characterization.

Methods in Molecular Biology (Clifton, N.J.), 83–91. https://doi.org/10.1007/978-1-60327-198-1_8.

497 Hall, J.B., Dobrovolskaia, M.A., Patri, A.K. and McNeil, S.E. (2007) Characterization of Nanoparticles for Therapeutics. *Nanomedicine*, 2, 789–803. https://doi.org/10.2217/17435889.2.6.789/ASSET/IMAGES/LARGE/GRAPHIC22.JPEG.

498 Sonam, Chaudhary, H. and Kumar, V. (2014) Taguchi Design for Optimization and Development of Antibacterial Drug-Loaded PLGA Nanoparticles. *Int. J. Biol. Macromol.*, 64, 99–105. https://doi.org/10.1016/J.IJBIOMAC.2013.11.032.

499 Vandervoort, J. and Ludwig, A. (2002) Biocompatible Stabilizers in the Preparation of PLGA Nanoparticles: A Factorial Design Study. *Int. J. Pharm.*, 238, 77–92. https://doi.org/10.1016/S0378-5173(02)00058-3.

500 Mistry, A., Stolnik, S. and Illum, L. (2009) Nanoparticles for Direct Nose-to-Brain Delivery of Drugs. *Int. J. Pharm.*, 379, 146–157. https://doi.org/10.1016/j.ijpharm.2009.06.019.

501 Piñeiro, L., Novo, M. and Al-Soufi, W. (2015) Fluorescence Emission of Pyrene in Surfactant Solutions. *Adv. Colloid Interface Sci.*, 215, 1–12. https://doi.org/10.1016/J.CIS.2014.10.010.

502 Stopková, L., Inová, J.G., Uchtová, Z., Márik, J.Č. and Andriamainty, F. (2018) Determination of Critical Micellar Concentration of Homologous 2-Alkoxyphenylcarbamoyloxyethyl-Morpholinium Chlorides. *Mol. 2018, Vol. 23, Page 1064*, 23, 1064. https://doi.org/10.3390/MOLECULES23051064.

503 Wolszczak, M. and Miller, J. (2002) Characterization of Non-Ionic Surfactant Aggregates by Fluorometric Techniques. *J. Photochem. Photobiol. A Chem.*, 147, 45–54. https://doi.org/10.1016/S1010-6030(01)00611-6.

504 Islam, Y., Ehtezazi, P., Cashmore, A., Marinsalda, E., Leach, A.G., Coxon, C.R., Fatokun, A.A., Sexton, D.W., Khan, I., Zouganelis, G., Downing, J., Pluchino, S., Sivakumaran, M., Teixido, M. and Ehtezazi, T. (2021) The Inclusion of a Matrix Metalloproteinase-9 Responsive Sequence in Self-Assembled Peptide-Based

Brain-Targeting Nanoparticles Improves the Efficiency of Nanoparticles Crossing the Blood-Brain Barrier at Elevated MMP-9 Levels. *J. Pharm. Sci.*, 110, 1349–1364. https://doi.org/10.1016/J.XPHS.2020.12.004.

505 Ryan, D.M., Anderson, S.B., Senguen, F.T., Youngman, R.E. and Nilsson, B.L. (2010) Self-Assembly and Hydrogelation Promoted by F 5 -Phenylalanine. *Soft Matter*, 6, 475–479. https://doi.org/10.1039/B916738B.

506 Ryan, D.M., Anderson, S.B. and Nilsson, B.L. (2010) The Influence of Side-Chain Halogenation on the Self-Assembly and Hydrogelation of Fmoc - Phenylalanine Derivatives. *Soft Matter*, 6, 3220–3231. https://doi.org/10.1039/C0SM00018C.

507 Hinchcliffe, M., Jabbal-Gill, I., Smith, A. and Hinchcliffe, M. (2005) Effect of Chitosan on the Intranasal Absorption of Salmon Calcitonin in Sheep. *J. Pharm. Pharmacol.*, 57, 681–687. https://doi.org/10.1211/0022357056073.

508 Casettari, L. and Illum, L. (2014, September 28) Chitosan in Nasal Delivery Systems for Therapeutic Drugs. Journal of Controlled Release, 189–200. https://doi.org/10.1016/j.jconrel.2014.05.003.

509 Illum, L. (1991) The Nasal Delivery of Peptides and Proteins. *Trends Biotechnol.*, 9, 284–289. https://doi.org/10.1016/0167-7799(91)90091-U.

510 Illum, L., Farraj, N.F. and Davis, S.S. (1994) Chitosan as a Novel Nasal Delivery System for Peptide Drugs. *Pharm. Res. 1994 118*, 11, 1186–1189. https://doi.org/10.1023/A:1018901302450.

511 Sarabandi, K., Gharehbeglou, P. and Jafari, S.M. (2019) Spray-Drying Encapsulation of Protein Hydrolysates and Bioactive Peptides: Opportunities and Challenges. *https://doi.org/10.1080/07373937.2019.1689399*, 38, 577–595. https://doi.org/10.1080/07373937.2019.1689399.

512 He, P., Davis, S.S. and Illum, L. (1999) Chitosan Microspheres Prepared by Spray Drying. *Int. J. Pharm.*, 187, 53–65. https://doi.org/10.1016/S0378-5173(99)00125-8.

513 Mitragotri, S., Burke, P.A. and Langer, R. (2014) Overcoming the Challenges in Administering Biopharmaceuticals: Formulation and Delivery Strategies. *Nat. Rev. Drug Discov. 2014 139*, 13, 655–672. https://doi.org/10.1038/nrd4363.

514 Nicolas, S. and Nicolas, D. (2020) Triptans. *StatPearls*. http://europepmc.org/books/NBK554507.

515 Edvinsson, L. and Lars Edvinsson, P. (2015) CGRP Receptor Antagonists and Antibodies against CGRP and Its Receptor in Migraine Treatment. *Br. J. Clin. Pharmacol.*, 80, 193–199. https://doi.org/10.1111/BCP.12618.

516 Diao, L. and Meibohm, B. (2013) Pharmacokinetics and Pharmacokinetic-Pharmacodynamic Correlations of Therapeutic Peptides. *Clin. Neuropharmacol.*, 52, 855–868. https://doi.org/10.1007/s40262-013-0079-0.